MEMBRANE ASSISTED FLUIDIZED BED REACTOR: EXPERIMENTAL DEMONSTRATION FOR PARTIAL OXIDATION OF METHANOL

DISSERTATION

to obtain
the doctor's degree at the University of Twente,
on the authority of the rector magnificus,
prof. dr. F. A. van Vught,
on account of the decision of the graduation committee,
to be publicly defended
on Thursday May 27th, 2004 at 16.45 hrs

by

Salim Abdul Rashid Khan Deshmukh

Born on June 1st, 1976

in Mahad, India

This dissertation is approved by the promoter

Prof.dr.ir. J.A.M. Kuipers

and the assistant promoter

Dr.ir. M. van Sint Annaland

To my parents
To all relatives and friends

Dissertation committee:

Prof.dr.ir. C. Hoed, chairman	University of Twente
Prof.dr.ir. J.A.M. Kuipers, promoter	University of Twente
Dr.ir. M. van Sint Annaland, assistant-promoter	University of Twente
Prof.dr.ir. L. Lefferts	University of Twente
Prof.dr.ir. W.P.M. van Swaaij	University of Twente
Prof.dr.ir. H.J. Heeres	University of Groningen
Dr.ir. P.H.M. Feron	TNO/MEP, Apeldoorn
Prof.dr. M.P. Dudukovic	University of Washington, USA

This research is a part of the research program carried out within the Center for Separation Technology, as a cooperation between the University of Twente and TNO, the Netherlands Organization for Applied Scientific Research.

Publisher:
PrintPartners Ipskamp
P.O. Box 333, 7500 AH Enschede, The Netherlands

ISBN: 90-365-2060-6

Contents

Summary

Strongly exothermic heterogeneously catalyzed gas phase partial oxidation reactions are an industrially important class of chemical conversions, which require reactors that need to be carefully designed to remove the large amount of energy generated by the reactions. In addition the formation of explosive gas mixtures should be avoided and a high selectivity for the intermediate product of interest should be achieved. In this thesis a new reactor concept is proposed and investigated for this class of reactions aiming at improved reactor safety and a higher product throughput, i.e. higher product yield at higher flow rates, using multifunctionality. The proposed reactor concept, the membrane assisted fluidized bed reactor (MAFBR), combines the advantages of good heat transfer characteristics of the fluidized bed with the possibility of controlled dozi 1 of air/oxygen via the (ceramic) membranes at high temperatures achieving an inherentıy safe and isothermal reactor operation. Due to the insertion of the membranes in the fluidized bed and the addition of gas via the membranes, the gas back mixing, usually a disadvantage of fluidized beds, is strongly reduced, while the good heat transfer characteristics can be retained. The potential of the membrane assisted fluidized bed reactor was investigated for the partial oxidation of methanol to formaldehyde, because this reactor concept is especially interesting for strongly exothermic partial oxidation reactions where the feed composition is restricted by the explosion regions of the reactants and products. For this reaction system the membrane assisted fluidized bed reactor allows operation at more severe reaction conditions with a higher productivity, while explosive mixtures or temperature runaways can be avoided. In this thesis the reactor concept has been developed on the basis of an experimental study on the effect of fluidization conditions on the membrane permeation rate in a MAFBR, the extent of gas back mixing and the tube-to-bed heat transfer rates in the presence of membrane bundles with and without membrane permeation. In addition the kinetics of the main reaction and important side reactions during the partial oxidation of methanol to formaldehyde were determined and finally the technical feasibility of the reactor concept was assessed in a small laboratory scale reactor was tested aiming for a proof of principle.

The effect of fluidization conditions, viz. the superficial gas velocity, particle size and freeboard pressure on the gas permeation rate through porous ceramic membranes has been studied experimentally for two different configurations of the membrane bundles, horizontal and vertical membrane bundles. The gas withdrawal rate through the membranes increased with an increase in the freeboard pressure, which could be well

described by the dusty gas model. In this model it was simply assumed that the membrane permeate flux was only a function of the local pressure in the fluidized bed, for which the hydrostatic head with the average bed porosity was taken. The superficial gas velocity as well as the particle size had no overall effect on the total amount of gas permeated through the membranes for both membrane configurations. This finding can be explained by the fact that the decrease in the average bed porosity at lower superficial gas velocities or larger particle sizes is counterbalanced by an increase in the bed height.

The effect of gas permeation through horizontally immersed membrane tubes on the heat transfer characteristics in a membrane assisted fluidized bed was investigated experimentally. Local time-averaged heat transfer coefficients from copper tubes arranged in a staggered orientation with respect to the membrane tubes to the fluidized bed were measured in a square bed (0.15 m x 0.15 m x 0.95 m) containing glass particles (75-110 μm) fluidized with air distributed via a porous plate, where the ratio of gas fed or removed through the membrane bundles and the porous plate distributor was varied. The experimental results revealed that high gas permeation rates through the membranes strongly decreased the heat transfer coefficient at high superficial gas velocities for tubes at the top of the tube bundle. This was attributed to the reduced mobility and increased bubble hold up and/or dilution of the emulsion phase, reducing overall heat capacity. However, the heat transfer coefficient in the membrane assisted fluidized beds is much higher than in packed bed reactors. In the design of membrane assisted fluidized beds care must be taken to include the effect of gas addition or withdrawal through the membranes on the required heat transfer surface area.

The extent of gas back mixing has been studied experimentally for fluidized beds with internals (membranes) using different membrane bundle configurations, viz. horizontally and vertically positioned membranes, with and without addition of gas via the membranes over a wide fluidization velocity range. The effect of the presence of the membranes, but especially the effect of gas addition via membranes on the axial gas back mixing in the fluidized beds has been studied experimentally using steady state tracer gas injection experiments. For a fluidized bed with vertical and horizontal internals the axial gas back mixing is strongly reduced compared to a bed without internals which can be attributed to the presence of the internals, which obstruct the lateral movement of the bubbles by preventing bubble growth. Thus the formation of macroscopic circulation patterns, as observed for the bed without internals is impeded. The addition of gas via the membranes in the bed with horizontal membranes reduced the gas back mixing enormously, even much more than due to the presence of internals. The membrane

permeation effectively annihilates the macro scale circulation in the fluidized bed. Furthermore, experiments with tracer gas injected via the membranes highlighted the importance of mass transfer limitations between the bubble phase and emulsion phase. The higher the ratio of he permeated through the membranes to the gas fed via the bottom distributor, the smaller the average bubble size and bubble fraction, the smaller the mass transfer limitations.

To assess the potential of the membrane assisted fluidized bed reactor for the methanol partial oxidation, reliable and accurate reaction rate expressions are required for the methanol partial oxidation reaction and its most important side reactions, which are valid over very wide concentration ranges. The kinetics of the methanol partial oxidation to formaldehyde reaction system over a commercial Fe-Mo catalyst has been determined experimentally in a differentially operated reactor at temperatures ranging from 230 to 260°C, over a wide range of methanol and oxygen concentrations. The principal products were formaldehyde, water, dimethyl ether (DME) and dimethoxymethane (DMM) while only traces of methyl formate were detected. The presence of water vapour lowered the formaldehyde formation rate significantly, especially at lower water partial pressures. The relative effect of the water concentration on the formation rate was much smaller at higher water partial pressures. For the most important side reactions, i.e. dimethyl ether formation as well as dimethoxymethane formation (both equilibrium reactions), the forward reaction rates were determined from the selectivity data. The backward reaction rates were obtained from the forward reaction rates and the thermodynamic equilibrium data. Dimethyl ether formation reaction rate (forward reaction) was found to be only dependent on the methanol concentrations with first order dependency. The dimethoxymethane formation rate (forward reaction) was found to be linear with both the formaldehyde and the methanol concentration. The formaldehyde oxidation to CO was studied separately in a dual bed, in which formaldehyde was first formed in an integral reactor at lower temperatures and subsequently converted to CO in a differential reactor. The rate of CO formation was first order in formaldehyde and the oxygen dependency was identical to that for the formaldehyde formation from methanol.

The kinetics of the formaldehyde formation from methanol could be well described by Langmuir-Hinshelwood kinetics, assuming two different metal oxide sites, one containing adsorbed oxygenates and the other one containing lattice oxygen and including competitive adsorption of water and methanol. The observed influences of the composition and temperature on the methanol partial oxidation, formaldehyde partial oxidation, dimethyl ether formation and dimethoxymethane formation reaction rates

could be well described. A multi-variable non-linear regression to fit the pre-exponential reaction and adsorption constants and activation energies was carried out with Levenberg-Marquard minimization technique, where the axial concentration profiles in the kinetics reactor were accounted for using a plug flow reactor model in order to properly take into account the influence of the water concentration on the reaction rates (even in the differentially operated kinetics reactor).

Finally, a small laboratory scale membrane assisted fluidized bed reactor (MAFBR) was constructed in order to experimentally demonstrate the reactor concept for the methanol partial oxidation to formaldehyde. The methanol conversion and product selectivities were measured at various overall fluidization velocities, reactor temperatures, methanol and oxygen overall feed concentrations, ratios of gas fed via membranes and the distributor and bed heights.

With steady state tracer injection experiments it was shown that in the experimental reactor effective compartmentalization was achieved with very low axial gas back-mixing due to the elimination of the macro scale circulation patterns induced by the presence of the membranes and the permeation of gas through the membranes. With an ultrasound technique the RTD of the MAFBR was determined over a wide range of fluidization velocities, enabling quantification of the axial gas back-mixing. The MAFBR exhibited approximately plug flow behaviour for all the operating conditions used in this investigation.

Subsequently the MAFBR was demonstrated successfully for the partial oxidation of methanol to formaldehyde. High methanol conversions and high selectivities to formaldehyde were achieved with safe and almost isothermal reactor operation at very high inlet methanol concentrations, much higher than currently used in industrial processes. It was experimentally demonstrated that distributive feeding of oxygen in a MAFBR produces an increased overall formaldehyde yield and throughput without pronounced undesirable conversion of formaldehyde to carbon monoxide.

Finally, a phenomenological reactor model has been developed considering the MAFBR as a series of ideally stirred tank reactors consisting of a bubble phase and an emulsion phase, where the addition of gas via the membranes and gas production due to chemical transformations was accounted for. The developed model can be considered as a two-parameter model, namely the number of CISTRs in series, which was determined on basis of separate RTD experiments and the average bubble size, assumed constant throughout the fluidized bed. With the developed model the experimentally observed trends as a function of the operating conditions could be well described.

Samenvatting

Sterk exotherme heterogeen gekatalyseerde gasfase partiële oxidatie reacties vormen een belangrijke klasse van chemische omzettingen, die uitgevoerd worden in reactoren waarby goed rekening moeten worden gehouden met de afvoer van de grote hoeveelheden energie die de reacties produceren. Daarnaast moet de vorming van explosieve gasmengsels worden vermeden en de gewenste hoge selectiviteit naar het tussenproduct gerealiseerd te worden. In dit proefschrift wordt een nieuw reactorconcept voorgesteld en bestudeerd voor deze klasse van reacties, waar – gebruik-makend van multi-functionaliteit – een verbeterde reactorveiligheid en een hogere productiviteit (hogere product yield bij hogere doorzetten) wordt nagestreefd. Het voorgestelde reactorconcept, de membraan gefluïdiseerde bed reactor, combineert de voordelen van de goede warmteoverdrachts-karakteristieken van een gefluïdiseerd bed met de mogelijkheid lucht of zuurstof gecontroleerd toe te voeren via (keramische) membranen bij verhoogde temperaturen, waarmee een intrinsiek veilige en isotherme reactoroperatie mogelijk wordt. Daarnaast kan via het inbrengen van membranen in het gefluïdiseerde bed en de gas-toevoer via de membranen de gas-terugmenging sterk verminderd worden, terwijl de goede warmte-overdrachtskarakteristieken behouden blijven. De geschiktheid van de membraan gefluïdiseerde bed reactor is onderzocht voor de partiële oxidatie van methanol naar formaldehyde, aangezien de membraan gefluïdiseerde bed reactor in het bijzonder interessant is voor dit sterk exotherme partiële oxidatie reactiesysteem, waar voor andere reactorconcepten de keuze van de voedingssamenstelling beperkt wordt door de explosiegrenzen van de reactanten en producten. Voor dit reactiesysteem kan de membraan gefluïdiseerde bed reactor bij andere procescondities met een verhoogde productiviteit bedreven worden, terwijl intrinsiek explosies en runaways voorkomen kunnen worden. In dit proefschrift is dit reactorconcept bestudeerd via een experimentele studie naar het effect van de fluïdisatiecondities in het membraan gefluïdiseerde bed op de membrane permeatie-snelheden. Daarnaast is de gas-terugmenging en de warmte-overdrachtssnelheid tussen het bed en ondergedompelde buizen in aanwezigheid van membraanbundels met en zonder membraan-permeatie onderzocht. De kinetiek van de hoofd- en de belangrijkste nevenreacties van de partiële oxidatie van methanol naar formaldehyde is bepaald om tenslotte de technische haalbaarheid van het voorgestelde reactorconcept te toetsen in een laboratoriumschaal reactor.

Het effect van de fluïdisatiecondities, d.w.z. de superficiële gassnelheid, de deeltjesdiameter en de freeboard-druk op de gas-permeatiesnelheid door proreuze

keramische membranen is experimenteel bestudeerd voor twee verschillende membraanbundelconfiguraties, te weten horizontaal en verticaal gepositioneerde membraanbundels. De gasontrekkingssnelheid door de membranen neemt toe bij hogere drukken in het freeboard, hetgeen goed beschreven wordt met het dusty gas model, waarbij aangenomen is dat de membraan permeatie-flux alleen een functie is van de locale druk in het gefluïdiseerde bed, waarvoor de hydrostatische druk is genomen met de gemiddelde bed porositeit. De superficiële gassnelheid en de deeltjesgrootte hadden geen effect op de totale snelheid waarmee het gas door de membranen werd onttrokken. Dit kan verklaard worden door het feit dat de verlaging in de gemiddelde bedporositeit bij lagere superficiële gassnelheden gecompenseerd wordt door een toename in de bedhoogte.

Het effect van gas-permeatie door horizontaal geplaatste membraanbuizen op de warmte-overdrachtseigenschappen van een membraan gefluïdiseerd bed is experimenteel bestudeerd. Locale tijdsgemiddelde warmte-overdrachtscoëfficiënten van koperen buizen gepositioneerd om en om met membraanbuizen naar een vierkant met lucht gefluïdiseerd bed (0.15 m x 0.15 m x 0.95 m) met glasdeeltjes (75-110 μm) zijn gemeten, waarbij de verhouding van gas gevoed of verwijderd via de membraanbuizen en de poreuze verdeelplaat werd gevarieerd. De experimentele resultaten lieten zien dat bij hoge superficiële gassnelheden de warmte-overdrachtssnelheid bovenin het bed sterk verlaagd wordt bij hoge gas-permeatiesnelheden door de membranen. Dit wordt toegeschreven aan de verlaagde bewegelijkheid en verhoogde bellenfractie en/of gasporositeit van de emulsiefase, wat in een verlaagde overall warmtecapaciteit resulteert. Evenwel zijn de warmte-overdrachtscoëfficiënten in membraan gefluïdiseerde bedden nog altijd veel hoger dan in gepakte bed reactoren. In het ontwerp van membraan gefluïdiseerde bed reactoren moet goed rekening gehouden worden met het effect van gas toevoer of onttrekking via membranen op de vereiste totale oppervlakte voor warmte-uitwisseling.

De mate van gas-terugmenging is experimenteel bepaald voor gefluïdiseerde bedden met membranen voor horizontaal en verticaal gepositioneerde membraanbundels en met en zonder gas-toevoer via de membranen voor een groot bereik van fluidisatiesnelheden. Het effect van de aanwezigheid van de membraanbundels, maar vooral ook het effect van gas-toevoer via de membranen op de axiale gas-terugmenging is gemeten met stationaire tracer-injectie experimenten. In een gefluïdiseerd bed met verticale of horizontale membraanbundels is de axiale gas-terugmenging sterk verminderd in vergelijking met een bed zonder buizen, doordat de buizen de laterale beweging van de bellen en daardoor de belgroei verminderen. De macroscopische

circulatie in het gefluïdiseerde bed, die in bedden zonder buizen worden waargenomen, wordt hierdoor sterk gereduceerd. Toevoer van gas via de membranen in een bed met horizontale membranen reduceerede de gas-terugmenging aanzienlijk, zelfs veel meer dan door de aanwezigheid van de membraanbundels. De membraan-permeatie verhindert effectief de macroscopische circulatie. Daarnaast hebben de experimenten met tracer-injectie via de membranen het belang van massatransportlimitaties tussen de bel en de emulsiefase laten zien. Hoe hoger de verhouding van de gasstroom toegevoerd via de membranen tot de gasstroom gevoed via de bodem-verdeelplaat, hoe kleiner de gemiddelde belgrootte en belfractie, dus hoe kleiner de massatransportlimitaties.

Om de mogelijkheden van de membraan gefluïdiseerde bed reactor voor de partiële oxidatie van methanol vast te stellen, zijn betrouwbare en nauwkeurige reactiesnelheidsvergelijkingen nodig voor de partiële oxidatie van methanol naar formaldehyde en de belangrijkste nevenreacties, die geldig zijn over een groot concentratiebereik. De kinetiek van dit reactiesysteem is bestudeerd over een commerciële Fe-Mo katalysator in een differentieel bedreven kinetiekreactor bij temperaturen van 230 tot 260 ºC. De belangrijkste reactieproducten van de partiële oxidatie van methanol waren naast formaldehyde en water, dimethyl ether (DME) en dimethoxymethaan (DMM), terwijl alleen sporen van methyl formiaat gedetecteerd werden. De aanwezigheid van waterdamp verlaagde de formaldehyde vormingssnelheid aanzienlijk, vooral bij lage water-partiaalspanningen. Het relatieve effect van de water-concentratie was veel geringer bij hogere partiaalspanningen van water. Voor de belangrijkste nevenreacties, d.w.z. de vorming van DME en DMM (beide evenwichtsreacties) zijn vormingsnelheden bepaald aan de hand van de selectiviteitsdata. De reactiesnelheden voor de omgekeerde reacties zijn afgeleid uit de voorwaartse reactiesnelheden en de thermodynamische evenwichtsdata. De DME-vormingssnelheid bleek alleen een functie van de methanolconcentratie volgens een eerste orde afhandelijkheid. De DMM-vormingssnelheid was lineair afhankelijk van de formaldehyde en de methanol concentratie. De oxidatiesnelheid van formaldehyde naar CO is afzonderlijk gemeten in een dual-bed reactor, waar in het eerste bed (integrale reactor) formaldehyde werd gevormd bij lage temperaturen, dat vervolgens werd omgezet naar CO in een differentiële reactor. De vormingssnelheid van CO bleek eerste orde in formaldehyde en de zuurstofafhankelijkheid was identiek aan die van de partiële oxidatie van methanol. De reactiesnelheden van dit reactiesysteem konden goed beschreven worden met een Langmuir-Hinshelwood kinetiek over twee verschillende typen metaaloxide plaatsen aan het katalysatoroppervlak, waarbij een type bestaat uit geadsorbeerde koolwaterstoffen en de andere uit roosterzuurstof, met daarnaast

competitieve adsorptie van water en methanol. De gemeten invloeden van de samenstelling en temperatuur op de partiële oxidatie van methanol en formaldehyde en de vormingssnelheden van DME en DMM konden hiermee goed worden beschreven. Middels de Levenberg-Marquardt techniek, een multi-variabele niet-lineare regressie, zijn de pre-exponentiële reactie- en adsorptieconstantes en de activeringsenergieën gefit, waarbij rekening gehouden is met axiale concentratieprofielen in de kinetiekreactor (gebruik makend van een plug flow reactor-model) teneinde de invloed van axiale waterconcentratie-profielen, zelfs in de differentieel bedreven kinetiekreactor, correct mee te nemen.

Tenslotte is een klein laboratorium-schaal membraan gefluïdiseerd bed reactor geconstrueerd om experimenteel het reactorconcept voor de partiële oxidatie van methanol te demonstreren. De methanol conversie en de product selectiviteiten zijn gemeten bij verschillende superficiële gassnelheden, temperaturen, methanol en zuurstof overall ingansconcentraties, verhoudingen van gas gevoed via de membranen t.o.v. gas gevoed via de bodemverdeelplaat en bedhoogtes. Met stationaire tracer-injectie experimenten is aangetoond dat de reactor erg weinig gas-terugmenging vertoont o.a. door het uitschakelen van macroscopische circulatiepatronen vanwege de aanwezigheid van de membraanbundels en gas-permeatie door de membranen. Met een ultrasound techniek is de RTD van het membraan gefluïdiseerde bed bepaald voor een groot bereik van fluidisatiesnelheden teneinde de overall axiale gas-terugmenging te kwantificeren. De experimentele reactor liet voor alle bestudeerde operatiecondities een vrijwel propstroom gedrag zien. Vervolgens is de partiële oxidatie van methanol naar formaldehyde in het membraan gefluïdiseerde bed uitgevoerd. Zonder problemen konden hoge methanol conversies en hoge product selectiviteiten gerealiseerd worden met een intrinsiek veilige en vrijwel isotherme reactoroperatie bij erg hoge methanol voedingsconcentraties, veel hoger dan momenteel gebruikelijk is bij conventionele industriële processen. Middels distributieve voeding van zuurstof in een membraan gefluïdiseerd bed reactor kunnen hogere formaldehyde yields en hogere doorzetten gerealiseerd worden zonder een significante ongewenste toename in CO vorming.

Een fenomenologisch model is ontwikkeld waarin het membraan gefluïdiseerde bed beschouwd wordt als een serie van ideaal geroerde tank reactoren, die elk bestaan uit een bellenfase en een emulsiefase, waarbij rekening gehouden is met de toevoer van gas via de membranen en gasproductie door de chemische omzettingen. Het ontwikkelde model kan beschouwd worden als een twee-parameter model, namelijk het aantal tanks in serie, dat bepaald is met onafhankelijke RTD metingen, en de gemiddelde (constant

veronderstelde) beldiameter. Met dit model konden de experimenteel waargenomen trends als functie van de verschillende operatiecondities goed worden beschreven.

Chapter 1

General introduction

Abstract

Strongly exothermic heterogeneously catalyzed gas phase partial oxidation reactions are an industrially important class of chemical conversions, which require complex reactors that need to be carefully designed to remove the large amount of energy generated by the reactions, to avoid the formation of explosive gas mixtures and to achieve a high selectivity for the intermediate product of interest. In this thesis a new reactor concept is investigated for this class of reactions aiming at improved reactor safety and a higher product throughput, i.e. higher product yield at higher flow rates, using multifunctionality. The proposed reactor concept, the membrane assisted fluidized bed reactor (MAFBR), combines the advantages of good heat transfer characteristics of the fluidized bed with the possibility of controlled dozing of air/oxygen via the (ceramic) membranes at high temperatures achieving an inherently safe and isothermal reactor operation. Due to the insertion of the membranes in the fluidized bed and the addition of gas via the membranes, the gas back mixing, usually a disadvantage of fluidized beds is strongly reduced, while the good heat transfer characteristics can be retained. In this chapter this novel reactor concept is introduced and qualitatively compared with conventional reactor technologies. Moreover, it is indicated that the reactor concept is especially interesting for strongly exothermic partial oxidation reactions, where the feed concentration of the reactant is bounded by the explosion regions of the reactant and products. Finally, the objectives of the research are presented, which are followed by an outline of the thesis.

1. Introduction

Strongly exothermic heterogeneously catalyzed gas phase partial oxidation reactions are an industrially important class of chemical conversions. Examples of large industrial scale processes based on this type of reactions are the methanol partial oxidation to formaldehyde and the oxidative dehydrogenation of ethyl benzene to styrene. Processes for highly exothermic reactions, where large amounts of heat needs to be removed, and often the formation of explosive gas mixtures needs to be avoided and a high selectivity for intermediate products in consecutive reaction scheme are important, require a complex and dedicated reactor technology. The reactors differ mainly in the mode of the reaction energy removal and the mode of addition of the reactants, which is determined by the permissible concentrations of the reactants and products because of explosion dangers and the heat transfer and mixing characteristics of the reactor. In this work a new reactor concept is investigated for this type of reactions aiming at improved throughput, i.e. higher product yield at higher flow rates on the basis of the process intensification via the integration of membranes inside the reactor.

High temperature catalytic processes performed using inorganic membranes have been in recent years a fast growing area of research. Chemical engineers, catalysts and material scientists have addressed this topic from different viewpoints in a combined effort. Despite the amount of work already carried out, the direct application of inorganic membrane reactors in the process industry is still limited because of a large number of technical and economical drawbacks. For application in high temperature catalytic membrane reactors, the inorganic membranes remain the only candidate, though by far less developed and commercialized than their organic counterparts. In particular, ceramic membranes have seen an enormous development due to successful improvement in several manufacturing techniques (Hsieh, 1988). This made them potentially interesting either as high temperature gas separators or as support for more selective, though less permeable metallic membranes.

2. Packed bed membrane reactor

In Figure 1 a schematic of a packed bed membrane reactor is given. The integration of membranes in the reactor allows to either doze one of the reactants in a controlled manner to achieve optimal axial concentration profiles and thus higher product

yield (high selectivity at high conversion) or alternatively to remove one of the products, typically used to circumvent the thermodynamic equilibrium.

The integration of ceramic membranes inside a reactor using either catalytically active or membranes that enclose a conventional fixed bed of catalyst pellets, has been studied and tested experimentally for a number of reactions (Figure 1 gives a schematic representation of a packed bed membrane reactor). An extensive survey of reactions performed in high temperature membrane reactors can be found in the article by Saracco et al., (1994). Most of the studies have been focused on heterogeneously catalyzed gas-solid reactions, aiming either at increasing the conversion of equilibrium limited reactions, or at enhancing the selectivity towards desired intermediate products (Table 1).

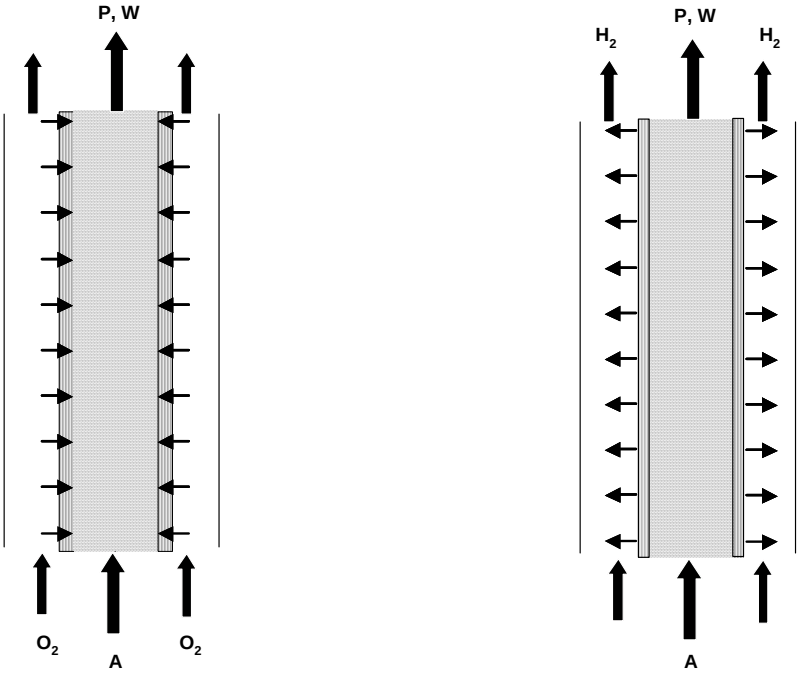

(a) Controlled dozing of one of the reactants e.g. partial oxidation (b) Removal of one of the products e.g. dehydrogenation

Figure 1. Schematic of packed bed membrane reactor for controlled dozing of one of the reactants (a) or removal of one of the products (b); A=reactant, P=product and W= waste.

Table 1: Some reactions of potential interest for inorganic membrane reactor application in the petrochemical industry (Saracco et al., 1994)

Equilibrium limited reactions via removal of product	*Selectivity enhancement via controlled dozing*
Methane steam reforming	Oxidative coupling of methane
Ethane dehydrogenation	Partial oxidation of propane to acrolein
Propane dehydrogenation	Partial oxidation of butane to maleic anhydride
Cyclohexane dehydrogenation	Partial oxidation of ethane
Ethyl benzene dehydrogenation	Partial oxidation of butane to methacrolene
Water gas shift reaction	Partial oxidation of methanol to formaldehyde (Diakov et al. 2001)

In the context of selectivity enhancement, potential benefits could arise because of the following reasons:

1. The membrane keeps the bulk of the two reactants separated, avoiding their premixing and consequently preventing side reactions (Veldsink et al., 1992).
2. The dense membranes (Pd alloys, solid electrolyte) can supply one of the reactants in a monatomic form, particularly active towards, for instance, partial oxidations (Anshits et al., 1989), or partial hydrogenations (Gryaznov et al., 1982 and Nagamoto and Inoue, 1986).
3. Porous membranes such as γ-alumina, modifies in an advantageous way the residence time and the concentration profile of the reactants in the catalytically active zone (Zaspalis, 1990 and Sloot, 1991, Sloot et al., 1990, 1992).

Moreover, especially for partial oxidation reactions a membrane reactor offers improved reactor safety and controllability, reduced separation costs in case of permselective membranes and a wider operating range resulting in higher productivity. However, packed bed membrane reactors also possess some disadvantages:

- High pressure drop and mass transfer limitations because of relatively large particle size.
- Radial temperature and concentration gradients.
- Difficulties in reaction heat removal.
- Low specific membrane surface area.

- No degree of freedom for membrane and cooling tube arrangement.

These disadvantages can be largely overcome by integrating the membranes inside a fluidised bed, referred to as the membrane assisted fluidized bed reactor (MAFBR).

3. Membrane Assisted fluidized bed reactor

A membrane assisted fluidized bed reactor (MAFBR) is a special type of reactor that combines the advantages of a fluidized bed and a membrane reactor (see Figure 2).

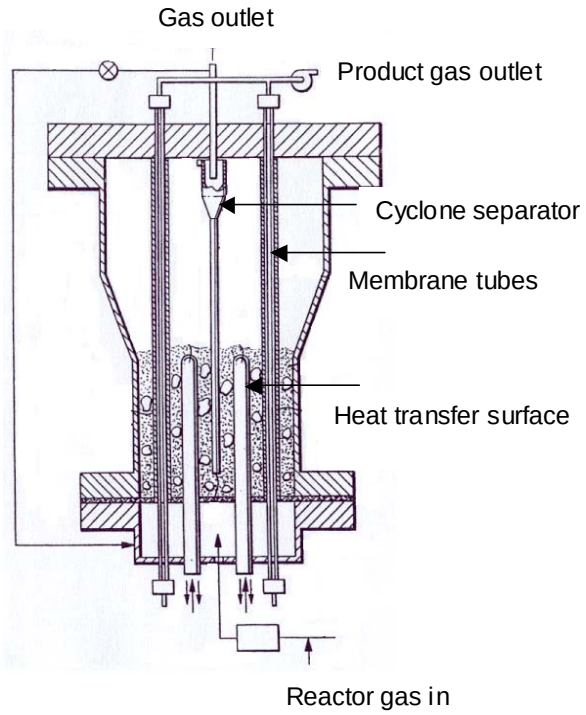

Figure 2. Schematic representation of membrane assisted fluidized bed reactor (Adris et al. 1994).

Fluidization is the operation by which solid particles are transformed into a fluid-like state through suspension in a gas or liquid (Kunii and Levenspiel, 1991). The phenomenon of fluidization has been widely applied to the commercial exploitation of catalytic reactions and gas fluidized beds employing fine powders are finding increased application in the chemical and petroleum industries. The gas velocity at which the solid weight is just balanced by the drag exerted on the particles is called the minimum fluidization velocity. As the superficial velocity is raised from the minimum fluidization velocity, the fluidized solids go through the bubbling, slugging, turbulent and fast fluidization regimes. Figure 3 shows a number of fluidization regimes, which are encountered with change in fluidization velocity. In this work fluidization in the bubbling regime is applied.

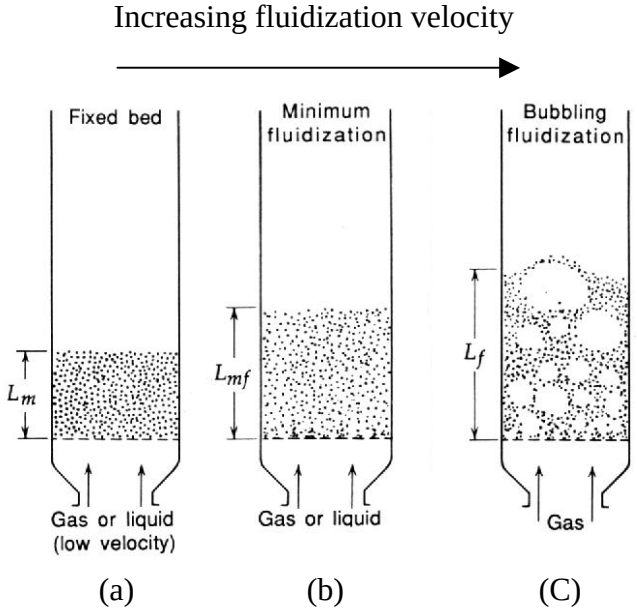

Figure 3. Evolution of fluidization regimes with a change in fluidization velocity (Kunii and Levenspiel, 1991).

3.1. Heat transfer characteristics of fluidized beds

One of the main advantages of the fluidized bed reactor is the excellent tube-to-bed heat transfer, which allows a safe and efficient reactor operation for highly exothermic reactions. Also for highly endothermic reactions without temperature gradients, where the hot catalyst is circulated between the reactor and the regenerator, the excellent gas-solid heat transfer characteristics of the fluidized beds can be effectively exploited. One of the remarkable features of the fluidized bed is its temperature

uniformity. The excellent heat transfer characteristics, caused by the intense macro scale solids mixing induced by the rising bubbles, results in a remarkable temperature uniformity, which exists in both the radial and axial direction, even in beds as large as 10 m (Miracca and Capone, 2001).

Numerous previous studies have been carried out to study the various aspects of tube-to-bed heat transfer in fluidized beds like the influence of the tube diameter, the tube arrangement, the pitch etc,. Studying the tube-to-bed heat transfer in a membrane assisted fluidized bed is novel and has never been done before. In this work the influence of the presence of membrane and heat transfer tube bundles and especially the effect of gas addition and removal via the membrane tubes on the spatial distribution of the tube-to-bed heat transfer coefficient at various fluidization velocities was studied experimentally.

3.2. Mixing characteristics of fluidized beds

Although the good mixing of the solids induced by the bubbles results in good heat transfer properties of the bed, it also causes significant gas back-mixing, which often decrease the conversion and product selectivity. Moreover a large part of the gas flows in the form of bubbles through the fluidized bed, which might cause reactant bypass due to bubble-to-emulsion mass transfer limitations. However, the insertion of membranes decreases the effective axial dispersion via compartmentalization of the fluidized bed. Insertion of membrane bundles in a suitable configuration impedes bubble growth and macroscopic circulation patterns in the fluidized bed, thereby reducing reactant by-pass via rapidly rising large bubbles. Furthermore, gas withdrawal as well as addition via the membranes decreases the bubble superficial gas velocities in the top section of the bed, resulting in smaller gas bubbles, which increases the inter-phase gas exchange favoring high conversions (Mleczko et al., 1996). Both vertical and horizontal inserts (membranes and heat transfer tubes) can be used to effectively retard the emulsion circulation and increase the bubble breakage. For the controlled dozing of one of the reactants a horizontal arrangement of inserts is usually preferred to directly control the local concentrations. For the removal of one of the intermediate products vertical membrane bundles might suffice, which are much easily integrated in the reactor.

In this work the effect of the presence of the membrane bundles including their configuration and the effect of gas addition via the membrane on the axial gas back-mixing is studied using steady state tracer injection experiments, from which detailed information on the flow patterns in the fluidized bed can be derived.

Thus by insertion of membranes in the fluidized bed a synergistic effect can be accomplished. Firstly, optimal concentration profiles can be created via controlled dozing or withdrawal and secondly the fluidization behaviour can be improved via the presence of the inserts and permeation of the gas through the membranes, so that large improvements in conversion and selectivity might be achieved. The main advantages of the MAFBR are:

- Negligible pressure drop; no internal mass and heat transfer limitations because of the small particle sizes that can be employed.
- Isothermal operation.
- Flexibility in membrane and heat transfer surface area and arrangement of the membrane bundles.
- Improved fluidization behavior:
    - Compartmentalization: reduced axial gas back mixing.
    - Reduced bubble size: improved bubble to emulsion mass transfer.

Some of the possible disadvantages of MAFBR are:

- Difficult reactor construction and membrane sealing at wall.
- Attrition of the reactor internals and the catalyst.

The main objective of the research presented in this thesis is the development and demonstration of the membrane assisted fluidized bed reactor for a highly exothermic partial oxidation reaction, to achieve higher product yield at higher reactant throughput, improved reactor safety by distributive addition of oxygen via membranes. Firstly, the effect of fluidization conditions on the gas permeation through the membrane has been studied experimentally. Subsequently, the effect of insertion of membranes, the membrane configuration, (i.e. horizontal or vertical) and gas addition via the membranes on axial gas phase back-mixing and the tube-to-bed heat transfer coefficient has been studied experimentally. Finally, the reactor concept is demonstrated experimentally for the industrially important partial oxidation of methanol to formaldehyde to assess whether the MAFBR can indeed approximate the ideal isothermal plug flow reactor.

By distributive addition of oxygen via ceramic membranes lower local oxygen concentrations in the fluidized bed can be achieved, which enables operation of the reactor outside the explosion limits of the reaction mixture. This opens the window for increased feed concentration of methanol of double the industrial level, with a corresponding increased formaldehyde productivity (per pass through-put), where the good heat transfer characteristics of the MAFBR are utilized to achieve isothermal reactor operation despite the much lager heat production.

4. Thesis outline

Firstly, in **Chapter 2** the morphological parameters of the micro porous membranes have been determined experimentally. Subsequently the effects of the fluidization conditions, such as the particle size, superficial gas velocity and freeboard pressure on the membrane permeate flow have been studied in order to describe the membrane permeation rates from the fluidized bed.

In **Chapter 3** the heat transfer characteristics of a membrane assisted fluidized bed was investigated experimentally. Firstly, the effect of membrane bundles on tube to bed heat transfer coefficient was studied. Secondly, the effect of gas addition rates through the membranes on the axial and lateral distribution of heat transfer coefficient was investigated over a wide range of fluidization velocities.

In **Chapter 4** the influence of the presence and configuration of membrane bundles and the effect of gas addition via the membranes on the effective axial gas dispersion was studied experimentally using tracer gas injection experiments. From the experiments, information on the prevailing macro scale flow pattern and bubble-to-emulsion mass transfer could be deduced.

Subsequently in **Chapter 5** a detailed kinetic study is reported on the methanol partial oxidation and the most important side reactions, viz. the formaldehyde partial oxidation, dimethyl ether and dimethoxy methane formation, for a wide temperature and concentration ranges. Reaction rate expressions are derived describing all the observed influences of temperature and composition.

Finally, in **Chapter 6** the benefits of the membrane assisted fluidized bed reactor concept for the methanol partial oxidation reaction have been demonstrated. Firstly, the

axial back mixing in the demonstration reactor is quantified to assess whether the MAFBR can indeed be considered as an isothermal plug flow reactor. Subsequently, the effects of various fluidization conditions, including the ratio of the gas fed via the membranes and via the distributor, and wide range of methanol concentrations on methanol conversion and formaldehyde selectivity were studied. This chapter concludes by predicting the description of a two-phase model developed to describe and study the experimental results.

References

Adris, A. E., Grace, J. R., Lim, C. J. and Elnashaie, S. S. (1994), USA Patent number 5326550.

Anshits, A. G., Shigapov, S. N. and Shevnin, V. N. (1989), " Oxidative conversion of methane into C2 hydrocarbons on silver membrane catalyst", Kinet. Catal., (30), 1103.

Diakov, V., Larfarga, D. and Varma, A. (2001), "Methanol oxidative dehydrogenation in a catalytic packed bed membrane reactor", Catalysis Today, (67), 159-167.

Gryaznov, V. M. and Slin'ko, M. G.. (1982), "Selectivity in catalysis with reagent transfer through the selectively permeable catalyst", Faraday Discuss. Chem. Soc., (72), 73-93.

Hsieh, H. P. (1988), "Inorganic membrane reactors – a review", AICHE Symp. Ser., (84), 31-43.

Kunii, D. and Levenspiel, O. (1991), "Fluidization Engineering", Wiley, New York.

Miracca, I. and Capone, G. (2001), "The staging in fluidized bed reactors: from CISTR to plug-flow", Chemical Engineering Journal (82), 259-266.

Mleczko, L., Ostrowski T., and Wurzel, T. (1996), "A fluidized bed membrane reactor for the catalytic partial oxidation of methane to synthesis gas", Chem. Eng. Sci., 51, 3187.

Nagamoto, H. and Inoue, H. (1986), " The hydrogenation of 1,3-butadiene over a palladium membrane", Bull. Chem. Soc. Jpn., (59), 3935-3939.

Ostrowski, T., Giroir-Fendler, A., Mirodatos, C. and Mleczko, L. (1998), "Comparative study of the catalytic partial oxidation of Methane to synthesis gas in fixed bed and fluidized bed membrane reactors. Part II: Development of membranes and catalytic measurements", Cat. Today. , 40, 191.

Saracco, G. and Specchia, V. (1994), “Catalytic inorganic membrane reactors: present experience and future opportunites”, Catal. Rev. Sci. Eng., (36), 305-384.

Sloot, H. J., Versteeg, G. F. and van Swaaij, W. P. M. (1990), “ A non-permselective membrane reactor for chemical processes normally requiring strict stoichiometric feed rates of reactants”, Chem. Eng. Sci., (45), 2415-2421.

Sloot, H. J. (1991), “ A non-permselective membrane reactor for catalytic gas phase reactions”, Ph. D. Thesis, Twente University, Enschede.

Sloot, H. J., Versteeg, G. F. and van Swaaij, W. P. M. (1992), “ High temperature membrane reactor for catalytic gas-solid reactions”, AICHE J., (38), 887-900.

Veldsink, J. W., van Damme. R. M. J., Versteeg, G. F. and van Swaaij, W. P. M. (1995), “A catalytically active membrane reactor for fast, exothermic, heterogeneously catalyzed reactions”, Chem. Eng. Sci., (47), 2939-2944.

Zaspalis, V. T. (1990), “ Catalytically active ceramic membranes, Synthesis, Properties and Application, Ph.D. Thesis, Twente University, Enschede.

Chapter 2

Effect of fluidization conditions on the membrane permeation rate in a membrane assisted fluidized bed

Abstract

The effects of fluidization conditions on the membrane permeation rate in a membrane assisted fluidized bed (MAFB) employing micro-porous membranes have been studied experimentally. A pseudo two-dimensional fluidized bed equipped with horizontal ceramic membranes and a square fluidized bed equipped with vertical ceramic membranes positioned in a staggered arrangement have been employed. Firstly, the morphological parameters of the micro porous membranes have been determined with separate experiments. The membrane gas permeation rates can be well described with Darcy's law and the dusty gas model for the membranes in the two-dimensional and three-dimensional bed respectively. Secondly, the effects of the fluidization conditions, such as the particle size, superficial gas velocity and freeboard pressure on the membrane permeate flow rate have been measured. The membrane permeation rates from the fluidized bed could be well described by taking into account the local pressure drop over the membrane, where the local pressure inside the fluidized bed was evaluated as the hydrostatic head using the average bed porosity.

1. Introduction

A membrane assisted fluidized bed reactor (MAFBR) is a special type of reactor that combines the advantages of a fluidized bed and a membrane reactor. Despite the excellent heat transfer properties of a fluidized bed axial gas back-mixing can considerably decrease the overall reactant conversion and product selectivity. By insertion of membranes in the fluidized bed, either perm-selective or porous membranes, large improvements in conversion and selectivity can be achieved.

Firstly, the product selectivity can be increased via optimization of the axial concentration profiles via distributive feeding of one of the reactants (e.g. controlled dozing of oxygen for partial oxidation reactions) or selective withdrawal of one of the products (e.g. selective removal of hydrogen in dehydrogenation reactions). Furthermore, controlled dozing of oxygen could be used to achieve high conversions and still avoid the formation of explosive reaction mixtures, rendering the reactor inherently safe.

Secondly, the insertion of membranes decreases the effective axial dispersion via compartmentalization of the fluidized bed. Insertion of membrane bundles in a suitable configuration impedes bubble growth and macroscopic circulation patterns in the fluidized bed, thereby reducing reactant by-pass via rapidly rising large bubbles. Furthermore, gas withdrawal through the membranes decreases the superficial gas velocities in the top section of the bed, resulting in smaller gas bubbles, which increases the inter-phase gas exchange favoring high conversions (Mleczko et al., 1996). Both vertical and horizontal inserts (membranes and heat transfer tubes) can be used to effectively retard the emulsion circulation and increase the bubble breakage. For the controlled dozing of one of the reactants a horizontal arrangement of inserts is usually preferred to directly control the local concentrations. For the removal of one of the intermediate products vertical membrane bundles might suffice, which are much easily integrated in the reactor.

The membrane assisted fluidized bed reactor (MAFBR) to reactions of industrial importance has been investigated in the recent past. Adris et al. (1994) demonstrated both by experiments and by modeling (1991) that for the steam reforming of natural gas the *in situ* separation and removal of hydrogen via perm-selective thin-walled palladium-based membranes shifted the conventional thermodynamic equilibrium and increased the synthesis gas yields in comparison to the industrial fixed bed steam reformer. Using simulations Abdalla and Elnashaie (1995) showed for the catalytic dehydrogenation of

ethyl benzene to styrene and Ostrowski et al., (1998) for the catalytic partial oxidation of methane to synthesis gas that with MAFBRs higher product selectivities could be realized compared to fixed bed reactors. In these studies the insertion of perm-selective hydrogen membranes in the fluidized bed was investigated.

This work focuses on the application of porous membranes, e.g. for the controlled dozing of oxygen in a fluidized bed for the partial oxidation of methanol to formaldehyde. It is investigated experimentally whether the fluidization conditions, such as particle size, superficial gas velocity and freeboard pressure as well as membrane bundle configuration (horizontal or vertical) influence the permeation rates through the porous membranes. Firstly, the experimental set-up for the membrane assisted fluidized bed is shortly described. Subsequently, the membrane morphology parameters are determined from separate experiments. And finally, the influence of the fluidization conditions on the permeate fluxes are discussed and modeled.

2. Experimental

In the membrane assisted fluidized bed under investigation, micro porous ceramic membrane tubes of very small outer diameter (2.5 mm) have been used. In order to investigate the influence of the membrane arrangement and fluidization conditions on the membrane permeation flux, separate fluidized beds with horizontal and vertical membranes have been designed with similar tube diameters.

First the experimental set-up of the membrane assisted fluidized beds and their inserts arrangement are presented. Then the experimental technique to determine the morphological parameters of the ceramic micro porous ceramic membranes is explained with special attention to the importance of the pore size, which determines the dominating transport mechanism through the membranes.

2.1. Experimental set-up

A square fluidized bed (0.15 m x 0.15 m x 0.95 m) was constructed from lexan, in which 39 ceramic membrane tubes (1.5 mm inner diameter, 2.5 mm outer-diameter, length 0.15 m and average pore size 0.15 μm) were positioned vertically in a staggered arrangement with an equilateral pitch of 0.02 m (see Figure 2b). Furthermore, a flat pseudo two-dimensional (0.185 m x 0.015 m x 0.4 m) gas fluidized bed was constructed of polycarbonate, which was equipped with four horizontal membrane bundles each

containing 18 membranes (1 mm inner diameter, 2.5 mm outer-diameter, length 0.185 m and average pore size 0.2 μm) as shown in Figure 2a. The fluidized beds were filled with glass beads (density, 2550 kg/m^3) and fluidized with air at ambient temperature via a porous plate distributor (with a pore size of about 10 μm). At the outlet a filter was placed to avoid carry-over of the fines. The freeboard pressure was controlled by passing the outlet gas through a water column. By maintaining atmospheric pressure at the permeate side of the membranes, gas was removed from the fluidized bed and the membrane permeate flow was measured with a Brooks mass flow meter. To investigate the influence of the fluidized bed hydrodynamic behavior on the membrane permeate flow, the permeate flow was measured at different superficial gas velocities and freeboard pressures for Geldart A and B type particles (see Table 1). A detailed flow diagram of the experimental set-up is shown in Figure 1.

Table 1. Different particles used in the experiments with their operating conditions at minimum fluidization conditions calculated from Kunii and Levenspiel (1991)

Exp.	Geldart classification	Particle size [μm]	u_{mf} [m/s]	ε_{mf} [-]
I	A	40-70	0.00439	0.454
II	B	80-110	0.0121	0.434
III	B	150-180	0.0327	0.418
IV	B	230-320	0.0905	0.398

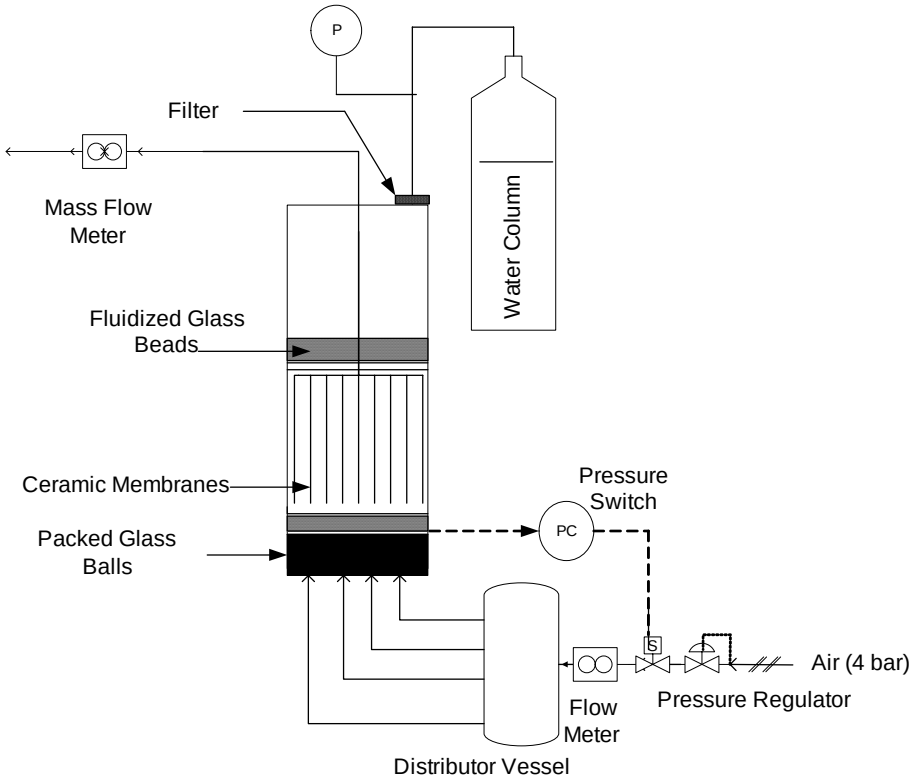

Figure 1. Schematic of the experimental set-up for the gas permeation measurements in a MAFB.

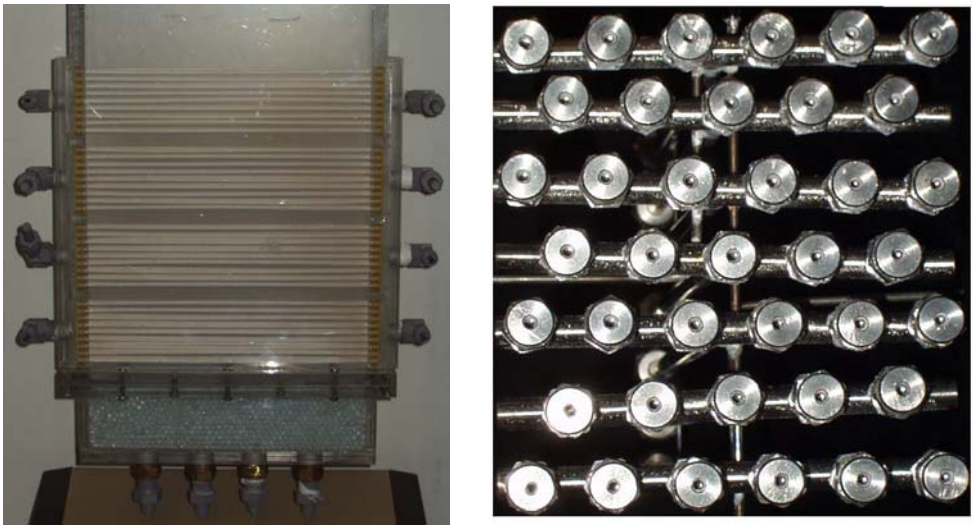

(a) (b)

Figure 2. Pictures of the membrane arrangement for the gas permeation measurements (a) front view of horizontal membranes and (b) top view of vertical membranes.

2.2. Permeability measurements to determine the membrane morphology parameters

Gas permeation through micro-porous inorganic membranes can in general be attributed to Knudsen diffusion, viscous flow and bulk diffusion mechanisms. To simplify the interpretation of the experimental results, the experiments were carried out without concentration gradients, so that the contribution due to bulk diffusion could be ignored in this work. Furthermore, as a rule of thumb, Knudsen diffusion dominates when the mean free path is larger than ten times the pore diameter (Smid et al., 1996). Since the estimated mean free path for air (90 nm) is in the same order of magnitude as the pore radius of the vertical ceramic membrane used in the set-up (75 nm), both the Knudsen diffusion and viscous flow will contribute to the total gas flux through the membrane, which can be described by the dusty gas model according to

$$N = -\frac{1}{RT}\left[K_0 v_M + B_0 \frac{P}{\mu_g}\right]\nabla P \tag{1}$$

where, N represents the molar gas flux, R the universal gas constant, T, the temperature, μ_g the gas viscosity and P and ∇P the pressure and pressure gradient. The mean molecular velocity v_M can be calculated with

$$v_M = \sqrt{\frac{8RT}{\pi M}} \tag{2}$$

where M is the average molar mass of air.

The Knudsen diffusion and viscous flow morphology parameters, K_0 and B_0 respectively, are membrane-specific constants and independent of the permeating gas, provided that no other gas-membrane interaction takes place than collision (e.g. no dissolution, adsorption or surface diffusion). For homogeneous membranes with cylindrical pores K_0 and B_0 can be calculated with

$$K_0 = \frac{2\varepsilon r_p}{3\tau} \quad \text{and} \quad B_0 = \frac{\varepsilon r_p^2}{8\tau} \tag{3}$$

Where ε is the membrane porosity, τ the membrane tortuosity and r_p the pore radius.

Since real membranes have very complex structures, K_0 and B_0 must be determined experimentally. Integrating Eq. (1) over a tubular membrane wall using that the gas permeate flow ($N \cdot r$) is constant results in:

$$N_o = \frac{1}{RT}\left[K_0 v_M + B_0 \frac{P_{av}}{\mu_g}\right] \frac{\Delta P}{r_o \ln\left(\frac{r_o}{r_i}\right)} \tag{4}$$

where N_o is the molar gas flux at the outer membrane area, P_{av} is the arithmetic mean of the gas pressure at both sides of the membrane, ΔP is the total pressure difference over the membrane and r_i and r_o are the inner and outer membrane radii respectively. Plotting $N_0 RTr_o \ln(r_o/r_i)/\Delta P v_M$ versus (P_{av}/v_M) in a graph will give K_0 as the intercept and B_0 as the slope.

2.2.1. Vertical membrane set-up

The membrane morphology parameters for vertical membranes were determined in a separate experimental set-up (see Figure 3). Using a dead-end membrane construction a controlled flow of N_2 was forced through the membrane and the resulting pressure drop was measured via pressure transducers (see for further details on the experimental technique Guijt et al., 2000). By blocking part of the membrane surface it was ensured that the axial pressure drop in the membrane tube was negligibly small, which was confirmed by constant values of K_0 and B_0. For the ceramic tubes the experimentally determined values for B_0 and K_0 are $1.00 \cdot 10^{-16}$ m^2 and $5.35 \cdot 10^{-9}$ m respectively (see Figure 4). With these values for B_0 and K_0 and assuming cylindrical pores, a pore radius of 100 nm can be estimated (using Eq. 3), which compares reasonably with the actual pore size (75 nm).

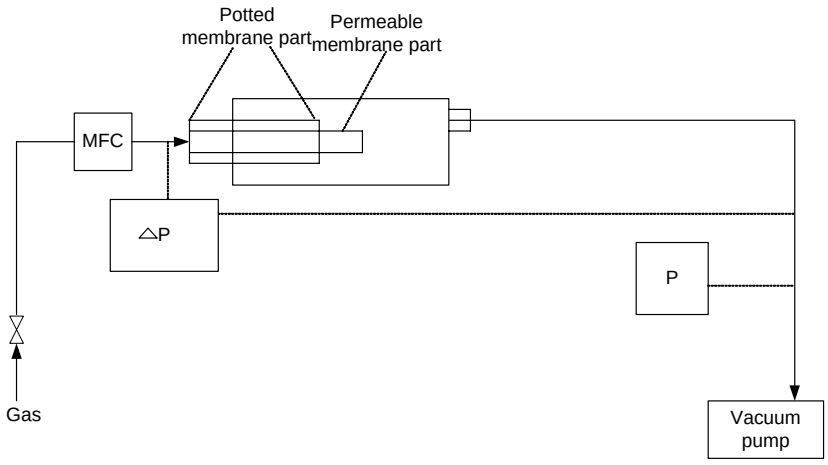

Figure 3. Schematic of the experimental set-up to determine the membrane morphology parameters.

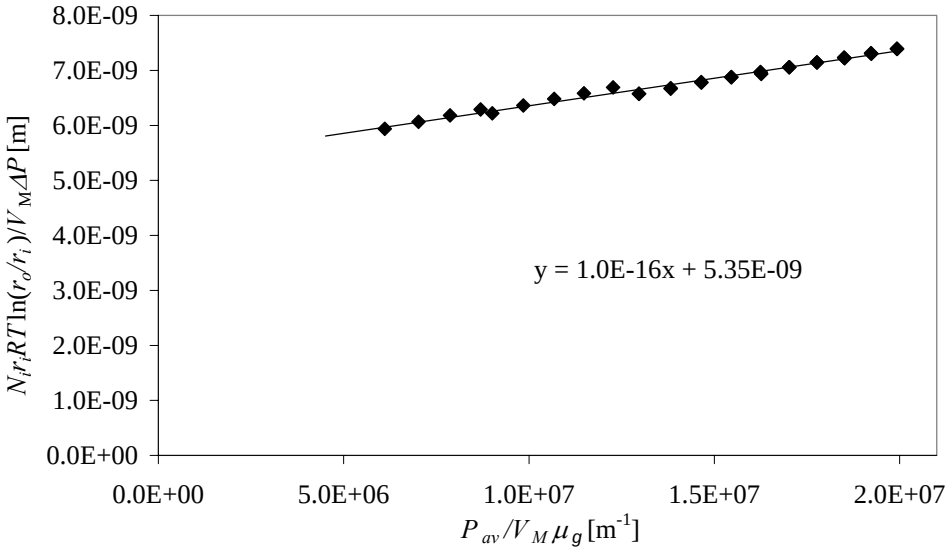

Figure 4. Determination of the membrane morphology parameters from the experiments

2.2.2. Horizontal membrane set-up

Ceramic membranes in the set-up with horizontal membranes were more porous than the vertical membranes (pore radius 100 nm), thus viscous flow is the dominating mechanism for the permeation through the membranes. Hence the molar flux through the membranes reduces to:

$$N = -\frac{1}{RT}\left[B_0 \frac{P}{\mu_g} \right] \nabla P \qquad (5)$$

where B_0 is the permeability constant, determined experimentally for each of the horizontal membrane bundles separately. In these experiments air was fed at the bottom of the bed without glass particles, where, one membrane bundle was allowed to permeate air while others were closed. The flow rate was recorded when the equilibrium pressure was reached. The permeability constants obtained for the different bundles are tabulated in Table 2.

Table 2. Results of permeability measurements for each membrane bundle

Bundle No.	Calculated B_0 (m^2)
1	$1.24 \cdot 10^{-15} \pm 1.778$ %
2	$1.46 \cdot 10^{-15} \pm 1.05$ %
3	$1.47 \cdot 10^{-15} \pm 1.35$ %
4	$1.34 \cdot 10^{-15} \pm 1.15$ %

3. Results and discussion

Experimental results on the effects of the fluidization conditions in the membrane assisted fluidized bed on the gas removal via membranes are presented below.

3.1. Effect of fluidization conditions on the membrane permeate flow

In order to study the effect of the operating conditions in the fluidized bed on the permeate flow through the porous membranes, the membrane permeate flow was measured at different superficial gas velocities and different freeboard-pressures for powders with different particle size ranges (see Table 1) and for horizontally and vertically positioned membrane tubes.

3.1.1. Bed with horizontal membranes

The effect of the particle size is given in Figure 5, while the effect of inlet gas velocity on the membrane permeation rate is shown in Figure 6. It can be seen from the graphs that there is hardly any effect of particle size and superficial gas velocity on membrane permeation at constant free-board pressure. This can be explained by the fact that the pressure drop across the fluidized bed (buoyant weight per unit cross sectional area) remains constant once minimum fluidization velocity is attained. Hence, the limiting factor for the increase in viscous flow driven membrane permeation is the free board pressure, which is kept constant for these studies. Smaller deviations in membrane permeation for studies with 80-110 micrometer diameter particles can be attributed to the plugging of the filter placed at the exit of the fluid bed by the fine particles.

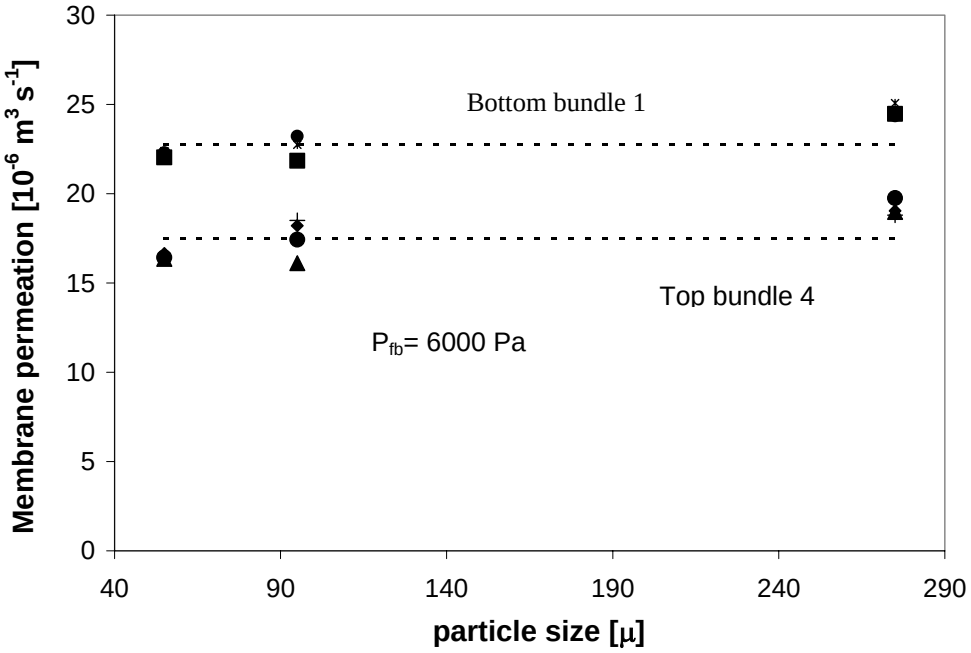

Figure 5. Effect of particle size on the membrane permeation rate over the range of fluidization velocities studied and for bottom most and top most bundles.

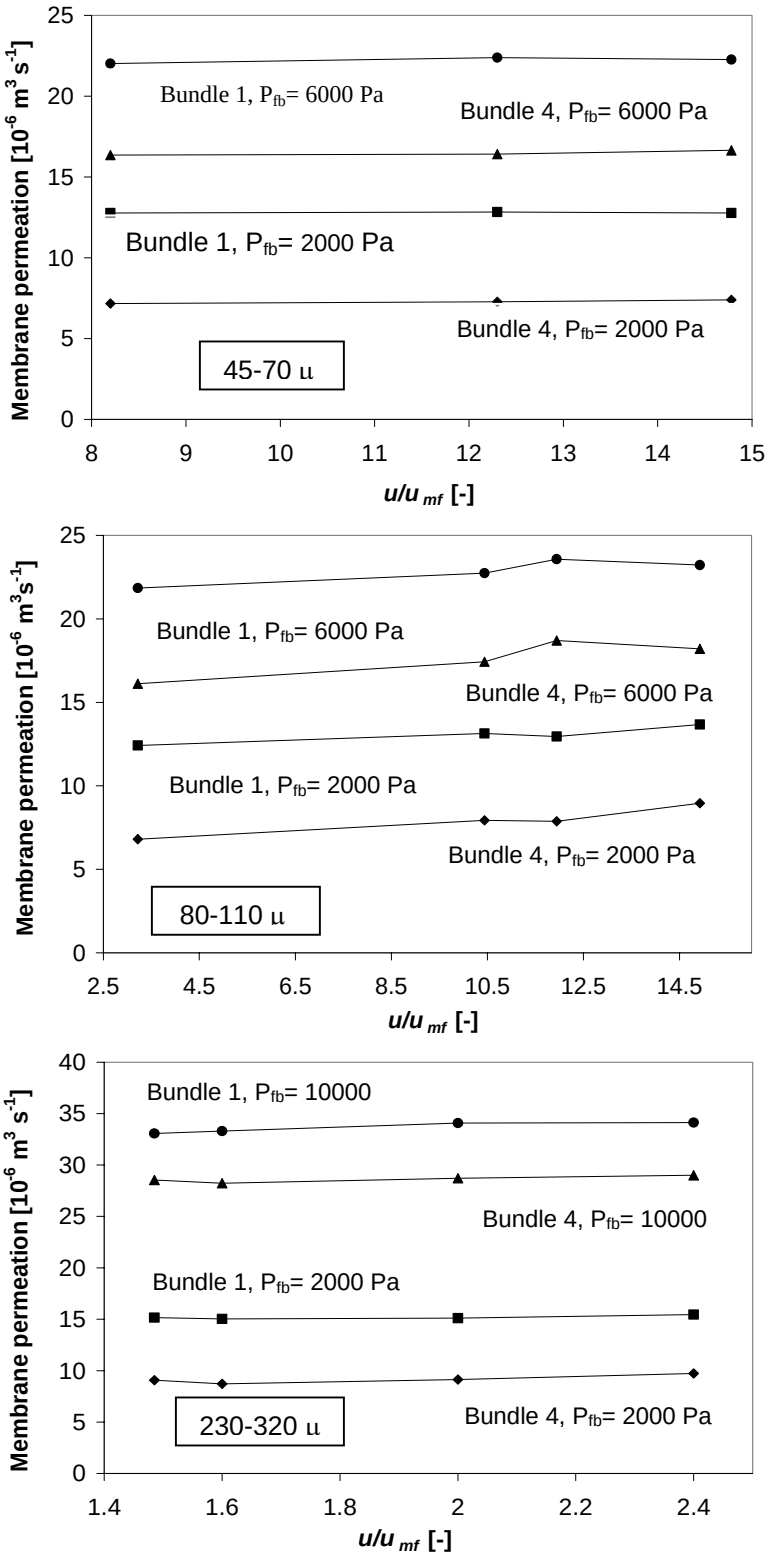

Figure 6. Effect of the relative superficial gas velocity (u/u_{mf}) and freeboard pressure (P_{fb}) on the measured permeation rate for different particle sizes and for bundle 1(bottom most) and bundle 2 (top most).

3.1.2. Bed with vertical membranes

Similar experiments were performed for the bed with vertical inserts to check the effect of inserts on the membrane gas permeation. The effect of the particle size is given in Figure 7, while the effect of the superficial gas velocity on the permeate flow is shown in Figure 8. The figures clearly show that there is hardly any effect of both the superficial gas velocity and the particle size on the permeate flow at the same freeboard pressure. Small deviations in the membrane permeation at high superficial gas velocities can be attributed to the plugging of the filter placed at the exit of the fluid bed by fine particles, which increases the freeboard pressure slightly.

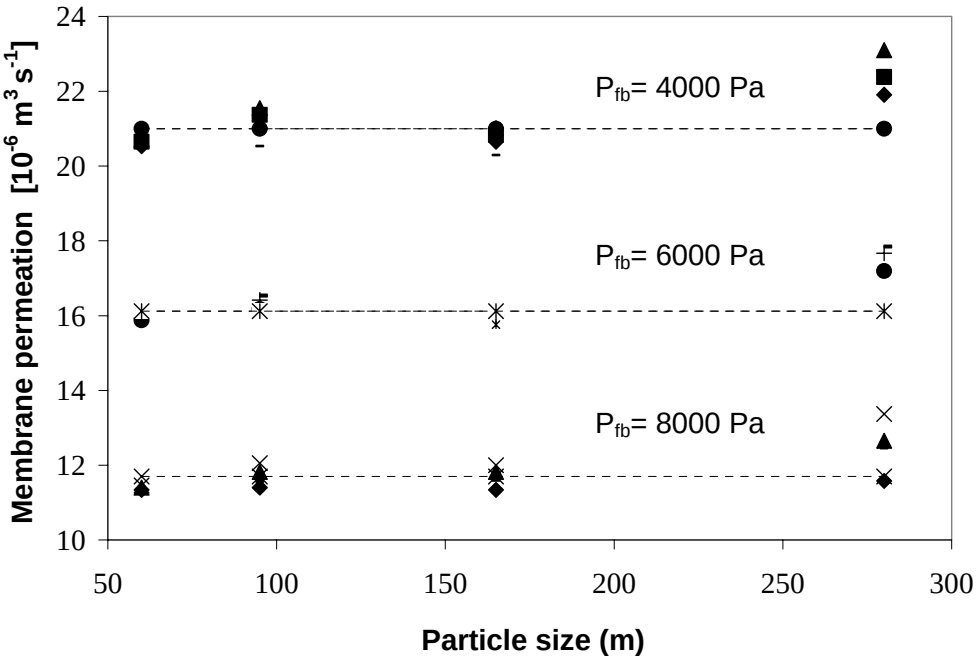

Figure 7. Effect of particle size on the membrane permeation rate over the range of relative superficial gas velocities (u/u_{mf}) and freeboard pressures (P_{fb}) studied.

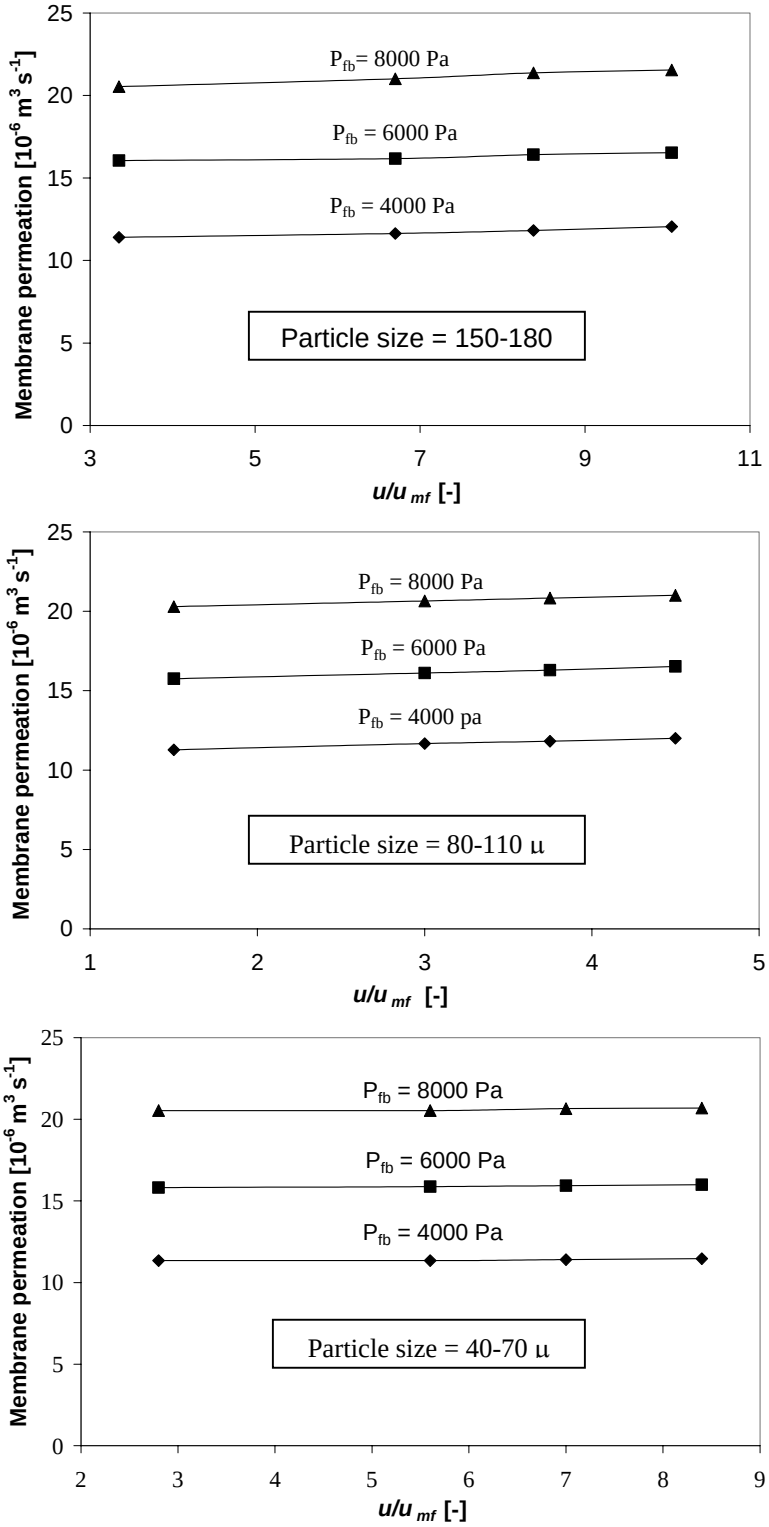

Figure 8. Effect of the relative superficial gas velocity (u/u_{mf}) and freeboard pressure (P_{fb}) on the measured permeation rate for different particle sizes.

4. Modeling of membrane gas permeation in MAFB

The experimental results have shown that the superficial gas velocity and the particle size in the fluidized bed have no effect on the gas permeation through the ceramic membrane tubes, indicating that the solids circulation patterns and the local bubble fraction do not influence the gas permeation fluxes. Moreover, from the experiments it can be concluded that only the freeboard pressure determines the overall gas permeation flow rate for the same type of solids, provided that concentration gradients are absent.

The local gas permeation rate is only determined by the local pressure drop across the membrane. The local pressure in the fluidized bed, P_0, at a vertical distance z from the distributor, can be estimated with the freeboard pressure, P_{fb}, augmented with the hydrostatic head of the bed:

$$P_o = P_{fb} + \left(H_f - z\right)\left(1-\varepsilon_{bed}\right)\left(\rho_p - \rho_g\right)g \tag{6}$$

Where H_f represents the total bed height and ε_{bed} the average bed porosity. The average bed porosity was taken here, since the bed porosity hardly changes as a function of height (Shiau and Lin 1993).

4.1. Vertical membrane set-up

The local permeate flow ϕ through a single vertical membrane tube varies as a function of the axial position z in the bed according to

$$\frac{d\phi}{dz} = 2\pi\left(N\cdot r\right)_i = \frac{2\pi}{RT\ln\left(\frac{r_i}{r_o}\right)}\left[K_0 v_M\left(P_o - P_i\right) + \frac{B_0}{2\mu_g}\left(P_o^2 - P_i^2\right)\right] \tag{7}$$

Where P_o and P_i represent the local pressures at the outside and inside of the membrane tube. The total gas flow permeated through a single vertical membrane tube can then be obtained via substitution of Eq. 6 into Eq. 7 and integration over the bed height. The average bed porosity varies considerably for different particle sizes and superficial gas velocities. However, the product of the expanded bed height and the average solid

porosity, and hence the total permeation flow, remained practically unaltered in the experiments, since the initial packed bed height was kept constant.

To compare the results between the theoretically calculated permeate flow rate and the measured permeate flow rate, all the data points in this study are plotted in a parity plot (Figure 9). This plot shows that the experimentally determined and theoretically calculated membrane permeate flow rates match closely and that the deviation is less than 6%. This also shows that the method used to obtain the membrane morphology parameters was correct and gave accurate measurements of the membrane properties within an experimental error of 10% and 6% for B_0 and K_0 respectively.

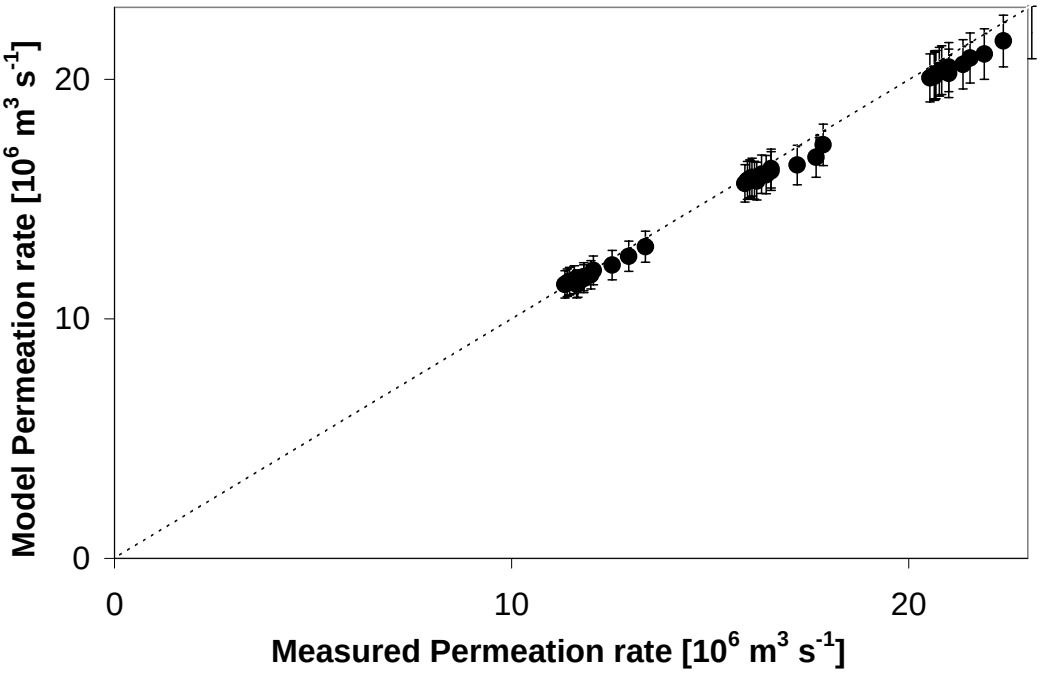

Figure 9. Parity plot for the experimentally determined and theoretically calculated membrane permeation rates in a MAFB with vertical membranes.

4.2. Horizontal membrane set up

The local permeate flow ϕ through a horizontal membrane tube bundle varies as a function of the axial position *z* in the bed and can be deduced by simplification of Eq. 7 by neglecting Knudsen diffusion for these membranes with large pore diameter as:

$$\frac{d\phi}{dz} = 2\pi\left(N \cdot r\right)_i = \frac{2\pi}{RT\ln\left(\frac{r_i}{r_o}\right)}\left[\frac{B_0}{2\mu_g}\left(P_o^2 - P_i^2\right)\right] \tag{8}$$

Again, to compare the results between the theoretically calculated permeate flow rate and the measured permeate flow rate, all the data points, obtained with set-up with horizontally positioned membranes have been plotted in parity plots (Figure 10). These plot also show that the experimentally determined and theoretically calculated membrane permeate flow rates agree well.

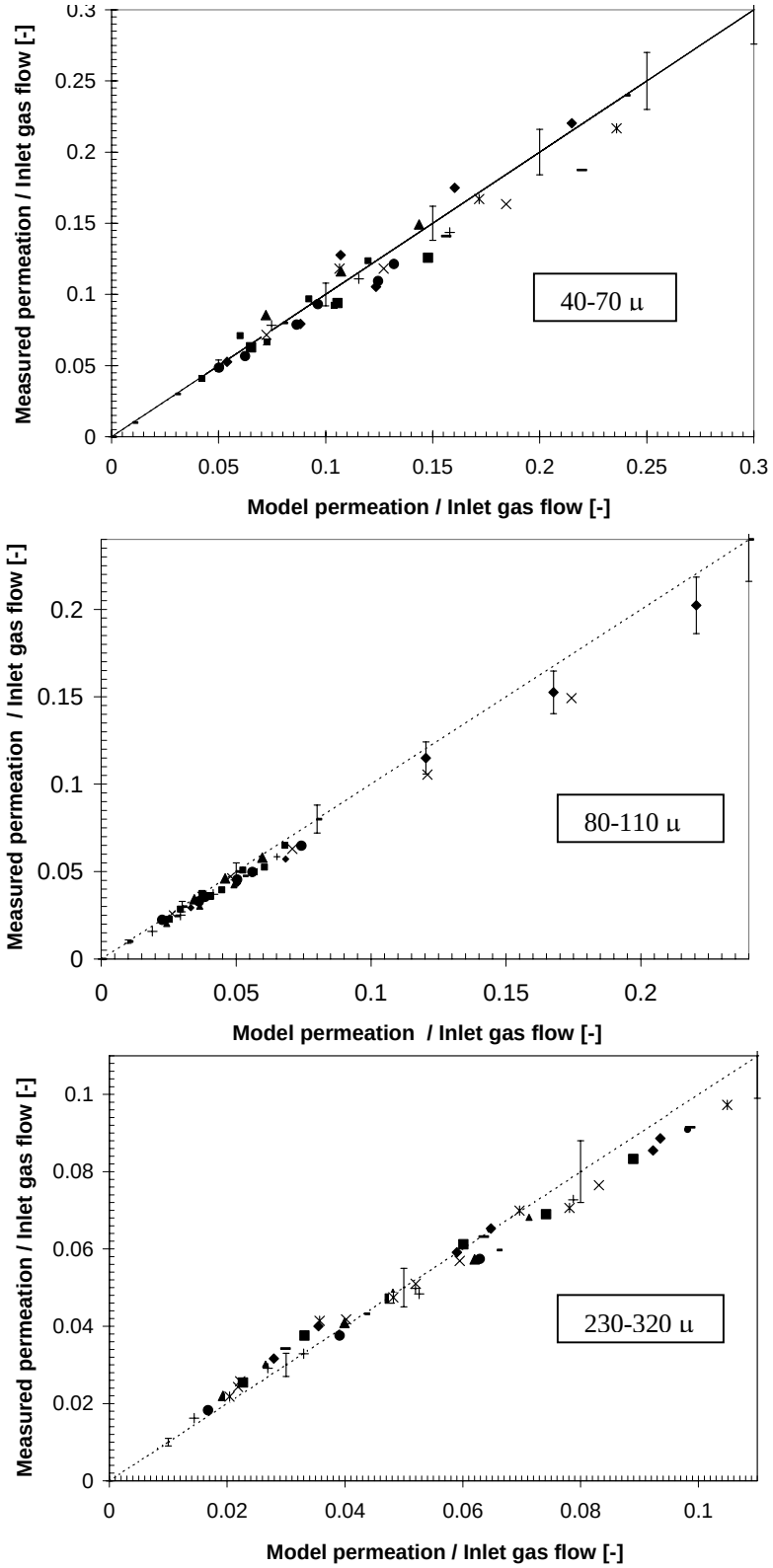

Figure 10. Parity plot for the experimentally determined and theoretically calculated membrane permeation rates in a MAFB with horizontal membranes.

5. Conclusions

The effect of fluidization conditions, viz. the superficial gas velocity, particle size and freeboard pressure on the gas permeation rate through porous ceramic membranes has been studied experimentally for two different configurations of the membrane bundles. The gas withdrawal through the membranes increased with an increase in the freeboard pressure, which could be well described by the dusty gas model, where it was simply assumed that the membrane permeate flux was only a function of the local pressure in the fluidized bed, for which the hydrostatic head with the average bed porosity was taken. The superficial gas velocity as well as the particle size had no overall effect on the total amount of gas permeated through the membranes for both membrane configurations, which can be explained by the fact that the decrease in the average bed porosity at lower superficial gas velocities or larger particle sizes is counterbalanced by an increase in the bed height. Although concentration gradients in the fluidized bed and the membranes were absent in this work, this can be easily included in the dusty gas model. Moreover, since the solids circulation patterns do not affect the membrane permeation fluxes, no effects of the arrangement (horizontal or vertical) and pitch of the vertical membranes were observed.

The membrane permeate flux expression can be directly incorporated into fluidized bed rector models, such as the two phase bubbling bed model by Kunii and Levenspiel (1991) or the improved bubble-assemblage model (BAM) of Shiau and Lin (1993), which is based on the model of Kato and Wen (1969), in order to model the performance of fluidized bed membrane reactors. However, in these models the effect of the membrane bundles on the heat transfer properties of submerged heat transfer tubes and the gas back-mixing behavior are not yet incorporated and additional experimental work on this subject is described in Chapter 3 and 4 respectively.

Acknowledgement

This research is part of the research program carried out within the Center for Separation Technology, as cooperation between the University of Twente and TNO, the Netherlands Organization for Applied Scientific Research. The author wishes to thank Gerrit Schorfhaar for construction and maintenance of the setup.

Nomenclature

A_m membrane surface area, [m^2]

B_0 membrane morphology parameter for viscous flow, [m^2]

g gravitational acceleration, [$m \cdot s^{-2}$]

H_{mf} minimum fluidization bed height, [m]

H_f actual fluidization bed height, [m]

K_0 membrane morphology parameter for Knudsen flow, [m]

M molecular weight, [$g \cdot mole^{-1}$]

N molar gas flux through the membrane, [$mole \cdot m^{-2} \cdot s^{-1}$]

P pressure, [Pa]

ΔP pressure drop across the membrane in the fluidized bed, [Pa]

P_{av} arithmetic mean of the pressure inside the membrane and the bed pressure, [Pa]

P_{fb} freeboard pressure, [Pa]

P_0 fluid bed pressure, [Pa]

r_i membrane tube inside radius, [m]

r_o membrane tube outside radius, [m]

r_p membrane pore radius, [m]

R gas constant, [$J \cdot mol^{-1} \cdot K^{-1}$]

T bed temperature, [K]

u_0 superficial gas velocity, [$m \cdot s^{-1}$]

u_{mf} minimum fluidization velocity, [$m \cdot s^{-1}$]

V_M mean molecular velocity of gas, [$m \cdot s^{-1}$]

z axial position, [m]

Greek symbols

ε_{bed} average bed voidage of the bed, [-]

ε_{mf} bed voidage at minimum fluidization conditions, [-]

ϕ molar flow of gas through the membrane, [$mole \cdot s^{-1}$]

μ_g gas viscosity, [Pa·s]

τ membrane pore tortuosity, [-]

ρ_g gas density, [$kg \cdot m^{-3}$]

ρ_p particle density, [kg·m^{-3}]

References

Abdalla, B.K. and Elnashaie, S.S.E.H. (1995), "Fluidized bed reactor without and with selective membranes for the catalytic dehydrogenation of ethylbenzene to styrene", Journal of Memb. Science, 101, 31.

Adris, A.M., Elnashaie, S.S.E.H. and Hughes, R. (1991),"A fluidized bed reactor for steam reforming of methane", The Canadian Journal of Chemical Engineering, 69, 1061.

Adris, A.M., Lim, C.J. and Grace J.R. (1994), " The fluid bed membrane reactor system: A pilot scale experimental study", Chem. Eng. Sci., 49, 5833.

Guijt, C.M., Racz, I. G., Reith, T. and de Haan, A.B. (2000), “Determination of membrane properties for use in the modelling of a membrane distillation module”, Desalination, 132, 255.

Kunii, D. and Levenspiel, O. (1991) "Fluidization engineering", Butterworth-Heinemann series.

Mleczko, L., Ostrowski T. and Wurzel, T. (1996), "A fluidized bed membrane reactor for the catalytic partial oxidation of methane to synthesis gas", Chem. Eng. Sci., 51, 3187.

Ostrowski, T., Giroir-Fendler, A., Mirodatos, C. and Mleczko, L. (1998), "Comparative study of the catalytic partial oxidation of Methane to synthesis gas in fixed bed and fluidized bed membrane reactors. Part II: Development of membranes and catalytic measurements", Cat. Today. , 40, 191.

Shiau, C. and Lin, C. (1993), “An improved bubble assemblage model for fluidized bed catalytic reactors”, Chem. Eng. Sci., 48, 1299.

Smid, J., Avci, C.G., Gunay, V., Terpstra, R.A. and Van Eijk, J.P.G.M. (1996), "Preparation and characterization of microporous ceramic hollow fiber membranes", Journal of Memb. Sci., 112, 85.

Chapter 3

Heat transfer in a membrane assisted fluidized bed with immersed horizontal tubes

Abstract

The effect of gas permeation through horizontally immersed membrane tubes on the heat transfer characteristics in a membrane assisted fluidized bed was investigated experimentally. Local time-averaged heat transfer coefficients from copper tubes arranged in a staggered formation with the membrane tubes to the fluidized bed were measured in a square bed (0.15 m x 0.15 m x 0.95 m) containing glass particles (75-110 μm) fluidized with air distributed via a porous plate, where the ratio of gas fed or removed through the membrane bundles and the porous plate distributor was varied. The experimental results revealed that high gas permeation rates through the membranes strongly decreased the heat transfer coefficient at high superficial gas velocities for tubes at the top of the tube bundle, which was attributed to the reduced mobility and increased bubble hold up and/or dilution of the emulsion phase, reducing overall heat capacity.

In the design of membrane assisted fluidized beds care must be taken to include the effect of gas addition or withdrawal through the membranes on the required heat transfer surface area.

1. Introduction

Fluidized beds employing fine powders are finding increased application in the chemical and petrochemical industry because of their excellent mass and heat transfer characteristics. However, in fluidized bed chemical reactors axial gas back-mixing can strongly decrease the conversion and product selectivities. By insertion of membranes in fluidized beds large improvements in conversion and selectivity can be achieved, firstly by optimizing axial concentration profiles via distributive feeding of one of the reactants or selective withdrawal of one of the products, and secondly, by decreasing the effective axial dispersion via compartmentalization of the fluidized bed. Moreover, insertion of membrane bundles in a suitable configuration impedes bubble growth, thereby reducing reactant by-pass via rapidly rising large bubbles. Often cooling or heating tubes are also submerged in the fluidized bed to withdraw or add thermal energy respectively. The effective heat transfer coefficient between the surface of these tubes and the fluidized bed is an important parameter in the design of these fluidized beds. The integrated gas addition or removal via membranes inside the fluidized bed strongly influences the bed hydrodynamics and thus the tube-to-bed heat transfer.

Numerous previous studies have been carried out to study the various aspects of tube-to-bed heat transfer in fluidized beds. However, studying the tube-to-bed heat transfer in a membrane assisted fluidized bed is novel and has never been done before, to the author's knowledge. In this work the influence of the presence of membrane and heat transfer tube bundles and the effect of gas addition and removal via the membrane tubes on the spatial distribution of the time averaged tube-to-bed heat transfer coefficient at various fluidization velocities was studied experimentally.

Before presenting and discussing experimental results, first the experimental set-up, the experimental technique and experimental procedure used to measure the tube-to-bed heat transfer coefficient are described in the next section. Finally the experimental data is compared with literature correlations.

2. Experimental

A very high specific membrane surface area cab be achieved with membrane tubes of very small tube diameter. However, to accomplish the desired heat exchange to withdraw the released reaction heat or to supply the required reaction energy, heat transfer tubes of similar smaller size are required. A membrane assisted fluidized bed has been constructed to measure the local heat transfer coefficient consisting of membranes and heat transfer tubes of comparable tube diameter of about 3 mm. Moreover, small heat transfer tubes allow an accurate measurement of tube-to-bed heat transfer coefficients by reducing the heat transfer resistance inside the heat transfer tubes as explained in section 2.2 and difficulties in the interpretation of the results due to the curvature effect of the heat transfer tubes can be avoided.

First the membrane assisted fluidized bed and the arrangement of the inserts is explained. Subsequently the experimental technique to measure tube-to-bed heat transfer coefficient is explained with special attention to the particle electrostatic effect on the tube-to-bed heat transfer coefficient.

2.1. Experimental set-up

To measure the spatial distribution of the heat transfer coefficient, a square fluidized bed (0.15 m x 0.15 m x 0.95 m) was constructed out of lexan and filled with glass beads (75-110 μm, 2550 kg/m^3) to a packed bed height of about 0.30 m. The bed was equipped with 18 horizontal copper heat transfer tubes (2 mm ID and 3 mm OD) and 40 horizontal ceramic membrane tubes (1.5 mm ID and 2.5 mm OD with a pore size of 0.15 μm), through which gas could be added or withdrawn, arranged in a staggered orientation with an equilateral pitch of 0.02 m. In Figure 1 top view of the membrane assisted fluidized bed and schematic side view of the tube arrangement is shown. Uniform fluidization was achieved with a porous plate distributor with a pore size of 10 μm. Fluidization was performed with humidified air (50-60 % humidity) at ambient conditions to avoid static electricity problems (see Figure 2). It was found that static charging of the particles strongly decreased the measured heat transfer coefficients, especially in experiments with tube bundles. Furthermore, it was verified experimentally that the bed temperature was uniform throughout the bed.

(a) Top view (b) Side view

Figure 1. Picture (top view) and schematic side view of the membrane assisted fluidized bed. •: Heating tube, o: Membrane tube.

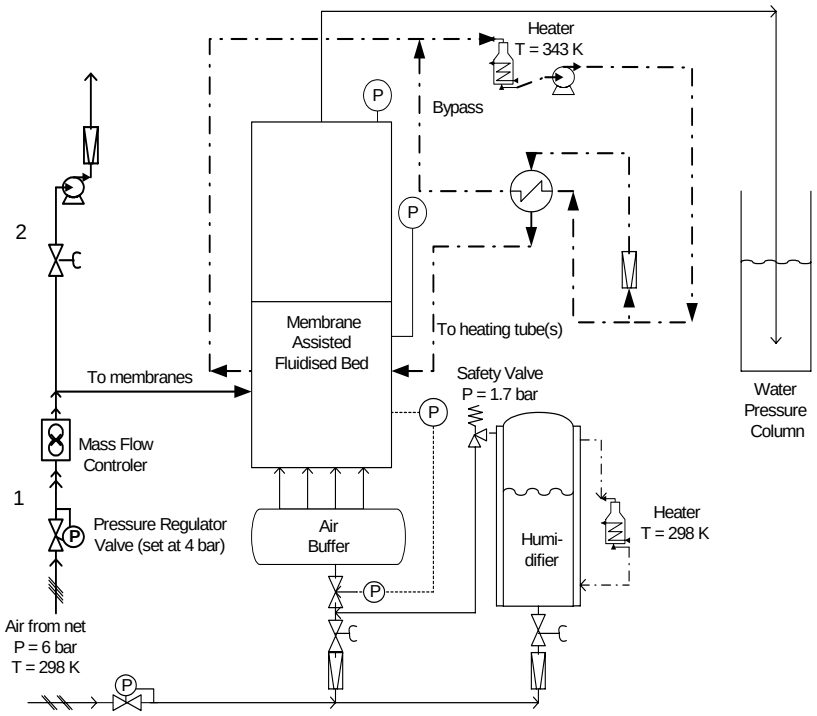

1: gas addition, 2: gas withdrawal

Figure 2. Schematic of the experimental set-up.

2.2. Experimental technique

Various experimental methods have been reported in the literature to measure the heat transfer coefficient between a submerged surface and the fluidized bed. The most frequently reported method is an electrically heated metallic film sensor (e.g. Tout and Clift, 1973 and Fitzgerald et al., 1981). This method is based on the change in the resistance of a metallic film with temperature. The film is heated to a certain temperature, which is different from the bed temperature, and kept constant by varying the power supplied to the film using a thermocouple or a reference resistance. Based on this principle, it is also possible to use long strips and measure along a surface. The problem of this method is that the metallic films are too large compared to the desired tube size.

A method based on thermocouples was used by George (1987), by Olsson and Almsted (1992), and by McKain et al. (1994). The advantage of using thermocouples as sensors is the relatively small area of the thermocouples, the low price, the commercial availability and easiness of construction. By using at least two thermocouples at different radial positions on the outer surface of the tube, information on bubble passage can be obtained. Again, heat transfer coefficients between the bed and the heat transfer tubes of very small size (3 mm) studied in this work cannot be measured with this method.

Karamavruc et al. (1994) and Kahn and Turton (1992) have used an experimental technique that only requires one thermocouple. The principle of the technique is that a thermocouple is positioned at the outside surface of a tube and that the inside temperature is kept at a constant value. This can be accomplished by using a very high water flow rate. A disadvantage of this method is that the thermocouple is incorporated in the tube, as is the case in the multiple thermocouple method. This means that every single tube has to have one thermocouple fitted at the surface. Furthermore, the temperature difference between the water at the inside and particles at the outside of the tube has to be considerable in order to accurately measure the heat transfer coefficient.

In this work the tube-to-bed heat transfer coefficient was determined by measuring the difference between the entrance and the exit mixing-cup temperatures of the heat transfer fluid, which was fed with preheated water with an average velocity of 4.6 cm/s, at about 50 °C, and the bed temperature using T-type thermocouples. An accurate measurement of the mixing cup temperature was ensured by positioning static mixers inside the tube (see Figure 3) and averaging over 2 to 5 minutes. An advantage of this technique to measure the heat transfer coefficient is that the thermocouples can be

switched easily from one tube to another to determine the axial and lateral variation of the heat transfer coefficient in the bed.

A thermal energy balance over single heat transfer tube submerged in the fluidized bed reads:

$$\phi_m C_p \frac{dT_{water}}{dz} = \pi d_i h_{total} \left(T_{water} - T_{bed} \right) \tag{1}$$

where the overall heat transfer coefficient, h_{total}, is given by:

$$\frac{1}{h_{total}} = \frac{1}{h_{tube}} + \frac{d_i \, ln(\frac{d_o}{d_i})}{2\lambda_{copper}} + \frac{1}{h_{bed}} \frac{d_i}{d_o} \tag{2}$$

Assuming constant physical properties and a constant bed temperature in the fluidized bed, $Nu = h_{tube} d_i / \lambda_{water} = 3.66$, i.e. $h_{tube} \cong 1150$ $Wm^{-2}k^{-1}$, can be taken for the heat transfer resistance in the hydrodynamically and thermally fully developed laminar flow inside the copper heat transfer tubes, as can be deduced from the measured axial temperature profile inside the heating tube (see Figure 4). With this technique the time averaged tube-to-bed heat transfer coefficient could be determined well within maximum experimental error of 10% with good reproducibility, provided that the fluidizing air was sufficiently humidified (see Figure 5) to avoid effects induced by electrostatic forces.

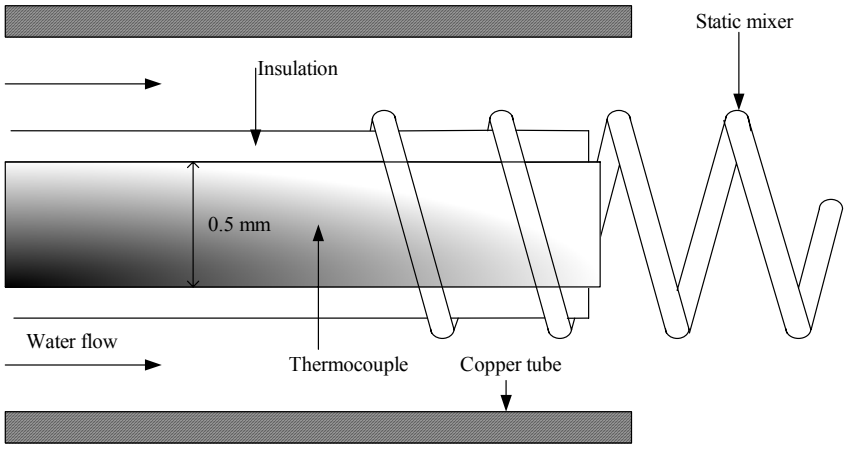

Figure 3. Schematic of the thermocouple arrangement in the tube for measuring the mixing cup temperature.

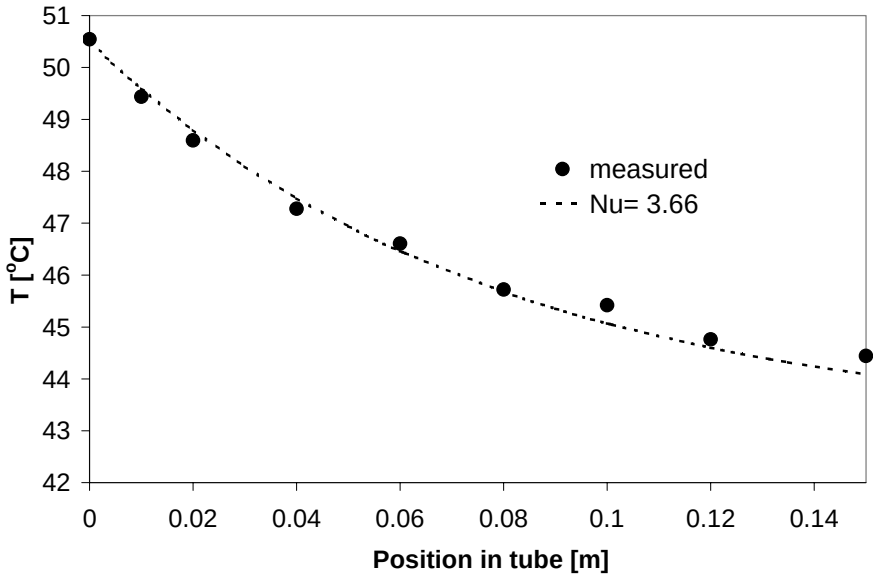

Figure 4. Experimental verification of water temperature profile inside the heat transfer tube.

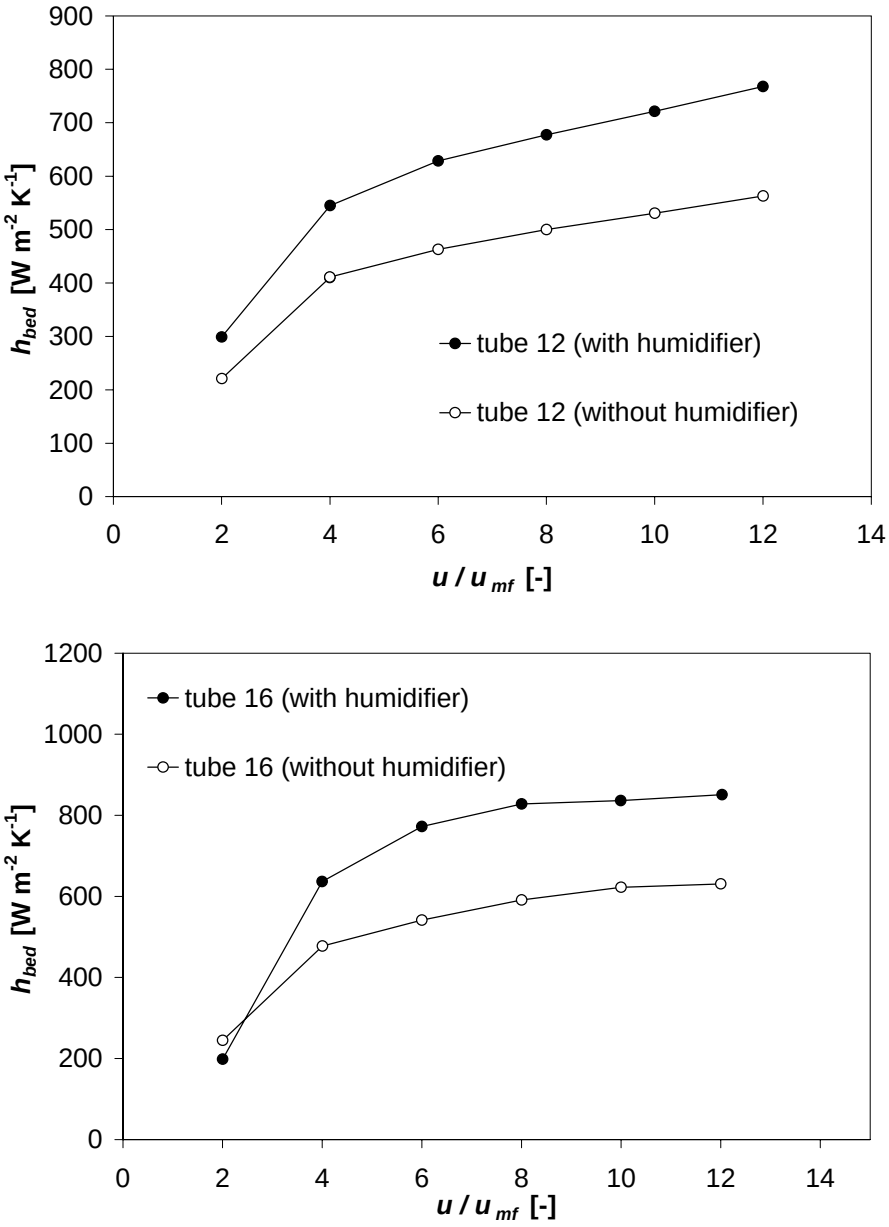

Figure 5. Static electricity effect on experimentally measured tube-to-bed heat transfer coefficient.

3. Experimental results

Firstly, experimental results for the time averaged tube-to-bed heat transfer coefficient for a single tube are presented and compared with reported experimental values in the literature. Subsequently, the results for tube banks without permeation through the membranes will be reported. Finally, the effect of permeation through the membranes will be discussed.

3.1. Heat transfer from a single tube

The heat transfer coefficient between the surface of a single tube submerged in a fluidized bed was measured at different positions in the fluidized bed in order to compare the observed heat transfer coefficients with reported literature values and as a reference for the experiments employing tube-banks. The experimentally determined tube-to-bed heat transfer coefficient increased with increasing superficial gas velocities and reached a maximum at about $8u_{mf}$. The maximum tube-to-bed heat transfer coefficient (h_{max}) increased as a function of height above the distributor (tube 16: 830 W/m^{2}K; tube 2: 970 W/m^{2}K; (see Figure 1b)), which is attributed to increased solids mobility higher in the bed due to bubble coalescence. In the lateral direction no significant changes in the heat transfer coefficient were observed even at high superficial gas velocities. Wall effects were not measured since the measurement closest to the wall was 1.7 cm.

3.2. Heat transfer with a tube bank without membrane permeation

The tube-to-bed heat transfer coefficients were measured in the fluidized bed for all the 18 tubes placed in the bed at different superficial gas velocities without permeation through the membrane tubes. As shown in Figure 6, the measured heat transfer coefficient increases with the superficial gas velocity and levels off at higher gas velocities to a maximum. Increasing the superficial gas velocity increases the mobility of the emulsion phase, which decreases the average residence time of an emulsion phase ‘packet’ at the tube surface, thereby increasing the heat transfer coefficient. However, at higher gas velocities more and larger bubbles are formed having a lower volumetric heat capacity, causing the heat transfer coefficient to level off and eventually decrease at very high gas velocities (see e.g. Kunii and Levenspiel, 1991). Furthermore, the heat transfer coefficient strongly decreases as a function of the distance from the distributor, caused by the bubble growth and coalescence.

When comparing the maximum heat transfer coefficient determined in the fluidized bed with a tube bank with the results obtained with a single tube, the tube-to-bed heat transfer coefficient decreased by almost 200 W/m^{2}K (see Figure 6 b) due to the reduced mobility of the emulsion phase caused by the additional internals, which obstruct the macro-scale movement of the emulsion phase. Moreover, the internals promote bubble breakage, which reduces the bubble rise velocity, resulting in decreased emulsion movement in the vicinity of the heat transfer surfaces.

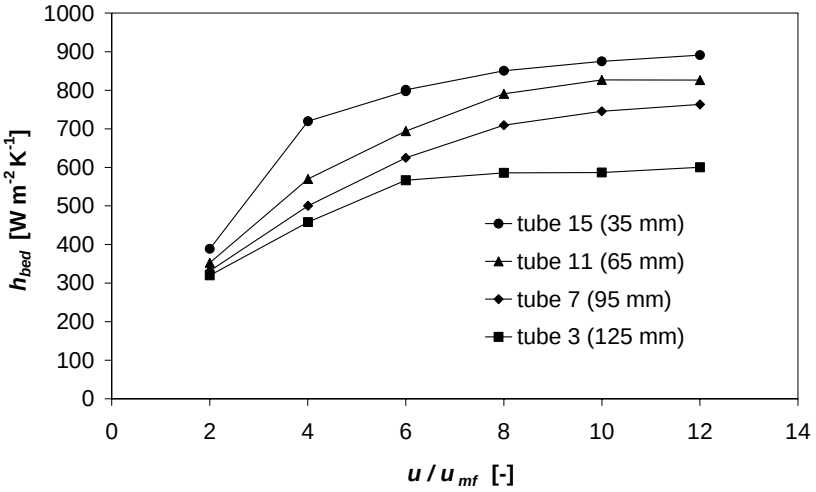

(a)

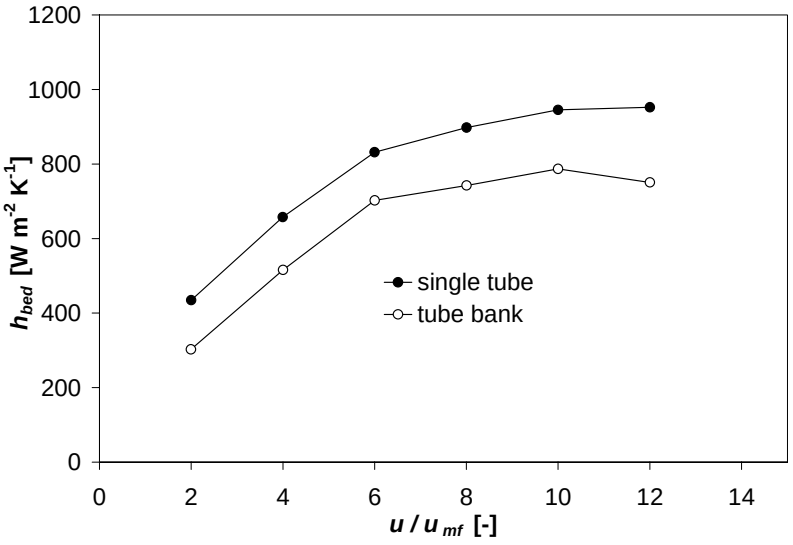

(b)

Figure 6. Tube-to-bed heat transfer coefficient as a function of the superficial gas velocity: a) for different heights above the distributor (Tube number refers to position indicated in Figure 1); b) for an experiment with a single tube and a tube bank, measured at position 2.

In Figure 7 the spatial distribution of the heat transfer coefficient for two different superficial gas velocities is shown. Increasing the superficial gas velocity from $6u_{mf}$ to $10u_{mf}$ increases the tube-to-bed heat transfer coefficient, but does not change its spatial distribution. The highest heat transfer coefficients were observed just above the distributor in the center of the bed. A slight lateral asymmetry in the spatial distribution is caused by the asymmetric configuration of the heat transfer tubes.

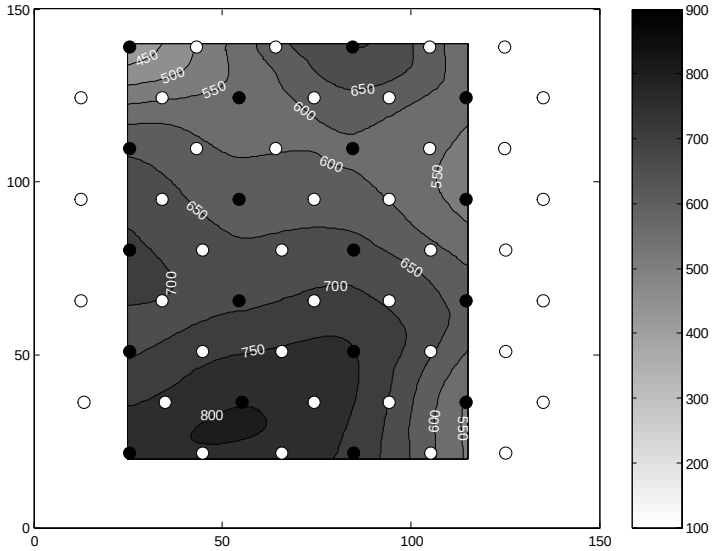

(a)

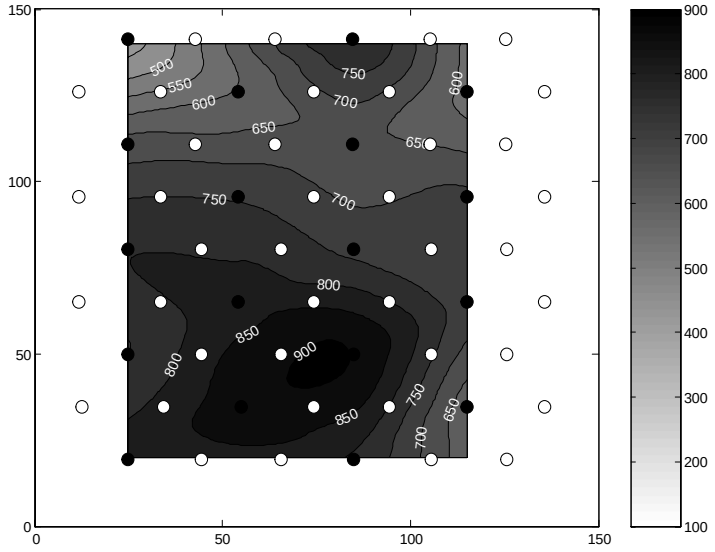

(b)

Figure 7. Spatial distribution of the tube-to-bed heat transfer coefficient for two different superficial gas velocities: (a) 6 u_{mf} and (b) 10 u_{mf}.

3.3. Heat transfer with a tube bank with membrane permeation

To study the effect of gas permeation via membranes on the tube-to-bed heat transfer coefficient, experiments were carried out by adding or removing part of the fluidizing gas via the membranes at different superficial gas velocities. Up to 40% of the total gas flow could be added via the membranes, whereas only 10% of the total gas flow could be removed due to pump limitations. In the experiments where gas was added through the membranes, the total gas feed was kept constant, which implies that experiments with higher permeation rates through the membranes were carried out at a lower gas flow through the distributor.

3.3.1. Effect of membrane permeation on heat transfer coefficient

In Figure 8 the spatial distribution of the tube-to-bed heat transfer coefficient is given at a superficial gas velocity of $6u_{mf}$ for different membrane permeations. The Figure clearly shows that with increasing gas permeations through the membrane the measured heat transfer coefficient at the bottom of the bed decreases and that the heat transfer coefficient decreases much more pronounced as a function of the axial position in the bed. The lower heat transfer coefficient at the bottom of the bed at higher gas permeations was caused firstly by the lower gas feed through the distributor and secondly by the suppressed macroscopic circulation pattern due to the reduced down flow at the walls and the reduced bubble growth in the centre of the bed. Furthermore, the heat transfer coefficient decreases strongly as a function of the height above the distributor and even much more pronounced than observed for the experiment without permeation, where the decrease in the heat transfer coefficient was caused by the bubble growth. The additional decrease in the heat transfer coefficient as a function of the axial coordinate is attributed to an increased bubble hold up due to the much smaller average bubble diameter and the dilution of the emulsion phase in case part of the gas is fed via the membranes, which results in a decreased volume and heat capacity of the emulsion phase.

3.3.2. Effect of superficial gas velocity on heat transfer coefficient

Figure 9 depicts the effect of the superficial gas velocity on the tube-to-bed heat transfer coefficient at different permeations and at two different tube locations. For a tube located at the top of the bed, the effect of membrane permeation on the tube-to-bed heat transfer coefficient was negligible at a low fluidization velocity of $2u_{mf}$, but very strong at

higher gas velocities (see (Figure 9 a). At a low superficial gas velocity the emulsion packet renewal rate at the tube surface was very low due to the absence of a large macroscopic circulation pattern caused by the absence of larger bubbles. Hence, the tube-to-bed heat transfer coefficient will mainly depend on the local superficial gas velocity. Remarkably, at high gas permeations through the membrane an increase in the total gas flow does not increase the heat transfer coefficient for a tube at the top of the bundle. The increased macroscopic emulsion circulation at higher gas velocities (because of the larger bubbles) is more than counterbalanced by the increased bubble hold-up and/or dilution of the emulsion phase.

For a tube in the center of the bed the effect of permeation through the membranes is very pronounced at a low fluidization velocity of $2u_{mf}$ (see Figure 9 b) because of the reduced local gas velocity at higher permeation rates. However, at high superficial gas velocities only a small decrease in the heat transfer coefficient at higher membrane permeations was observed, because of the smaller local effect on the bubble hold-up and/or dilution of the emulsion phase, since the tube in the center of the tube bundle experiences only part of the total gas fed via membranes.

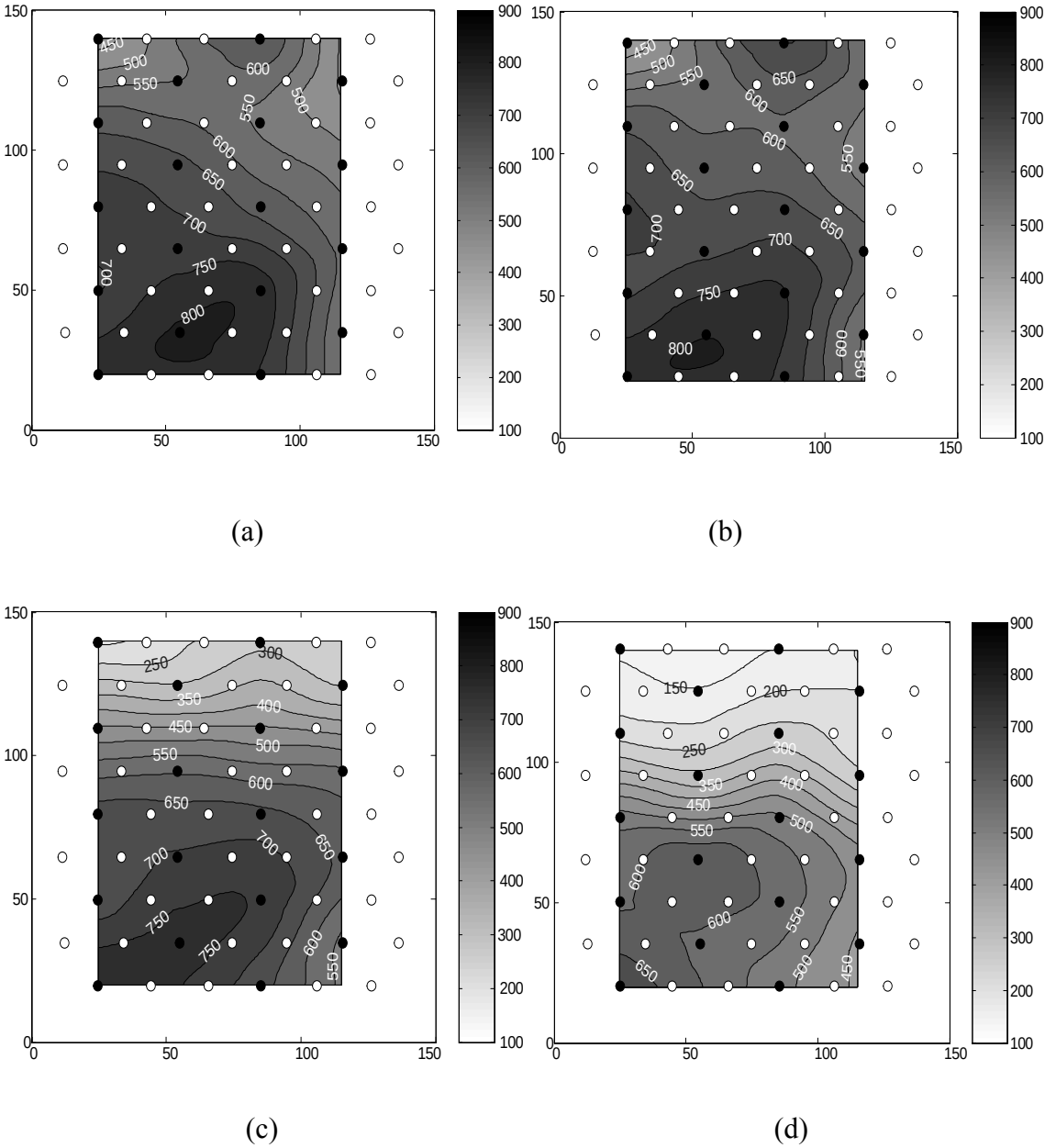

Figure 8. Heat transfer coefficients of the bed at various positions in the bed at 6 u_{mf}
a) -10 % permeation; b) no permeation; c) 20% permeation; d) 40% permeation.

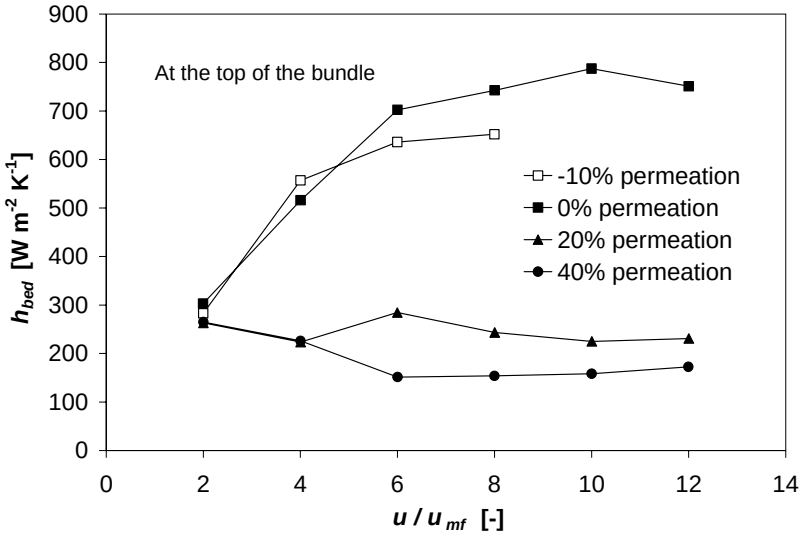

(a)

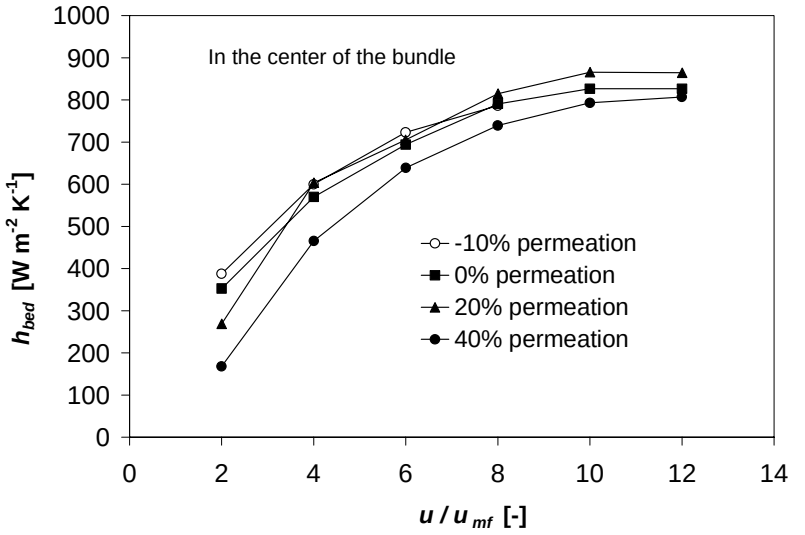

(b)

Figure 9. Tube-to-bed heat transfer coefficient as a function of the superficial gas velocity; a) Tube position 2 (top of the tube bundle); b) Tube position 11 (center of the tube bundle).

4. Literature description of fluidized bed to immersed tube heat transfer

Modelling of heat transfer in fluidized bed has been attempted since the 1940's. Lots of models have been proposed since then, but none of them have actually led to a satisfying description of heat transfer in fluidized beds. It is not the scope of this chapter to give a full review on modelling of heat transfer in fluidized beds, but instead a short overview on models that have gained most attention in the past is given in this section and a comparison is made with our experimental observations in the next section.

The models reported in literature can be divided in three groups based on the level of sophistication.

4.1. Predictive empirical correlations

It has been generally accepted that the heat transfer coefficient consists of a convective and radiative part. Since the radiative contribution only becomes important at elevated temperatures, it will not be considered here.

The earliest approaches (e.g. Leva et al., 1949) to model the convective heat transfer assigned the thermal resistance to a gaseous boundary layer at the heat transfer surface. The enhancement of heat transfer found in fluidized beds is then attributed to the scouring action of solid particles on the gas film, decreasing the "effective film thickness". Models following this approach generally attempt to correlate a heat transfer Nusselt number in terms of the fluid Prandtl number and a modified Reynolds number (with either the particle diameter or the tube diameter as characteristic length scale) or the Archimedes number:

$$Nu = f\left(\mathrm{Pr}, Ar, \mathrm{Re}_p, \mathrm{Re}_{D_T}\right) \tag{3}$$

Numerous studies have been performed on immersed tubes for cooling or heating purposes and several reviews can be found in literature (e.g. Saxena et al. 1978, Saxena, 1989, Tsukada, 1992, and Grewal, 1994). No correlation has been found that is based on a system of tubes with a diameter of 3 mm and particles of 100 μm as employed in this work. Also, no experimental data was found for heat transfer in a membrane assisted fluid bed with heat transfer to a surface.

Since many correlations can be found, only a few are presented here, which are of interest in this investigation.

According to Grewal (1994), the best correlation to predict the maximum heat transfer coefficient of a tube bank is given by Grewal and Saxena (1980). This relation was tested on the experimental data of various authors and gives the tube to bed heat transfer coefficient within an overall error of about 20%. The relation was originally derived for a staggered tube bundle with tubes of 12.7 mm in diameter, and sand particles with a diameter of 286 μm. It was verified for particle diameters ranging from 167 to 504 μm, Ar in the range of 75-20,000 and pitch/tube diameter ratios (P/D_t) from ranging from 1.75 to 9:

$$Nu_{wp,\max} = \frac{h_{bed} D_t}{k_e} = 0.9 \left(Ar \cdot \frac{D_{12.7}}{D_t} \right)^{0.21} \left(\frac{C_{p,p}}{C_{p,g}} \right)^{0.2} \left[1 - 0.21 \left(\frac{P}{D_t} \right)^{-1.75} \right] \tag{4}$$

where D_t is the tube diameter and $D_{12.7}$ is a reference diameter of 12.7 mm.

A correlation by Prins (1989) incorporates the effect of curvature, which is believed to be significant in the current set-up because of the small tube diameters employed. Various particles sizes ranging from 14 μm to 1000 μm were used in his investigation. The correlation was derived for fixed spheres submerged in the fluidized bed, so the heat transfer coefficient is probably overestimated by this correlation.

$$Nu_{wp,\max} = \frac{h_{bed} D_t}{k_e} = 4.175 \cdot Ar^{0.087\left(D_t/d_p\right)^{0.128}} \left(0.844 + 0.0756 \left(\frac{T_{bed}}{273} \right) \right)_T \left(\frac{D_T}{d_p} \right)^{-0.278} \tag{5}$$

Another commonly used correlation was proposed by Molerus (1995). This correlation is based on particle convection and was tested for particles of 74 μm diameter. The gas velocity ranged from 0 to 0.5 m/s. This equation is valid for low Archimedes numbers (<100), resulting in laminar flow, where heat transfer via gas convection can be neglected.

$$Nu = \frac{h_{pc} l_l}{k_g} = \frac{0.125\left(1-\varepsilon_{mf}\right)}{1+\dfrac{k_g}{2C_p\mu}} \cdot \frac{1}{1+25\left\{ \sqrt[3]{\dfrac{u-u_{mf}}{u_{mf}}} \sqrt[3]{\dfrac{\rho C_{p,p}}{k_g g}} \left(u-u_{mf}\right) \right\}^{-1}} \tag{6}$$

In this relation l_l is the laminar flow length scale, defined as a function of the maximum heat transfer coefficient.

$$l_l = \frac{0.09}{1 + k_g / 2C_p \mu} \frac{k_g}{h_{\max}} \tag{7}$$

These are correlations however and not fundamental models, so although they might give a good prediction, they don't really represent the underlying physical phenomena. So, another class of description, which is based on phenomenological aspects of fluidization, is described below.

4.2. Phenomenological description

These descriptions closely resemble the empirical description of the bed-to-tube heat transfer, however more detailed knowledge of the fluidized bed is incorporated. Bed parameters such as the bubble frequency, the thickness of a stagnant particle or gas layer or the bubble fraction are incorporated. In literature, two types of descriptions can be found. The first type is based on a gas-film resistance (e.g., Martin, 1984a, and Molerus, 1997). It assumes that heat transfer is governed by the resistance in a thin gas film around the surface. And the second and more fundamental approach was introduced by Mickley and Fairbanks (1955). In their model, the heat transfer surface is alternately contacted by gas bubbles with a porosity of 1 and packets of closely packed particles with porosity approximately equal to the minimal fluidization porosity. The convective heat transfer coefficient is then expressed as:

$$h_{bs} = \sqrt{k_e \rho_e C_{p,e} S} \tag{8}$$

where S is a stirring factor. The difficulties of this model comes with the requirement of packet phase conductivity, the average residence time of the packet and the time fraction of contact of the bubble phase.

Chandran and Chen (1985) derived a correlation taking into account both the bubble phase and the emulsion phase. In terms of a frequency number, $N_f = f d_p^2 \rho_e C_{p,e} / k_e$ the correlation reads:

$$Nu_e \cong \frac{2}{\sqrt{\pi}} \exp\left[-a_1 N_f^{\left(a_2 + a_3 \ln\left[1/N_f\right]\right)} \right] \sqrt{N_f} \tag{9}$$

where,

$$\begin{aligned} a_1 &= 0.213 + 0.117 \ln\left(k_e/k_g\right) + 0.041\left[\ln\left(k_e/k_g\right)\right]^2 \\ a_2 &= 0.398 - 0.049 \ln\left(k_e/k_g\right) \\ a_3 &= 0.022 - 0.003 \ln\left(k_e/k_g\right) \end{aligned} \tag{10}$$

Kunii and Levenspiel (1991) developed a general expression for the heat transfer coefficient between a fluidized bed and the heat exchange surface, which accounts for the fact that part of the time the surface is bathed by gas and part of the time by emulsion packets:

$$h_{bed} = \left[\delta\left(h_r + h_g\right)\right]_{bubble} + \left[\frac{1-\delta}{\dfrac{1}{h_r + 2k_{ew}^0/d_p + \alpha_w C_{pg} \rho_g u_0} + \dfrac{1}{h_{packet}}} \right]_{emulsion} \tag{11}$$

For the case of fine particles at low temperatures, the radiation term (h_r) can be ignored. And the gas flow through the emulsion phase is negligible (small Re_p). Since the wall temperature reaches many particle layers into the emulsion packet in contact with the surface, the additional resistance of the first surface layer can be neglected. The equation then reduces to:

$$h_{bed} = \left[\frac{1-\delta}{\dfrac{1}{h_{packet}}} \right]_{emulsion} = 1.13\left[k_e^0 \rho_p (1-\varepsilon_{mf}) C_{p,p} f \left(1-\delta\right)\right]^{1/2} \tag{12}$$

where, f is the bubble frequency at the surface, $k_e^{\,0}$ is the heat conductivity of the emulsion at u_{mf} and δ is the bubble fraction.

Using rough estimations for the bubble frequency, the contact time and the near-wall porosity, the model of Kunii and Levenspiel (1991) can give a good first approximation, however their model remains semi-empirical and dependent on hydro-dynamical input.

4.3. Models based on first principles

These models are the most sophisticated models. The hydrodynamics and heat transfer are calculated on the particle level and from first principles using computational fluid dynamics (e.g., Kuipers, 1990, Schmidt and Renz, 2000, Patil, 2003). Based on the conservation equations for both phases, it is in principle possible to predict instantaneous particle volume fractions, velocity distributions as well as the local pressure field, at least for Geldart B and D type of particles. With the implementation of energy equations of both phases, the relevant heat transfer coefficients can now be calculated provided that the porosity distribution in the vicinity of the wall is properly accounted for (Patil, 2003). However, microscopic models were beyond the scope of this investigation.

5. Comparison with literature correlations

In this section the experimental results for the tube-to-bed heat transfer coefficient are compared with experimental data from the literature. Then, these values are compared with various correlations for the tube-to-bed heat transfer coefficients, only for the case of a membrane assisted fluidized bed without membrane permeation, since the effect of membrane permeation has not been accounted for in these correlations.

The measured tube-to-bed heat transfer coefficients compare well with experimental values reported in the literature, which were measured with heat transfer probes for similar systems under comparable fluidization conditions (Sharma, 1997 and Sharma and Turton, 1998) (see Table 1).

Table 1. Experimentally determined heat transfer coefficients for a single tube submerged in a fluidized bed without inserts reported in the literature for similar system under comparable fluidization conditions

Material	d_p (μm)	h_{max} ($W \cdot m^{-2} \cdot K^{-1}$)	h_{avg} ($W \cdot m^{-2} \cdot K^{-1}$)	Reference
Glass	76	-	766	Sharma, 1997
Glass	76	-	825	Sharma and Turton, 1998
Glass	100	850	-	Sharma and Turton, 1998

The experimentally determined tube-to-bed heat transfer coefficients for the tube bank without membrane permeation through the membranes are compared with the literature correlations described in section 4 (see table 2).

All correlations (except Molerus et al., 1995) determine a maximum heat transfer coefficient. Since no maximum in the heat transfer coefficient was observed in the current investigation, the heat transfer coefficient at $12u_{mf}$ was used as a comparison. At $12u_{mf}$ the average heat transfer coefficient of the bed was experimentally found to be about 800 W/m^2 K. The macroscopic relations all underestimate h_{bed}. Especially the correlation of Grewal and Saxena grossly underestimates h_{bed} (about 600%). The correlation by Prins et al also gives a too low value of the heat transfer coefficient, but only about 25%. In Figure 10, the experimental results of tube 8 are compared with the results of the correlation of Molerus. It predicts much lower values for h_{bed} than is experimentally found.

The mesoscopic models give a better prediction of the maximum heat transfer coefficient. The correlation of Chandran and Chen gives the best approximation of the maximum heat transfer coefficient.

Table 2. Comparison of maximum tube-to-bed heat transfer coefficient predicted by various literature correlations

No.	Author	Correlation	h_{bed} ($W \cdot m^{-2} \cdot k^{-1}$)
1	Grewal and Saxena (1980)	$Nu_{wp,\max} = \frac{h_{bed} D_t}{k_e} = 0.9 \left(Ar \cdot \frac{D_{12.7}}{D_t} \right)^{0.21} \left(\frac{C_{p,p}}{C_{p,g}} \right)^{0.2} \left[1 - 0.21 \left(\frac{P}{D_t} \right)^{-1.75} \right]$	127
2	Prins et al. (1989)	$Nu_{wp,\max} = \frac{h_{bed} D_t}{k_e} = 4.175 \cdot Ar^{0.087\left(D_t/d_p\right)^{0.128}} \left(0.844 + 0.0756 \left(\frac{T_{bed}}{273K} \right) \right)_T \left(\frac{D_T}{d_p} \right)^{-0.278}$	640
3	Molerus et al. (1995)	$Nu = \frac{h_{pc} l_l}{k_g} = \frac{0.125\left(1-\varepsilon_{mf}\right)}{1+\frac{k_g}{2C_p \mu}} \cdot \frac{1}{1+25\left\{ \sqrt[3]{\frac{u-u_{mf}}{u_{mf}}} \sqrt[3]{\frac{\rho C_{p,p}}{k_g g}} \left(u-u_{mf}\right) \right\}^{-1}}$	550 (at $12u_{mf}$)
4	Mickley and Fairbanks (1955)	$h_{bs} = \sqrt{k_e \rho_e C_{p,e} S}$	963
5	Chandran and Chen (1985)	$Nu_e \cong \frac{2}{\sqrt{\pi}} \exp\left[-a_1 N_f^{\left(a_2 + a_3 ln\left[1/N_f \right] \right)} \right] \sqrt{N_f}$	780
6	Kunii and Levenspiel (1991)	$h_{bed} \cong \left[\frac{1-\delta}{\frac{1}{h_{packet}}} \right]_{emulsion} = 1.13 \left[k_e^0 \rho_p (1-\varepsilon_{mf}) C_{p,p} f \left(1-\delta\right) \right]^{1/2}$	636

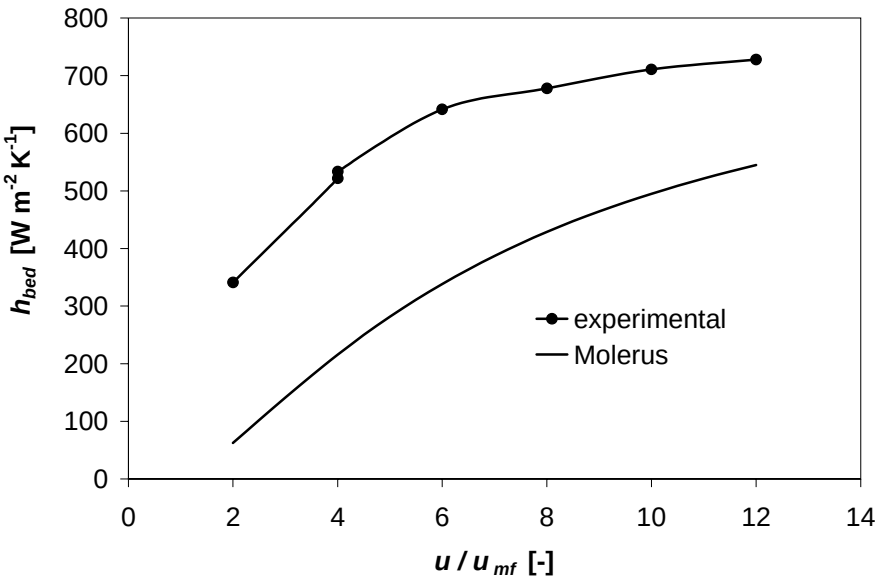

Figure 10. Comparison of experimental value of the h_{bed} with model of Molerus et al. (1995).

6. Summary and conclusions

The effect of presence of and the gas permeation through horizontally submerged membrane tubes in a fluidized bed on the time averaged tube-to-bed heat transfer coefficient was investigated experimentally by measuring the bed temperature and the inlet and outlet mixing-cup temperatures of water flowing through heat transfer tubes.

The presence of the membrane and heat transfer tubes decreases the heat transfer coefficient due to the reduced mobility of the emulsion phase, caused by the internals obstructing the macro-scale movement of the emulsion phase, and by the enhanced bubble breakage decreasing the bubble rise velocity.

Without gas permeation through the membranes, the heat transfer coefficients increase with increasing superficial gas velocity and level off at high gas velocities to a maximum, where the increased emulsion phase mobility is counterbalanced by the larger bubbles. The heat transfer coefficient decreased as a function of the distance from the distributor, which was attributed to bubble growth due to coalescence. The experimentally determined tube-to-bed heat transfer coefficient compare reasonably well with the mesoscopic correlations from the literature for the case of no gas permeation through the membranes. At high gas permeation rates through the membranes the

decrease in the heat transfer coefficient at the top of the tube bundle was even stronger at high superficial gas velocities, caused by the increased bubble hold-up and/or dilution of the emulsion phase. However, lower in the tube bundle the decrease in the heat transfer coefficient was less pronounced, since these tubes experienced only part of the total gas fed via membranes.

Concluding, in a membrane assisted fluidized bed the product selectivity and/or operational safety can be enhanced, but care must be taken to include the effect of gas addition through the membranes on the required heat transfer surface area.

Acknowledgement

This research is part of the research program carried out within the Center for Separation Technology, as cooperation between the University of Twente and TNO, the Netherlands Organization for Applied Scientific Research. The author wishes to thank S. Volkers for his valuable contribution to the experimental work. Also the help by W. Leppink and G. Schorfhaar for construction and maintenance of the set-up is gratefully acknowledged.

Notations

a	constant
Ar	Archimedes number $\left(\frac{d_p^3 \rho_g \left(\rho_s - \rho_g\right) g}{\mu_g^2}\right)$
C_p	heat capacity [$J \cdot kg^{-1} \cdot K^{-1}$]
d	diameter of the copper tube [m]
D	tube diameter [m]
f	bubble frequency [s^{-1}]
h_{bed}	bed heat transfer coefficient [$W \cdot m^{-2} \cdot K^{-1}$]
h_{total}	overall heat transfer coefficient [$W \cdot m^{-2} \cdot K^{-1}$]
h_{tube}	tube side heat transfer coefficient [$W \cdot m^{-2} \cdot K^{-1}$]
k	thermal conductivity [$W \cdot m \cdot K^{-1}$]
k_e^0	thermal conductivity at minimum fluidization [$W \cdot m \cdot K^{-1}$]
L	Tube length [m]
l_l	laminar flow length scale [m]

N_f number frequency
P pitch [m]
Re Reynolds number $\left(\frac{du\rho}{\mu}\right)$
S stirring factor
T temperature (°C)
u Superficial gas velocity [m·s^{-1}]
u_{mf} minimum fluidization velocity [m·s^{-1}]
v_{av} average velocity of water in the tube [m·s^{-1}]
Z bed height [m]
Nu Nusselt number $\left(h_{bed}d_o/\lambda\right)$
Gz Graetz number $\left(K/\rho C_p = L/\upsilon_{av}d_i^2\right)$

Greek letters

ε voidage
ϕ_m mass flow rate of water [kg·s^{-1}]
λ_{copper} thermal conductivity of copper [W·m·K^{-1}]
λ_{water} thermal conductivity of water [W·m·K^{-1}]
ρ density of water [kg·m^{-3}]
μ viscosity [pa·s]
δ bubble fraction

Subscripts

b bubble phase
bs bed to surface
D inside tube diameter
e emulsion phase
ew emulsion to wall
g gas phase
i inside
max maximum
mf minimum fluidization

o outside
p particle
pc particle convection
r radiative
t,T tube
wp particle to wall

References

Chandran, R. and Chen, J.C. (1985), AICHE J. 31, 244.

Fitzgerald, T.J., Catipovic, N.M. and Jovanovic, G. N. (1981), "Instrumented cylinder for studying heat transfer to immersed tubes in fluidized beds", Ind. Eng. Chem. Fund. 20, 82-88.

George, A.H. (1987), "A transducer for the measurement of instantaneous local heat flux to surfaces immersed in high temperature fluidized beds", Int. J. Heat. Mass. Transfer, 30 (4), 763-769.

Grewal, N.S. (1994), "Heat transfer between immersed horizontal tubes and bubbling fluidized beds", Trends in Chem. Eng., 2, 33-58.

Grewal, N. S. and Saxena, S. C. (1980), Ind. Eng. Chem. Proc. Dev., 20, 109-116 (1980).

Kahn, T. and Turton, R. (1992), "The measurement of instantaneous heat transfer coefficients around the circumference of a tube immersed in a high temperature fluidized bed", J. Heat Mass Transfer, 35 (12), 3397-3406.

Karamavruc, A.I., Clark, N.N. and McKain, D.L. (1994), "Deduction of fluidized bed heat transfer coefficients using one- and two-dimensional analyses", Powder Technology, 80, 83-91.

Kuipers, J.A.M. (1990), A Two-Fluid Micro Balance Model of Fluidized Beds, PhD report, University of Twente.

Kunii, D. and Levenspiel, O. (1991), "Fluidization Engineering, second edition", Butterworth-Heinemann series in chemical engineering, chapter 13.

Leva, M., Weintrub, M. and Grummer, M. (1949), "Heat transmission trough fluidized beds of fine particles", *Chem. Eng. Prog.*, 45 (9), 563-572.

Martin, H. (1984) "Heat transfer between Gas Fluidized Beds of Solid Particles and the Surfaces of Immersed Heat Exchanger Elements- Part I", Chem. Eng. Process, 18, 157-169.

McKain, D., Clark, N., Atkinson, C. and Turton, R. (1994), "Correlating local tube surface heat transfer with bubble presence in a fluidized bed", Powder Technology, 79, 69-79.

Mickley, H.S. and Fairbanks, D.F. (1955), Mechanism of Heat Transfer to Fluidized Beds, A.I.Ch.E. J., Vol. 1, No. 1. 374-384.

Molerus, O., Buschka, A. and Dietz, S (1995), "Particle migration and heat transfer in fluidized beds- II: Prediction of heat transfer in bubbling fluidized beds", Chem. Eng. Sci. Vol.50, No. 5, 879-885.

Molerus, O. and Wirth, K.E. (1997), "Heat transfer in fluidized beds", London, Chapman and Hall, 1997.

Olsson, S.E. and Almsted, A.E. (1992), "Local instantaneous and time-averaged heat transfer in pressurised fluidized beds with horizontal tubes: influence of the pressure, fluidization velocity and tube-bank geometry", Chem. Eng. Sci., 50 (20), 3231-3245.

Patil, D. J. (2003), " An experimental and computational study of dense gas-solid fluidized beds", Ph. D. Thesis, Twente University, Enschede.

Prins, W., Harmsen, G. J., De Jong, P. and Van Swaaij, W. (1989),"Heat transfer from an immersed fixed silver sphere to a gas fluidized bed of very small particles", Fluidization VI, Grace, J.R. eds., Engineering Foundation, New York, 677-684.

Saxena, S. C., Grewal, N. S., Gabor, J. D, Zabrodsky, S. S. and Galershtein, D. M. (1978), "Heat transfer between a gas fluidized bed and immersed tubes", Adanced heat transfer, 14, 149-247.

Saxena, S.C. (1989), "Heat transfer between immersed surfaces and gas-fluidized beds", Adv. Heat Transfer, 19, 97-190.

Schmidt, A. and Renz, U. (2000), "Numerical prediction of heat transfer in fluidized beds by a kinetic theory of granular flows", Int. J. Therm. Sci., 39, 871-885.

Sharma, K.R. (1997), "Relative contributions from particle conduction and gas convection to the heat transfer coefficient between dense gas-solid fluidised beds and surfaces", Powder Technology, 91, 75-80.

Sharma, K.R. and Turton, R. (1998), "Mesoscopic approach to correlate surface heat transfer coefficient with pressure fluctuations in dense gas solid fluidized beds", Powder Technology, 99, 109-118.

Tsukada, M. and Horio, M. (1992), "Maximum heat transfer coefficient for an immersed body in a bubbling fluidized bed", Ind. Eng. Chem. Res., 31, 1147-1157.

Tuot, J. and Clift, R. (1973), "Heat transfer around single bubbles in a two-dimensional fluidized bed", A.I.Ch.E.J., 69 (128), 78-84.

Chapter 4

Gas back-mixing studies in membrane assisted fluidized beds

Abstract

Fluidized beds employing fine powders are finding increased application in the chemical and petrochemical industry because of their excellent mass and heat transfer characteristics. However, in fluidized bed chemical reactors axial gas back mixing can strongly decrease the conversion and selectivity. By insertion of membranes in fluidized beds large improvements in conversion and selectivity can be achieved, firstly by optimizing axial concentration profiles via distributive feeding of one of the reactants or selective withdrawal of one of the products, and secondly, by decreasing the effective axial dispersion via compartmentalization of the fluidized bed. Moreover, insertion of membrane bundles in a suitable configuration impedes bubble growth, thereby reducing reactant by-pass via rapidly rising large bubbles. In this work the influence of the presence and configuration of membrane bundles and the effect of gas addition via the membranes on the effective axial dispersion was studied.

Steady state concentration profiles of a CO_2-tracer injected at different locations through a probe (point injection) or via the membranes (line injection) in a square fluidized bed (0.15 m x 0.15 m x 0.95 m) containing glass particles (75-110 μm, 2550 kg/m^3) fluidized with nitrogen distributed via a porous plate were measured for different bed configurations, viz. without internals, with vertical or horizontal membrane bundles and for different gas flow ratios of gas fed through the membrane bundles and the porous plate distributor.

Experimental results revealed that the vertical and horizontal membrane bundle configuration decrease the effective axial dispersion considerably compared to bed without internals. The point injection experiments indicated the importance of a non-uniform lateral emulsion phase velocity profile. The line injection experiments clearly

pointed out the importance of bubble-to-emulsion phase mass transfer limitations. Gas addition through the membrane bundles decreases the effective axial dispersion enormously by almost annihilating the solids down flow along the walls and by decreasing the average bubble size and bubble fraction.

1. Introduction

Fluidized beds employing fine powders are finding increased application in the chemical and petrochemical industry because of their excellent mass and heat transfer characteristics. However, in fluidized bed chemical reactors axial gas back mixing can strongly decrease the conversion and selectivity. By insertion of membranes in fluidized beds large improvements in conversion and selectivity can be achieved, firstly by optimizing axial concentration profiles via distributive feeding of one of the reactants or selective withdrawal of one of the products, and secondly, by decreasing the effective axial dispersion via compartmentalization of the fluidized bed. Moreover, insertion of membrane bundles in a suitable configuration impedes bubble growth, thereby reducing reactant by-pass via rapidly rising large bubbles.

Gas back mixing in a fluidized bed is generally attributed to the down flow of particles. Stephen et al. (1967) already pointed out that down flow of gas could occur when the velocity of descending solids exceeds the interstitial velocity of the gas in the dense (emulsion) phase. In bubbling beds without internals gas back mixing typically commences at about $3u_{mf}$ (Nguyen at al., 1981, Latham and Potter 1970). The effective gas back mixing coefficient then increases somewhat with increasing gas velocity (Van Deemter, 1980), where particle properties and the bed diameter have a considerable effect on the extent of gas back mixing. Many experiments have been conducted to measure gas back mixing in fluidized beds with and without internals in the bubbling regime, as reviewed by van Deemter (1985). Nguyen at al. (1981) studied the gas back mixing in large fluidized beds containing tube assemblies. They found that horizontal tubes completely suppressed gas back mixing at gas velocities of up to 0.3 m/s (u/u_{mf} = 12). Also the horizontal tube assemblies reduce the bubble size and promote more uniform distribution of bubble size. Vertical tubes suppressed back mixing at lower velocities but were less effective in suppressing gas back mixing at higher velocities. A noteworthy result was the development of marked non-uniformity in the radial gas back mixing.

To the author's knowledge the effect of membrane permeation on the gas back mixing in the fluidized beds has not been reported before in the literature. Moreover, in order to increase the specific membrane surface area membrane tubes with a very small diameter were used in this work, typically much smaller than used before in gas back mixing studies.

In this work the influence of the presence and configuration of membrane bundles and especially the effect of gas addition via the membranes on the effective axial and lateral dispersion was studied experimentally using steady state tracer gas experiments.

Before presenting and discussing the experimental results, first the experimental set-up, the experimental technique and experimental procedure used to measure the gas back mixing in the bed are described in the next section.

2. Experimental

In the MAFBR porous ceramic membranes have been employed for controlled dozing of oxygen as air. The optimal configuration of the membrane bundles inside the fluidized bed is dictated by the allowable degree of gas back mixing (low solid down flow rate) and the required heat transfer characteristics (high solids mobility for high heat transfer rates). Three bed geometries, viz. a bed without internals, a bed with vertically positioned membranes and a bed with horizontal membranes, have been employed and compared to study the effect of the presence and arrangement of the membranes, where the bed without internals was chosen as a reference for the other two geometries. Furthermore, the effect of addition of gas via membranes on the gas back mixing in the bed with horizontal membranes has been investigated.

Before presenting the experimental results, details of the insert arrangements for the geometries used are explained. Subsequently the experimental technique to measure the axial gas back mixing in all the fluidized beds is explained and finally, the experimental procedure to obtain accurate and reproducible experimental data on tracer gas concentration profiles is presented.

2.1. Experimental set-up

To measure the axial gas back mixed concentration of the tracer gas, a square fluidized bed (0.15 m x 0.15 m x 0.95 m) was constructed out of lexan and filled with glass beads (75-110 μm, 2550 kg/m^3) to a packed bed height of about 0.30 m. The bed with vertical membranes was equipped with 39 equilaterally placed vertical ceramic membranes having horizontal separation of 0.02 m as shown in Figure 1. The bed with horizontal inserts was equipped with 18 horizontal copper tubes (2 mm ID and 3 mm OD) and 40 horizontal ceramic membrane tubes, arranged in a staggered arrangement

with an equilateral pitch of 0.02 m. In Figure 2 the top view of the membrane assisted fluidized bed with horizontal membranes and a detailed side view of the tube arrangement is shown. The membranes had inner diameter of 1.5 mm, outer diameter of 2.5 mm with a pore size of 0.15 μm. In all the set ups uniform fluidization was achieved with a porous plate distributor with a pore size of approximately 10 μm and nitrogen at ambient conditions was used as the fluidization agent. Figure 3 depicts a detailed flow sheet of the experimental set up used to measure the axial back mixing in the three different bed geometries.

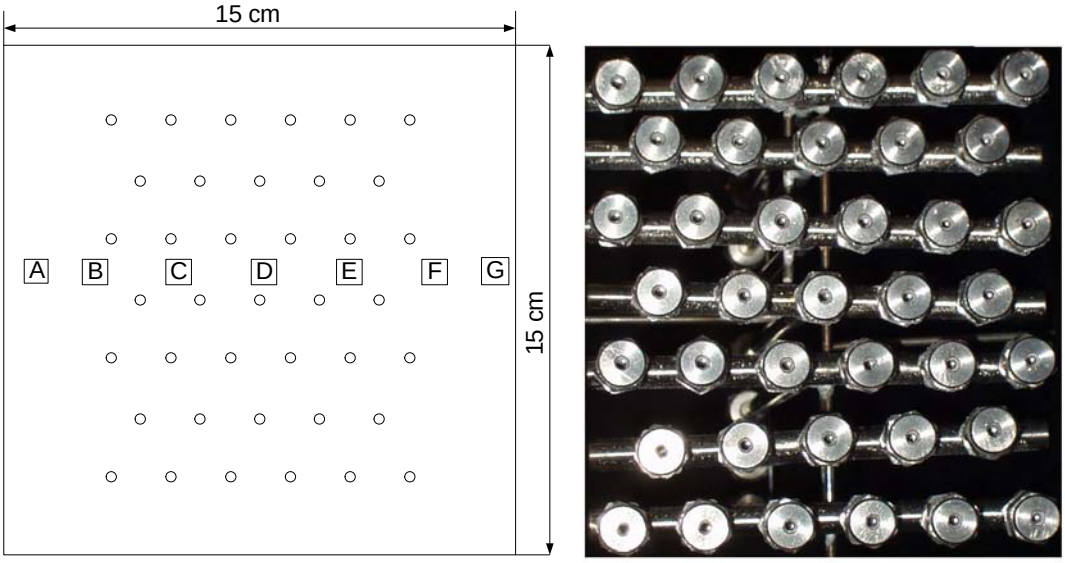

(a) Schematic top view (b) Picture (top view)

Figure 1. Schematic top view and a picture of the membrane assisted fluid bed with vertical membranes showing the injection and detection points indicated with A-G.

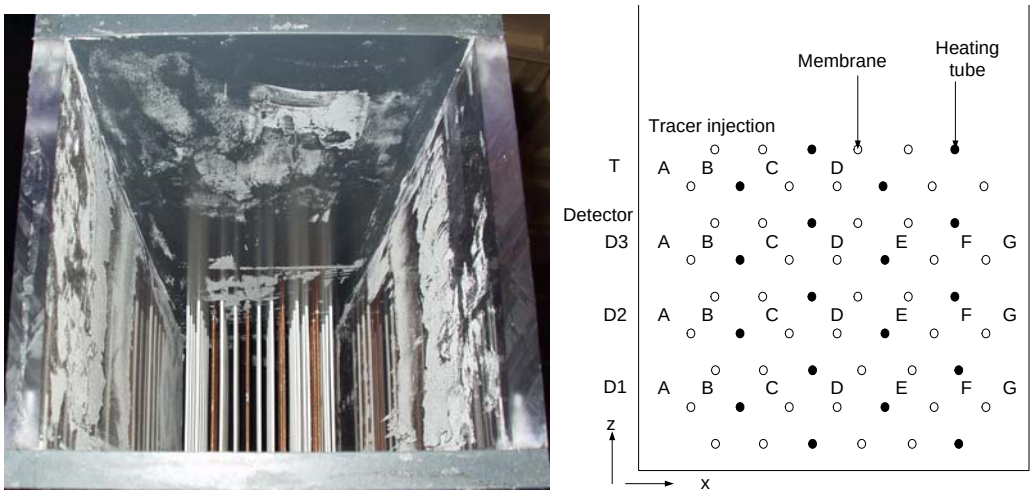

(a) Picture (top view) (b) Schematic side view

Figure 2. Picture (top view) and schematic side view of the membrane assisted fluid bed with horizontal inserts showing the tracer injection and detection points, indicated with A-G for the lateral position and D1-D3 for the axial position.

•: Heating tube, o: Membrane tube.

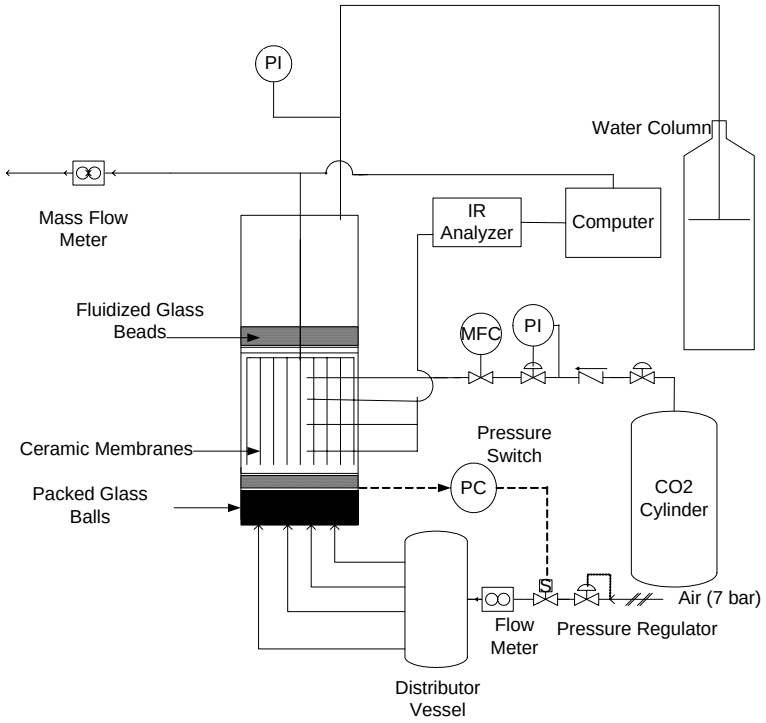

Figure 3. Schematic of the experimental set-up.

IR = infra red	MFC = mass flow controller
PC = pressure controller	S = solenoid valve
PI = pressure indicator	

2.2. Experimental technique

Steady state axial and lateral concentration profiles of a CO_2-tracer injected at different locations through a probe (point injection) or via the membranes (line injection) were measured for the three different bed configurations, for different gas flow ratios of gas fed through the membrane bundles and the porous plate distributor. CO_2 was used as a tracer gas. For the point injection measurements a small steady stream of tracer gas was injected at a single point by a traversing probe, which could be located at seven lateral positions. As shown in Figure 4, experiments were carried out with consecutive injection of steady tracer at points A to D while the gas was sampled at seven sampling locations A to F for each of three axial positions indicated by detecting probes (D1-D3). The sample gas was analyzed with an IR analyzer connected to a computer based data acquisition

system. For the line injection measurements CO_2 was fed via the ceramic membrane bundles such that CO_2 concentration in the freeboard was 1.5 %.

2.3. Experimental procedure

Before actually measuring the back mixed tracer gas concentration profile in the fluidized bed, the analyzer was calibrated with a standard mixture of 1.6% CO_2 in N_2. The output signal of the analyzer gives the concentration at the point of measurement as percent CO_2. The fluctuations in the signal from the analyzer were smoothened by time averaging the analyzer signal. Maximum averaging time of 16 minutes was used for the near wall detection points and somewhat smaller averaging time was sufficient for other locations in the bed (typically 2 to 4 min.). It was ensured that the selected averaging time was sufficiently long enough to give reproducible results.

The effect of the completely mixed CO_2 injection concentration, C_0, on the gas back mixing results was investigated first to find the optimal value of the CO_2 concentration in the injected gas stream. With smaller CO_2 concentrations in the injected gas the physical properties are less affected, but with a higher concentration the accuracy of the measurement is better because of the better detectability of the analyzer. A CO_2 injection concentration (C_0) of 0.25% was chosen. With somewhat lower and somewhat higher concentration the linearity in the detected concentrations with respect to C_0 was assessed.

Since very small particles (75-110 μ) have been used in this investigation, the detector probe tip was equipped with larger fine filter having 60 μ pores and larger surface area (see Figure 4 b). Steady flow (10-20 liter/h) to the analyzer was maintained by a vacuum pump installed at the exit of he analyzer.

Finally, in order to demonstrate the reproducibility of the results, selected runs were repeated after a few days and the results from the second run did not show any significant deviation form the original run (deviation < 5%).

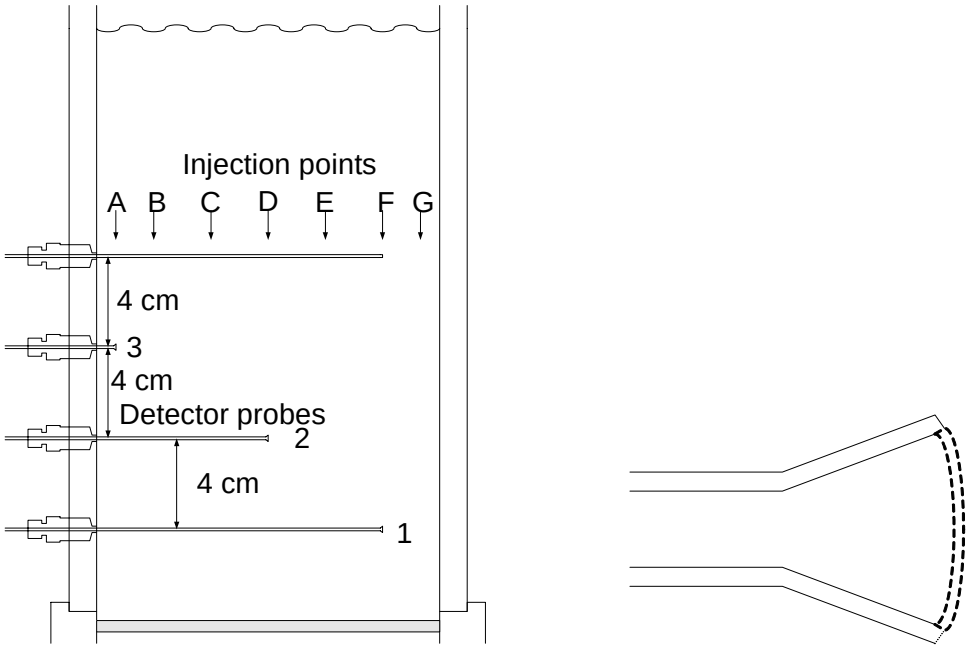

(a) (b)

Figure 4. Schematic overview of (a) tracer injection and detection system and (b) detector tip. (Positions from left wall: A: 0.825 cm, B: 2.5 cm, C: 5.0 cm, D: 7.5 cm and rest are mirror image).

3. Experimental results and discussion

Firstly, experimental results on the extent of axial and lateral back mixing deduced from the tracer gas concentration profile for the beds with three different geometries, viz. a bed without internals, a bed with vertical membranes and a bed with horizontal membranes are presented for different fluidization velocities and subsequently compared. Finally, the effect of gas addition via membranes on axially back mixed tracer gas concentration profiles for a bed with horizontal membrane bundles will be discussed.

3.1. Gas back mixing studies without gas addition via membranes

Experiments have been carried out at three fluidization velocities of 4, 6 and 8 times u_{mf} with the tracer gas injections consecutively at positions A to D (see Figure 4a). Three set-up configurations, viz. bed without internals, bed with vertical membranes and bed with horizontal membranes have been used as shown in Figures 1 and 2. The

experimental observations for all the three geometries will be discussed below successively.

3.1.1. Fluidized bed without internals

Steady state relative tracer gas concentration measured at three axial locations in the bed with the tracer gas injection near wall (Figure 5) or in the centre of the bed (Figure 6) for three different fluidization velocities are plotted as a function of the dimensionless distance from the centre of the bed. Probe 1 was positioned lowest in the bed and was located 4 cm above the distributor. Other probes were separated by 4 cm from the neighboring one. Note the differences in scale for the C/C_0 axes in the figures.

The following important observations and conclusions were discerned from the experimental results.

1. For tracer gas injection at the centre of the bed (position C and D), the relative tracer gas concentrations detected just below the injection point were significantly higher at a fluidization velocity of 4 u_{mf} for all axial positions (probes 1, 2 and 3) than at higher fluidization velocities, indicating that strong up flow prevails at the centre of the bed at higher fluidization velocities (see Figure 6).

2. With the tracer gas injection near wall (position A) and with a relatively low fluidization velocity of 4u_{mf}, rather low relative tracer gas concentrations were detected close to the wall below the injection point at all the three axial positions, indicating that the down flow near wall is not significant at low fluidization velocities. When the fluidization velocity is increased, the near wall down flow also increases and very pronounced at a fluidization velocity of 8u_{mf} and higher as can be clearly observed by the high tracer concentrations detected near the wall below the injection point (see Figure 5, Injection A). Interestingly, with the injection point near the wall and at a fluidization velocity of 6u_{mf} high relative tracer concentrations were detected just below the injection point (probe 3), but very low concentrations at somewhat lower axial positions (probe 1 and 2), which indicates that at a fluidization velocity of 6u_{mf} the down flow does not extend completely to the bottom of the fluidized bed (see Figure 5, Injection B).

3. With the tracer gas injection point at position B, the relative tracer gas concentrations detected at position C are higher than at position A for all of the three detector probes and all the three fluidization velocities, despite the fact that position A is closer to position B

than position C, indicating that the average lateral position between the up flow and the down flow regions in the bed is just between position A and B (see Figure 5, Injection B).

From the above observations it is very clear that with increasing fluidization velocity the down flow of solids near the wall becomes prominent and the gas flows upward in the centre of the bed due to increased bubble activity in the centre of the bed at higher fluidization velocities. Two macroscopic circulation loops can be envisaged depending on the superficial velocity as schematically depicted in Figure 7. This profile is consistent with previous literature studies for aspect ratios of about two as used in this study (Kunii and Levenspiel, 1991).

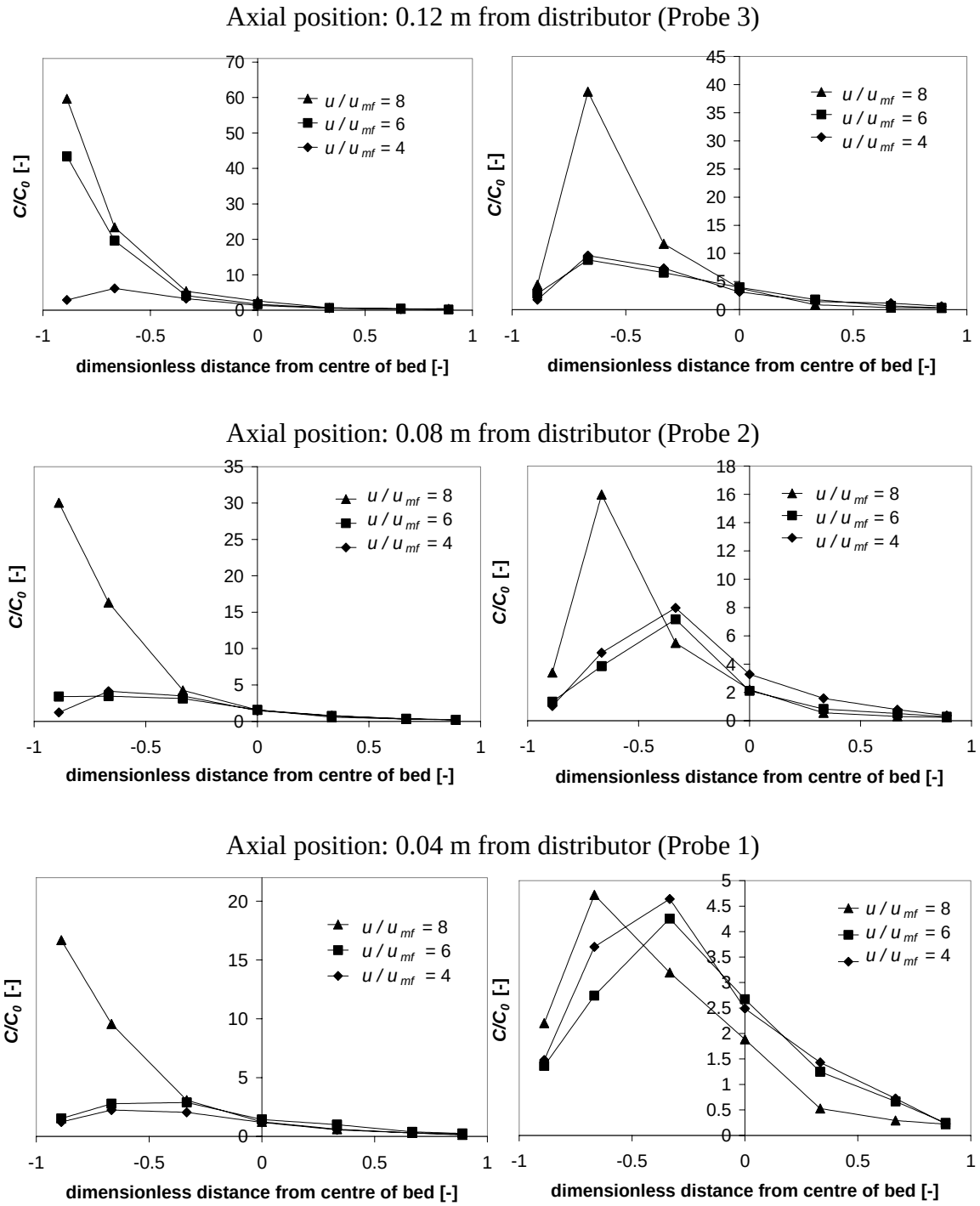

Figure 5. Effect of the superficial fluidization velocity on the experimentally measured lateral tracer gas concentration profile (relative to the free board conc. C_0) at three different axial positions in a bed without internals with the tracer gas injections point *near the wall*. (see Figure 4 for position A and B).

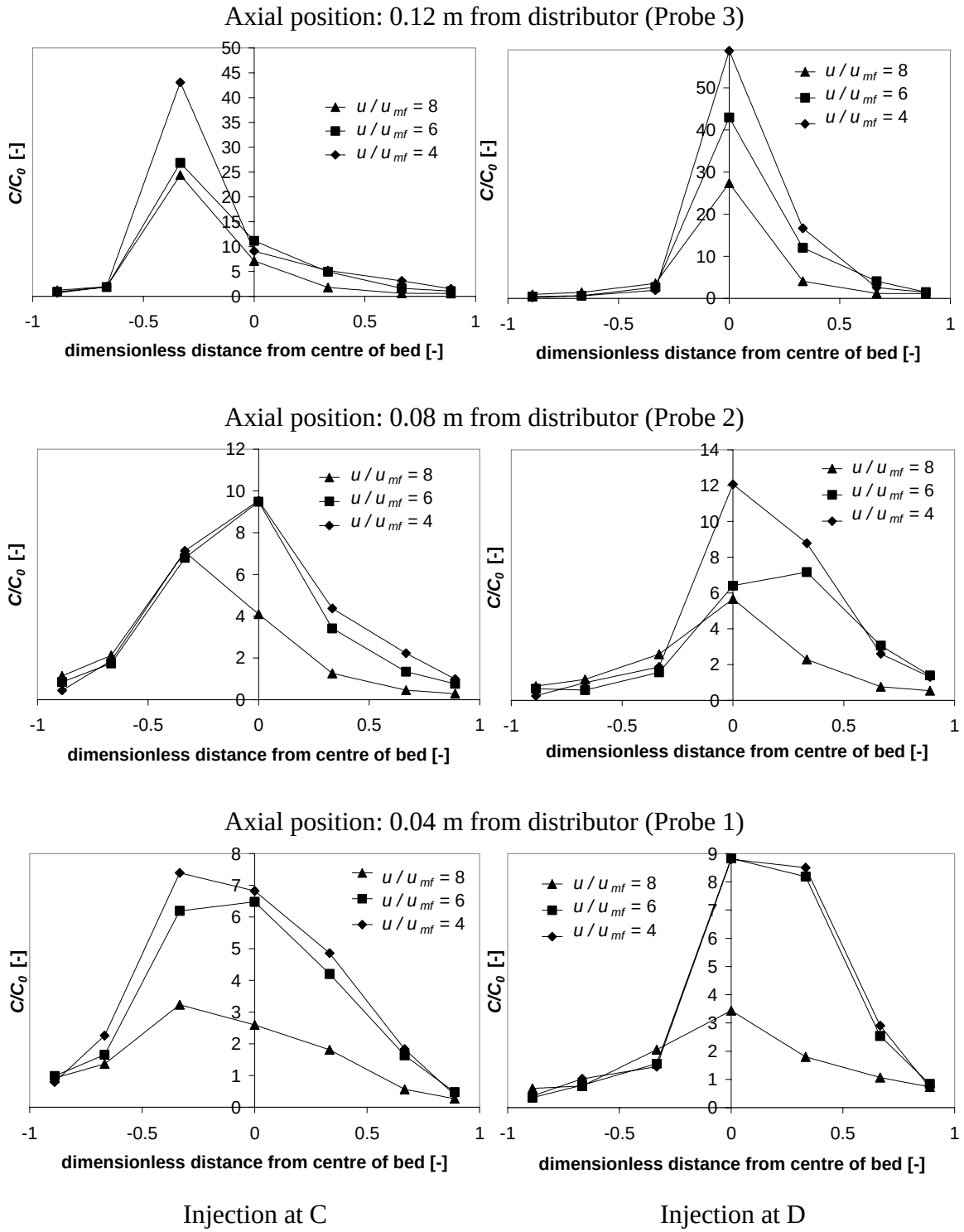

Figure 6. Effect of the superficial fluidization velocity on the experimentally measured lateral tracer gas concentration profile (relative to the free board conc. C_0) at three different axial positions in a bed without internals and with the tracer gas injection point *near the centre of the bed*. (see Figure 4 for position C and D).

(a)

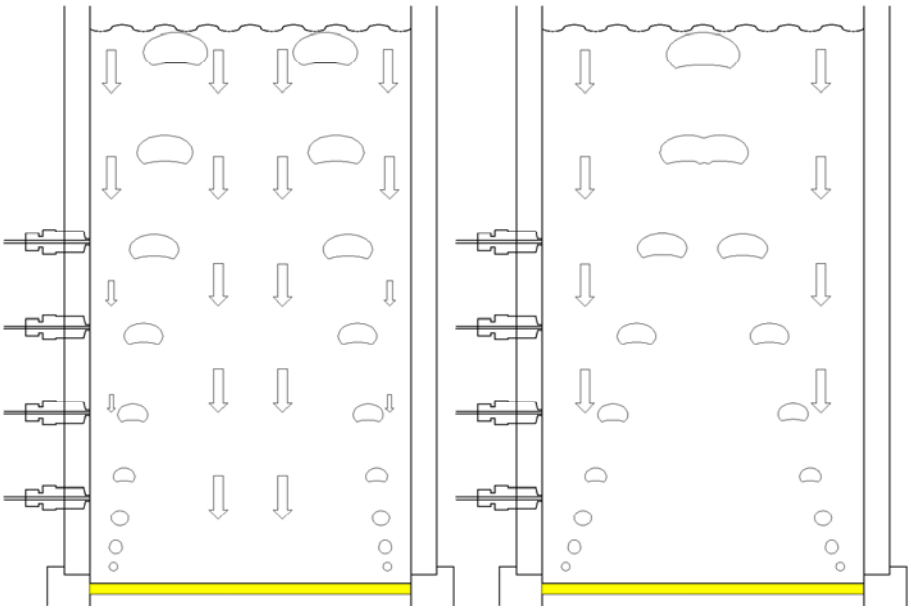

(b)

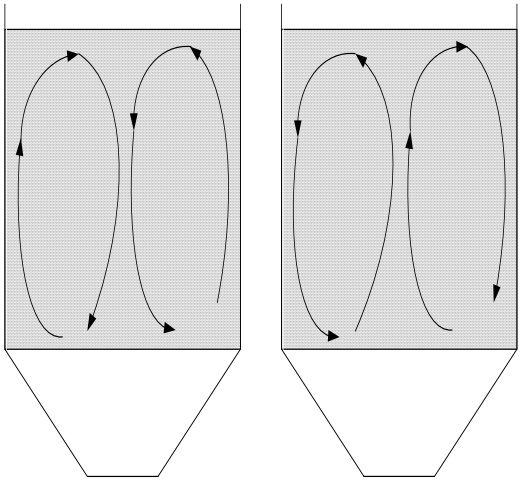

$u_0/u_{mf} = 4\ u_{mf}$ $u_0/u_{mf} = 8\ u_{mf}$

Figure 7. Schematic of the macroscopic circulation patterns changing with the fluidization velocity in the fluidized bed without internals: (a) bubble pattern (b) emulsion circulation pattern at aspect ratio (L/D) of 2.

Qualitatively our experimental results for a bed without internals agree quite well with literature data at similar fluidization conditions. Nguyen et al. (1977) reported that if a stable bubble pattern exists at the top of the bed, it leaves a persistent central area bubble free, leading to pronounced solids down flow in this area and associated strong gas back mixing. They observed this at fluidization conditions of $u/u_{mf} = 6$ and an aspect ratio of nearly two. We observed the same in our investigation at similar fluidization conditions. The increase in gas back mixing with increase in fluidization velocity is well-known and was also observed in our study.

3.1.2. Fluidized bed with vertical membranes

Steady state concentration profiles measured at three axial locations in the bed with the tracer gas consecutively injected at four positions and at three different fluidization velocities are plotted as a function of the dimensionless distance from the centre of the bed and are shown in Figures 8 and 9.

The following important observations were made from the experimental results.

1. For the tracer gas injection near the centre of the bed (position C and D), the relative tracer gas concentrations detected just below the injection point were very low for all the fluidization velocities studied compared to the experiments without internals. Again the highest relative concentrations were measured for the fluidization velocity of $4u_{mf}$, however the magnitudes of C/C_0 are much smaller indicating that the upflow in the centre of the bed is very pronounced even at low velocities and becomes even stronger at higher gas velocities (see Figure 9).

2. With the tracer gas injection point near the wall, the tracer concentrations detected at the top most probe just below the injection point (probe 3) were very high for all fluidization velocities. However for lower gas velocities of $4u_{mf}$ and $6u_{mf}$ the relative concentrations detected at lower axial positions were very small, but for a high superficial velocity of $8u_{mf}$ the tracer concentration remain high also at the lower axial positions in the bed. This indicates that only for high gas velocities ($>8u_{mf}$) the macroscopic circulation extends completely extended over the entire bed height (see Figure 8, Injection A).

3. As the tracer gas injection point is moved to position B, magnitudes of C/C_0 become significantly smaller for all of the probes, even just below the injection point. At the low

fluidization velocities of $4u_{mf}$ and $6u_{mf}$, the tracer concentrations detected were very small even just below the injection point, which indicates that up flow prevails at injection position B at these velocities. Only at $8u_{mf}$, higher tracer concentrations were detected at lower positions in the bed, indicating a more pronounced down flow. This is supported by the increase in the concentration detected near the wall only for the high velocity of $8u_{mf}$ for the case with the injection at the centre (point D) at probe 2.

From the above observations it is clear that the down flow near the wall becomes more prominent only at relatively high fluidization velocities. However, the presence of the vertical membranes suppressed the macroscopic circulation loops by directing the gas bubbles upwards and obstructing the lateral movement of the bubbles yielding a more uniform up flow in the bed and small down flow region near the wall with decreased downward velocity. Thus the vertical membranes strongly suppress axial back mixing.

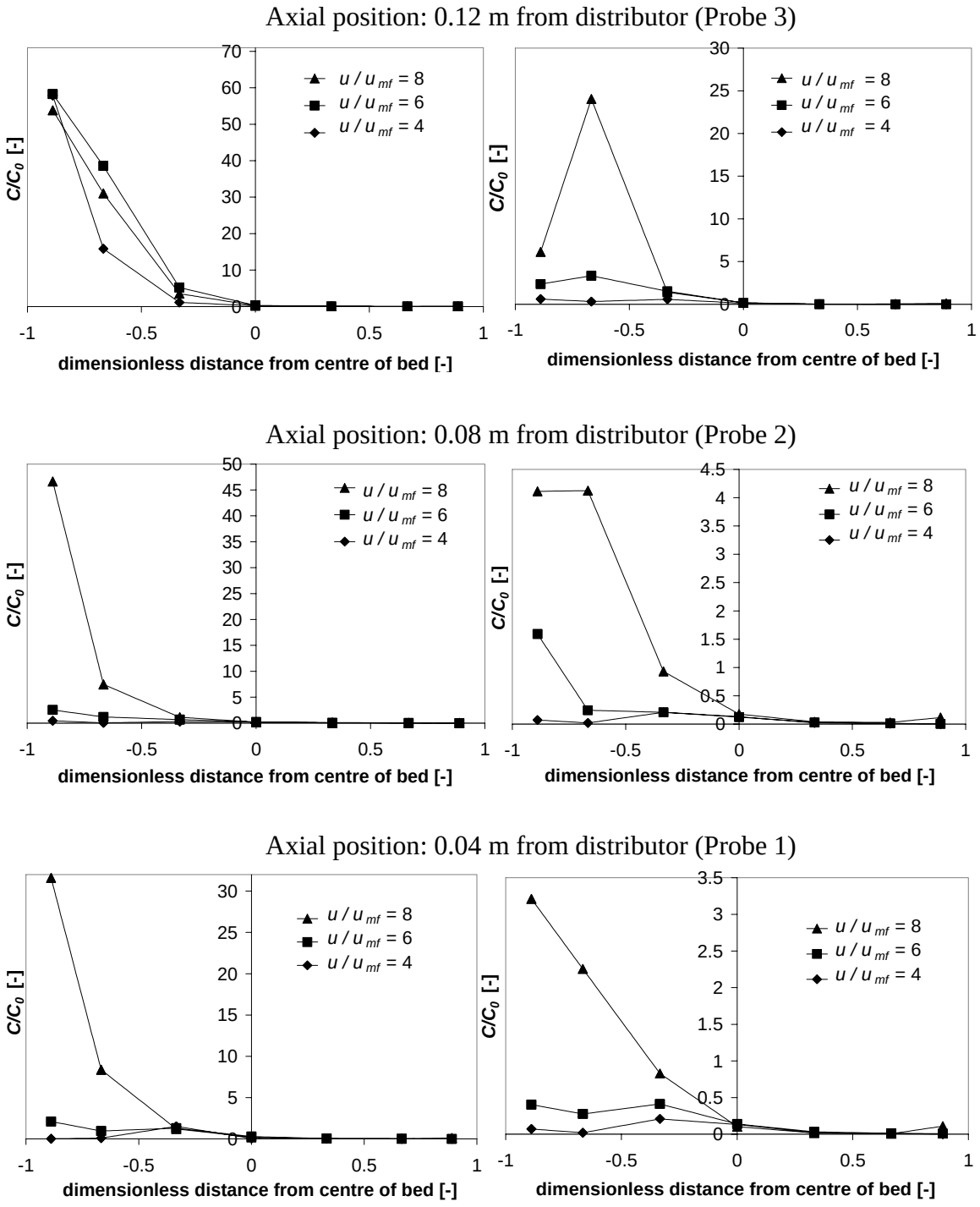

Figure 8. Effect of the superficial fluidization velocity on the experimentally measured lateral tracer gas concentration profile (relative to the free board conc. C_0) at three different axial positions in a bed with vertical membranes and with the tracer gas injections point *near the wall*. (see Figure 4 for position A and B).

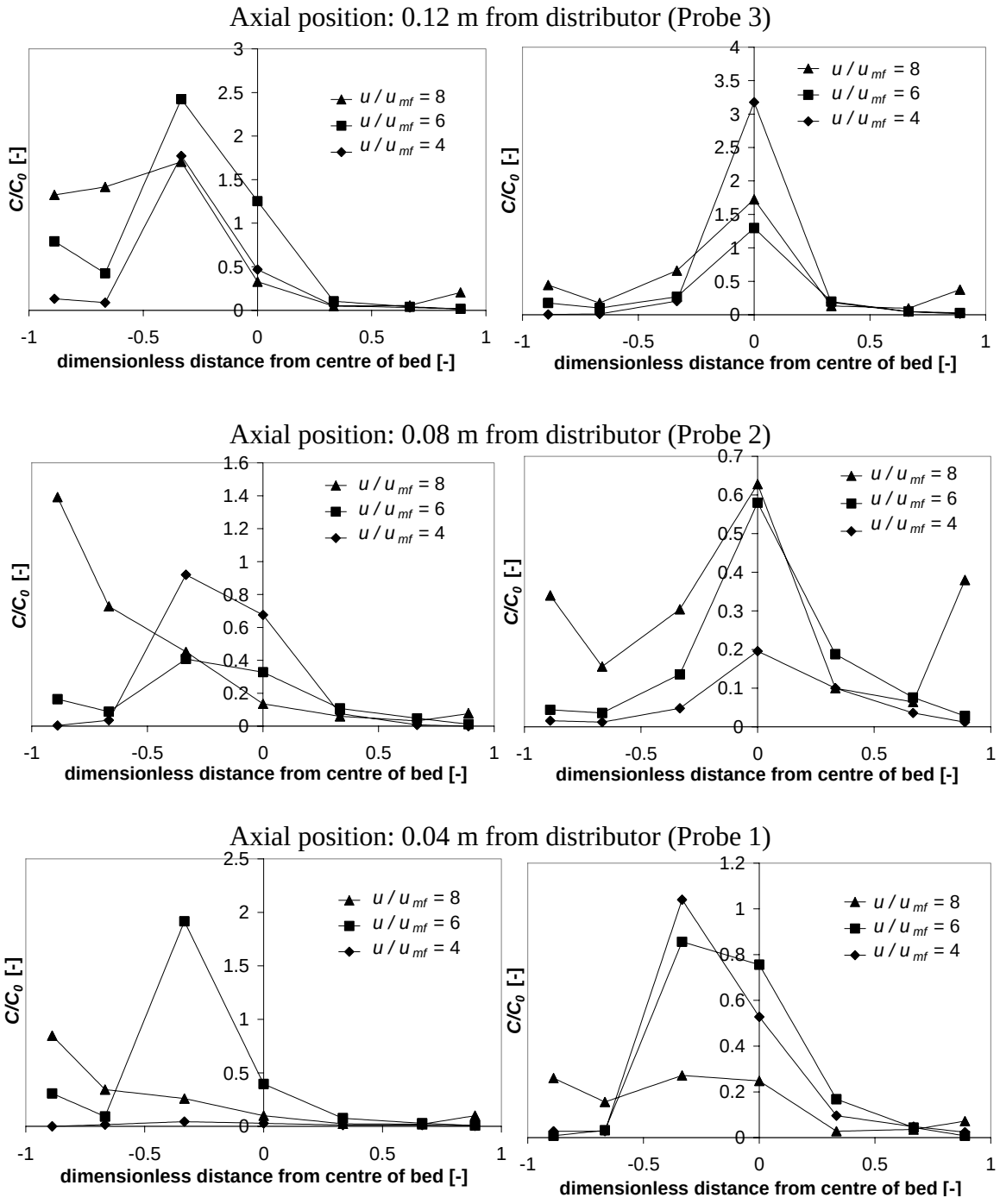

Figure 9. Effect of the superficial fluidization velocity on the experimentally measured lateral tracer gas concentration profile (relative to the free board conc. C_0) at three different axial positions in a bed with vertical membranes and with the tracer gas injection point *near the centre of the bed*. (see Figure 4 for position C and D).

3.1.3. Fluidized bed with horizontal membranes

In order to investigate the macroscopic circulation patterns in a fluidized bed with horizontal membranes, tracer gas experiments were carried by again measuring steady state lateral relative concentration profiles at three axial locations in the bed and for four different tracer gas injection points at three different fluidization velocities. The results have been plotted in Figure 10 and Figure 11. Note that a small asymmetry in the profiles exists, which is caused by slight asymmetry in the geometry of the inserts.

Very similar effects can be observed as shown before for the fluidized bed with vertical membranes, i.e. only significant down flow for high superficial gas velocities ($>8u_{mf}$). Apparently horizontal membranes also obstruct the lateral movement of the bubbles due to bubble breakage. A remarkable difference with the results for the fluidized bed with vertical membranes is the increase in the relative tracer gas concentration detected near the wall, opposite to the side of the bed where the tracer gas was injected, especially at higher superficial gas velocities. This can be attributed to the lateral mixing in the fluidized bed above the top most membrane, which comes all the way till the bottom of the bed via the small down flow zone, hence relatively faster down flow zone is located higher.

Nguyen et al. (1981) also studied the gas back mixing in large fluidized beds with tube assemblies (vertical and horizontal internals). They observed that horizontal tubes immersed in the fluidized bed suppressed the gas back mixing completely up to fluidization velocities of u/u_{mf} = 12 with a fluidized bed of similar aspect ratio of about two. This effect has been observed in our investigation as well. They also observed that vertical membranes suppressed the gas back mixing up to fluidization velocities of u/u_{mf} = 5, but were less effective in suppressing the gas back mixing at higher velocities, with pronounced back mixing at the center of the bed.

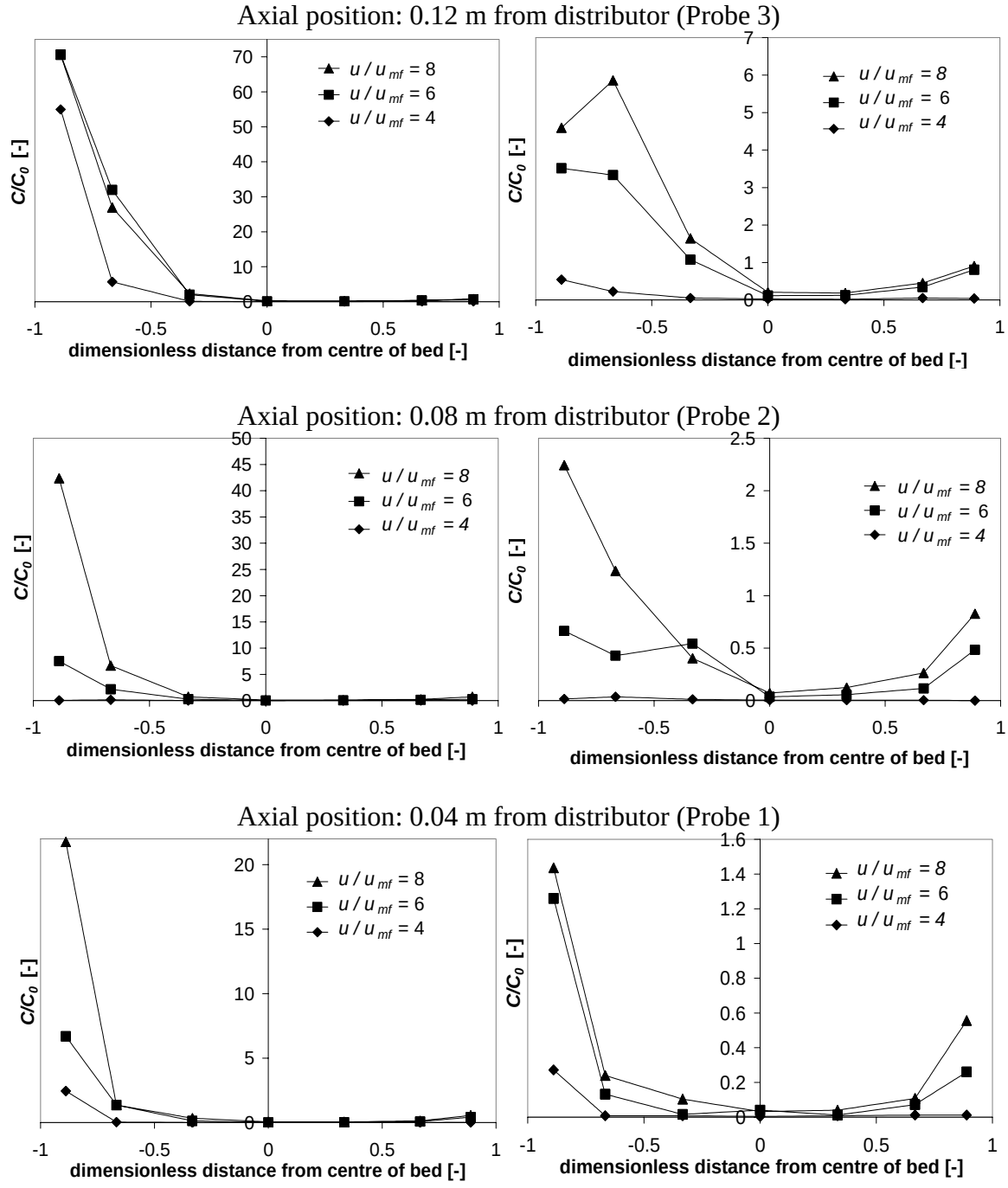

Figure 10. Effect of the superficial fluidization velocity on the experimentally measured lateral tracer gas concentration profile (relative to the free board conc. C_0) at three different axial positions in a bed with horizontal internals with the tracer gas injections point *near the wall*. (see Figure 4 for position A and B).

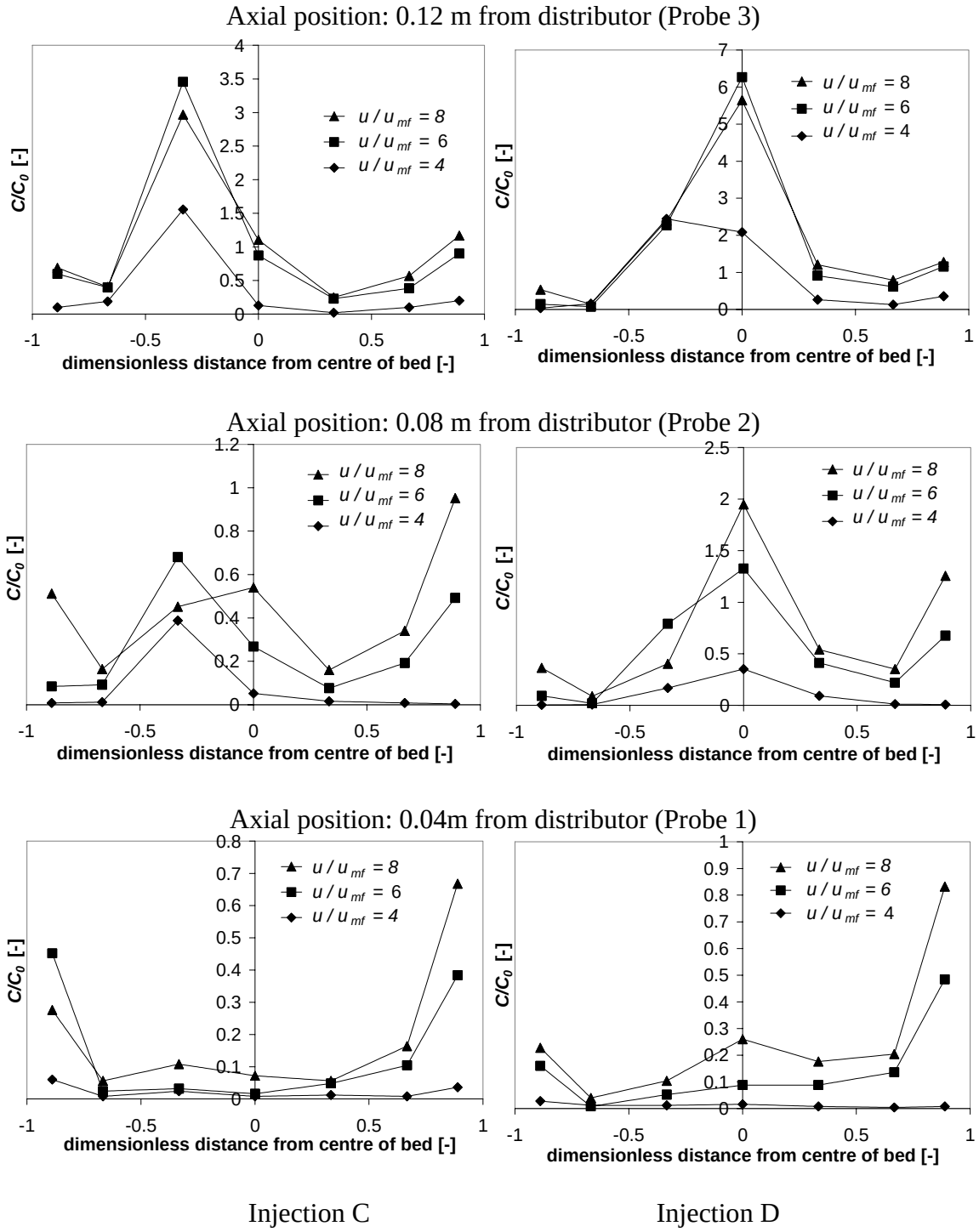

Figure 11. Effect of the superficial fluidization velocity on the experimentally measured lateral tracer gas concentration profile (relative to the free board conc. C_0) at three different axial positions in a bed with horizontal internals and with the tracer gas injection point *near the centre of the bed*. (see Figure 4 for position C and D).

3.1.4. Comparison of gas back mixing in the three geometries

Steady state concentration profiles (C/C_0) measured at three different axial locations, in the bed, with the tracer gas injection at four different positions and at fluidization velocity of $8u_{mf}$ have been plotted as a function of the dimensionless distance from the centre of the bed for the three different geometries in Figure 12 and Figure 13.

The following conclusions can be drawn from these figures.

1. With the tracer injection near the wall (point A), the tracer gas concentrations are quite similar for the fluidized bed without inserts and with vertical and horizontal membranes. In the top half of the bed (probe 2 and probe 3) the tracer concentrations for the bed with horizontal membranes are somewhat higher than the bed without inserts and somewhat lower further away from the wall, which indicates reduced lateral mixing at the wall. The same holds for the bed with vertical membranes, however the down flow is extended further towards the bottom of the bed, as can be concluded from the highest relative tracer concentrations near the wall for vertical membranes in the bottom zone of the bed (probe 1) (see Figure 12).

2. With the tracer gas injection at position B, the highest tracer concentrations were detected for the bed without inserts. The concentrations were much smaller for the bed with vertical membranes and even again much smaller for the bed with horizontal membranes. From this it can be concluded that the down flow region was smallest for the bed with horizontal membranes.

3. The results with the injection point in the centre of the bed show that both the vertical and horizontal membranes very effectively suppress the axial back mixing.

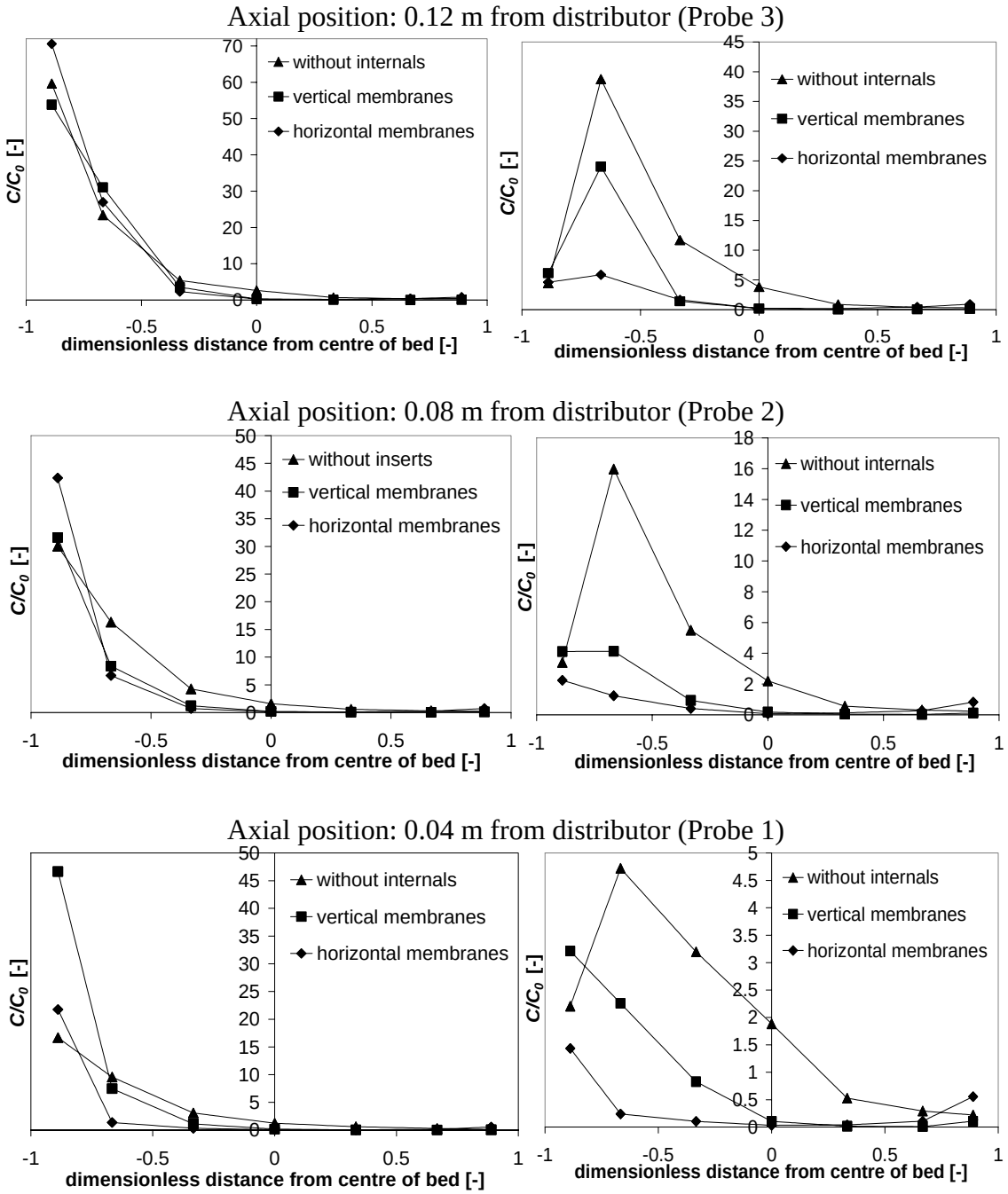

Figure 12. Comparison of experimentally measured lateral relative tracer gas concentration profiles for the three axial positions and for three geometries (without inserts and with vertical or horizontal inserts) with the tracer gas injection *near the wall* for a superficial gas velocity of $8u_{mf}$.

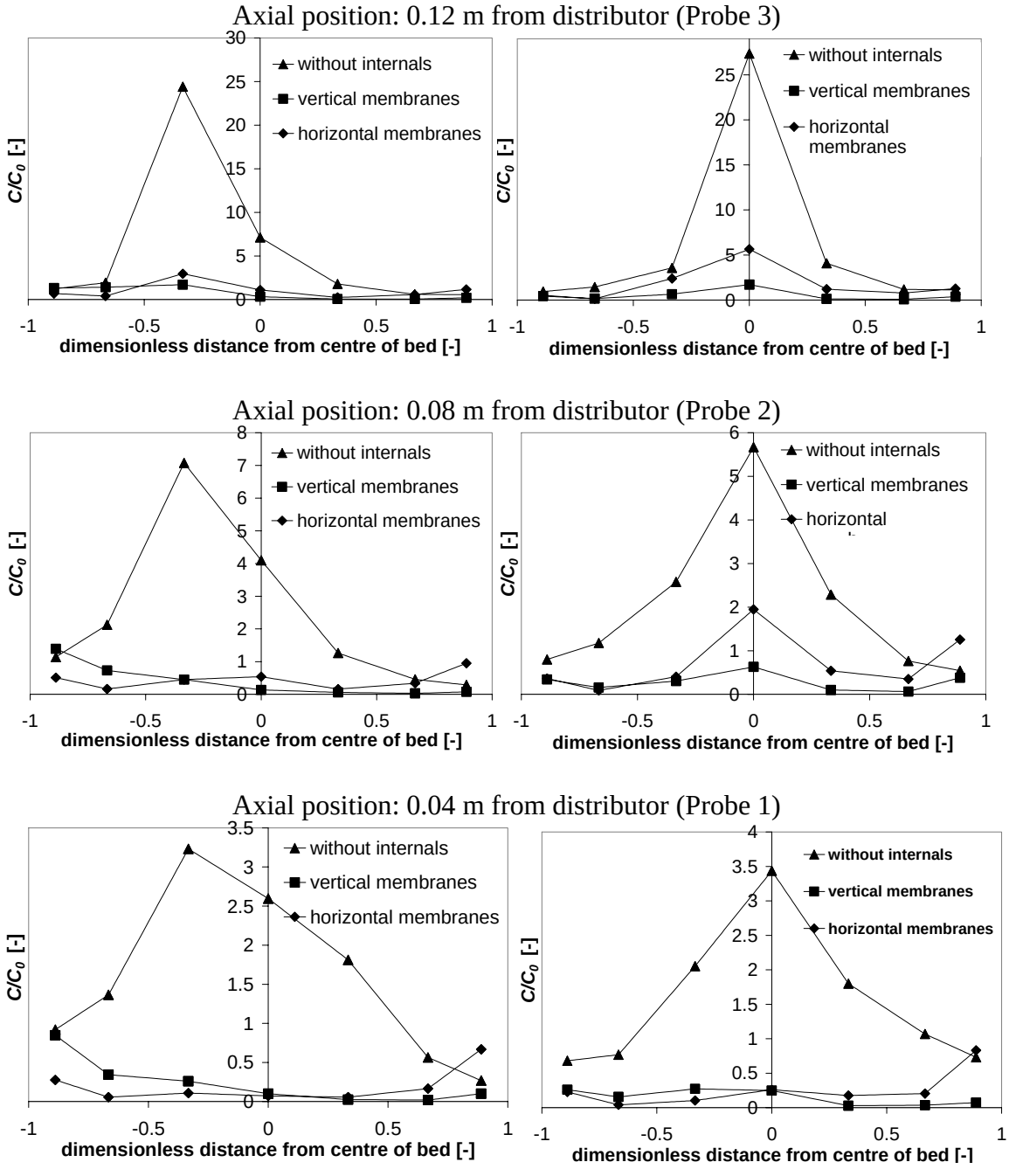

Figure 12. Comparison of experimentally measured lateral relative tracer gas concentration profiles for the three axial positions and for three geometries (without inserts and with vertical or horizontal inserts) with the tracer gas injection *near the center* for a superficial gas velocity of $8u_{mf}$.

3.2. Gas back mixing studies with addition of gas via membranes

In a membrane assisted fluidized bed reactor a portion of the feed can be supplied through the membranes to achieve optimal axial concentration profiles from conversion and selectivity point of view. Therefore the effect of membrane permeation on the gas back mixing was also studied experimentally. A bed with horizontal membranes was selected, since it allows a better control to doze one of the reactants and it is believed that horizontal membranes improve the bubble-to-emulsion phase mass transfer due to bubble breakage, resulting in smaller average bubble diameter. In order to study the effect of gas addition via the membranes on the gas back mixing, point injection as well as line injection experiments were carried out.

3.2.1. Point injection of tracer gas

Tracer gas point injection experiments were performed in the fluidized bed with horizontal membranes at superficial gas velocities of $6u_{mf}$ and $8u_{mf}$ with the injection at position A (near the wall) and D (in the centre), where part of fluidizing gas was fed via membranes (0-20%), keeping the total flow rate corresponding to $6u_{mf}$ and $8u_{mf}$ respectively (see Figure 14 and 15).

The relative tracer concentrations detected in the bed both with the injection near the wall and in the centre of the bed are very small and considerably smaller when compared to those obtained without membrane permeation at otherwise similar conditions. The concentrations detected decreased even further with an increase in the gas flow rate permeated via membranes. The observed trends are essentially the same for both the velocities studied. The small increase in the concentration near the wall is again the result of lateral mixing in the top of the bed above the top most membrane. Furthermore, asymmetry in the lateral concentration profiles is due to the geometry of the bed, because one side of the bed has one row of membrane tubes less, so that less gas is added via the membranes at this side resulting in higher tracer concentrations. The somewhat higher near wall tracer concentrations at $8u_{mf}$ than $6u_{mf}$ indicate the larger circulation flows near the wall at higher superficial gas velocities.

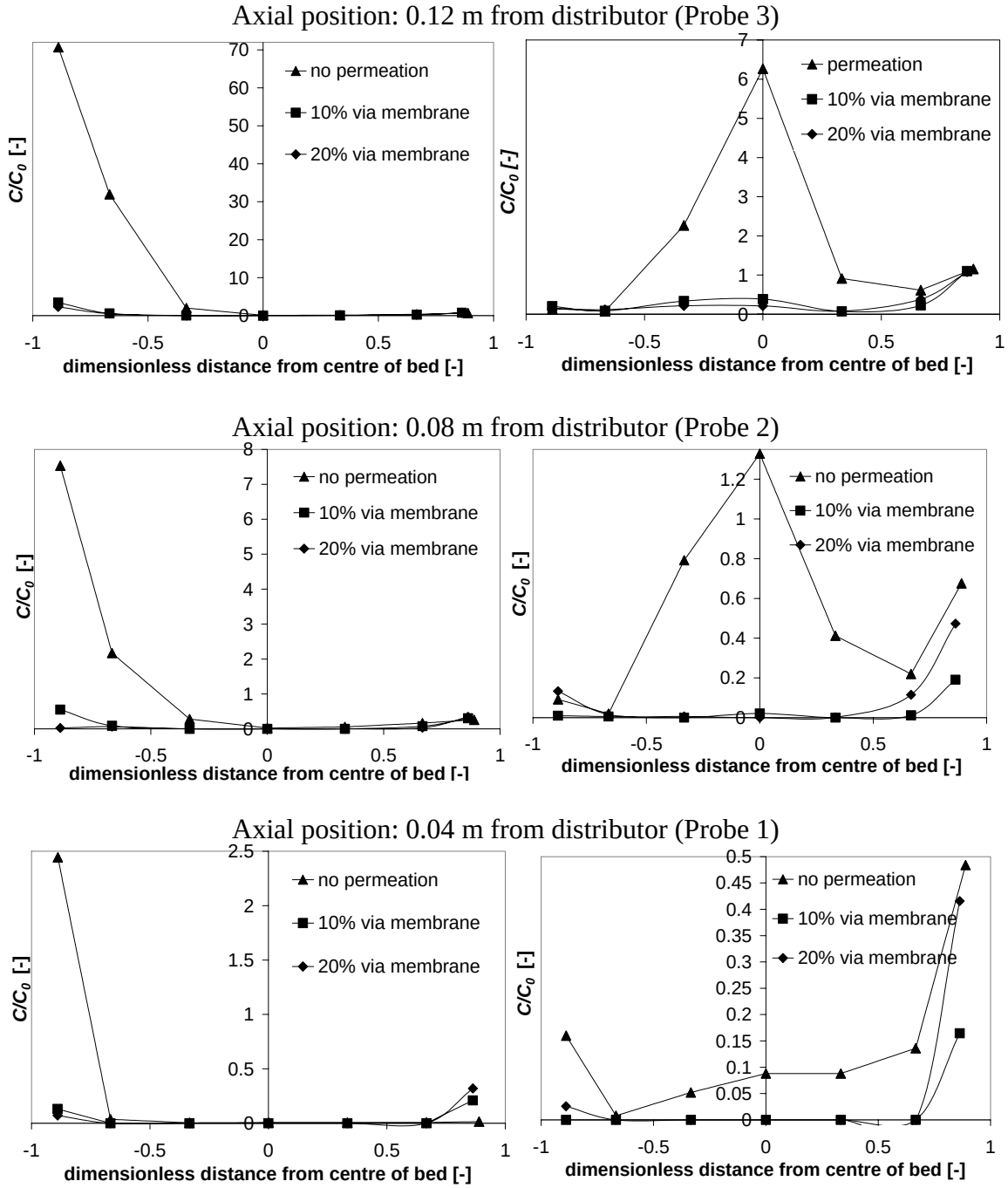

Figure 14. Effect of gas addition via the membranes on the experimentally measured lateral relative tracer gas concentration profile at three different axial positions with the injection point near wall (A) or near the centre (D) for superficial gas velocity of $6u_{mf}$.

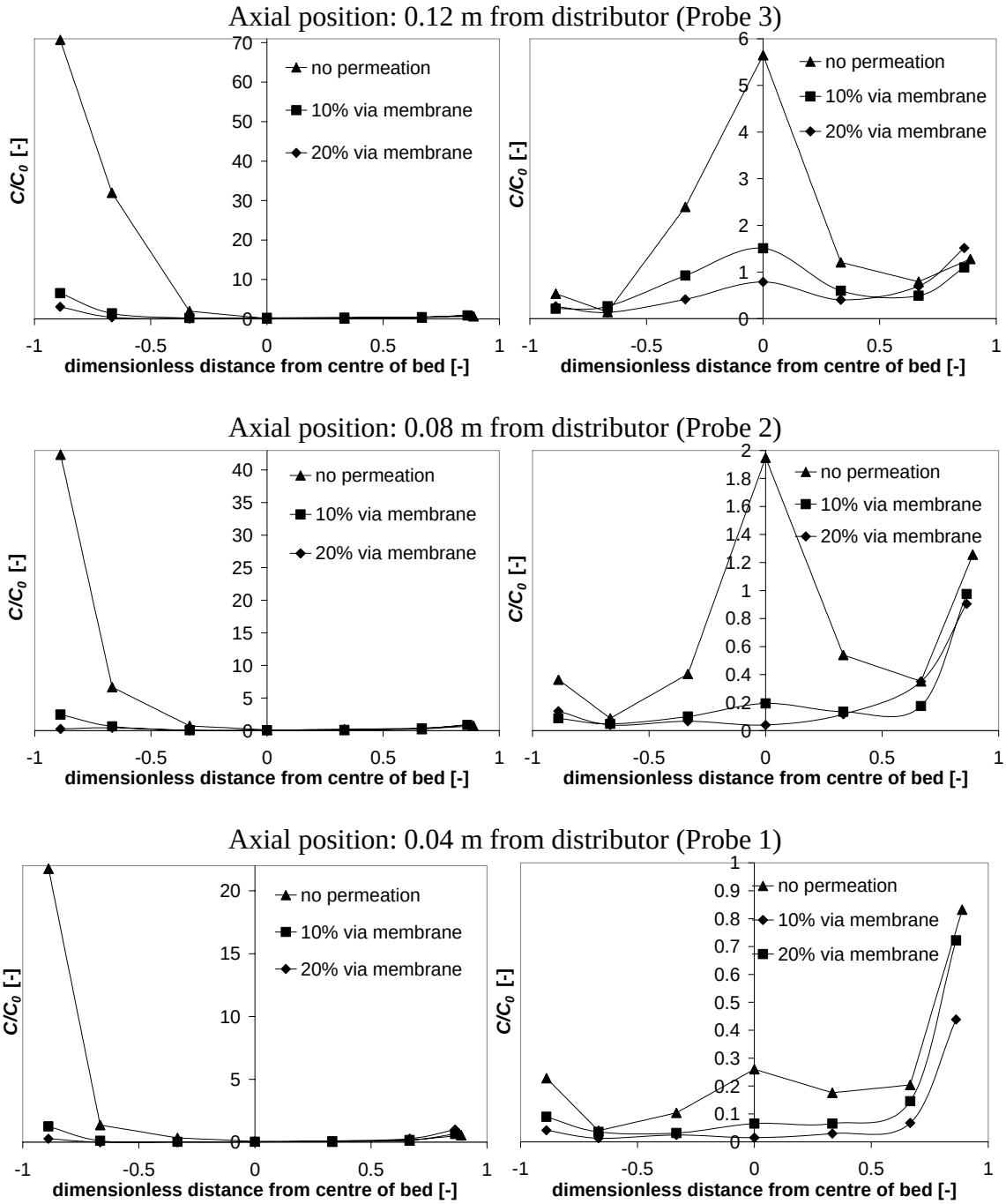

Figure 15. Effect of gas addition via the membranes on the experimentally measured lateral relative tracer gas concentration profile at three different axial positions with the injection point near wall (A) or near the centre (D) for superficial gas velocity of $8u_{mf}$.

3.2.2. Line injection of tracer gas (via the membranes)

Tracer gas line injection experiments were performed at superficial gas velocities of 2, 4, 6 and 8u_{mf}, where the tracer gas was fed distributively via the membranes, such that the tracer gas freeboard concentration amounted 1.5 mol% at the exit of the reactor. In these experiments the conditions were selected to approach those existing in the membrane assisted fluidized bed reactor. The probe, which was used to inject tracer gas for the point injection measurements, was used as additional detection probe and shown as probe 4 (at the higher axial location of 0.16 m from the distributor).

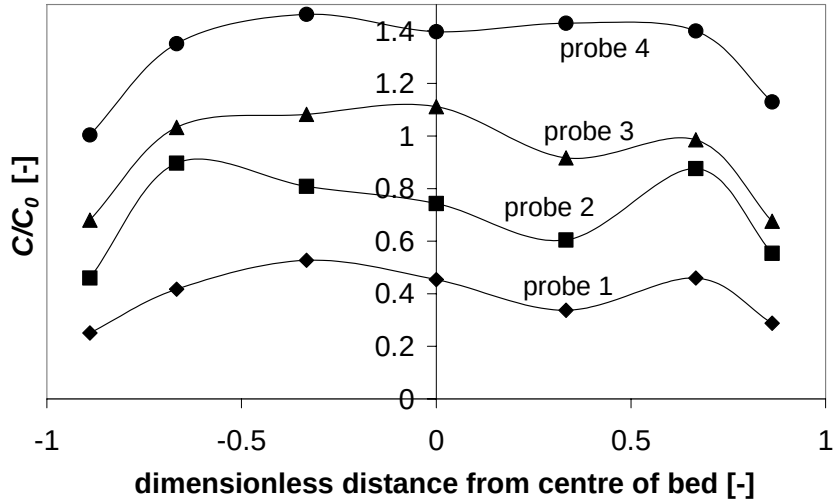

Figure 16. Lateral relative tracer gas concentration profiles in the bed at four different bed heights (probe 1-4), for a superficial gas velocity of 4u_{mf} with 20% of the fluidizing gas fed via the membranes.

Figure 16 shows the steady state lateral concentration profile relative to the well-mixed freeboard concentration C_0 detected at the four different heights in the membrane assisted fluidized bed with horizontal membranes operated at superficial gas velocity of 4u_{mf} and with 20% of the gas fed via membranes.

Firstly, Figure 16 shows an increase in the detected tracer concentrations at higher axial positions, directly resulting from the large amounts of tracer gas fed higher in the bed. Remarkably the tracer gas concentrations detected at the highest axial position are higher than the freeboard concentrations over the entire cross section of the bed (C/C_0>1). This clearly demonstrates the presence of mass transfer limitations in the bed between the gas bubbles and the emulsion phase. Without mass transfer limitations the emulsion

phase and bubble phase concentrations, indicated with C_e and C_b respectively would be the same and equal to the freeboard concentration at the top of the bed. However, if the tracer gas mainly fed to the emulsion phase with a reasonably good lateral mixing the emulsion phase concentration of tracer gas will be higher than the free board concentration and the bubble concentration smaller. If we can now assume that the concentration detected is the volumetric average of the emulsion phase and the bubble phase (since the gas is sucked out of the bed), the detected tracer concentration is given by

$$C_{CO_2} = \delta_b C_{b,CO_2} + (1-\delta_b) C_{e,CO_2} \quad (1)$$

where δ_b represents the local bubble fraction.

Since the bubble fraction is typically about 0.1 – 0.2, the detected concentrations are determined by the emulsion phase concentration, which exceeds the freeboard concentration in case mass transfer limitations prevail.

Secondly, Figure 16 shows that higher concentrations prevail at the centre of the bed than at the wall, which is contrary to what was observed in the point injection measurements. Moreover, concentration profiles at the centre of the bed are reasonably flat. This can be explained by the lateral profile of the bubble fraction. Due to higher bubble fraction at the centre of the bed, the tracer gas, which is assumed to be mainly fed to the emulsion phase, will be mixed into a smaller emulsion phase volume, yielding higher local emulsion phase concentrations.

3.2.2.1. Effect of membrane permeation

Figure 17 shows the effect of the addition of gas via the membrane on the time averaged steady state concentration profiles measured at four axial locations in the bed.

As the gas fraction added via the membrane is increased, the magnitude of C/C_0 detected at all the four axial positions decreased. This is because of the following two reasons: Firstly, when a large portion of the gas is fed via the membrane the tracer concentration in the stream permeating through the membranes was set to a lower value in order to fix the freeboard concentration of 1.5% for all the three permeations studied. Secondly, the larger the flow rate through the membranes, the smaller the flow rate through the distributor, since the total flow rate has been kept the same. This results in a

smaller bubble size and bubble fraction for the case of the largest permeation and hence a somewhat lower concentration detected as discussed earlier.

The differences observed between the concentration levels detected at different permeation flow rates were not significant at overall fluidization velocity of $4u_{mf}$ because of the rather homogeneous nature of the fluid bed and good mass transfer between the two phases due to the smaller bubble size compared to higher fluidization velocities.

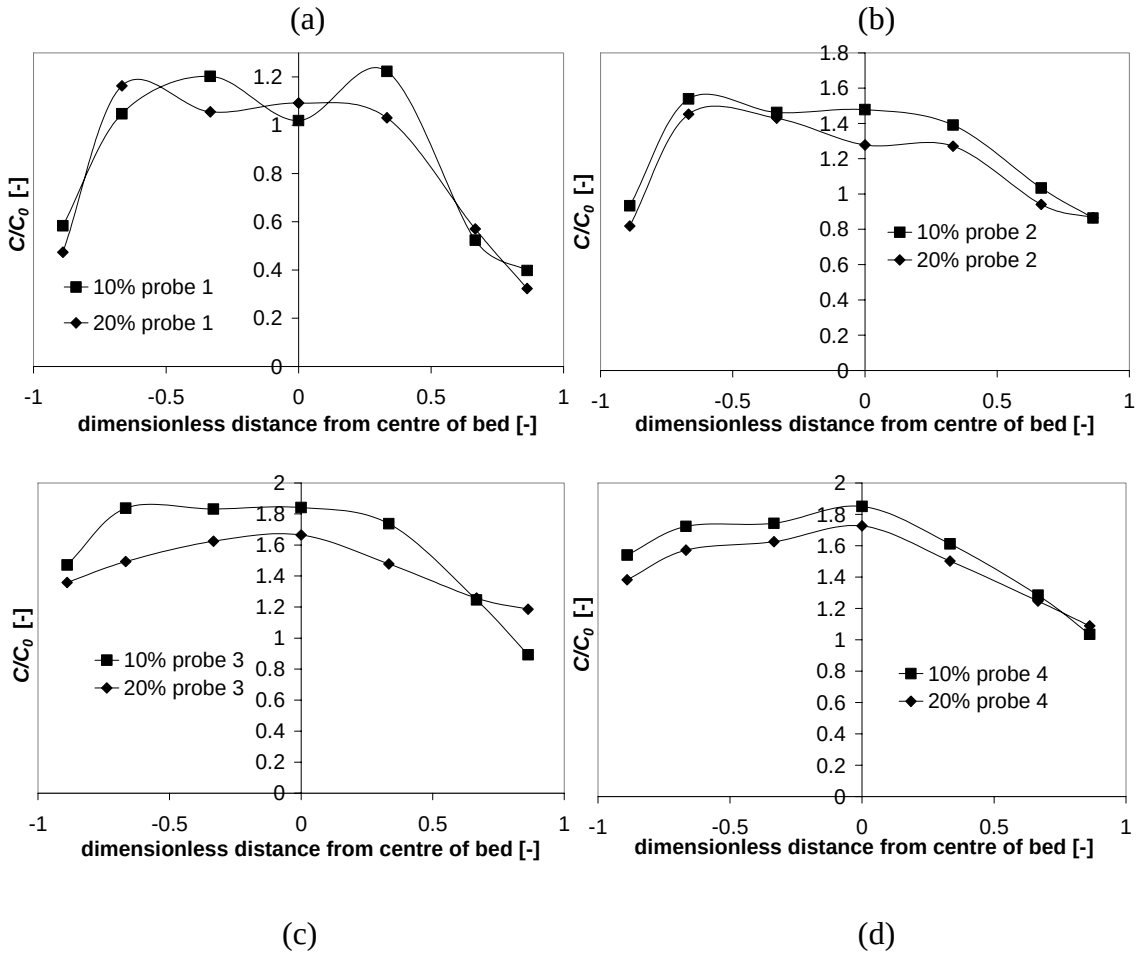

Figure 17. Effect of membrane permeation on the lateral relative concentration profiles detected at a superficial gas velocity of $8u_{mf}$, at four different axial positions: (a) at 0.16 m from distributor; (b) at 0.12 m from distributor; (c) at 0.08m from distributor and (d) at 0.04 m from distributor

3.2.2.2. Effect of the superficial gas velocity

Figure 18 shows the effect of the superficial gas velocity on the time-averaged steady state lateral tracer concentration profiles at four different axial positions with 20% of the gas fed via the membranes.

The figure clearly shows that at lower overall gas velocities the lateral relative concentration profile is much flatter and smaller concentrations are detected. With a lower overall gas velocity the bubble fraction will be smaller and the bubbles will be more uniformly distributed over the cross section of the bed. Furthermore, the average bubble size will be smaller, which will result in a better bubble-to-emulsion phase mass transfer, yielding smaller detected tracer concentrations.

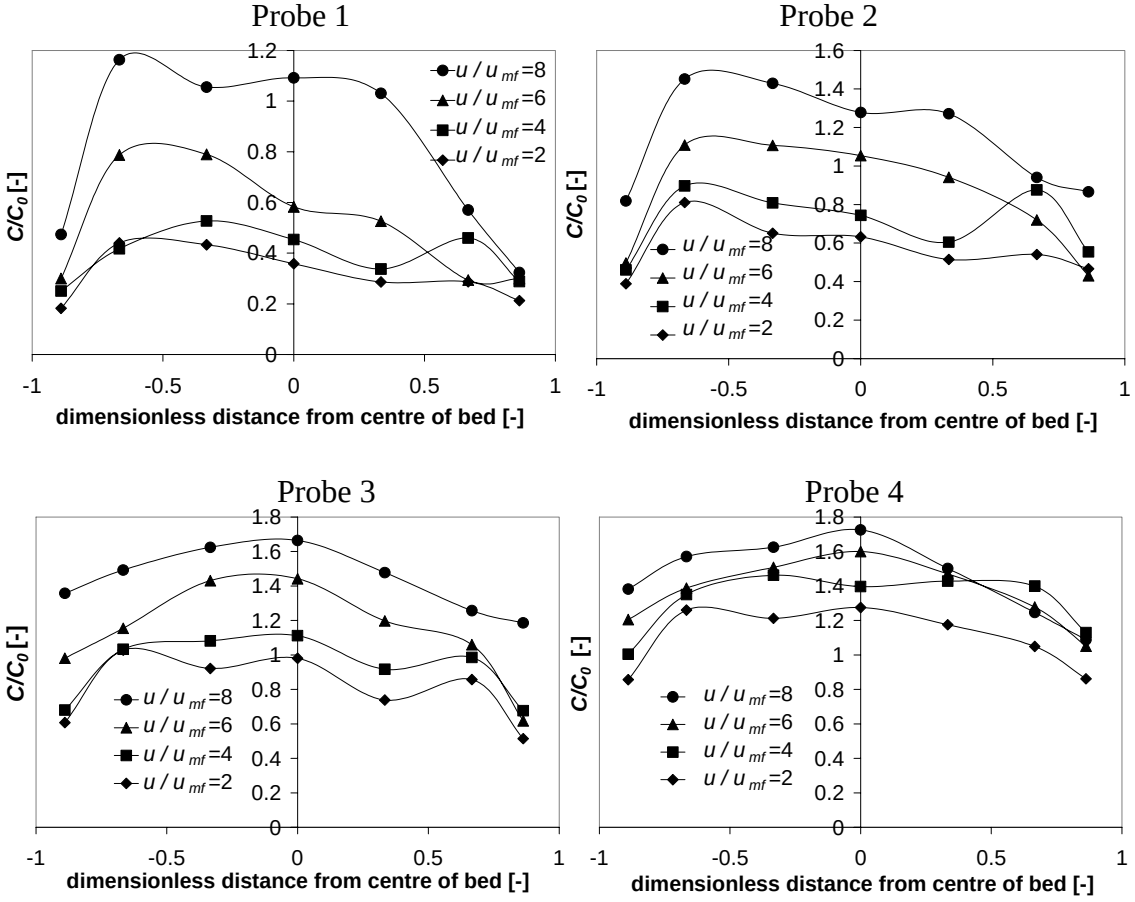

Figure 18. Effect of the overall superficial gas velocity on the lateral relative concentration profiles in the membrane assisted fluidized bed at various bed heights and at 20% of the total fluidization gas added via membrane. Probe 1 at 0.04 m from distributor; Probe 2 at 0.08 m from distributor; Probe 3 at 0.12m from distributor and Probe 4 at 0.16 m from distributor.

4. Summary and conclusions

To assess the potential of the membrane assisted fluidized bed reactor for methanol partial oxidation, the extent of gas back mixing has been studied experimentally for fluidized beds with internals (membranes) with different membrane bundle configurations, viz. horizontally and vertically positioned membranes, with and without addition of gas via the membrane over wide fluidization velocity range. The effect of the presence of the membranes, but especially the effect of gas addition via membranes on the axial gas back mixing in the fluidized beds has been studied experimentally using steady state tracer gas injection experiments.

For a fluidized bed with vertical and horizontal internals the axial gas back mixing is strongly reduced compared to a bed without internals, simply due to the presence of the internals, which obstruct the lateral movement of the bubbles by preventing bubble growth. Thus the formation of macroscopic circulation patterns, as observed for the bed without internals is impeded.

The addition of gas via the membranes in the bed with horizontal membranes reduced the gas back mixing enormously, even much more than due to the presence of internals. The membrane permeation effectively annihilates the circulation in the fluidized bed.

Furthermore, experiments with tracer gas injected via the membranes highlighted the importance of mass transfer limitations between the bubble phase and emulsion phase. The higher the permeation through the membranes, the smaller the average bubble size and bubble fraction, hence mass transfer limitations are reduced.

Acknowledgement

This research is part of the research program carried out within the Center for Separation Technology, as a cooperation between the University of Twente and TNO, the Netherlands Organization for Applied Scientific Research. The author wishes to thank Gerrit Schorfhaar and Wim Leppink for the construction and maintenance of the experimental set-ups. Also the contribution by Jan Stroomer and Mattijs van der Ham in the experimental work is greatly appreciated.

Notations

C	concentration [%]
D	detector
u	superficial gas velocity to the bed, [m·s^{-1}]
u_{mf}	minimum fluidization velocity, [m·s^{-1}]

Greek letters

δ	bubble phase fraction in [-]

Subscripts

0	free board region
b	bubble phase
e	emulsion phase
mf	at minimum fluidization condition

References

Kunii, D. and Levenspiel, O. (1991), "Fluidization Engineering", Wiley, New York.

Lathem, R. and Potter, E. (1970), "Back-mixing of gas in a 6-in diameter fluidized bed", The Chemical Engineering Journal, (1), 152.

Nguyen, H. V., Whitehead, A. B. and Potter O. E. (1977),"Gas back mixing, solid movement and bubble activities in scale large fluidized beds", AIChE Journal (23-6), 913-922.

Nguyen, H. V., Potter O. E., Dent, D. C. and Whitehead, A. B. (1981), "Gas back mixing in large fluidized beds containing tube assemblies", AIChE Journal (27-3), 509-514.

Stephens, G. K., Sinclair, R. L. and Potter, O. E., (1967), " Gas exchange between bubbles and dense phase in a fluidized bed", Powder Technol., 1, 157.

Van Deemter, J. J., (1980), "Mixing patterns in large scale fluidized beds", In Fluidization, Edited by J. R. Grace J. M. Matsen), Plenum Press, New York, 69.

Van Deemter, J. J., (1985), “Mixing”, In Fluidization, (Edited by J. F. Davidson, R. Clift and D. Harrison), Chap. 9. Academic Press, New York.

Chapter 5

Kinetics of partial oxidation of methanol over Fe-Mo catalyst

Abstract

Kinetics of the methanol partial oxidation to formaldehyde over a commercial Fe-Mo catalyst has been studied experimentally in a differentially operated reactor at temperatures of 230-260 ℃, over a wide range of methanol and oxygen concentrations. The principal products were formaldehyde, water, dimethyl ether (DME) and dimethoxymethane (DMM). The kinetics of the formaldehyde formation from methanol could be well described by Langmuir-Hinshelwood kinetics, assuming two different metal oxide sites, one containing adsorbed oxygenates and the other one containing lattice oxygen. The presence of water vapour lowered the formaldehyde formation rate significantly, especially at lower water partial pressures. The relative effect of the water concentration on the formation rate was much smaller at higher water partial pressures. These results could be well explained in terms of competitive adsorption of water with methanol on the free active catalyst sites.

For the most important side reactions, i.e. dimethyl ether formation as well as dimethoxymethane formation the forward reaction rates were determined from the selectivity data. The backward reaction rates were obtained from the forward reaction rates and the thermodynamic equilibrium data. Dimethyl ether formation reaction rate (forward reaction) was found to be only dependent on the methanol concentrations with first order dependency. The dimethoxymethane formation rate (forward reaction) was found to be linear with both the formaldehyde and the methanol concentrations.

Carbon monoxide was not formed during differential kinetics measurements of formaldehyde formation from methanol. Therefore, formaldehyde oxidation to CO was studied separately in a dual bed catalyst, in which formaldehyde was first formed in an integral reactor at lower temperatures and subsequently converted to CO in a differential

reactor. The rate of CO formation was first order in formaldehyde and oxygen dependency was the same as that for formaldehyde formation from methanol.

These experimental observations were interpreted by assuming that the oxidation reactions take place on two different metal oxide sites, one containing adsorbed oxygenates and a second one containing lattice oxygen.

The observed influences of the composition and temperature on the methanol partial oxidation, formaldehyde partial oxidation, dimethyl ether formation and dimethoxymethane formation reaction rates could be well described with rate equations based on the above assumptions. Minimization of the standard deviations of the reaction rates was carried out with Levenberg-Marquard minimization technique, where the axial concentration profiles in the kinetics reactor were accounted for using a plug flow reactor model in order to properly take into account the influence of the water concentration on the reaction rates (even in the differentially operated kinetics reactor).

1. Introduction

Formaldehyde is a base chemical of major industrial importance. In spite of fluctuations in the world economy, the growth of formaldehyde production has been remarkably steady and is expected to continue. The main industrial use of formaldehyde is in the production of urea-phenolic and melamine resins, which are used in the manufacture of chipboard (compressed wood) and plywood. Other well-established applications are in the production of paints, cosmetics, explosives, fertilizers, dyes, textiles and papers. Industrial processes for formaldehyde production can be divided in silver-catalyzed and metal oxide catalyzed processes. A brief comparison of both processes is outlined below.

1.1. Silver catalyzed process

A typical silver catalyst based process consists of an adiabatic reactor containing a bed of extremely pure silver in a granular crystalline form or silver gauze. The reactor feed is on the methanol rich side of the flammability limit and complete conversion of oxygen is obtained. The reactions occur essentially at atmospheric pressure and at 600 to 650°C and can be represented by two simultaneous parallel reactions:

$$CH_3OH + 0.5O_2 \rightarrow HCHO + H_2O \quad \Delta H = -156 \text{ KJ/mol} \tag{1}$$

$$CH_3OH \rightarrow HCHO + H_2 \quad \Delta H = +85 \text{ KJ/mol} \tag{2}$$

Between 50 and 60% of the formaldehyde is formed by the exothermic reaction and the remainder by the endothermic reaction. Carbon monoxide and dioxide, methyl formate and formic acid are the by-products formed. Overall yields of 86-90% based on methanol are possible. The product stream from the reactor is fed to the bottom of an absorption tower, where the bulk of the methanol, water and formaldehyde is condensed in the bottom section and formaldehyde from the tail gas is recovered by fresh water in the top section. The bottom stream of the absorption tower is fed to a distillation tower to recover the unconverted methanol for recycling to the reactor. The bottom stream from the distillation tower, an aqueous solution of formaldehyde, is usually sent to an anion exchange unit to reduce the formic acid content. The product contains up to 50% formaldehyde and less than 1.5% methanol. The main disadvantages of this process are the low catalyst lifetime due to poisoning and the high costs associated with the product

purification. The catalyst is subjected to poisoning by transition metals (chlorine and sulphur compounds) and especially iron dust, resulting in low catalyst lifetime ranging from 2 to 6 months. The catalyst activity can be restored by an electrolytic recovery process. Moreover it is costly to obtain highly concentrated formaldehyde because of the incomplete conversion of methanol and the use of an energy intensive distillation process (Gerberich and Seaman, 1994).

1.2. Metal oxide (Fe-Mo) catalyst process

Most of the newly built formaldehyde plants (more than 70%) are based on the metal oxide catalyst (Fe-Mo) due to near complete conversion of methanol (exceeding 99%) as well as a very high formaldehyde selectivity (95%) and most importantly due to stringent environmental regulations being imposed. In this process, all of the formaldehyde is produced by the exothermic partial oxidation of methanol (eq.1) essentially at atmospheric pressures and temperatures of 250-400°C. Overall plant yields are 88-92% (Gerberich and Seaman, 1994).

Generally, a multitubular non-adiabatic packed bed reactor, with the heat transfer fluid flowing on the shell side, is used. The feed to the reactor is lean in methanol and rich in oxygen. However, if the oxygen in the reactor is reduced to 10% by substituting tail gas for air, it has been demonstrated that the methanol content in the feed can be increased to 9-12%, thus reducing the flow rate through the reactor gases and associated compression costs. Using this operation mode, up to 80% of the tail gas can be recycled in the steady state such that only 20% must be incinerated to destroy the small amounts of side products. The most significant advantage of this process is that products containing typically 50% formaldehyde with less than 1% methanol can be produced directly without distillation. Moreover, catalyst life is between one to two years (Gerberich and Seaman, 1994).

In this work the application of a novel membrane assisted fluidized bed reactor for the partial oxidation of methanol to formaldehyde over a Fe-Mo catalyst is studied. Due to the excellent mixing and heat transfer characteristics of fluidized reactors, operation at much higher methanol concentration is possible without safety problems associated with heat removal or explosion dangers, thereby increasing the reactor productivity. For the development of this novel reactor concept an accurate, complete and consistent description of the reaction kinetics of all chemical transformation steps, valid

over a wide range of operating conditions, especially at higher methanol concentrations (>> 6%) is required. This is the main objective of the research reported in this chapter.

The main chemical transformations prevailing during partial oxidation of methanol are: methanol to formaldehyde, formaldehyde to CO, dimethyl ether (DME) from methanol and dimethoxymethane (DMM) from formaldehyde and methanol. Several authors have studied the kinetics of the methanol partial oxidation to formaldehyde over a Fe-Mo catalyst. However, most of the previous work was limited to the formation of formaldehyde only and not much attention was paid to the formation of side products, viz. CO, DME and DMM. Moreover, all the kinetics data reported in the literature were measured at low methanol concentrations (maximum 6%). Also, most of the previous kinetic studies have been carried out either in a basket type of reactor or an integral reactor, where it is difficult to completely exclude mass and heat transfer limitations due to the highly exothermic nature of this reaction system. In order to avoid problems in the interpretation of the experimental data due to temperature and/or concentration gradients and to achieve reliable intrinsic kinetics, a gradient-less (differential) reactor was used in this work. Before going into details of the experimental set-up, experimental procedure and experimental results, a brief literature survey on the reaction kinetics of the aforementioned reactions is given below.

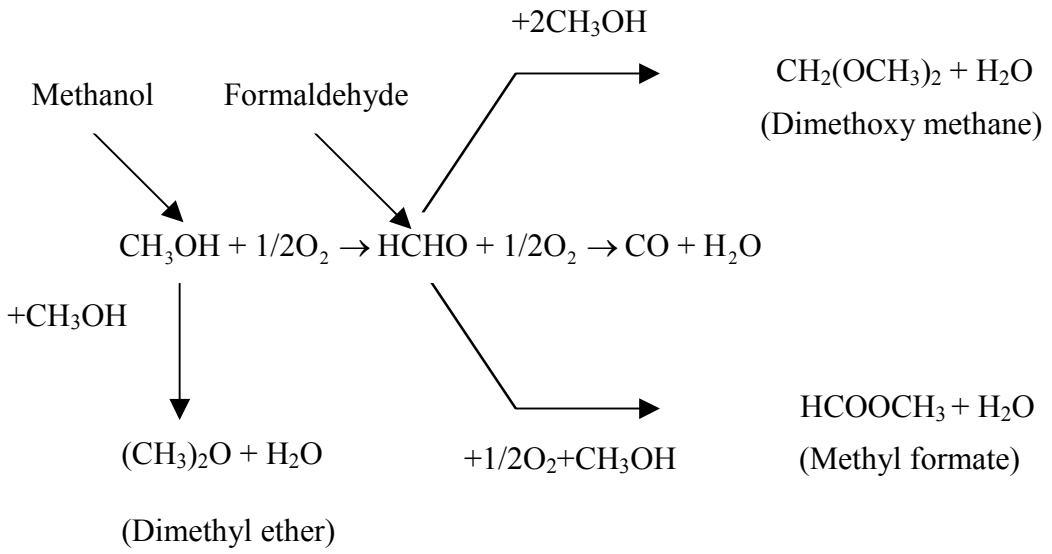

Figure 1. Reaction scheme of main reaction and side reactions during partial oxidation of methanol.

2. Literature overview

Over the last decade several authors have studied the kinetics of the partial oxidation of methanol to formaldehyde. Jiru et al. (1964) suggested a redox mechanism similar to the one adopted by Mars and van Krevelen (1954) for description of the oxidation of aromatic hydrocarbons over vanadium pentoxide. Edward et al. (1977) studied this reaction in a recycle reactor over Fe-Mo catalyst, and they showed that mass and heat transfer limitations disguise the obtained kinetic data at temperatures exceeding 280°C. Furthermore, in another paper Jiru et al. (1966) studied the influence of the reaction products on the reaction rate. According to them, the formaldehyde concentration affects the reaction rate, while the water concentration does not. On the other hand Pernicone et al. (1968) observed a significant effect of water, decreasing the reaction rate.

Santacesaria et al. (1981) performed methanol partial oxidation in a CSTR reactor by operating at a temperature below 250°C to avoid transport limitations. They used different criteria to select the most suitable kinetics model to describe the oxidation of methanol to formaldehyde over an iron molybdate catalyst. Their criteria were in order of importance: (a) the values of the parameters must have physical significance, (b) the model must fit the experimental runs and (c) the number of parameters must be increased only when significant improvements are obtained in satisfying the preceding criteria. They confirmed the redox mechanism for this reaction. Moreover they observed that the presence of water lowers the rate of reaction by reducing the number of available active centers on the catalyst. Furthermore, they found that the amount of DMM decreased with an increase in the residence time, which could be explained by taking into account the gas phase equilibrium of the following reaction:

$$CH_2O + 2CH_3OH \rightleftarrows CH_2(OCH_3)_2 + H_2O \quad K_{DMM}^{eq} = \left[\frac{P_{g,DMM} P_{g,H_2O}}{P_{g,CH_3OH}^2 P_{g,HCHO}} \right]_{eq} \qquad (3)$$

Based on thermodynamic calculations, using the data reported in Stull et al. (1969), they estimated a value of 0.2 for the equilibrium constant K_{DMM}^{eq} at 500 K. The formation of DMM at low contact time could be explained by assuming that DMM is formed according to Eq. 3 and that the desorption of DMM is faster than that of formaldehyde. This hypothesis agrees well with the findings of Edwards et al. (1977), who also found that a temperature increase decreases the formation of all the by-products.

Schwedock et al. (1989) carried out a comprehensive study of the partial oxidation of methanol in a packed bed reactor. They reported the results of a large number of high-quality steady state and transient kinetic experiments. These include a large number of measurements taken at different temperatures during transient operation, measurements at different composition at several locations in the bed under steady state conditions, and data spanning a wide range of reactor operating conditions. Several comprehensive non-sequential non-linear parameter estimation schemes were used together with sophisticated steady state and dynamic models to determine model parameters. For partial oxidation of methanol, they found activation energy of 71.13-79.42 kJ/mol with a reaction order of one half in methanol. However they concluded that a redox rate expression was needed to describe the kinetics of carbon monoxide production. Activation energies reported for this reaction were in the range of 41.8-71.13 kcal/mol.

Edwards et al. (1977) investigated the partial oxidation of methanol in a mixed flow reactor at atmospheric pressure using lean methanol-air mixtures. Steady state reaction rates were obtained over a commercial iron molybdate catalyst at temperatures ranging from 170 to 367°C. Their work contributed further to the knowledge on the reaction kinetics, with particular emphasis on the role of the adsorbed methoxyl intermediates. Furthermore, they suggested that at low methanol partial pressures the rate equation of Mars and van Krevelen (1954) may be satisfactory, but for high conversions the effect of water must be included, as proposed earlier by Evmenenko and Gorokhovataskii (1969). They observed that the reaction was first order in methanol at low concentrations followed by saturation of the surface and shift of the rate-determining step to desorption, especially at low temperatures. They also confirmed the rate inhibition by other reaction products.

Pernicone et al. (1968) found a marked inhibiting effect of water on the reaction rate for the formaldehyde formation, especially at low water partial pressures. Their experimental results could be explained in terms of competitive adsorption of water and methanol on the free active catalyst surface. Surface acidity seemed to be important and the competitive adsorption could be explained on the basis of a higher basicity of water than methanol. The influence of water on the formaldehyde formation rate was not observed by previous researchers because of the use of a recycle reactor or CSTR reactor and hence at relatively high water concentrations.

Recently Holstein and Machiels (1996) studied the kinetics of the methanol oxidation to formaldehyde over an iron molybdenum oxide catalyst in a continuous flow reactor with external recycling at temperatures of 200-300°C. The kinetics of the reaction could be well described by a power law rate expression, with the power of the methanol, oxygen and water partial pressures equal to 0.94±0.06, 0.1±0.05 and –0.45±0.07 respectively. The measured activation energy was 98 ± 6 kJ/mol. When product inhibition by water vapour was not taken into account in their rate expression, the apparent reaction orders in methanol and oxygen and the activation energies were all lower than the true values. They also reported that methanol chemisorbs dissociatively to form methoxy and hydroxyl groups, and additionally that the rate-determining step was the decomposition of the methoxy intermediate. Product inhibition was suggested to occur through kinetic coupling, whereby water vapour chemisorbs dissociatively to form hydroxyl groups, which reduce the steady state concentration of the methoxy groups on the catalyst surface by reacting with them to form methanol.

More recently, Diakov et al. (2002) experimentally investigated the kinetics of methanol partial oxidation to formaldehyde and formaldehyde partial oxidation to carbon monoxide. With a plug flow reactor model they demonstrated that the methanol reaction order for the formaldehyde formation reaction is one half and the oxygen reaction order is zero. For CO formation, first order in the formaldehyde concentration was found. They found peculiar maxima in the carbon monoxide formation as a function of oxygen partial pressure, which they described with a bimolecular Langmuir-Hinshelwood type of kinetics for oxygen. The apparent activation energy was found to be 146 kJ/mol for the formaldehyde formation reaction and 72 kJ/mol for the CO formation reaction.

In order to develop an accurate description of the reaction kinetics, a kinetic study has been carried on the methanol partial oxidation reaction system, where the experiments have been performed in a differential reactor in order to obtain kinetic data not affected by transport limitations and over a wide range of methanol, oxygen and water concentrations in the feed stream.

Before presenting and discussing the experimental results, first the experimental set-up and the experimental procedure to determine the reaction kinetics is described in the next section.

3. Experimental

A differential reactor has been designed to determine reaction kinetics over a commercial Fe-Mo catalyst. First the kinetics reactor and the experimental set-up are described. Then the experimental procedure used to determine the reaction kinetics is presented with special attention to ensure that the kinetics can be determined free of mass and heat transfer limitations.

3.1. Experimental set-up

The partial oxidation of methanol was performed over a commercial Fe-Mo catalyst kindly provided by Perstorp. The original catalyst was available in the form of hollow cylindrical pellets having a height of 2.4-2.8 mm, an internal diameter- 2.4-2.6 mm, an outer diameter- 4.8-5.2 mm and a surface area of 6 m^2/g. The catalyst was crushed to the size of 220-300 micron particles. 0.11 g of this crushed catalyst was placed into a differential quartz reactor having a 5 mm inner diameter. The detailed experimental set-up is shown in Figure 2. Inlet and exit gas temperatures were measured with a transversing thermocouple. The reactor temperature was set and controlled by heaters. The reactor was fed with a preheated air, methanol and nitrogen gas mixture. Methanol was fed by saturating nitrogen via a liquid methanol bubbler. Isothermal conditions in the bubbler were maintained by circulating hot water on the shell side.

The pressure and temperature of the bubbler were measured digitally to set the methanol concentration in the feed. The feed concentration was analyzed accurately with a Varian 3400 gas chromatograph having thermal conductivity detector. A Molsieve-5A column was used for the separation of oxygen, nitrogen and carbon monoxide and Hayesep-T column was used to separate the formaldehyde, methanol, water, dimethyl ether and dimethoxymethane mixture. Helium was used as a carrier gas and temperature programmed analysis was carried out at 60-160°C. Special precautions were taken to avoid condensation of methanol and polymerization of formaldehyde to para-formaldehyde by tracing the lines from the outlet of the reactor to the outlet of the gas chromatograph at 135 °C.

The partial oxidation of formaldehyde to CO was performed over the same Fe-Mo catalyst in a dual catalyst bed differential reactor, where first bed was used to convert methanol into formaldehyde at relatively low temperatures (integrally), which was subsequently converted to CO in the second bed (differentially). The feed stream

compositions to the to the second bed could be measured before raising the temperature of the second catalyst bed to the desired reactor temperature, where the temperature of the second bed was maintained low enough to be virtually catalytically inactive and still avoid condensation of water and polymerization of formaldehyde. Temperature of the reactor was controlled as mentioned above and the same analysis system was used.

The partial oxidation of methanol to formaldehyde was studied in the temperature range of 220-260°C, whereas the partial oxidation of formaldehyde was studied in the temperature range of 250-290°C, since the catalyst was relatively inactive for this consecutive reaction at these low temperatures and even with a relatively large amount of catalyst (2 g), which is almost 20 times the amount used in methanol partial oxidation experiments. All the kinetic runs have been performed at near atmospheric conditions. Reactor flow rates and catalyst size have been chosen in such a way that transport limitations could be ruled out.

Secondary products such as dimethyl ether, dimethoxymethane and in few cases traces of methyl formate were also detected during the partial oxidation of methanol other than formaldehyde and water. No carbon monoxide and carbon dioxide was detected in the experiments for the partial oxidation of methanol, whereas carbon monoxide was the only product of the formaldehyde oxidation.

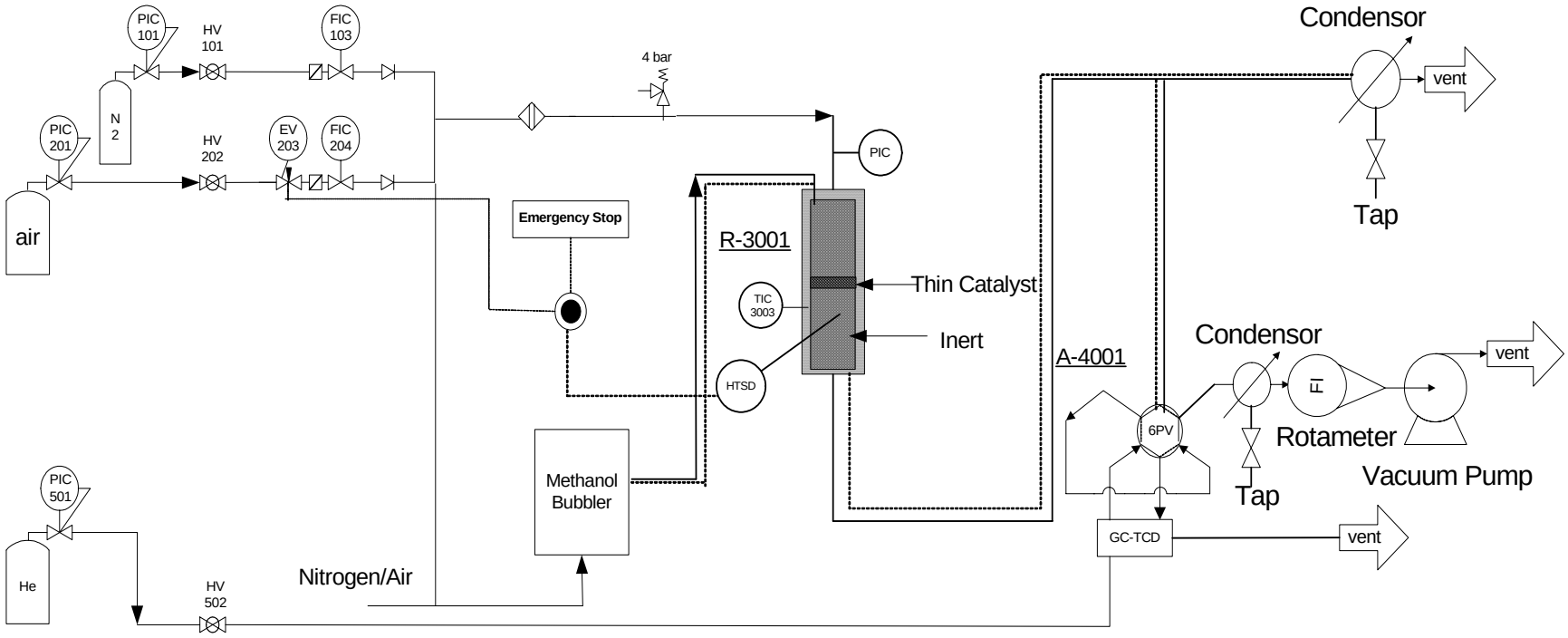

PIC - pressure indicator and control	FIC - Flow indicator and controller
EV - emergency valve	GC-TCD - gas chromatograph with thermal conductivity detector
TIC - temperature indicator and controller	6PV- six port valve
HTSD - high temperature shut down	HV- manual valve

Figure 2. Schematic diagram of the experimental setup.

3.2. Experimental procedure

The partial oxidation of methanol to formaldehyde was performed over an industrial Fe-Mo catalyst with steady state experiments. The catalyst activity as well as the reproducibility of the measurements were regularly checked by performing a standard experiment with the same methanol and oxygen concentrations at the same temperature and residence time during the kinetic research. The total carbon balance was always satisfied within 6%. Before presenting and discussing the experimental results it is demonstrated that the kinetic experiments were carried out in absence of mass and heat transfer limitations.

3.2.1. Absence of temperature and concentration gradients in the kinetics reactor

Through differential reactor operation i.e. at low reactant conversions, typically less than 5-10%, intra-reactor temperature gradients are avoided. A small amount of catalyst was used to assure a low conversion level so that the temperature, pressure and composition through the thin catalyst bed are almost constant. The axial variation of the temperature was measured by transversing a thermocouple through the catalyst bed. The maximum measured temperature difference between the inlet and exit gas streams was only 2°C.

Generally interphase temperature gradients are more difficult to overcome than intraparticle temperature gradients. The fundamental reason for this is the relatively low thermal conductivity of the exterior fluid surrounding the catalyst particles compared to the relatively high thermal conductivity of the catalyst particle itself. Considering intraparticle transfer limitations, concentration gradients are generally more important than temperature gradients. The most effective way to reduce the inter and intra particle temperature and concentration gradients is to reduce the particle size while still avoiding pressure drop problems. This has been investigated experimentally using two different particle sizes but keeping all other operating conditions identical for two different feed concentrations of methanol (see Figure 3). The absence of an influence of the particle size on the conversion rate demonstrates that the system is kinetically controlled.

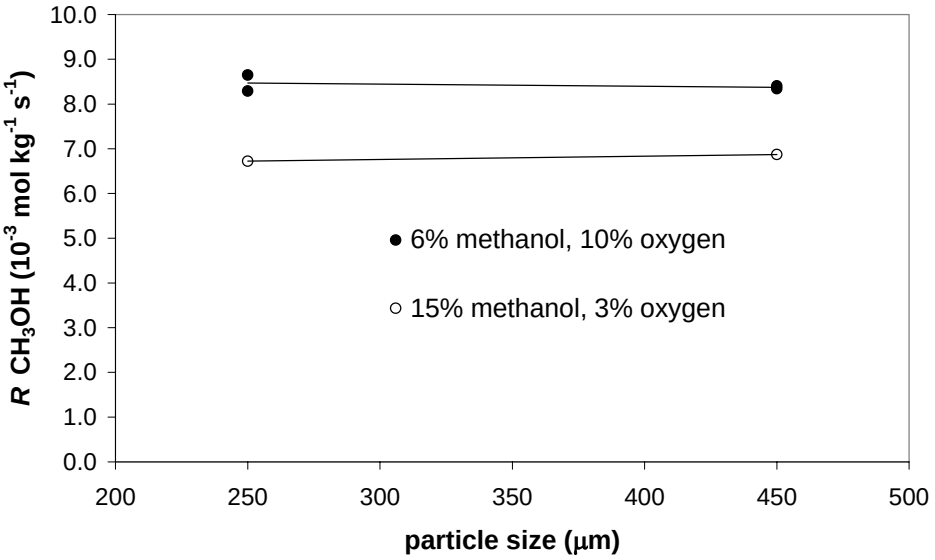

Figure 3. Methanol conversion rate dependency on catalyst particle size at 250°C.

Furthermore, experiments have been carried out where the gas residence time was varied by changing the catalyst mass or the gas flow rate. The results of these experiments are presented in Figure 4, showing a linear dependence of the conversion as a function of the gas residence time. This also demonstrates the differential and isothermal operation of the reactor.

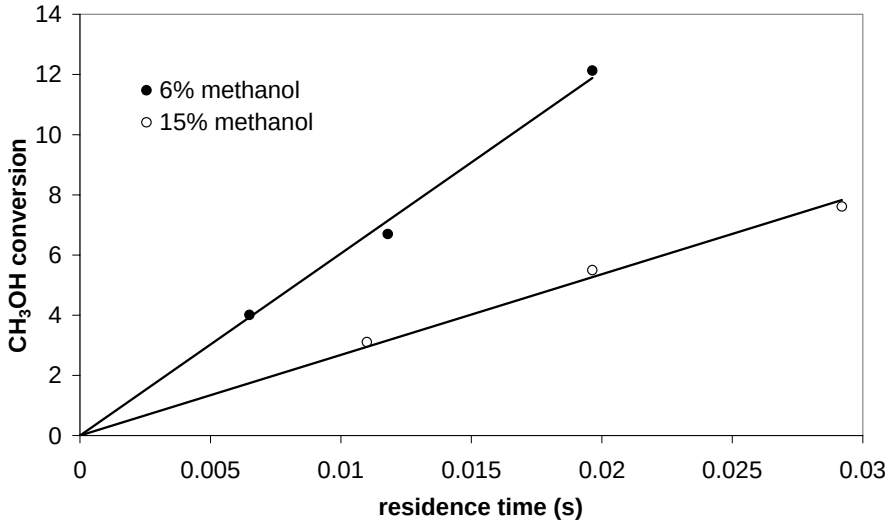

Figure 4. Methanol conversion dependency on residence time at 5% oxygen in the feed, 0.11 g of catalyst and 250°C.

The presence of mass transfer limitations can also be inferred by experimentally determining the apparent activation energy. In case of a gas-solid reaction, if the apparent activation energy is less than 20 kJ/mol, mass transfer limitations could play a role. In our case the experimentally determined apparent activation energy was 85.1 kJ/mol for the methanol partial oxidation to formaldehyde. This value agrees very well with the values found by Santacesaria et al. (1981) (80.25 kJ/mol) and Edwards et al. (1977) (81.5 kJ/mol).

4. Experimental results

In order to investigate the influences of methanol and oxygen concentration and the catalyst temperature on the reaction rate of methanol partial oxidation and the influences of the concentration of formaldehyde and oxygen and the catalyst temperature on the formaldehyde partial oxidation rate, steady state reaction rates for several series of experiments have been carried out. The overview of the experimental conditions is given in Table 1. By appropriate choice of the gas residence time differential reactor operation could be assured.

Table 1. Overview of experimental program.

Reaction	Series	T (°C)	Gas composition (inlet mole percentage)	
			Methanol (%)	Oxygen (%)
Methanol partial oxidation to formaldehyde	1	230-260	2-10	10
	2	230-260	2-15	5
	3	230-260	6	0.4-10
	4	230-260	15	1-5
Formaldehyde partial oxidation to CO	1	250-290	0.7-7.5	5
	2	250-290	3.5	1-15

Firstly, the experimental results for the steady state methanol partial oxidation to formaldehyde and the influence of water are described and secondly, those for the formaldehyde partial oxidation to carbon monoxide are described. Furthermore, from the selectivity data information on the kinetics of the most important side reactions during the partial oxidation of methanol is deduced.

4.1. Methanol partial oxidation to formaldehyde

In Figures 5-10 the steady state formaldehyde production rates during methanol partial oxidation are given as a function of composition and temperature. In these figures the results of the kinetic rate expressions derived in the next section have also been included.

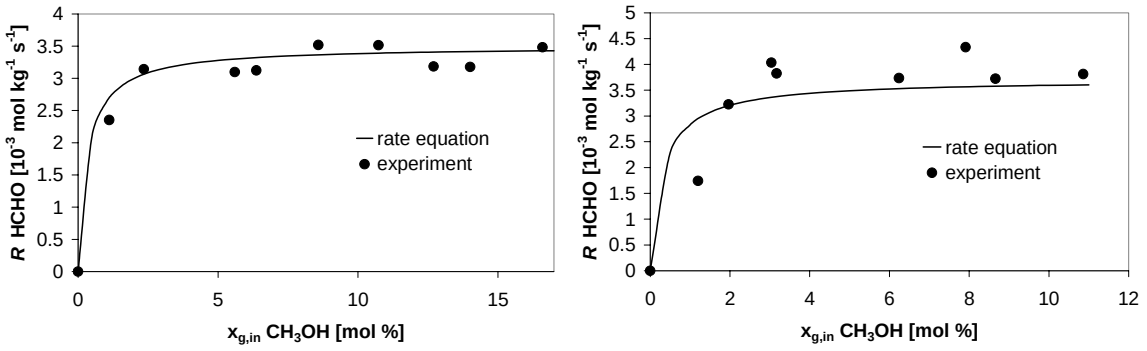

(a) (b)

Figure 5. Formaldehyde production rate as a function of the methanol inlet concentration at 230°C; (a) 5% oxygen and (b) 10% oxygen.

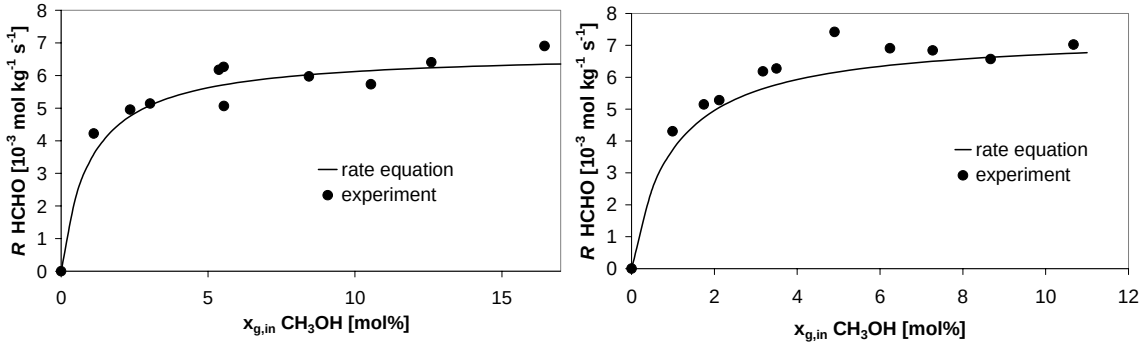

(a) (b)

Figure 6. Formaldehyde production rate as a function of the methanol inlet concentration at 250°C; (a) 5% oxygen and (b) 10% oxygen.

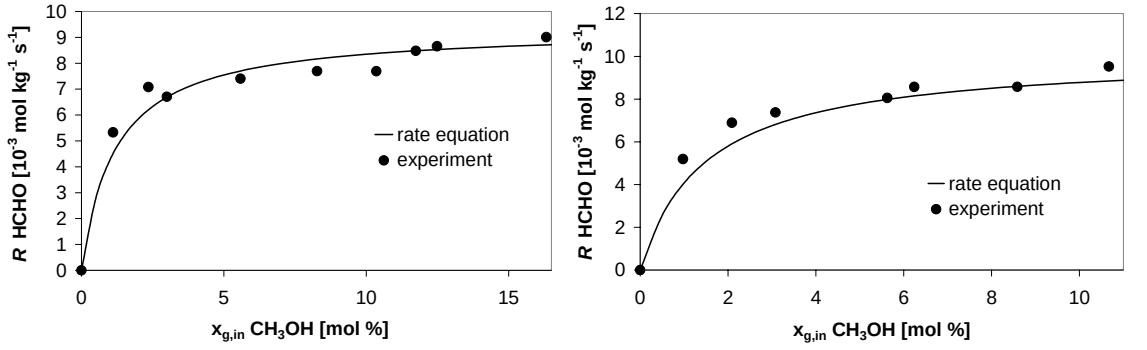

(a) (b)

Figure 7. Formaldehyde production rate as a function of the methanol inlet concentration at 260°C; (a) 5% oxygen and (b) 10% oxygen.

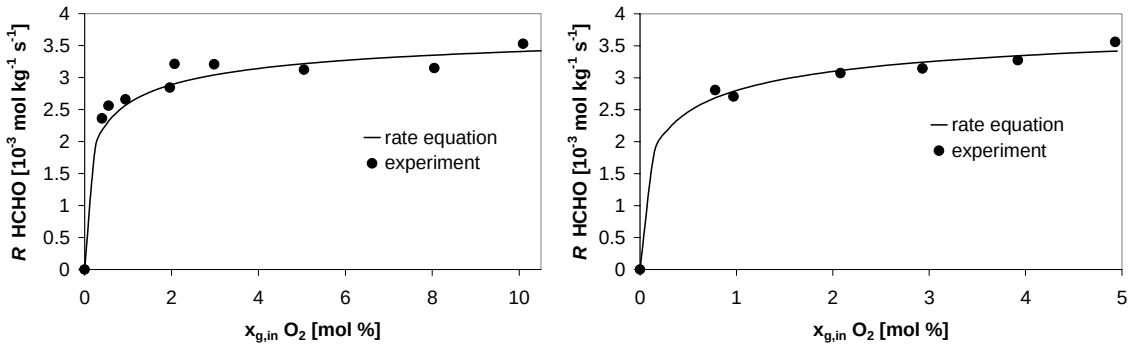

(a) (b)

Figure 8. Formaldehyde production rate as a function of the oxygen inlet concentration at 230°C; (a) 6% Methanol and (b) 15% Methanol.

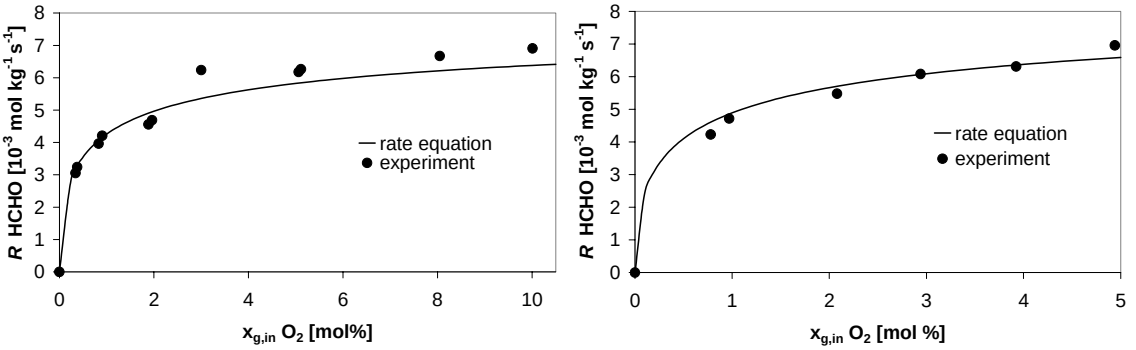

(a) (b)

Figure 9. Formaldehyde production rate as a function of the oxygen inlet concentration at 250°C; (a) 6% Methanol and (b) 15% Methanol.

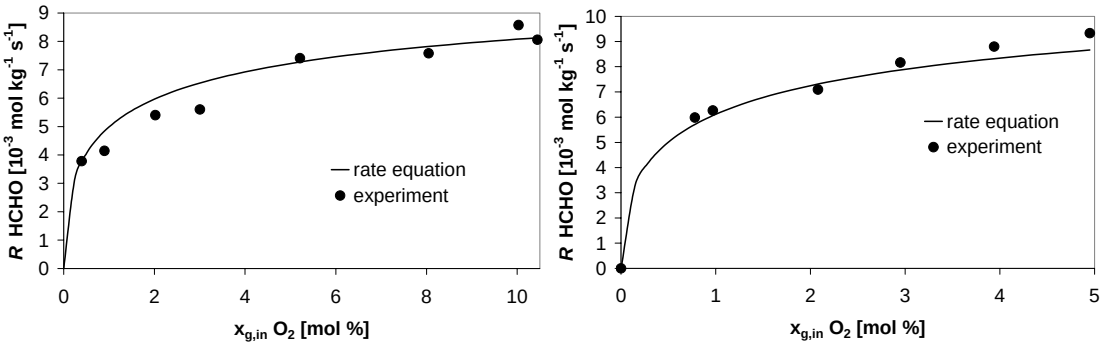

(a) (b)

Figure 10. Formaldehyde production rate as a function of the oxygen inlet concentration at 260°C; (a) 6% Methanol and (b) 15% Methanol.

The following important observations can be discerned from the experimental results:

1. The methanol partial oxidation rate at a fixed oxygen concentration shows linear dependence on the methanol concentration at low methanol concentrations. The reaction rate increases with the methanol inlet concentration at least up to a methanol inlet concentration of about 5% and then reaches a plateau (see Figures 5-7), following Langmuir type kinetics for methanol. These figures also show the temperature dependency of the reaction rate and it can be seen that the plateau in the reaction rate is reached at higher methanol concentrations at higher temperatures, showing temperature effect on the methanol adsorption.

2. The methanol partial oxidation also exhibits Langmuir type kinetics with the oxygen inlet concentration at a fixed methanol concentration (Figures 8-10).

4.2. Dependency of the methanol partial oxidation rate on the water concentration

Many studies have shown the effect of water on the methanol partial oxidation reaction rate (Edwards et al., 1977; Santacesaria et al., 1981; Pernicone et al., 1968). Additional experiments were performed to quantify the effect of water on the decrease of the methanol partial oxidation reaction rate. In Figures 11-16 the steady state formaldehyde production rates during methanol partial oxidation in the presence of water are given as a function of inlet composition and temperature. Again, in these figures the results of the kinetic rate expressions derived in the next section are also shown.

The following important observations can be made from the experimental results:

1. A marked inhibition effect of the water on the reaction rate to formaldehyde can be seen from Figures 11 and 12.

2. From Figures 13 and 16, it is clear that the effect of water on the formaldehyde formation rate is more pronounced at lower water partial pressures and slowly becomes independent of water concentration. However, the inhibition effect of water is larger at lower temperatures. Similar results were obtained by Pernicone et al. (1968).

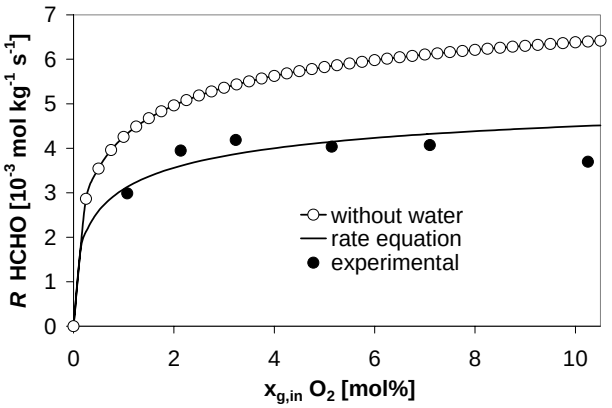

Figure 11. Formaldehyde production rate as a function of the oxygen inlet concentration at 6% methanol, 2.5% water and 250°C.

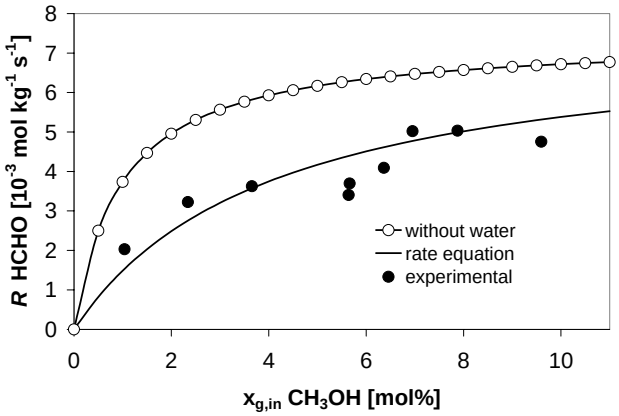

Figure 12. Formaldehyde production rate as a function of the methanol inlet concentration at 10% oxygen, 2.5% water and 250°C.

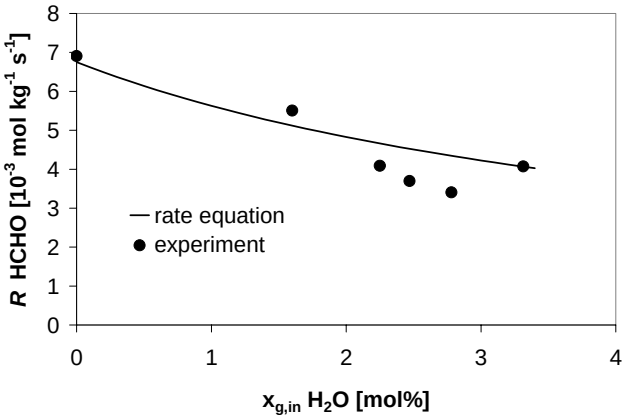

Figure 13. Formaldehyde production rate as a function of the water inlet concentration at 10% oxygen, 6% methanol and 250°C.

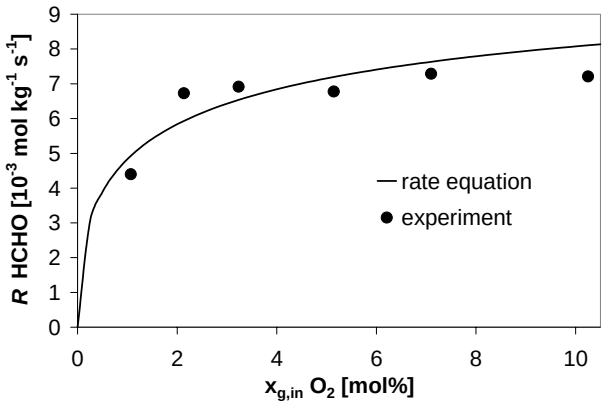

Figure 14. Formaldehyde production rate as a function of the oxygen inlet concentration at 6% methanol, 2.5% water and 270°C.

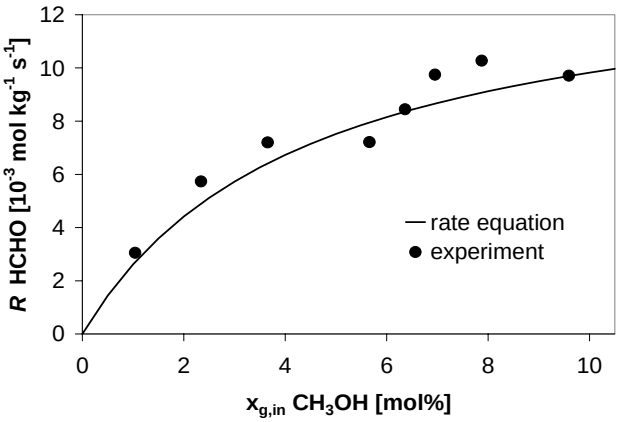

Figure 15. Formaldehyde production rate as a function of the methanol inlet concentration at 10% oxygen, 2.5% water and 270°C.

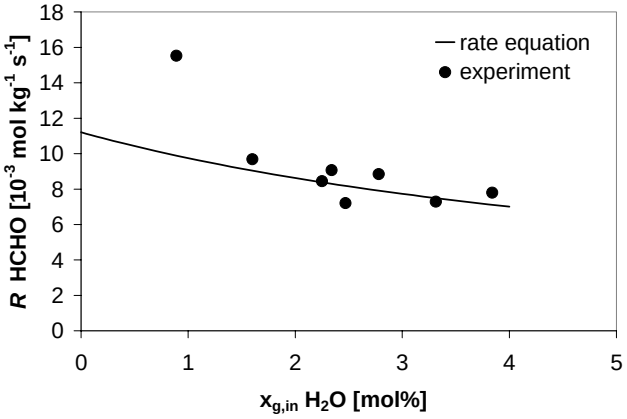

Figure 16. Formaldehyde production rate as a function of the water inlet concentration at 10% oxygen, 6% methanol and 270°C.

4.3. Formaldehyde partial oxidation to CO

In Figures 17-19 the steady state CO formation rates from formaldehyde are given given as a function of composition and temperature. In these figures the results of the kinetic rate expressions derived in the next section have been included again.

The following important observations can be noted from the experimental results:

1. The CO formation rate from formaldehyde oxidation at constant oxygen concentration increases linearly with formaldehyde concentration indicating a first order in the formaldehyde concentration.

2. The CO formation rate from formaldehyde oxidation at constant formaldehyde concentration shows Langmuir Hinshelwood type kinetics for oxygen, similar to the one observed for the methanol oxidation to formaldehyde.

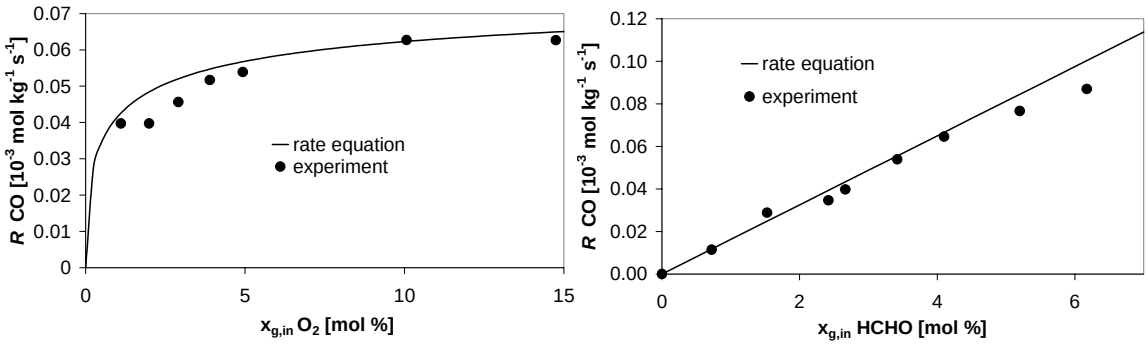

(a) (b)

Figure 17. Carbon monoxide production rate at 250°C; (a) as a function of the oxygen inlet concentration at 3.5% formaldehyde and (b) as a function of the formaldehyde inlet concentration at 5% oxygen.

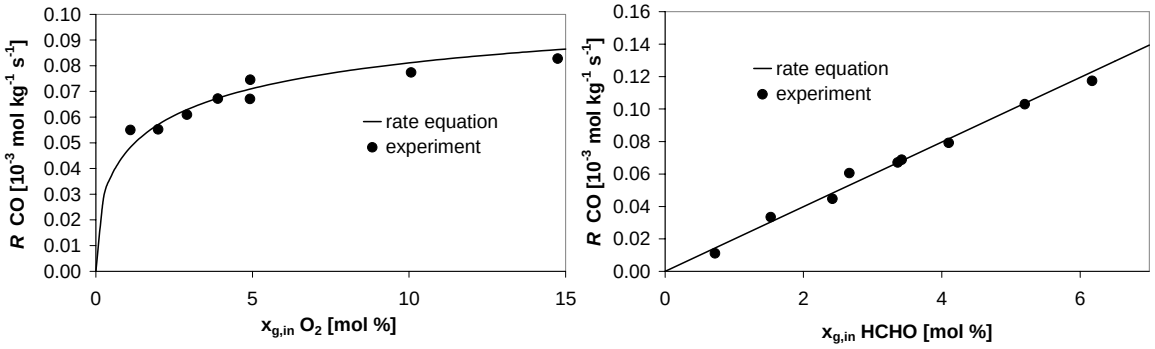

(a) (b)

Figure 18. Carbon monoxide production rate at 270°C; (a) as a function of the oxygen inlet concentration at 3.5% formaldehyde and (b) as a function of the formaldehyde inlet concentration at 5% oxygen.

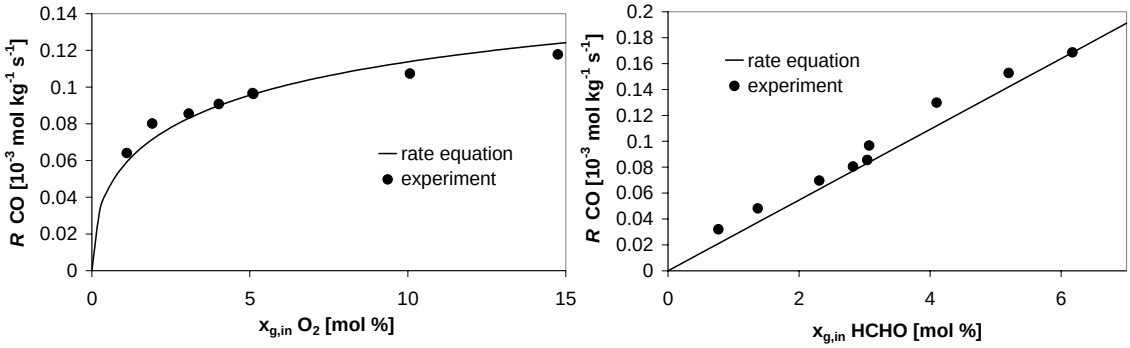

(a) (b)

Figure 19. Carbon monoxide production rate at 290°C; (a) as a function of the oxygen inlet concentration at 3.5% formaldehyde and (b) as a function of the formaldehyde inlet concentration at 5% oxygen.

4.4. Side reactions during the methanol partial oxidation

Only dimethyl ether and dimethoxymethane were detected at the exit stream from the reactor as side products. In very few cases traces of methyl formate were also observed. Since a differential reactor was used to determine the kinetics, the methanol conversion to these side products was extremely low (< 0.5% in most cases) which lead to some scatter in the experimental data. However, rate expressions for these side reactions can be derived in the next section based on these results (selectivity data) and their predictions have been included in the figures.

4.4.1. Dimethyl ether formation

Since methanol is the only reactant leading to the formation of dimethyl ether, steady state dimethyl ether formation rates as a function of methanol inlet concentration at various temperatures were plotted in Figures 20 to 22. The most important conclusion discerned from these figures is that the dimethyl ether formation rate increases approximately linearly with the methanol concentration.

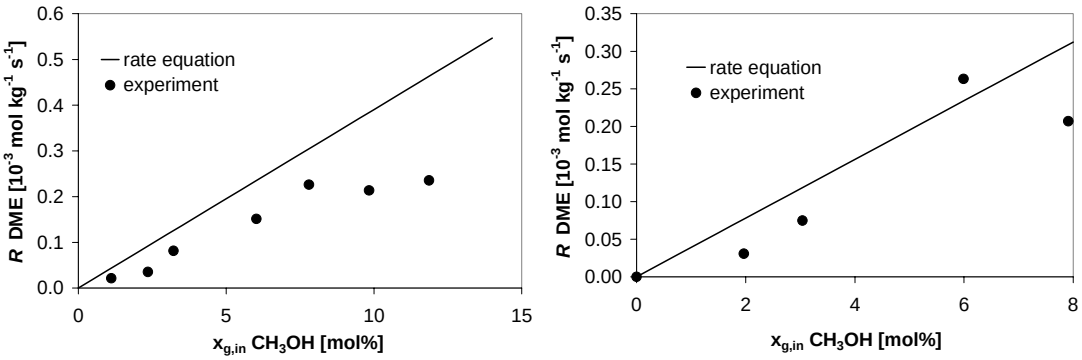

(a) (b)

Figure 20. Dimethyl ether production rate as a function of the methanol inlet concentration at 230°C; (a) 5% oxygen and (b) 10% oxygen.

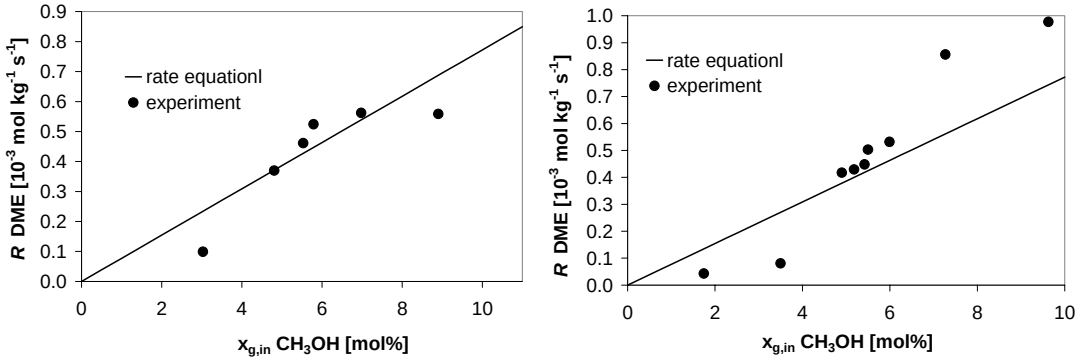

(a) (b)

Figure 21. Dimethyl ether production rate as a function of the methanol inlet concentration at 250°C; (a) 5% oxygen and (b) 10% oxygen.

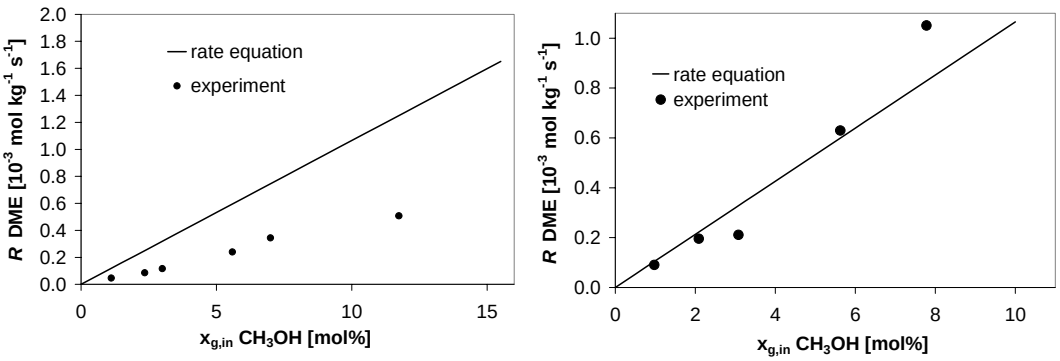

(a) (b)

Figure 22. Dimethyl ether production rate as a function of the methanol inlet concentration at 260°C; (a) 5% oxygen and (b) 10% oxygen.

4.4.2. Dimethoxymethane formation

The dimethoxymethane formation rate is a function of the methanol as well as the formaldehyde concentration. Since this reaction was not studied separately, steady state dimethoxymethane formation rates over formaldehyde partial pressure were plotted as a function of the methanol concentration at various temperatures to check the dependency of the methanol concentration on the dimethoxymethane formation rates (see Figures 23 to 25). The average formaldehyde concentration between the inlet and exit of the reactor has been used in these graphs. The solid lines show the linear dependency of the dimethoxymethane formation rate on methanol concentration and formaldehyde concentration.

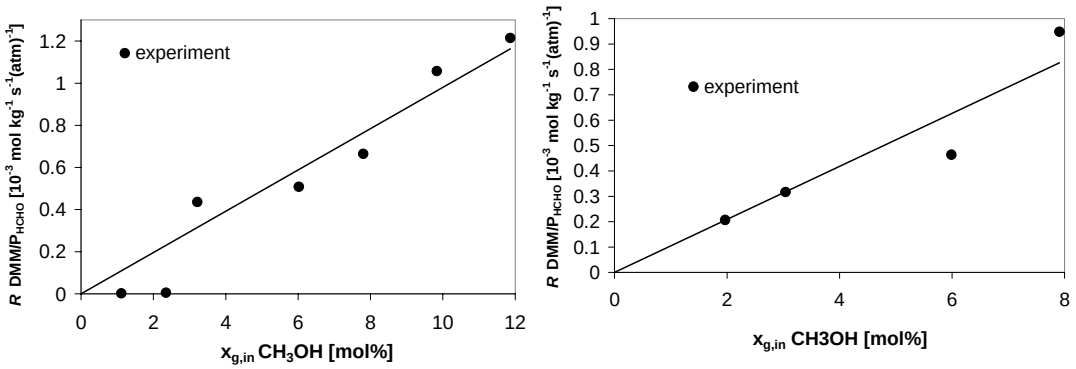

(a) (b)

Figure 23. Dimethoxymethane production rate over formaldehyde partial pressure as a function of the methanol inlet concentration at 230°C; (a) 5% oxygen and (b) 10% oxygen.

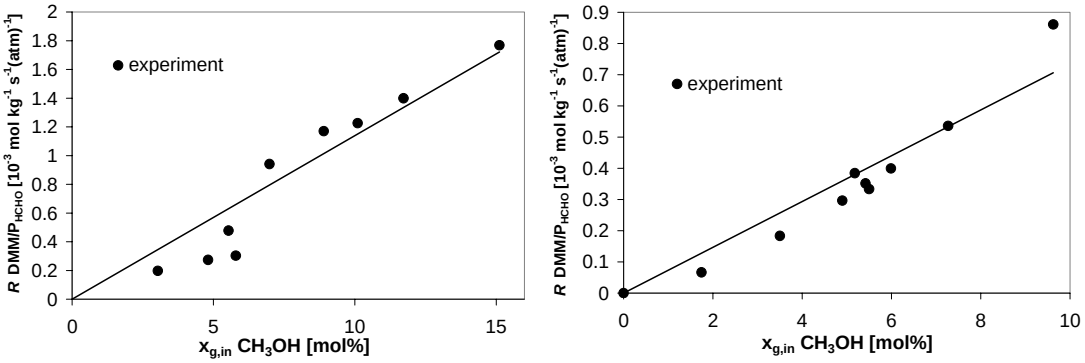

(a) (b)

Figure 24. Dimethoxymethane production rate over formaldehyde partial pressure as a function of the methanol inlet concentration at 250°C; (a) 5% oxygen and (b) 10% oxygen.

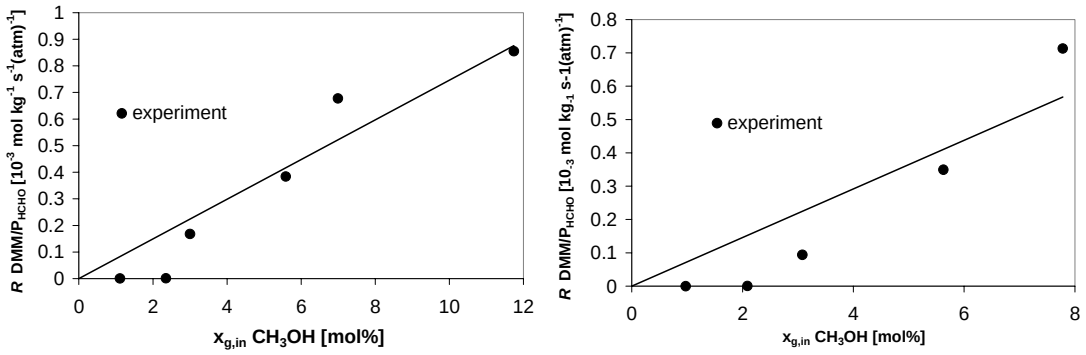

(a) (b)

Figure 25. Dimethoxymethane production rate over formaldehyde partial pressure as a function of the methanol inlet concentration at 260°C; (a) 5% oxygen and (b) 10% oxygen.

5. Derivation of rate equations

In this section we will focus on the derivation of steady state reaction rate equations for the methanol partial oxidation and its most important side reactions, viz. formaldehyde partial oxidation and DME and DMM formation, which can capture all experimental observations reported in the previous section as a function of composition and temperature over a wide concentration and temperature range. A brief description of a plausible reaction mechanism for the various reactions taking place on the Fe-Mo catalyst is given first, followed by the main conclusions drawn from our experimental study on the concentration and temperature dependency of the reaction rates.

Pernicone et al. (1969) have proposed that oxygen doubly bonded to Mo interacts with methanol to form:

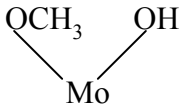

(4)

The $–OCH_3$ group is then dehydrogenated to adsorb formaldehyde; the removed hydrogen adsorbs on the neighbouring oxygen atom to form a –OH group. Abstraction of hydrogen from the $–OCH_3$ group to form adsorbed formaldehyde also takes place at neighbouring sites (Santacesaria et al., 1981, Machiels, 1982, Farneth et al., 1986, Edwards et al., 1977, Allison and Goddard, 1985, Goddard, 1985, Niwa et al., 1981). As formaldehyde and water desorb, the exposed Mo sites are reoxidised by the mobile oxygen from the lattice. The –OH groups desorb slowly and the water in the gas phase being a strong inhibitor, reacts with Mo–O to form:

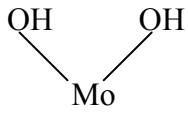

(5)

At low methanol partial pressures the rate equation of Mars and van Krevelen (1954) may be satisfactory (Jiru et al 1964), but at high conversions the effect of water must be included, as proposed by Evmenenko and Gorokhovatskii (1969), where water and methanol are supposed to possess similar adsorption characteristics at the Fe-Mo catalyst surface.

With this reaction mechanism the observed dependencies of the reaction rates on the composition and temperature can be explained. The experiments showed that methanol partial oxidation reaction rate to formaldehyde consists of two contributions, where the first contribution is a function of the methanol concentration and the second contribution depends on the oxygen concentration. Both these contributions are important for the, moreover both show Langmuir-Hinshelwood type dependency.

Furthermore, the formaldehyde oxidation rate to carbon monoxide also consists of two contributions. The first is proportional to the formaldehyde concentration and the second is proportional to the oxygen concentration. The formaldehyde concentration dependency is linear with gas phase formaldehyde concentration, whereas the oxygen exhibits again a Langmuir-Hinshelwood type dependency. The oxygen contribution terms for the formaldehyde oxidation are the same as those of the methanol oxidation, as expected. Inhibitive effect of methanol concentration on the carbon monoxide formation rate was not studied experimentally in our investigation, in order to avoid complications in the interpretation of the results (by methanol conversion to formaldehyde). This inhibitive effect of methanol and water has been accounted for in the rate expressions, though not verified experimentally (see Table 2).

For the rates of the side reactions, it can be concluded that the dimethyl ether formation rate is proportional to the methanol concentration because it does not need oxidative dehydrogenation and it leaves the catalyst in the oxidized state. Its formation is more probable at higher conversions when there is less oxygen available on the surface than at low conversion (Edwards et al. 1977).

The adsorbed formaldehyde at the catalyst surface may further react with methanol to form methyl formate, which further reacts with gas phase methanol to form dimethoxymethane (methylal). Hence, dimethoxymethane formation consists of two contributions. The first is proportional to the formaldehyde concentration and the second is proportional to the methanol concentration. Both these contributions show a linear dependency with respect to formaldehyde and methanol, respectively. Dimethoxymethane is especially formed at lower conversions (high methanol partial pressures) through the reaction of desorbed oxygenates with methanol.

The experimental results for all the reaction rates could be well described with a rate equation based on the assumption that the reaction takes place between two adsorbed species at two different sites, and that gas phase oxygen adsorbs dissociatively on the lattice oxygen sites of the catalyst. Furthermore, it has been assumed that adsorption equilibria are established instantaneously. For the dimethyl ether and dimethoxymethane formation reactions the thermodynamic equilibrium calculated using Aspen plus, was included (see Table 2). The reaction rate equations are given in Table 2.

For the rate constants and adsorption coefficients an Arhenius type dependency was assumed. The pre-exponential constants, adsorption coefficients and their activation energies have been fitted using the Levenberg-Marquardt method and results are given in Table 3. Initial guesses of all the constants were found by first minimising the standard deviation of the predicted and experimentally obtained reaction rates in Microsoft Excel. Since the water concentration influences the reaction rates and equilibrium reactions also play a role, the system of differential equations for mass balances of all the components describing the axial concentration profiles of all the components in detail, was integrated, followed by minimization of the standard deviation using the Levenberg-Marquardt method. Results of these integral analyses are plotted as parity plots for all these reactions and are shown in Figures 26 to 29. The results of these rate equations have been presented before in the figures showing the experimental results (Figures 5-25). With the derived kinetic model the reaction rates could be well described within typically 5-15%

accuracy (deviation). Different reaction orders in the Langmuir-Hinshelwood rate expressions did not significantly improve the description of the reaction rates. Finally, it is again emphasized that it is not possible to deduce the precise reaction mechanisms from the experiments described in this work, which was outside the scope of this study. The reaction rates should be considered as overall lumped reactions, accounting for possibly several elementary reaction steps.

Table 2. Reaction rate equations for the methanol oxidation *(R_{HCHO})*, formaldehyde oxidation *(R_{CO})*, dimethyl ether formation *(R_{DME})* and dimethoxymethane formation *(R_{DMM})*.

$CH_3OH + 1/2\ O_2 \xrightarrow{R_{HCHO}} HCHO + H_2O$	$R_{HCHO} = k_{HCHO}\theta_{CH_3OH}\theta_{O_2}$ (6)
$HCHO + 1/2\ O_2 \xrightarrow{R_{CO}} CO + H_2O$	$R_{CO} = k_{CO}\theta_{HCHO}\theta_{O_2}$ (7)
$2CH_3OH \underset{}{\overset{R_{DME}}{\rightleftarrows}} CH_3\text{-}O\text{-}CH_3 + H_2O$	$R_{DME} = k_{DME,f}P_{g,CH_3OH} - \frac{k_{DME,f}}{K_{DME}^{eq}}\frac{P_{g,DME}P_{g,H_2O}}{P_{g,CH_3OH}}$ (8)
$2CH_3OH + HCHO \overset{R_{DMM}}{\rightleftarrows} CH_2\text{-}(O\text{-}CH_3)_2 + H_2O$	$R_{DMM} = k_{DMM,f}P_{g,HCHO}P_{g,CH_3OH} - \frac{k_{DMM,f}}{K_{DMM}^{eq}}\frac{P_{g,DMM}P_{g,H_2O}}{P_{g,CH_3OH}}$ (9)

where

$$\theta_{CH_3OH} = \frac{K_{CH_3OH}P_{g,CH_3OH}}{1 + K_{CH_3OH}P_{g,CH_3OH} + K_{H_2O}P_{g,H_2O}} \quad (10)$$

$$\theta_{O_2} = \frac{K_{O_2}P_{g,O_2}^{1/2}}{1 + K_{O_2}P_{g,O_2}^{1/2}} \quad (11)$$

$$\theta_{HCHO} = \frac{P_{HCHO}}{1 + K_{CH_3OH}P_{g,CH_3OH} + K_{H_2O}P_{g,H_2O}} \quad (12)$$

$$K_{DME}^{eq} = \left[\frac{P_{g,DME}P_{g,H_2O}}{P_{g,CH_3OH}^2}\right]_{eq} \quad (13)$$

$$K_{DMM}^{eq} = \left[\frac{P_{g,DMM}P_{g,H_2O}}{P_{g,CH_3OH}^2 P_{g,HCHO}}\right]_{eq} \quad (14)$$

Table 3. Reaction rate constants (pre-exponential constants and activation energies) and equilibrium constants for the Methanol (R_{HCHO}) and formaldehyde partial oxidation (R_{CO}), dimethyl ether formation (R_{DME}) and dimethoxymethane formation (R_{DMM}).

	K_{CH_3OH}	[atm^{-1}]	$3.12\cdot10^{-4}$	E_{CH_3OH}	[kJ.mole^{-1}]	- 54.19
(R_{HCHO})	K_{O_2}	[atm$^{-1/2}$]	$1.23\cdot10^{-5}$	E_{O_2}	[kJ.mole^{-1}]	- 60.72
	K_{H_2O}	[atm^{-1}]	$2.30\cdot10^{2}$	E_{H_2O}	[kJ.mole^{-1}]	11.45
	k_{HCHO}	[mol kg^{-1}s^{-1}]	$2.08\cdot10^{6}$	E_{HCHO}	[kJ.mole^{-1}]	84.00
(R_{CO})	k_{CO}	[mol kg^{-1} atm^{-1} s^{-1}]	$1.32\cdot10^{2}$	E_{CO}	[kJ.mole^{-1}]	47.00
(R_{DME})	$k_{DME,f}$	[mol kg^{-1}atm^{-1}s^{-1}]	$1.9\cdot10^{5}$	$E_{DME,f}$	[kJ.mole^{-1}]	77.00
$K_{DME}^{eq} = \exp(-2.2158 + 2606.8/T)$						
(R_{DMM})	$k_{DMM,f}$	[mol kg^{-1}atm^{-2}s^{-1}]	$2.58\cdot10^{-6}$	$E_{DMM,f}$	[kJ.mole^{-1}]	-56.50
$K_{DMM}^{eq} = \exp(-20.416 + 9346.8/T)$						

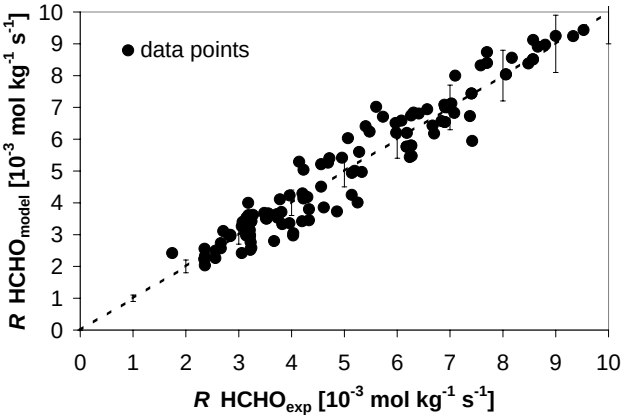

Figure 26. Parity plot for formaldehyde formation rate.

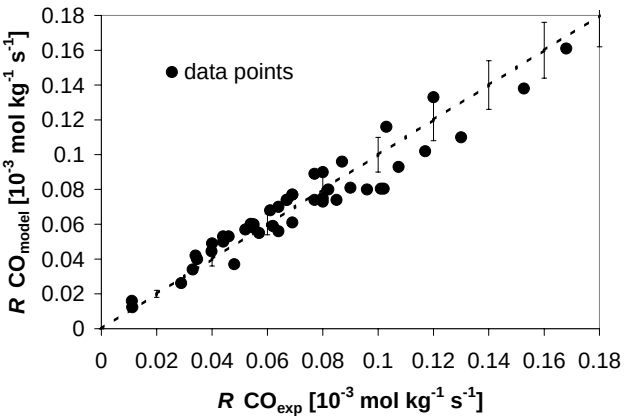

Figure 27. Parity plot for carbon monoxide formation rate.

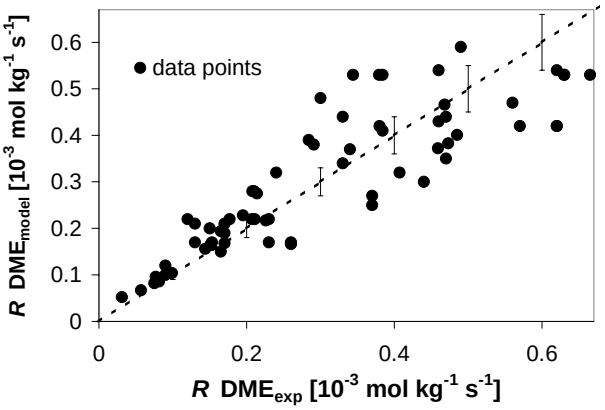

Figure 28. Parity plot for dimethyl ether formation rate.

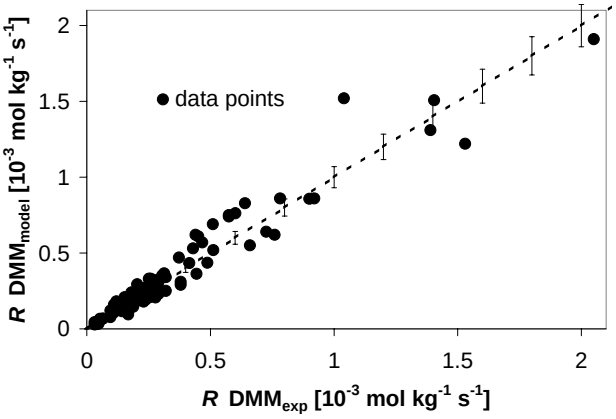

Figure 29. Parity plot for dimethoxymethane formation rate.

6. Discussion

In this section the experimental results for the steady state reaction rates are discussed. The experimentally determined reaction rates for methanol partial oxidation to formaldehyde and formaldehyde partial oxidation to carbon monoxide are compared with literature values. No rate expressions were found in literature for the formation of DME and DMM during the methanol partial oxidation reaction.

6.1. Comparison of the methanol partial oxidation reaction rate with literature

The experimentally determined steady state methanol partial oxidation reaction rate is compared with kinetic data given by Edwards et al. (1977) and Santacesaria et al. (1981). Edwards et al. (1977) have shown that reaction is approximately first order in methanol at low methanol concentrations followed by a saturation of the surface and shift of the rate-determining step to desorption of formaldehyde, especially at low temperatures. In our measurements as well, the rate is approximately first order in methanol at low methanol concentrations and then becomes almost independent of the methanol concentration because of catalyst surface saturation (Langmuir - Hinshelwood mechanism). Our reaction rates compared to those of Santacesaria et al. (1981) were higher by factor of 1.5 to 3.0 at the same experimental conditions. These differences in catalytic activity are relatively small and can be expected considering the different sources of the catalyst. Experimental data from Edwards et al. (1977) for similar experimental conditions showed reactions rates lower by factor of 2 compared to our experimental data. Experimentally determined apparent activation energy for partial oxidation of formaldehyde in this study was 85.1 kJ/mole (see Figure 30), which agrees very with the literature values (see Table 4). Also Table 5 shows various rate expressions taken from the literature and rate expressions obtained in our studies. The correlations proposed in literature correspond to lower methanol concentrations of about 6% and a temperature range of 230-275 °C.

Table 4. Comparison of the apparent activation energy for formaldehyde formation.

No.	Activation energy (kJ/mol)	Reference
1	81.5	Edwards et al. (1977)
2	80.3	Santacesaria et al. (1981)
3	85.11	Present work (experimental)

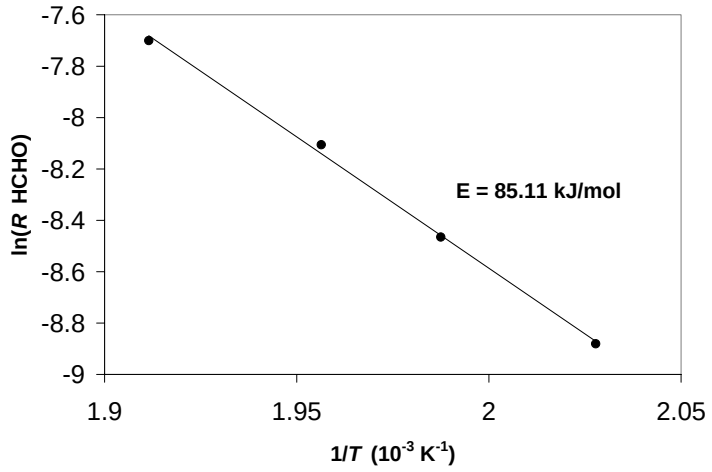

Figure 30. Arhenius plot for the formaldehyde production rate at 6% methanol and 10% oxygen in the feed.

Table 5. Steady state rate expressions for formaldehyde formation.

No.	Rate expression	Reference
1	$k_{CH_3OH} P_{CH_3OH}^{1/2} \Big/ \left(1+\left(K_{CH_3OH}.P_{CH_3OH}\right)^{1/2}\right)$	Schwedock et al. (1989)
2	$P_{CH_3OH}^{1/2} P_{O_2}^{1/2} \Big/ \left(K_{CH_3OH} P_{CH_3OH}^{1/2} + K_{O_2} P_{O_2}^{1/2}\right)$	Dente et al. (1964)
3	$\frac{K_{CH_3OH} K_{O_2} P_{CH_3OH} P_{O_2}^{1/2}}{K_{CH_3OH} P_{CH_3OH} + K_{O_2} P_{O_2}^{1/2}} . \frac{1}{(1+K_{H_2O} P_{H_2O})}$	Santacesaria et al. (1981)
4	$k_{CH_3OH} \frac{P_{CH_3OH}}{1+K_{CH_3OH}.P_{CH_3OH}+K_{H_2O}.P_{H_2O}} . \frac{P_{O_2}}{1+K_{O_2}.P_{O_2}}$	Evmenenko and Gorokhovatskii (1969)
5	$\frac{k_{CH_3OH} K_{CH_3OH} P_{CH_3OH} K_{O_2} P_{O_2}^{1/2}}{\left(1+K_{CH_3OH} P_{CH_3OH} + K_{H_2O} P_{H_2O}\right)\left(1+K_{O_2} P_{O_2}^{1/2}\right)}$	Present work

6.2. Comparison of formaldehyde partial oxidation reaction rate with literature

The experimentally determined steady state formaldehyde partial oxidation reaction rates have been compared with literature data from Edwards et al. (1977), Diakov et al. (2002), Schwedock et al. (1989) and Dente et al. (1964). Although the formaldehyde partial oxidation is the most important consecutive reaction during the partial oxidation of methanol to formaldehyde, relatively few kinetic studies have been carried out to determine the reaction rate for this reaction. Experimental data for the carbon monoxide formation from Edwards et al. (1977) match quite well our experimental results. The reported linear dependency of the reaction rate with formaldehyde concentration was also obtained in our study. Also, Diakov et al. (2002) and Dente et al. (1964) observed the linear dependency of the carbon monoxide reaction rates with formaldehyde concentrations. In fact Dente et al. (1964) found a pseudo first order in the formaldehyde concentration for the carbon monoxide formation rates at high oxygen concentrations, which is consistent with our experimental results, which showed that the oxygen dependency of the carbon monoxide formation rate diminishes at oxygen concentrations exceeding 5% (dissociative Langmuir-Hinshelwood isotherm). Most of the kinetic studies performed in the past have been carried out at relatively high oxygen concentrations because the industrial process itself used to be operated under oxygen rich conditions. Schwedock et al. (1989) found that a redox rate expression was needed for the kinetics of carbon monoxide production. Table 6 compares our activation energy with the literature data. Moreover, in Table 7, the reported reaction rate expressions for carbon monoxide formation have been summarised for comparison with the rate expression proposed in this work.

Table 6. Comparison of the apparent activation energy for the carbon monoxide formation rate from formaldehyde.

No.	Activation energy (kJ/mol)	Reference
1	78.7	Edwards et al. (1977)
2	41.84 - 71.13	Schwedock et al. (1989)
3	72.4	Diakov et al. (2002)
4	47.0	Present work

Table 7. Steady state rate expressions for carbon monoxide formation.

No.	Rate expression	Reference
1	$k_{CO}P_{HCHO}^{1/2}\Big/\left(1+\left(K_{HCHO}.P_{HCHO}\right)^{1/2}\right)$	Schwedock et al. (1989)
2	$K_{CO}P_{HCHO}$	Dente et al. (1964)
3	$k_{CO}P_{HCHO}P_{O_2}\Big/\left(1+K_{O_2}P_{O_2}\right)^2$	Diakov et al. (2002)
4	$k_{CO}P_{HCHO}P_{O_2}$	Bipin and Popov (1968)
5	$\dfrac{k_{CO}P_{HCHO}K_{O_2}P_{O_2}^{0.5}}{\left(1+K_{O_2}P_{O_2}^{0.5}\right)}$	Present work

7. Summary and conclusions

To assess the potential of the membrane assisted fluidized bed reactor for methanol partial oxidation, reliable and accurate reaction rate expressions are required for the methanol partial oxidation reaction and the most important side reactions, which are valid over very wide concentration and temperature ranges. The reaction rates published in literature are often valid only for relatively small methanol concentrations and high oxygen concentrations. Moreover, never before all the reaction rates for all relevant reactions were measured and fitted simultaneously.

Methanol partial oxidation and formaldehyde partial oxidation reaction rates and their most important side reactions were measured over a commercial Fe-Mo catalyst in a differentially operated reactor, which made it possible to perform the experiments in the kinetically controlled regime. The absence of temperature and concentration gradients was demonstrated experimentally. For both the methanol partial oxidation and formaldehyde partial oxidation steady state reaction rates were determined over a wide range of temperatures and concentrations. The observed reaction rates and activation energies for the methanol partial oxidation as well as for the formaldehyde partial oxidation correspond well with reported literature values. From the selectivity data information about the kinetics of the most important side reactions was deduced. Only the formation of dimethyl ether and dimethoxymethane needed to be considered as side reactions, taking the thermodynamic equilibrium into account.

From the experiments it was concluded that the methanol partial oxidation as well as the formaldehyde partial oxidation consist of two contributions each. The methanol partial oxidation reaction rate is approximately first order in methanol concentration at low concentrations but reaches a maximum plateau value suggesting the saturation of the active catalyst sites. The methanol partial oxidation reaction rate also shows a Langmuir-Hinshelwood dependency for the oxygen concentration, suggesting that only lattice oxygen takes part in the reaction, which is deoxidized by the gas phase oxygen once consumed in the surface reactions. The formaldehyde partial oxidation reaction rate was first order in the formaldehyde concentration, indicating small concentration of the adsorbed formaldehyde, whereas the oxygen dependency was identical to that for the methanol oxidation reaction rate, indicating that same oxygen sites were taking part in both the reactions.

For the most important side reactions, i.e. dimethyl ether formation as well as dimethoxymethane formation the forward reaction rates were determined from the selectivity data. The backward reaction rates were obtained from the forward reaction rate and the thermodynamic equilibrium data. Dimethyl ether formation rate (forward reaction) was found to be only dependent on the methanol concentration with first order dependency. The dimethoxymethane formation rate (forward reaction) was found to be linear with the both the formaldehyde and the methanol concentrations.

These experimental observations were interpreted by assuming that the oxidation reactions take place at two different metal oxide sites, one containing adsorbed oxygenates and a second one containing lattice oxygen.

The observed influences of the composition and temperature on the methanol partial oxidation, formaldehyde partial oxidation, dimethyl ether formation and dimethoxymethane formation reaction rates could be well described with rate equations based on the above assumptions (see Table 2 and Table 3). Minimization of the standard deviations of the reaction rates was carried out with Levenberg - Marquard minimization technique, where the axial concentration profiles in the kinetics reactor were accounted for using a plug flow reactor model in order to properly take into account the influence of the water concentration on the reaction rates (even in the differentially operated kinetics reactor).

Finally, the derived rate expressions for the methanol and formaldehyde partial oxidation as well as its most important side reactions provide important information for

the optimization of the process conditions-especially the temperature and methanol and the oxygen concentrations in the methanol partial oxidation reactor, and for the design, development and optimization of the membrane assisted fluidized bed in particular.

Acknowledgement

This research is part of a research program carried out within the Center for Separation Technology, as a cooperation between the University of Twente and TNO, the Netherlands Organization for Applied Scientific Research. The author wishes to thank Beno Knaken for the construction of the set-up and Wim Leppink for the maintenance of the set-up. Also the help by B.G.J Kamp for the GC analysis section is greatly appreciated.

Notations

E	activation energy [kJ·mol^{-1}]
ΔH	reaction enthalpy [kJ·mol^{-1}]
k	reaction rate constant [s^{-1}]
K	adsorption constant
K^{eq}	thermodynamic equilibrium constant
P_i	partial pressure of component i [atm]
R	gas constant [= 8.314 J mol^{-1} K^{-1}]
R_i	reaction rate of component i [mol·kg^{-1}·s^{-1}]
T	temperature [K] or [°C]
x_g	gas phase molar fraction [mol·mol^{-1}]

Greek symbols

θ_i	surface fraction of component i [-]

Subscripts

DME dimethyl ether
DMM dimethoxy methane
eq at thermodynamic equilibrium
exp experimental
f forward reaction
g gas phase
in inlet

References

Allison, J. N. and Goddard, W. A., (1985), J. Catalysis, 92, 127.

Bipin, V. N. and Popov, B. I. (1968), "Oxidation of formaldehyde by atmospheric oxygen on iron-molybdenum oxide catalyst", Kinetics and Catalysis, 9, 510-514.

Davies, P. Donald, R. T. and Harbord, N. H. (1989), "Catalytic oxidations", in Catalyst Handbook, (M. V. Twigg ed., 2nd ed.), Wolfe publishing Ltd., London. , 490.

Dente, M., Poppi, R. and Pasquon, I. (1964), " Cinetica dell'Ossidazione del Metanolo a Formaldeide con catalizzatore a base di ossidi di Fe e Mo.", Chim & Ind., 46, 1326.

Diakov, V., Blackwell, B. and Varma, A. (2002), "Methanol oxidative dehydrogenation in a catalytic packed bed membrane reactor: experiments and model", Chem. Eng. Sci., 57, 1563-1569.

Edwards, J., Nicolaidis, J., Cutlip, M. B. and Bennet, C. O. (1977), " Methanol partial oxidation at low temperatures", J. Catal., 50, 24.

Evmenenko, N. P. and Gorokhovataskii, Ya. B. (1969), Kinet. Katal. 10, 1071.

Farneth, W. E., McCarron, E. M. and Sleight, A. W. (1986), J. Am. Chem. Soc., 108, 2327.

Gerberich, H. R., Seaman, G. C., (1994), "Formaldehyde", in Kirk-Othmer Encyclopedia of Chemical Technology, Vol. 11, 4th edition, Wiley, New York, 929-951.

Goddard, W. A., (1985), Science, 227, 917.

Holstein, W. L. and Machiels, C. J., (1996), " Inhibition of methanol oxidation by water vapour-effect on measured kinetics and relevance to the mechanism", Journal of Catalysis, 162, 118-124.

Jiru, P., Wichterlova, B. and Tichy, J., (1964), Proc. 3rd Cong. Catal., p-199.

Jiru, P., Tichy, J. and Wichterlova, B., (1966), Coll. Czezh. Chem. Commun., 31, 674.

Machiels, C. J., (1982), in "Catalysis Under Transient Conditions", (A. T. Bell and L. L. Hegedus, Eds.), ACS Symposium series, Vol. 178, 239.

Mars, P. and Van Krevelen, D. W., (1954), Chem. Eng. Sci., 3, 41.

Niwa, M., Mizutani, M., Takahashi, M. and Murakami, Y., (1981), J. Catal., 70, 14.

Pernicone, N., Lazzerin, F., Liberti, G. and Lanzavecchia, G., (1968), " The effect of water on the catalytic oxidation of methanol to formaldehyde", J. Catal., 10, 83.

Pernicone, N., Lazzerin, F., Liberti, G. and Lanzavecchia, G., (1969), J. Catal., 14, 391.

Santacesaria, E., Morbidelli, N. and Carra, S. (1981), " Kinetics of the catalytic oxidation of methanol to formaldehyde", Chem. Eng. Sci., 36, 909.

Schwedock, M. J., Windes, L. C. and Ray, W. H., (1989), " Steady state and dynamic modelling of a packed bed reactor for the partial oxidation of methanol to formaldehyde II. Experimental results compared with model predictions", Chem. Eng. Comm., Vol. 78, 45-71.

Stull, D. R., Westrum, E. F. and Sinke, G. C., (1969), The Chemical Thermodynamics of organic compounds. McGraw-Hill, New York.

Chapter 6

Experimental demonstration of membrane assisted fluidized bed reactor for partial oxidation of methanol

Abstract

*A small laboratory scale membrane assisted fluidized bed reactor (*MAFBR*) was constructed in order to experimentally demonstrate the reactor concept for the methanol partial oxidation to formaldehyde. The methanol conversion and product selectivities were measured at various overall fluidization velocities, reactor temperatures, methanol and oxygen overall feed concentrations, ratios of gas fed via membranes and the distributor and the aspect ratios of the fluidized bed.*

With steady state tracer injection experiments it was shown that in the experimental reactor effective compartmentalization was achieved with very low axial gas back-mixing due to the elimination of the macro scale circulation patterns induced by the presence of the membranes and the permeation of gas through the membranes. With an ultrasound technique the RTD of the MAFBR *was determined over wide range of fluidization velocities, enabling quantification of the axial gas back-mixing. The experimental* MAFBR *exhibited approximately plug flow behavior for all the operating conditions used in this investigation.*

Subsequently the MAFBR *was demonstrated successfully for the partial oxidation of methanol to formaldehyde. High methanol conversions and high selectivities to formaldehyde were achieved with safe reactor operation at very high methanol concentrations, much higher than currently used in industrial processes. It was experimentally demonstrated that distributive feeding of oxygen in a* MAFBR *produces an increased overall formaldehyde yield and throughput without pronounced undesirable conversion of formaldehyde to carbon monoxide.*

Finally, a reactor model has been developed considering the MAFBR *as a series of ideally stirred tank reactors consisting of a bubble phase and an emulsion phase, where the addition of gas via the membrane and gas production due to chemical transformations was accounted for. The developed model can be considered as a two-parameter model, namely the number of CISTRs in series, which was determined on basis of separate RTD experiments and the average bubble size, assumed constant throughout the fluidized bed. With the developed model the experimentally observed trends as a function of the operating conditions could be well described.*

1. Introduction

Highly exothermic heterogeneously catalyzed gas phase partial oxidation reactions are an industrially important class of chemical reactions and require carefully designed reactors because of the large amount of heat liberated and the high selectivity requirement for the intermediate product of interest. A new reactor concept is proposed which offers improved reactor safety and higher product throughput via the concept of multifunctionality. Our concept aims to combine the advantages of good heat transfer and gas-solid mixing characteristics of the fluidized bed with the controlled dozing capability of membranes to achieve an inherently safe and isothermal reactor operation. Moreover, this reactor concept is especially interesting for highly exothermic oxidation reactions, where the explosion region of the reactants and products imposes restrictions on the feed concentration of the reactants. Reactor operation can be rendered inherently safe via distributive addition of oxygen, enabling lower local oxygen concentrations in the fluidized bed and thus operation outside the flammability limits of the hydrocarbons.

The behavior of the membrane assisted fluidized bed, i.e., tube to bed heat transfer and gas back-mixing has been studied extensively in Chapter 3 and 4 respectively. In this chapter the feasibility of the reactor concept is investigated experimentally for a model reaction system, the partial oxidation of methanol to formaldehyde for which the kinetics were studied in detail in Chapter 5. In this chapter we aim to demonstrate that the advantages of the fluidized bed and controlled dozing via membrane can indeed be integrated into a single unit, the membrane assisted fluidized bed reactor (MAFBR).

The application of fluidized bed membrane reactors to reactions of industrial importance has been investigated in the recent past. Adris et al., (1991) and (1994), demonstrated that for the steam reforming of natural gas the *in situ* separation and removal of hydrogen via perm-selective thin-walled palladium-based membranes the thermodynamic equilibrium can be overcome leading to increased synthesis gas yields in comparison to the industrial fixed bed steam reformer. Using simulations Abdalla and Elnashaie (1995) showed for the catalytic dehydrogenation of ethyl benzene to styrene and Ostrowski et al. (1998) for the catalytic partial oxidation of methane to synthesis gas that with fluidized bed membrane reactors higher product selectivities could be realized compared to fixed bed reactors. In these studies the insertion of perm-selective hydrogen membranes in the fluidized bed was investigated.

In this chapter the application of porous non-selective ceramic membranes for controlled dozing of air for the partial oxidation of methanol to formaldehyde was studied experimentally in a lab scale membrane assisted fluidized bed demonstration unit. With a two-phase model accounting for gas production due to chemical reaction and permeation through the membranes, the experimental results are interpreted to facilitate understanding of the experimental observations.

Due to financial limitations and restrictions imposed by safety regulations the aspect ratios (height-to-diameter) used in the demonstration unit were significantly higher than those used in the fluidized bed for the heat transfer characteristics and the gas back-mixing studies described in Chapters 3 and 4. Moreover, iron molybdate catalyst particles were used instead of glass particles. Sine the hydrodynamics and therefore gas back-mixing and heat transfer characteristics strongly depend on the aspect ratio of the fluidized bed and the particle properties, additional gas phase back-mixing experiments were carried out to quantify the effective axial dispersion in this reactor. Steady state tracer gas experiments were carried out as described in detail in Chapter 4. Furthermore the gas residence time distribution in the MAFBR was measured with an ultrasound measurement technique (Cents et al., 2003), using helium as tracer gas.

Before presenting and discussing the experimental results, the experimental set-ups and the experimental procedures will be described in the next section.

2. Experimental

This section starts with a description of the MAFBR, followed by a description of experimental set-ups and experimental techniques used to measure the extent of the gas phase back-mixing in the MAFBR. Subsequently, the experimental set-up and procedure for methanol partial oxidation to formaldehyde in the MAFBR is explained in detail.

2.1. Experimental set-ups and procedures

2.1.1. Membrane Assisted Fluidized Bed Reactor (MAFBR)

A square fluidized bed (0.05 m x 0.05 m x 1 m) was constructed from stainless steel and filled to a packed bed height of 0.1 - 0.30 m with a commercial iron molybdate catalyst, kindly provided by Perstorp and crushed and sieved to a diameter range of 75-150 μm, (particle density of 1750 kg/m^3). The bed was equipped with 21 horizontal stainless steel heat transfer tubes (2 mm ID and 3 mm OD) and 21 horizontal ceramic membrane tubes (1.5 mm ID and 2.5 mm OD with a pore size of approximately 0.15 μm), through which gas could be added, arranged in a staggered arrangement with a pitch (horizontal and vertical) of 0.016 m. In Figures 1 and 2a schematic front and side view of the membrane assisted fluidized bed is given, showing the tube arrangement in detail. Uniform fluidization was achieved with a porous plate distributor with a pore size of 10 μm.

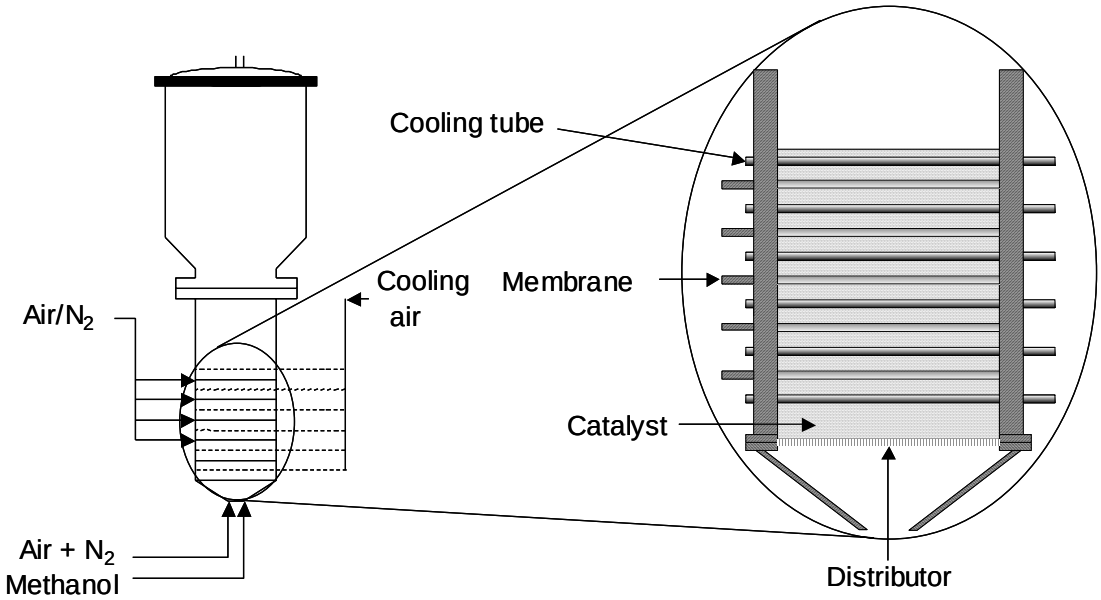

Figure 1. Schematic representation of the Membrane Assisted Fluidized Bed Reactor.

2.1.2. Gas back-mixing in membrane assisted fluidized bed reactor

Firstly, the experimental set-up used to measure the gas back-mixing by steady state tracer gas experiments is shown. Subsequently, the experimental set-up to measure the gas residence time distribution using the ultrasound technique is described.

2.1.2.1. Steady state tracer gas experiments

Figure 2 depicts the details of the experimental set-up used to measure the axial back-mixing in the MAFBR. The measuring technique and the procedures are the same as described in Chapter 4. In these studies the freeboard tracer gas concentration was set to 1%. Fluidization was performed with nitrogen distributed via a porous plate distributor.

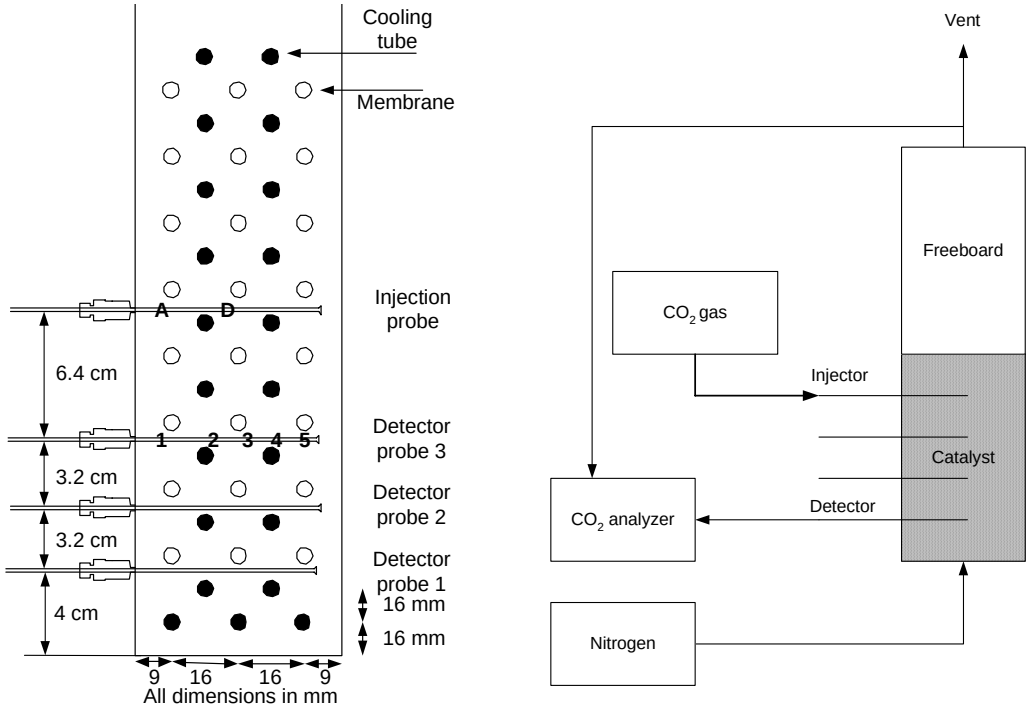

Figure 2. Schematic of the experimental set-up to measure gas back-mixing in the membrane assisted fluidized bed reactor by steady state tracer experiments: (a) detailed side view of the reactor; (b) simplified flow-sheet.

2.1.2.2. Measurement of the gas residence time distribution by an ultrasound technique

The measurement principle is based on the dependency of the speed of sound in a material on the bulk modulus (of elasticity) and the density of this medium. Thus with the ultrasound technique the concentrations of a component in a gas stream can be measured continuously and with a high frequency allowing the measurement of the residence time distribution in systems having a very small average residence time. Details about the technique are discussed in detail by Cents et al. (2003). Helium was selected as the tracer gas, firstly because of its pronounced difference in sound velocity compared to nitrogen (965 vs. 353 m/s at 23 °C) and, secondly because it does not adsorb on the catalyst surface.

The experimental set-up consists of an arbitrary waveform generator (AWG), which sends any desired electric signal to a piezoelectric transducer (T) with a center frequency of 800 kHz. The signal is amplified to a maximum of 44 dB with a variable power amplifier. The transmitting transducer converts the electric signal to a pressure wave that is received in another transducer (R). The converted electric signal is, after 31-dB amplification, acquired with a maximum sampling rate of 2 GS/s ($2 \cdot 10^9$ samples per second) and with 8-bit resolution in a digital oscilloscope. At the same time as the AWG sends the electric signal, a trigger signal is transmitted both to the oscilloscope and to an electrically controlled valve to start tracer injection. In this way, in every measurement, the starting point, t=0, is well defined. Data from the oscilloscope are transferred to a computer using a GPIB interface bus. The overall sampling frequency in this experimental set-up is limited by the data transfer rate and is 33 Hz. Of course, this problem could be overcome, which means that the theoretical maximum sampling frequency is in the order of 10000 Hz. The complete set-up is schematically represented in Figure 3.

Continuously a mixture of helium (10%) and nitrogen mixed in a union tee was fed to the reactor. At a given time the helium flow was stopped, i.e. a step-down for helium tracer gas concentration. The helium concentration was measured continuously at the exit of the reactor using the ultrasound technique. Thus the residence time distribution (RTD) of the tracer gas in the MAFBR could be determined accurately, despite the small average gas residence times. The helium concentration was varied between 5-10% to check the influence of the slight decrease in flow rate on the average residence time of the gas in the fluidized bed, which turned out to be negligible.

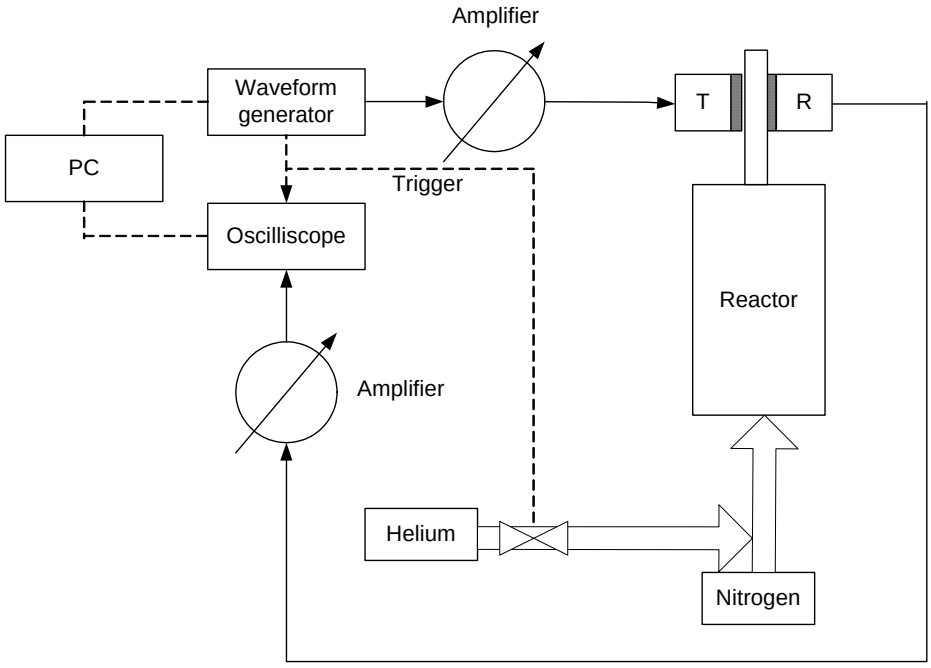

Figure 3. Schematic of the experimental set-up used to measure the gas residence time distribution in the membrane assisted fluidized bed reactor by an ultrasound technique.

2.1.2.3. Interpretation of RTD Measurements

The normalized pulse response function E(t) given by:

$$\int_0^\infty E(t)dt = 1 \tag{1}$$

is related to the step response function F(t) as follows:

$$F(t) = \int_0^t E(t)dt \tag{2}$$

The mean residence time (first moment) can be calculated using either the E or F-function as follows:

$$\bar{t} = \int_0^\infty tE(t)dt = \int_0^t tdF(t) \tag{3}$$

The comparison of the obtained mean residence time with the holding time of the system, defined as $\tau = \frac{V_{gas}}{\Phi_v}$ will yield information on the presence of dead zones and/or by-pass streams that have poor exchange with the main flow passing through the system.

Normally the E-curve is presented using the reduced time and given by:

$$\theta = \frac{t}{\tau} \tag{4}$$

Another important quantity is the spread in residence time, characterized by the variance:

$$\sigma^2 = MO_2 - \left(\bar{t}\right)^2,\ \sigma_\theta^2 = \frac{\sigma^2}{\tau^2},\ N = \frac{1}{\sigma_\theta^2} \tag{5}$$

where the second momentum MO_2 is given by:

$$MO_2 = \int_0^\infty t^2 E(t)dt = 2\int_0^\infty t(1-F(t))dt$$

In our experiments a step function was used as input function, which yields the F-curve as output signal. The RTD-curves obtained were interpreted using a model consisting of a cascade of N ideally mixed tanks of equal volume. Assuming a perfect input stepwise distribution at the inlet, the analytical solution for $F(\theta)$ is given by:

$$F(\theta) = \int_0^\theta \frac{N^N \theta^{N-1}}{(N-1)!} e^{-N\theta} d\theta = \frac{\Gamma_{in}(N, N\theta)}{\Gamma(N)} \tag{6}$$

Involving the complete and incomplete gamma-functions respectively given by:

$$\Gamma(x) = \int_0^\infty u^{x-1} x^{-u} du \tag{7}$$

$$\Gamma_{in}(x,y) = \int_0^y u^{x-1} e^{-u} du \tag{8}$$

The RTD curves obtained were interpreted directly on the basis of the *F* curve using equations 3 and 5 to obtain the number of CISTRs in series *N* and the average residence time $\bar{t}$. The effective axial dispersion coefficient (the Peclet number) is directly related to the number of CISTRs in series via (Westerterp et al. 1993).

$$\mathrm{Pe} = 2N + 2 \text{ for } N<5 \text{ and } \mathrm{Pe} = 2N \text{ for } N>5 \qquad (9)$$

Before actually measuring the RTD in the MAFBR over a range of fluidization velocities with and without gas addition via the membranes, the ultrasound technique was tested for two different single-phase reactors: (a) a reactor vessel with a volume of 1.250 l equipped with a magnetic stirrer to ensure nearly ideal gas-phase mixing (CISTR) and (b) two stainless steel tubular reactors with inner diameters of 20.0 and 18.4 mm and lengths of 2000 and 815 mm, respectively, to approximate plug-flow (PFR) behavior (*Pe* > 50).

2.1.2.4. Validation of the ultrasound technique with single phase model reactors

Figure 7 shows a typical step-down response for the stirred tank. It can be seen that the obtained mean residence time is in very good agreement with the holding time. Several RTD curves were obtained for different gas flow rates and the number of CISTRs obtained varied between 1.0 to 1.3, indicating that the single tank reactor is indeed almost ideally mixed.

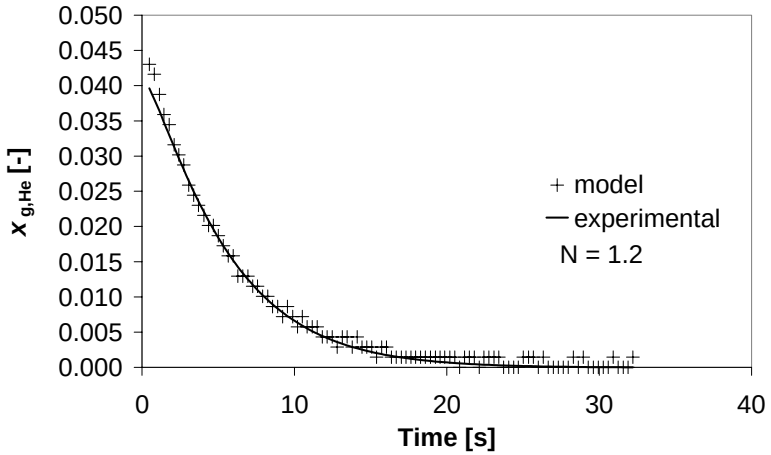

Figure 7. Typical response of a stirred tank reactor to a step-down input ($x_{g,He}$ = mole fraction helium in the outlet gas). Experimental data and the best-fit line (N_{CISTR} model) are plotted.

Moreover, Figure 8 shows a typical measured step-down response for one of the empty tubes used (PRF) and the best fit of the tanks in series model. Figure 9 shows the parity plot of the mean residence time calculated from this model and the actual holding time. As expected the empty tube shows approximately plug flow behavior.

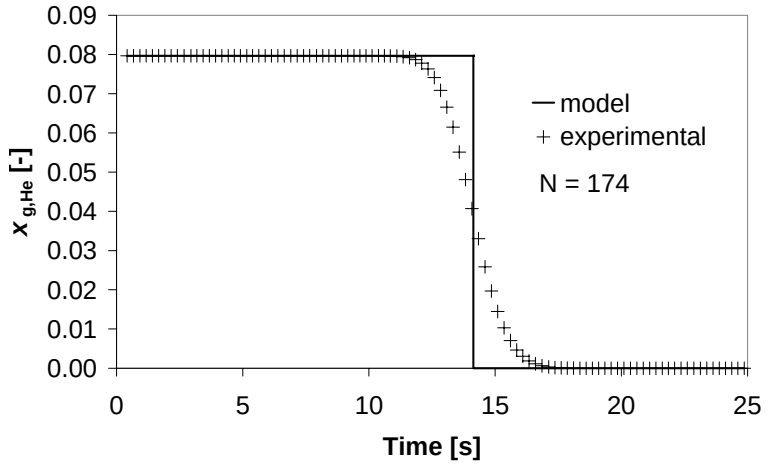

Figure 8. Typical response of one of the PFRs subjected to a step-down input ($x_{g,He}$ = mole fraction helium in the outlet gas). Experimental data and the best-fit line (N_{CISTR} model) are plotted.

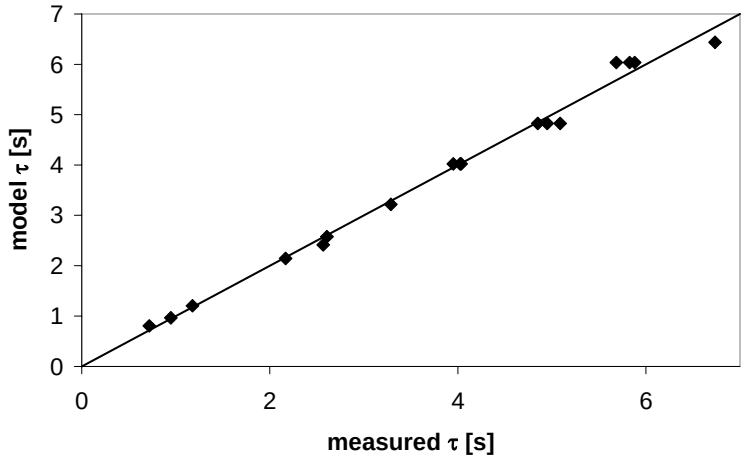

Figure 9. Parity plot of the measured mean residence time and the holding time of the PFR.

On the basis of the results described above, it was concluded that the ultrasound measurement technique was accurate and reliable.

2.1.3. Methanol partial oxidation to formaldehyde

The partial oxidation of methanol was preformed over a commercial Fe-Mo catalyst in a membrane assisted fluidized bed reactor. The original catalyst was available in the form of hollow cylindrical pellets having a height of 2.4-2.8 mm, an internal diameter of 2.4-2.6 mm and an outer diameter of 4.8-5.2 mm and a surface area of 6 m^2/g. The catalyst was crushed to the size of 75-150 μm particles. Typically about 800 gm (for 0.30 m packed bed height) of this crushed catalyst was packed into the square (0.05 m x 0.05 m x 1 m) membrane assisted fluidized bed reactor (see section 2.1). The detailed experimental set-up is shown in Figure. 4. Temperature control of the reactor was accomplished via two thermocouples connected to the heaters, which were fixed on the wall of the reactor. Temperatures inside the reactor were measured at four different axial locations in the catalyst bed and at one location in the freeboard region above the catalyst bed. The reactor was fed with a air, methanol and nitrogen mixture. Methanol was fed via the distributor by saturating nitrogen via a liquid methanol bubbler. Oxygen and nitrogen were also fed via the distributor and additionally via the membranes in case of experiments with membrane permeation. Isothermal conditions in the bubbler were maintained by circulating hot water on the shell side. The pressure and temperature of the bubbler were measured and controlled digitally in order to provide constant methanol concentrations in the feed, which were measured with a Varian 3400 gas chromatograph

equipped with a thermal conductivity detector. A Molsieve-5A column was used for the separation of oxygen, nitrogen and carbon monoxide and a Hayesep-T column was used to separate formaldehyde, methanol, water, dimethyl ether, dimethoxymethane and methyl formate, where Helium was used as a carrier gas and temperature programmed analysis was applied at 60-160°C. The detector signals (chromatograms) were stored in a PC using the data acquisition package Chromatographic Separation for Windows (CSW 32). Special precautions were taken to avoid condensation of methanol and polymerization of formaldehyde to para-formaldehyde by heating the freeboard and outlet of the reactor and the lines to the GC, as well as the outlet of the gas chromatograph at 135 °C. The partial oxidation of methanol to formaldehyde was studied in the temperature range of 250-300 ^{0}C. All the experiments were performed at near atmospheric pressure.

Before the experiments were initiated the reactor was preheated using a heater attached to the membrane-free walls of the reactor. Air was used to fluidize the reactor avoiding temperature gradients in the reactor. The reactor was heated to a temperature well below the desired reactor temperature and the methanol oxidation reaction heat was utilized to reach the final reactor temperature. Subsequently methanol was fed by bubbling nitrogen through the saturator and subsequently the airflow rate was slowly increased to avoid the formation of explosive mixtures and a sudden rise in reactor temperature. For each set of experiments, the feed concentrations were measured by bypassing the feed directly to the GC.

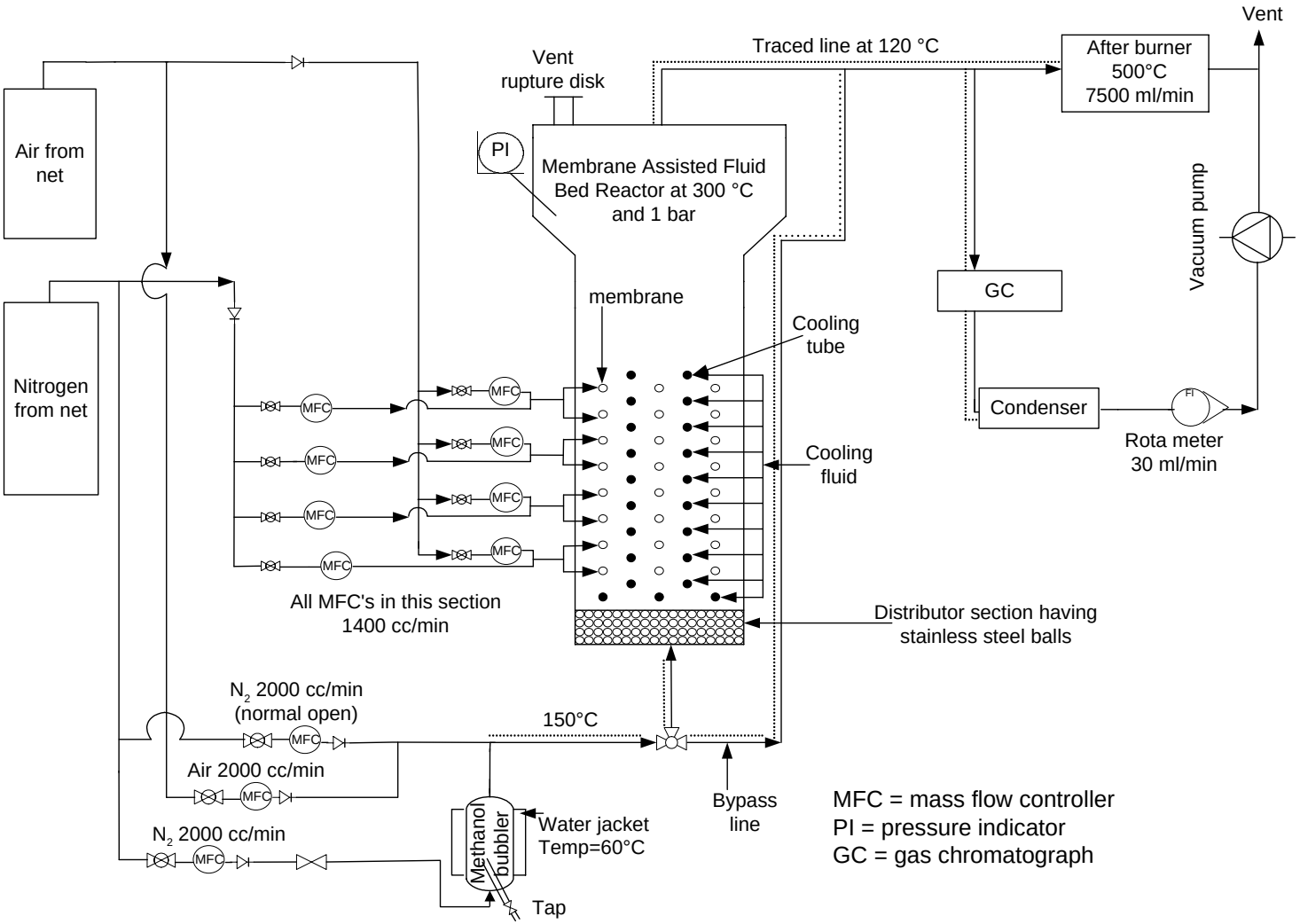

Figure 4. Schematic of the experimental set-up for partial oxidation of methanol to formaldehyde in a MAFBR.

3. Experimental results

In this section the obtained experimental results on the gas back-mixing experiments using steady state tracer gas injection and tracer response experiment using ultrasound technique will be discussed. Subsequently the experimental results obtained for the partial oxidation of methanol over a commercial iron molybdate catalyst will be presented. Finally these results will be interpreted in terms of a two-phase model.

3.1. Gas back-mixing

3.1.1. Steady state tracer injection experiments

In order to investigate the mixing behavior in our lab scale membrane assisted fluidized bed reactor, equipped with horizontal membranes, tracer gas experiments similar to those presented in Chapter 4 were performed. Steady state lateral concentration profiles were measured at three different axial locations in the bed with consecutive tracer injection at two different positions (near the wall and in the centre of the bed) for three different fluidization velocities (see Figure 5).

The most important observations obtained from the experiments are as follows:

1. For near wall tracer gas injection at of $8u_{mf}$ and $10u_{mf}$, very low relative tracer concentrations are detected at points below the injection point for all the three probes, indicating that down flow near the wall is not significant at these fluidization velocities and that the near wall circulation pattern does not extend over the entire bed. When the fluidization velocity is increased to $12u_{mf}$, the downflow near wall increases but still does not extend over the entire height of the reactor (see Figure 5, Injection A).

2. With the tracer gas injection located at the centre of the bed, the relative tracer gas concentrations detected just below the injection point were very small for all of the three detection probes at all fluidization velocities studied (See Figure 5, injection D). This pinpoints the strong upflow in the centre of the bed. The slightly higher concentrations at the wall observed at all axial positions and gas velocities applied are attributed to a weak near-wall downflow.

The observed phenomena correspond very well to the experimental results presented in Chapter 4. However that the extent of back-mixing is much smaller and near-wall down flow becomes significant at somewhat higher fluidization velocities, which can be attributed to the larger aspect ratio of this reactor.

In order to study the effect of gas addition via the membranes on the mixing behavior of the membrane assisted fluidized bed reactor, tracer gas point injection experiments were performed at superficial gas velocities of 8-12u_{mf} with tracer injection at position A (near the wall) and D (centre). In these experiments part of fluidizing gas was fed via the membranes (25-50%), keeping the total flow rate corresponding to 8-12u_{mf} respectively.

Figure 6 shows the effect of gas addition via the membrane on gas back-mixing at a fluidization velocity of 12u_{mf}. The relative tracer concentrations detected near the wall (injection A) are substantially smaller than detected (for the same conditions) without membrane permeation. Furthermore, the concentrations detected near the wall decrease with an increase in the gas flow rate permeated through the membranes. This indicates that the local near-wall downflow is effectively annihilated by gas permeation through the membranes. Moreover, the concentrations detected at the centre (injection D) also decreased substantially in case of gas addition via the membranes and reach nearly very low values demonstrating the near plug flow behavior of the bed.

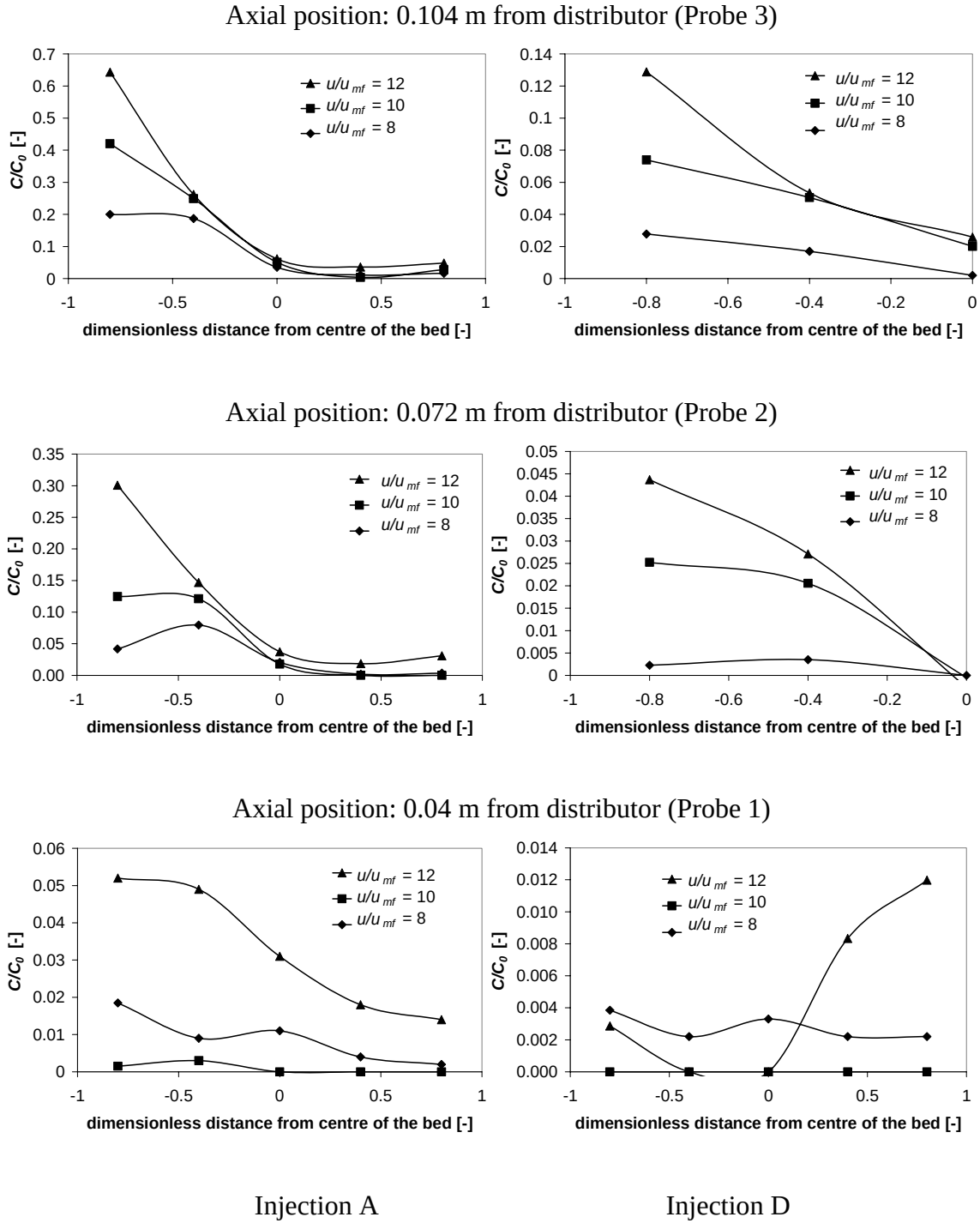

Figure 5. Effect of the superficial gas velocity on the experimentally determined lateral relative tracer gas concentration profile with injection point near the wall (Injection A) and at the centre (Injection D), injection point 0.168 m above the distributor.

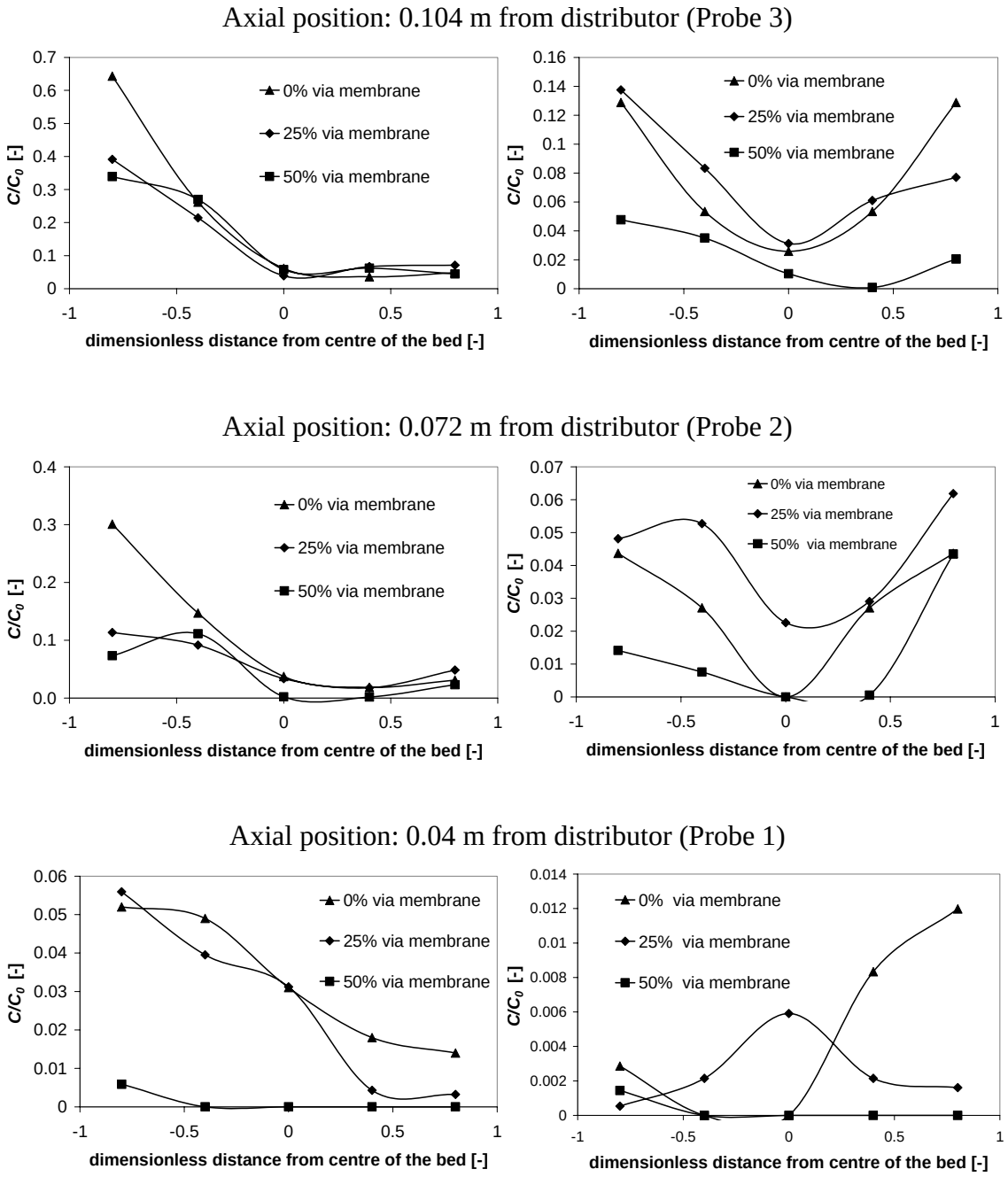

Figure 6. Effect of gas addition via the membranes on the experimentally determined lateral relative tracer gas concentration profile for a fluidization velocity of $12u_{mf}$, with injection near the wall (injection A) and at the centre (Injection D), injection point 0.168 m above the distributor.

3.1.2. Step response experiments using ultrasound technique

The ultrasound technique was used to measure the gas phase RTD in the membrane assisted fluidized bed reactor in order to quantify the extent of gas back-mixing in terms of an overall effective axial dispersion coefficient or equivalently the number of ideally stirred tank reactor (CISTR) in series.

Figure 10 shows the effect of the fluidization velocity on the equivalent number of CISTRs required to describe the overall effective axial back-mixing in the membrane assisted fluidized bed for different ratios of gas added via the membranes. The following conclusions can be drawn from the experiments.

1. For a fixed ratio of gas flow fed via the membranes relative to the gas flow fed via the distributor at the bottom of the bed, further referred to as permeation ratio, the number of CISTRs decreases with increasing fluidization velocity, corresponding to an increase in the effective axial gas dispersion.

2.For higher permeation ratios, the number of CISTRs also increases, again indicating decreased gas back-mixing. The gas added via the membranes, counteracts the down-flow of solids near the wall thereby reducing the macroscopic circulation patters and large-scale axial gas dispersion. However, this effect is noticeable in case the fractional amount of gas permeating through the membranes exceeds 25%.

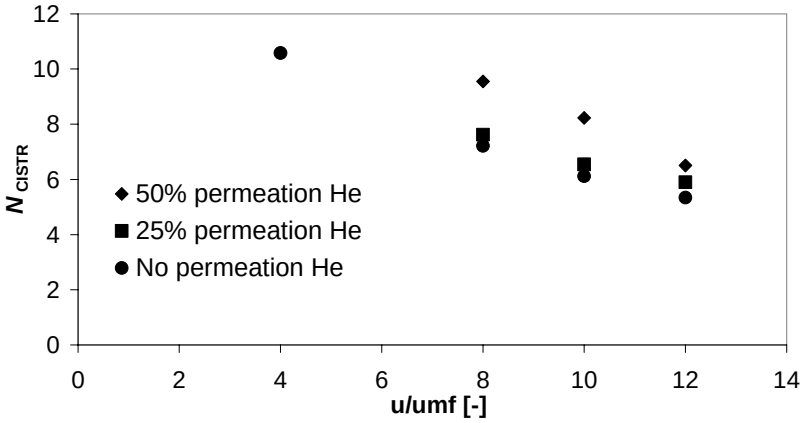

Figure 10. Effect of the fluidization velocity and the membrane permeation ratio on the number of CISTRs representing the MAFBR.

In order to assess the validity of these results, the average residence time calculated on the basis of the RTD (τ model) is plotted against the actual holding time in the reactor in Figure 11 showing a deviation less than 5%.

Finally, it is concluded that the number of tanks in series required to represent the MAFBR varies between 6 to 10, depending upon the fluidization velocity and permeation ratio, indicating a plug flow like behavior of MAFBR.

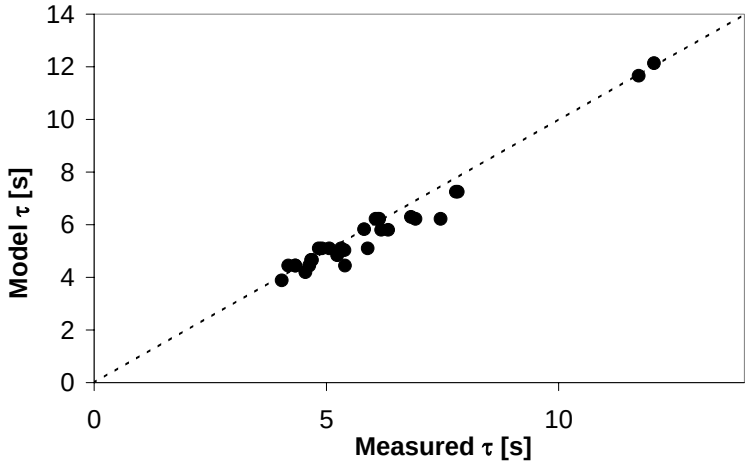

Figure 11. Parity plot of the mean residence time (calculated by the model) and the holding time of the MAFBR over a wide range of fluidization velocities and membrane permeation ratios.

3.2. Methanol partial oxidation to formaldehyde

In order to demonstrate the benefits of the novel membrane assisted fluidized bed reactor concept for the partial oxidation of methanol over a Fe-Mo catalyst, experiments were conducted over a wide range of methanol and oxygen concentrations, fluidization velocities, permeation ratios, catalyst bed heights and bed temperatures.

For experiments at fixed reactor temperature, the maximum temperature difference throughout the active part of the reactor was only 1-2°C indicating nearly perfect isothermal conditions.

3.2.1. Effect of the temperature

Figure 12 shows the effect of reactor temperature on the methanol conversion and formaldehyde selectivity and yield in a MAFBR at a fluidization velocity of $10u_{mf}$, a packed bed height of 0.3 m and 20% methanol and 12% oxygen inlet concentrations based on the total feed.

Firstly, it can be observed that the methanol conversion increases drastically when the temperature increases from 250 to 275°C. With a further temperature increase the methanol conversion does not increase because mass transfer limitations arise preventing the unreacted methanol to transfer from bubble phase to emulsion phase. Secondly, the formaldehyde selectivity decreases with higher temperatures because the formaldehyde in the emulsion phase is more susceptible to further oxidation at higher temperatures, because of the more pronounced mass transfer limitations and higher reaction rates to CO at higher temperatures.

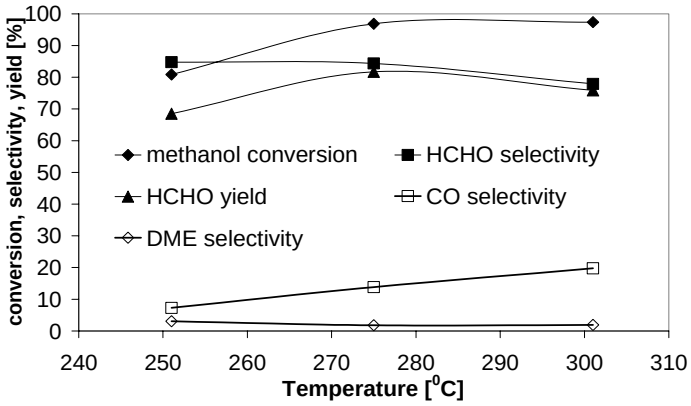

Figure 12. Effect of reactor temperature on the methanol conversion and selectivities to the reaction products at overall fluidization velocity of $10u_{mf}$, initial packed bed height of 0.3 m, 20% methanol and 12% oxygen overall inlet concentrations (no permeation through the membranes).

3.2.2. Effect of the methanol concentration

Figure 13 shows the effect of the methanol inlet concentration on the methanol conversion, formaldehyde selectivity and yield at 275°C and $10u_{mf}$ overall fluidization velocity, where 50% of the total gas was fed via the membranes. The methanol

conversion decreases with an increase in the methanol concentration, keeping the inlet oxygen concentration the same at 10%. Assuming that the methanol mass transfer rate increases linearly, the decrease in the methanol conversion indicates that the overall conversion rate is at least partly influenced by the reaction kinetics, where the lower oxygen concentrations decrease the reaction rates. However, the selectivity to formaldehyde increases with the increase in the methanol concentration because the oxygen concentration approaches the stoichiometric value, favoring the formation of formaldehyde rather than carbon monoxide. It is also important to notice that the selectivity towards dimethyl ether increases at higher methanol concentration, where the catalyst surface becomes more saturated with methoxy group and thereby favoring dimethyl ether formation.

These experiments also demonstrate that the formaldehyde productivity of the MAFBR can be increased almost linearly by increasing the methanol concentration, since the formaldehyde yield remains almost constant.

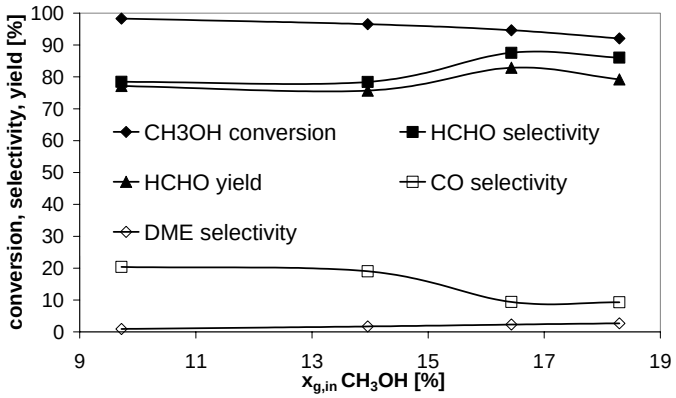

Figure 13. Effect of the methanol feed concentration on the methanol conversion and selectivity to the reaction products at overall fluidization velocity of $10u_{mf}$, where 50% of the total gas was fed via the membranes, using a 10% overall oxygen concentrations in the feed, initial packed bed height of 0.3 m and a reactor temperature of 275^{o}C.

3.2.3. Effect of the oxygen concentration

Figure 14 clearly shows that when oxygen is fed in excess of the stoichiometric value, the methanol conversion is strongly increased because the higher local oxygen concentrations in the emulsion phase increase the reaction rates. Also the CO selectivity

increases and formaldehyde selectivity decreases because of the higher local oxygen concentration as expected.

Hence it is clear that stoichiometric oxygen concentrations in the feed and a reactor temperature of 275°C are optimal (highest formaldehyde yield) and have been selected to study experimentally the effect of the fluidization velocity, the flow rate of the gas added via the membranes and initial catalyst packed bed height.

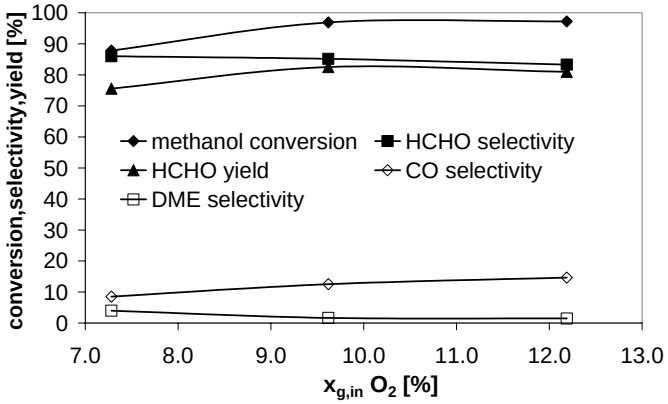

Figure 14. Effect of the oxygen overall feed concentration on the methanol conversion and selectivity to the reaction products at overall superficial velocity of $10u_{mf}$, catalyst packed bed height of 0.3 m, reactor temperature of 275°C, 15% overall methanol concentration in the feed and 50% of the total gas added via the membranes.

3.2.4. Effect of the fluidization velocity

Figure 15 shows the effect of the dimensionless fluidization velocity (u/u_{mf}) on the methanol conversion (C), formaldehyde selectivity (S), formaldehyde yield (Y) and carbon monoxide selectivity for overall inlet methanol and oxygen concentrations of 17% and 9% respectively, i.e. nearly stoichiometric feed concentration and different membrane permeation ratios of (0-40%).

The following important observations can be made on the basis of the experimental data.

1. Methanol conversion decreases with an increase in the fluidization velocity (also for 0% permeation), which can be attributed to mass transfer limitations of methanol from

the bubbles, formed at the distributor, to the emulsion phase. Since the average bubble diameter increases with increase in bed height and fluidization velocity.

2. The selectivity towards formaldehyde increases at higher fluidization velocities, mainly because of the lower formaldehyde residence time. Bubbles help to increase the selectivity by trapping the formaldehyde formed lower in the bed, which is not readily transferred back to the emulsion phase in the top of the bed due to the increased mass transfer resistance because of bubble growth.

3. The formaldehyde yield decreases with an increase in the fluidization velocity, because of the stronger decrease in the methanol conversion compared to the increase in formaldehyde selectivity.

4. Addition of part of the total gas via the membranes (distributive addition of oxygen) increases the methanol conversion, firstly because of the higher methanol residence time caused by the reduction in the gas flow rate fed via the distributor, and secondly because of the smaller bubble size which improves the methanol transfer rate to the emulsion phase. However, the selectivity to formaldehyde decreases because of the increased formaldehyde residence time in the bed and also because of the addition of oxygen at the top of the bed via the ceramic membranes where the formaldehyde concentrations are the highest.

5. It is striking to notice that the carbon monoxide selectivity remains at about 5% at higher overall fluidization velocities of $10u_{mf}$ even with addition of gas via membranes. Hence low selectivities to carbon monoxide can be maintained while achieving higher conversions by using distributed feeding of oxygen via the membranes. The byproducts in our experiments were dimethyl ether and methyl formate and occasionally dimethoxy methane, especially at high methanol concentrations above 15%, which can be recovered and recycled to be converted back to formaldehyde and CO eventually.

6. Finally, the same trends for the conversion and selectivities as a function of the fluidization velocity and membrane permeation ratio were observed for all the three bed heights studied.

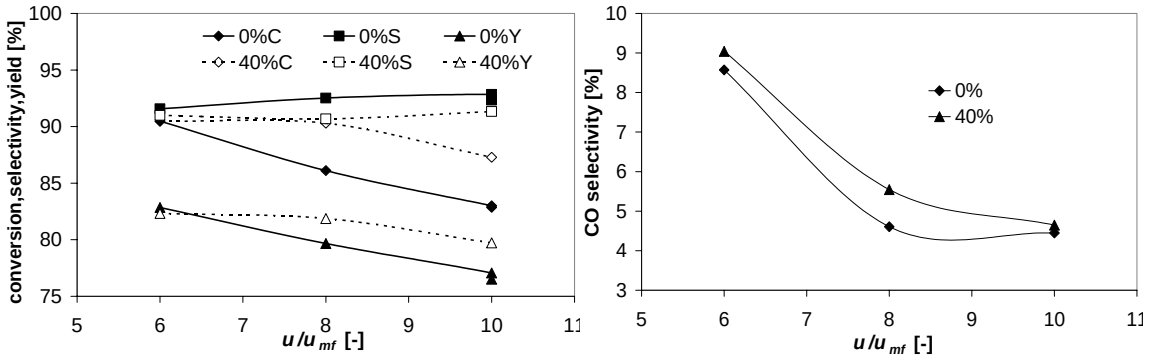

(a; packed bed height of 0.15 m)

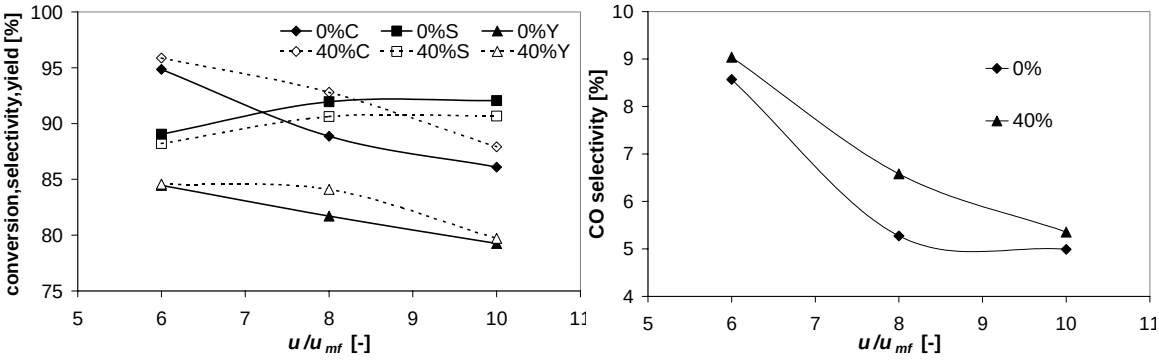

(b; packed bed height of 0.2 m)

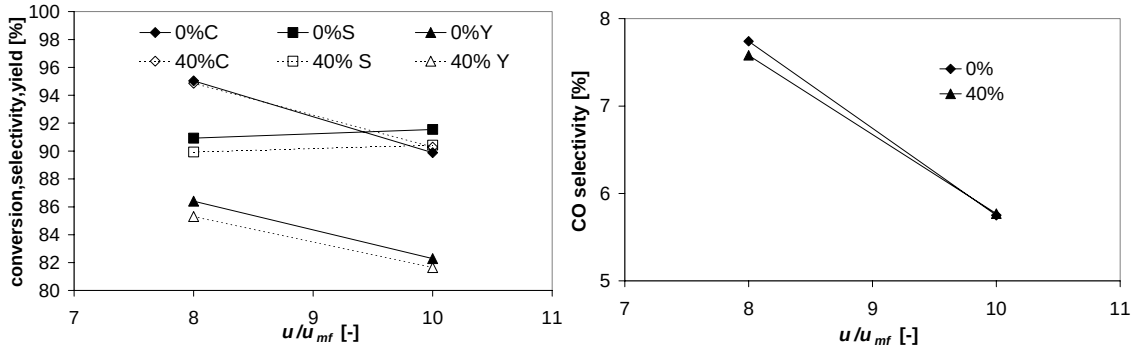

(c; packed bed height of 0.25 m)

Figure 15. The effect of the dimensionless overall fluidization velocity (u/u_{mf}) on the methanol conversion (C), formaldehyde selectivity (S), formaldehyde yield (Y) and carbon monoxide selectivity for overall inlet methanol and oxygen concentrations of 17% and 9% respectively, 275°C and for different membrane permeation ratios: (a) packed bed height of 0.15 m (L/D=3), (b) packed bed height of 0.20 m (L/D=4) and (c) packed bead height of 0.25 m (L/D=5).

3.2.5. Effect of the catalyst bed height

Figure 16 shows the effect of initial packed bed height on the methanol conversion (C), formaldehyde selectivity (S), formaldehyde yield (Y) and carbon monoxide selectivity at overall methanol and oxygen concentrations of 17% and 9% respectively for different membrane permeation ratios (0-40%).

Figure 16 shows that the methanol conversion increases with higher catalyst bed heights. However, the selectivity to formaldehyde decreases and to carbon monoxide increases, mainly because of the increased residence time of methanol and formaldehyde respectively.

Moreover, increasing the part of the total fluidizing gas fed via the membranes increases the conversion. However, the conversion levels off at a bed height of 0.25 m (L/D = 5) at both overall velocities studied. Apparently distributing the fluidizing gas via the membranes to increase the methanol conversion is most effective at lower aspect ratios because of the relatively large residence times required to achieve near complete conversion of methanol.

From the CO selectivity data it is also evident that a large flow rate of the gas fed via the membranes is favorable at large aspect ratios because CO selectivity is hardly increased and the conversion in increased giving an opportunity to increase the overall yield without affecting the methanol conversion and formaldehyde selectivity, rendering the reactor safe and away from explosion regions even at high methanol concentrations.

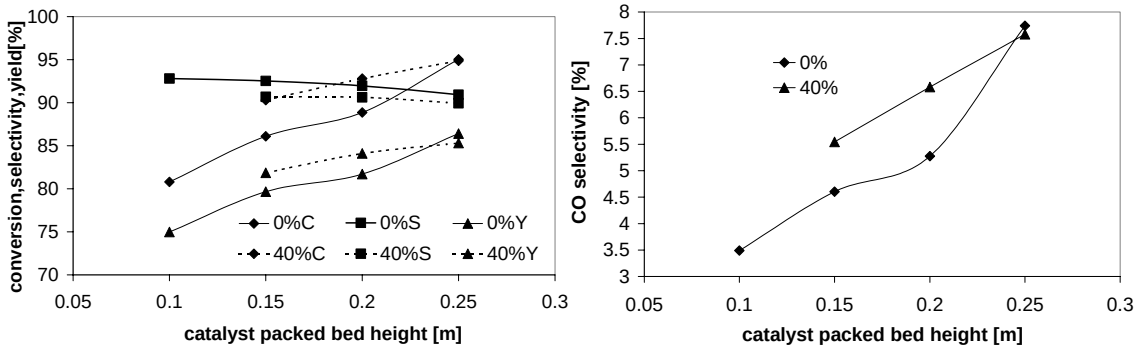

(a) $u/u_{mf} = 8$

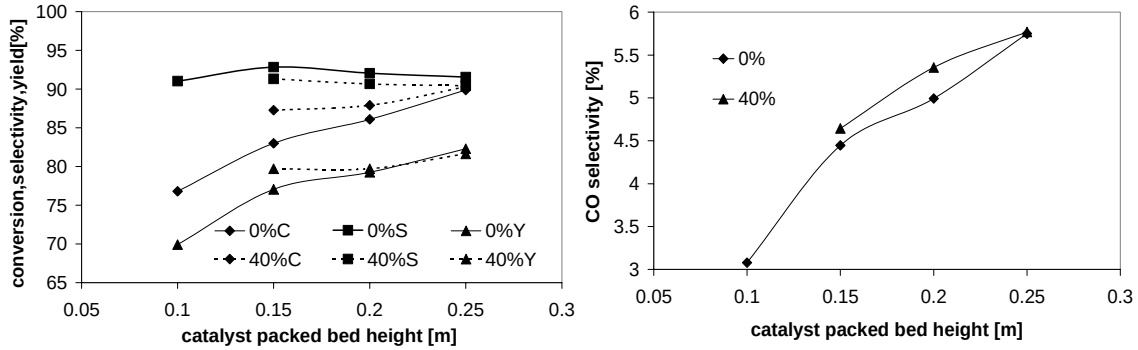

(b) $u/u_{mf} = 10$

Figure 16. Effect of catalyst packed bed height (L/D=aspect ratio) on the methanol conversion (C), formaldehyde selectivity (S), formaldehyde yield (Y) and carbon monoxide selectivity for an overall methanol and oxygen concentrations of 17% and 9% respectively, at 275°C for different membrane permeations ratios: (a) $u/u_{mf} = 8$ and (b) $u/u_{mf} = 10$.

3.2.6. Effect of influencing the axial oxygen concentration profile via axially varying membrane permeation flows

Table 1 shows the effect of imposing different oxygen concentration profiles created by distributing different air flow rates via the membrane bundles. These experiments were carried out at an overall superficial velocity of $8u_{mf}$, overall inlet methanol and oxygen concentrations of 17% and 9% respectively, a packed bed height of 0.25 m, reactor temperature of 275 °C and with 20% of the total gas added via the membranes at various distribution ratios within the three membrane bundles.

The experimental results clearly show that there is little effect of imposing different axial oxygen concentration profiles in the reactor by feeding different air flow rates via each of the bundles. The overall formaldehyde yield was always about 85%. Little effect on the product selectivities was also to be expected since the oxygen order is identical for both reactions, the methanol partial oxidation to formaldehyde and the formaldehyde partial oxidation to carbon monoxide.

However, the results show that by feeding relatively more oxygen at the bottom of the bed and simultaneously feeding a corresponding lower flow rate at the top, the methanol conversion is slightly decreased, the formaldehyde selectivity slightly increased and CO selectivity slightly decreased. Thus the CO losses can be somewhat reduced at the same formaldehyde yield. The lower methanol conversion indicates a slightly more pronounced bubble-to-emulsion phase mass transfer limitation due to the less optimal flow distribution over all the membranes resulting in slightly larger average bubble size. On the other end the mass transfer limitations for the formaldehyde helps keeping the CO selectivity low.

Table 1. Effect of imposing different axial oxygen concentration profiles via distributing different flow rates through the three bundles on the methanol conversion and product selectivities, where 20% of the total gas was added via the membrane, with a reactor temperature 275 ^{0}C, overall inlet methanol and oxygen concentrations of 17% and 9% respectively, a catalyst packed bed height of 0.25 m, an overall fluidization velocity of $8u_{mf}$. The centre of bundles 1, 2 and 3 were at 6.4, 12.8 and 19.2 cm above the distributor respectively, and each bundle consisted of 6 membranes.

Bundle 1 (%)	Bundle 2 (%)	Bundle 3 (%)	Methanol Conversion [%]	Formaldehyde Selectivity [%]	Formaldehyde yield [%]	CO Sel. [%]	DME Sel. [%]
33	33	33	95.40	89.63	85.51	8.43	1.43
50	50	0	94.05	90.30	84.93	7.23	1.62
66	33	0	93.32	91.02	84.94	6.60	1.63
33	66	0	94.22	90.65	85.41	7.11	1.53
50	0	50	92.69	91.21	84.54	6.14	1.75
40	40	20	94.01	91.42	85.41	6.86	1.73
50	30	20	92.98	91.38	84.96	6.36	1.74

4. Modeling

A one-dimensional two-phase model is developed to describe the partial oxidation of methanol in our MAFBR. The most common phenomenological description of the two-phase flow phenomena in fluidized bed reactor is based on the Bubble Assemblage Model, originally proposed by Kato and Wen (1969). In their model the fluidized bed is divided in the axial direction into number of CISTRs, where the size of each CISTR is calculated from the bubble diameter at the axial location in the bed and the number of CISTRs is calculated on the basis of the total expanded bed height. The model presented here also divides the fluidized bed into a number of CISTRs, following Kato and Wen (1969), however, the number of CISTRs corresponding to the extent of gas back-mixing in the MAFBR, has been measured with independent experiments using the ultrasound technique. Furthermore, all CISTRs are assumed to be of equal volume and consequently their size is no longer directly related to the local bubble size. A schematic representation of the gas flows between the bubble and emulsion phases of the CISTRs constituting the fluidized bed is shown in Figure 17. The model assumptions and model parameters are described in the following section.

4.1. Model assumptions

Our model is based on the following main assumptions:

- In the axial direction the bed is divided into several compartments of equal size where the height of each compartment is given by the total expanded bed height and the number of CISTRs representing the experimentally observed axial gas back-mixing.
- Each compartment consists of two phases, viz. the bubble and emulsion phase.
- The gas flowing through each phase is considered to be completely mixed within each compartment.

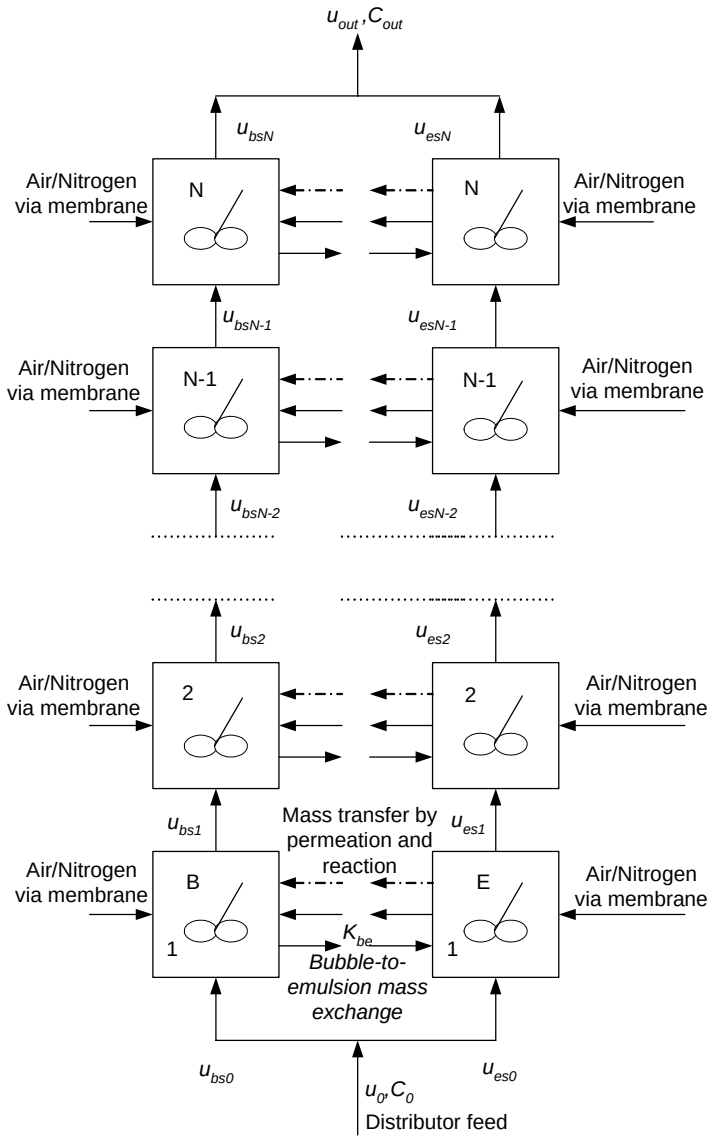

Figure 17. Schematic representation of the proposed model, B= bubble phase, E= emulsion phase

4.1.1. Bubble phase

The superficial bubble velocity (u_{bs}) is an important parameter in fluidized bed reactor modeling, since it influences many other parameters such as the volume fraction of each phase and superficial gas velocities of the other phases. The earliest and most common postulate to compute u_{bs}, which is known as the two-phase theory of fluidization (Toomey and Jonhnstone, 1952), suggests that the gas flow rate in the bubble phase is equal to excess gas flow rate above what is required for minimum fluidization. This

model assumes that u_{bs} remains constant through out the bed. This observation is however contrary to what Werther (1974) has observed in his experiments. Werther's data indicate that u_{bs} increases monotonically with the bed height. His data showed that a smaller diameter bed results in significantly higher u_{bs} compared to larger diameter beds. Thus, when bubbles rise in a fluidized bed, the dense phase continues to transfer gas to the rising bubbles. This, in turn causes the bubbles to grow in size and ascend with higher velocities. Moreover, because of the wall effect, the bed diameter has a strong effect on the rate of gas withdrawal from the dense phase. Due to the relatively smaller wall effect in a larger-diameter-bed, the withdrawal rate of the dense phase is less and consequently, the bubble size as well as the bubble gas flow rate at a given height will be smaller in a large diameter bed.

Furthermore, bubbles are known to move laterally towards the center, which actually induces the micro-scale lateral mixing in the emulsion phase, which is assumed to be laterally perfectly mixed. However, a uniform distribution of the bubble phase is assumed. It is therefore assumed that the bubbles disperse uniformly in each CISTR. The extent of the axial dispersion in the bubble phase induced by bubble breakage and coalescence caused by the presence of the membrane bundles, is assumed equal to the back-mixing in the emulsion phase and accounted for with the number of CISTRs in series. The following assumptions have been made for the bubble phase:

- A laterally uniform bubble fraction is assumed and lateral concentration differences in the bubble phase are assumed negligibly small due to assumed frequent bubble coalescence and break-up.
- The extent of the axial back-mixing equals that of the emulsion phase.
- The bubble phase is considered to be free of catalytic particles, so that no reactions occur in the bubble phase.

4.1.2. Emulsion phase

In a fluidized bed without internals a macro scale circulation pattern prevails with downflow of the emulsion phase near the wall and upflow at the centre of the bed. However, as shown with tracer gas experiments in the bed with horizontal inserts the macroscopic circulation is effectively annihilated, especially in case of gas permeation through the membranes. The following assumptions have therefore been made regarding the emulsion phase.

- The emulsion phase gas only flows upwards. This is based on the fact that the reactor approximates plug flow behavior (large number of CISTRs), which improves even further with addition of gas via membranes.
- The emulsion phase velocity remains constant and close to the minimum fluidization velocity, so that it is assumed that all the excess gas formed due to chemical reaction in the emulsion phase is transferred directly to the bubble phase. Analogously the gas flow rate fed to the emulsion phase via membranes is assumed to be perfectly mixed in the emulsion phase and instantaneously transferred to the emulsion phase.
- Constant emulsion phase porosity is assumed, which remains at the minimum fluidization porosity.

4.2. Model equations and model parameters

On the basis of the aforementioned assumptions the bubble and emulsion phase total and component mass conservation equations have been formulated for each CISTR and are shown in Table 2. For an explanation of the symbols used, the reader is referred to the symbol list at the end of the chapter. The empirical correlations for the model parameters have been taken from the literature, although they were originally obtained for beds without internals (see Table 3). It is assumed that these correlations can reasonably well describe the MAFBR. The kinetic rate expressions for the partial oxidation of methanol and its consecutive and parallel reactions, as determined in Chapter 5, are summarized in table 5 and 6.

Basically, our reactor model is a two-parameter model: the number of CISTRs in series and the average bubble size are considered as input parameters, where it is assumed that the bubble diameter remains relatively constant over the bed height in the MAFBR.

Despite the fact that some experimental results have been reported in the literature on the effect of horizontal inserts on the local bubble size considering bubble growth and coalescence and break up (Yates et al., 1990), no correlations have been found that account for the important effects of the membrane permeation and gas production due to the chemical reactions on the evolution bubble size. Therefore a constant bubble size throughout the reactor has been assumed. According to Kunii and Levenspiel (1991), powders of A and B type according to Geldart classification have a more constant bubble size at higher temperatures.

Table 2. Mass conservation equations for the bubble and emulsion phase.

Total mass balance

$$u^s_{b,n-1}A_T - u^s_{b,n}A_T + u^s_{e,n-1}A_T - u^s_{e,n}A_T + \frac{u_{tot}A_T F}{N} + \sum_j \left(\sum_i \nu_{i,j} \right) R_j m_{cat} \frac{RT}{P} = 0$$

Where:

$$u^s_{e,n}A_T = u_{e,n}A_T \left(1-\delta_{b,n}\right),$$
$$u^s_{b,0}A_T = \left(1-F\right)u_{tot}A_T\delta_{b,0},$$
$$u^s_{e,0}A_T = \left(1-F\right)u_{tot}A_T\left(1-\delta_{b,0}\right)$$

Bubble phase component mass balances

$$u^s_{b,n-1}A_T C_{b,n-1,i} - u^s_{b,n}A_T C_{b,n,i} + \frac{u_{tot}A_T F C_{p,n,i}\delta_{b,n}}{N}$$
$$+\left[\left(u^s_{e,n-1}A_T - u^s_{e,n}A_T\right) + \frac{u_{tot}A_T F\left(1-\delta_{b,n}\right)}{N} + \sum_j \left(\sum_i \nu_{i,j} \right) R_j m_{cat} \frac{RT}{P}\right] C_{e,n,i} \quad \text{for i= 1 to } n_c$$
$$-K_{b,e,n}V_{b,n}\left(C_{b,n,i} - C_{e,n,i}\right) = 0$$

Emulsion phase component mass balance

$$u^s_{e,n-1}A_T C_{e,n-1,i} - u^s_{e,n}A_T C_{e,n,i} + \frac{u_{tot}A_T F C_{p,n,i}\left(1-\delta_{b,n}\right)}{N}$$
$$-\left[\left(u^s_{e,n-1}A_T - u^s_{e,n}A_T\right) + \frac{u_{tot}A_T F\left(1-\delta_{b,n}\right)}{N} + \sum_j \left(\sum_i \nu_{i,j} \right) R_j m_{cat} \frac{RT}{P}\right] C_{e,n,i} \quad \text{for i=1 to } n_c$$
$$+K_{b,e,n}V_{b,n}\left(C_{b,n,i} - C_{e,n,i}\right) + \sum_j \nu_{i,j} R_j m_{cat} = 0$$

Table 3. Hydrodynamic parameters used in the model (without the effect of internals).

Parameter	Equation	Reference
Archimedes number	$Ar = \frac{d_p^3 \rho_g (\rho_p - \rho_g) g}{\mu_g^2}$	Kunii and Levenspiel (1991)
Minimum fluidization velocity	$u_{mf} = \left(\frac{\mu_g}{\rho_g d_p}\right)\left(\sqrt{(27.2)^2 + 0.0408 Ar} - 27.2\right)$	Shiau and Lin (1993)
Bed voidage at minimum fluidization velocity	$\varepsilon_{mf} = 0.586 Ar^{-0.029}\left(\frac{\rho_g}{\rho_p}\right)^{0.021}$	Shiau and Lin (1993)
Projected tube area for a square bed	$A_T = D_T^2$	
Rise velocity of a single bubble	$u_{br} = 0.711\ (g d_b)^{1/2}$	Kunii and Levenspiel (1991)
Velocity of rise of swarm of bubbles	$u_b = u_0 - u_{mf} + 0.711\ (g d_b)^{1/2}$	Kunii and Levenspiel (1991)
Initial Bubble diameter (Porous plate distributor)	$d_{b0} = 0.376(u_0 - u_{mf})^2$	Kunii and Levenspiel (1991)
Superficial bubble gas velocity	$\frac{u_{b,max,s} - u_{b,s}}{u_{b\,max,s} - U_{b,0,s}} = exp(-\frac{0.55z}{H_{mf} D_T})$	Mori and Wen (1975)
Maximum superficial bubble gas velocity	$u_{b,max,s} = u_0 - u_{mf}$	Pyle and Harrison (1967)
Initial superficial bubble gas velocity	$u_{b,0,s} = u_{br,0}\delta_{b0}$ Where $\delta_{bo} = (1 - H_{mf} / H_f)$	Shiau and Lin (1991)
Superficial emulsion gas velocity	$u_{es} = u_0 - u_{bs}$	Toomy and Johnstone (1952)
Bubble phase fraction	$\delta_b = \frac{u_{bs}}{u_b}$	Shiau and Lin (1993)
Emulsion phase fraction	$\delta_{en} = 1 - \delta_{bn}$	Kato and Wen (1969)

Height of bed expansion Average bubble rise velocity	$H_f = H_{mf}\frac{C_1}{C_1 - C_2}$ Where, $C_1 = 1 - \frac{u_{b0}}{\overline{u_b}} exp\left(-\frac{0.275}{D_T}\right)$ $C_2 = \frac{u_{bs}}{\overline{u_b}}\left[1 - exp\left(-\frac{0.275}{D_T}\right)\right]$ $\overline{u_b} = u_0 - u_{mf} + 0.711\left(g\overline{d_b}\right)^{1/2}$	Shiau and Lin (1993)
Gas exchange coefficient	$K_{bc} = 4.5\left(\frac{u_{mf}}{d_b}\right) + 5.85\left(\frac{D_g^{1/2} g^{1/4}}{d_b^{5/4}}\right)$ $K_{ce} = 6.77\left(\frac{D_g \varepsilon_{mf} u_b}{d_b^3}\right)^{1/2}$ $\frac{1}{K_{be}} = \frac{1}{K_{bc}} + \frac{1}{K_{ce}}$	Kunii Levenspiel (1991)
Volume of emulsion phase in the nth compartment	$V_{e,n} = A_T \frac{H_f}{N} \frac{\left(1 - \delta_{b,n}\left(u_{b,r,n} + \frac{2u_{mf}}{\varepsilon_{mf}}\right)\right)}{\frac{u_{b,r,n} - u_{mf}}{\varepsilon_{mf}}}$	Kato and Wen (1969)
Volume of bubble in the nth compartment	$V_{b,n} = A_T \frac{H_f}{N} \delta_{b,n}$	Kato and Wen (1969)

Table 4. Literature correlations for bubble size in fluidized bed without internals.

Mori and Wen (1975)	Darton et al. (1977)
$d_b = d_{b,\max} - \left(d_{b.\max} - d_{b,0}\right) e^{\left(\frac{-0.3h}{D_T}\right)}$	$d_b = 0.54\left(u - u_{mf}\right)^{0.4}\left(h + 4A_c^{0.5}\right)^{0.8} g^{-0.2}$

Table 5. Kinetic rate equations for the methanol partial oxidation reaction system.

Parameter	Equation
Surface fraction of methanol	$\theta_{CH_3OH} = \frac{K_{ads,\,CH_3OH} P_{g,CH_3OH}}{1 + K_{ads,\,CH_3OH} P_{g,CH_3OH} + K_{ads,\,H_2O} P_{g,H_2O}}$
Surface fraction of oxygen	$\theta_{O_2} = \frac{K_{ads,\,O_2} P_{g,O_2}^{1/2}}{1 + K_{ads,\,O_2} P_{g,O_2}^{1/2}}$
Surface fraction of formaldehyde	$\theta_{HCHO} = \frac{P_{g,HCHO}}{1 + K_{ads,\,CH_3OH} P_{g,CH_3OH} + K_{ads,\,H_2O} P_{g,H_2O}}$
Reaction rate towards formaldehyde	$R_{HCHO} = k_{HCHO} \theta_{CH_3OH} \theta_{O_2}$
Reaction rate towards CO	$R_{CO} = k_{CO} \theta_{HCHO} \theta_{O_2}$
Reaction rate towards DME	$R_{DME} = k_{DME,f} P_{g,CH_3OH} - \frac{k_{DME,f}}{K_{DME,eq}} \frac{P_{g,DME} P_{g,H_2O}}{P_{g,CH_3OH}}$
Reaction rate towards DMM	$R_{DMM} = k_{DMM,f} P_{g,HCHO} P_{g,CH_3OH} - \frac{k_{DMM,f}}{K_{DMM,eq}} \frac{P_{g,DMM}}{P_{g,CH}}$

Table 6. Reaction rate constants (pre-exponential constants and activation energies) and equilibrium constants for the methanol (R_{HCHO}) and formaldehyde partial oxidation (R_{CO}), dimethyl ether formation (R_{DME}) and dimethoxymethane formation (R_{DMM}).

	K_{CH_3OH}	[atm^{-1}]	$3.12 \cdot 10^{-4}$	E_{CH_3OH}	[kJ.mole^{-1}]	- 54.19
(R_{HCHO})	K_{O_2}	[atm$^{-1/2}$]	$1.23 \cdot 10^{-5}$	E_{O_2}	[kJ.mole^{-1}]	- 60.72
	K_{H_2O}	[atm^{-1}]	$2.30 \cdot 10^{2}$	E_{H_2O}	[kJ.mole^{-1}]	11.45
	k_{HCHO}	[mol kg^{-1}s^{-1}]	$2.08 \cdot 10^{6}$	E_{HCHO}	[kJ.mole^{-1}]	84.0
(R_{CO})	k_{CO}	[mol kg^{-1} atm^{-1} s^{-1}]	$1.32 \cdot 10^{2}$	E_{CO}	[kJ.mole^{-1}]	47.0
(R_{DME})	$k_{DME,f}$	[mol kg^{-1}atm^{-1}s^{-1}]	$1.9 \cdot 10^{5}$	$E_{DME,f}$	[kJ.mole^{-1}]	77.0
$K_{DME}^{eq} = \exp(-2.2158 + 2606.8/T)$						
(R_{DMM})	$k_{DMM,f}$	[mol kg^{-1}atm^{-2}s^{-1}]	$2.58 \cdot 10^{-6}$	$E_{DMM,f}$	[kJ.mole^{-1}]	-56.5
$K_{DMM}^{eq} = \exp(-20.416 + 9346.8/T)$						

4.2.1. Parametric sensitivity of the model

Before actually comparing the predictive capabilities of the model, simulations were performed to assess the sensitivity of the two model parameters, namely the number of CISTRs in series and the average bubble size, on the methanol conversion and product selectivities. Figure 18 shows the sensitivity of the number of CISTRs, thus the degree of plug flow behavior, on the methanol conversion and product selectivities for a base case experiment. An average bubble diameter of 19 mm was assumed. It is very clear that the number of CISTRs hardly affects the methanol conversion in case the number exceeds 2 to 3, while the formaldehyde and CO selectivities are basically independent of the number of CISTRs. Since the ultrasound experiments have demonstrated that the MAFBR can be represented by 6 to 10 CISTRs in series, depending on the fluidization velocity and permeation flow rates, the number of CISTRs is not a very critical parameter.

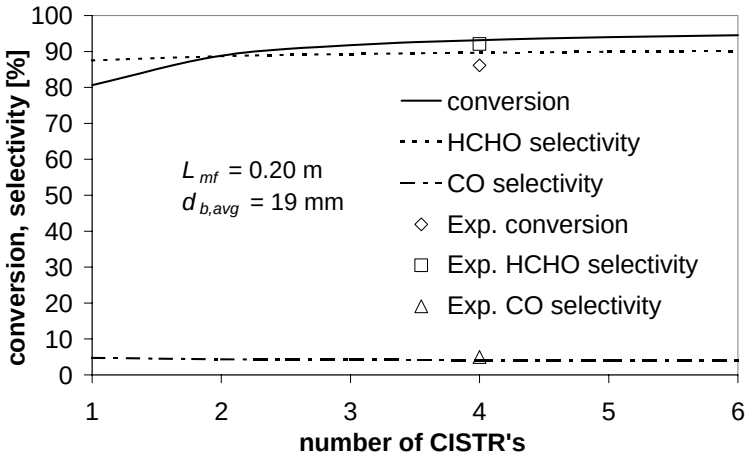

Figure 18. Sensitivity of the predicted methanol conversion and product selectivities with respect to the number of CISTRs in series. Conditions: 17% methanol and 9% oxygen overall inlet concentration, at 275°C reactor temperature, packed bed height of 0.2 m and overall fluidization velocity of $10u_{mf}$. The average bubble diameter was assumed as 13 mm.

Figure 19 shows the effect of the average bubble diameter on the methanol conversion and product selectivities for a fixed number of CISTRs of six. It is very obvious that the methanol conversion strongly depends on the average bubble diameter as expected because of the prevailing bubble-to-emulsion phase mass transfer limitation, which becomes more pronounced for bigger bubbles. However, the selectivity to

formaldehyde and carbon monoxide is not significantly influenced by the average bubble diameter. Smaller bubbles improve the transfer of the formaldehyde formed in the emulsion phase to the bubble phase, which thereby increases the selectivity to formaldehyde by trapping the formaldehyde inside the bubbles and hence preventing CO formation (see Figure 19 at lower bubble size), however, this effect is very small.

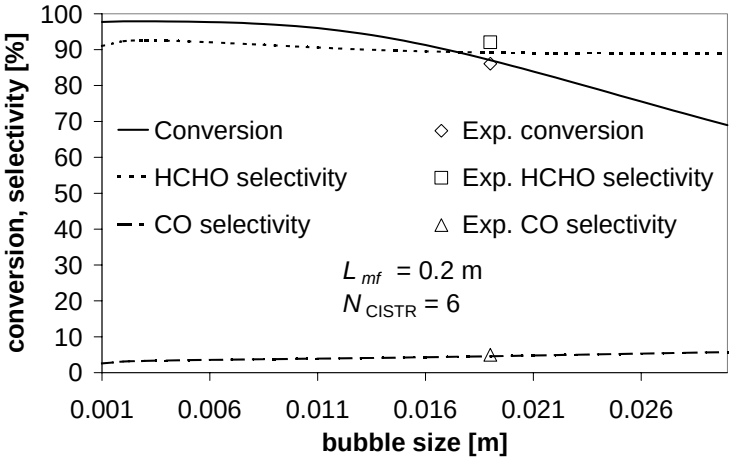

Figure 19. Sensitivity of the predicted methanol conversion and product selectivities with respect to the average bubble diameter (d_b). Conditions: 17% methanol and 9% oxygen overall inlet concentration, at 275°C reactor temperature, packed bed height of 0.2 m and overall fluidization velocity of $10u_{mf}$. The number of CISTRs was fixed at 6.

4.3. Comparison of model predictions with experiments

In this section the predictive capabilities of the model are assessed by simulating the experimental conditions employed in the experimental demonstration unit. Subsequently the model is used to further facilitate the understanding of the phenomena prevailing in the MAFBR in order to permit optimization of the reactor geometry and operating conditions.

Since no information is available on the average bubble size as a function of fluidization velocity and the bed height in a MAFBR with gas production (due to chemical reaction and permeation through the membranes) and the bubble size only influences the methanol conversion significantly and the product selectivity only moderately, the average bubble size was fitted to the methanol conversion for all the

experiments, where a constant bubble diameter throughout the fluidized bed was assumed.

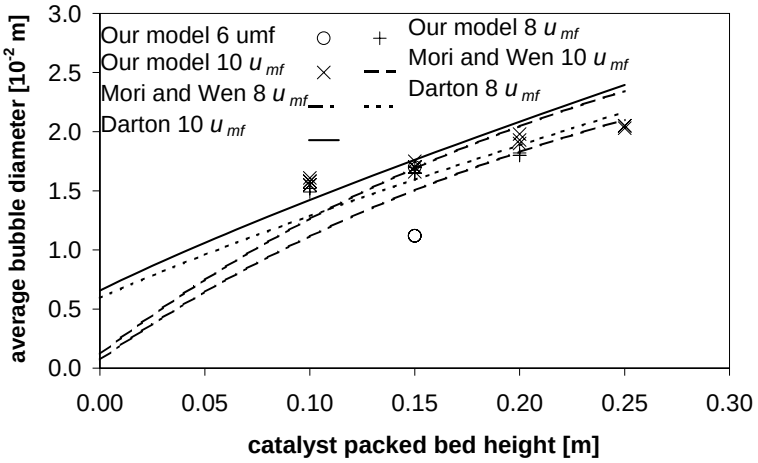

Figure 20. Comparison of the average bubble diameter fitted to the experimental data using literature correlations by Mori and Wen (1975) and Darton et al. (1977).

In Figure 20 the fitted average bubble size for all the experiments using different fluidization velocities, permeation ratios, methanol and oxygen overall inlet concentrations has been plotted as a function of the bed height. In this figure also the well-known correlations proposed by Mori and Wen (1975) and Darton et al. (1977) (see table 4), obtained for fluidized beds without internals at room temperature without chemical reactions, have been included.

The figure shows that the fitted average bubble size matches quite well with the literature correlations, despite the presence of horizontal membranes and gas addition via the membranes. The slightly larger bubble size at higher superficial gas velocities calculated on the basis of the literature correlations is also observed in the fitted results for the average bubble diameter. Furthermore, the results for the fitted average bubble size also show a consistent linear dependency on the bed height, as expected based on the correlations, however, the increase in the average bubble size is about a factor of 2 smaller compared to the literature correlations for the fluidized bed without internals.

Interestingly, for a relatively small bed height of 0.1 m, the fitted average bubble size was larger than calculated using the correlations for a fluidized bed without internals, indicating a faster bubble growth in the MAFBR. This is attributed to the increase in volumetric flow rate due to the reactions, especially in the bottom of the bed where most of the methanol conversion takes place. The gas produced in the emulsion phase is

assumed to be directly transferred to the bubble phase, thus increasing the average bubble size directly. However, the fitted bubble size is slightly smaller than predicted based on the literature correlations at higher bed heights, which could be attributed to the much more pronounced bubble break-up and coalescence in the MAFBR.

Moreover for type A-B particles according to Geldart classification at higher temperatures smaller bubbles and smoother fluidization can be expected (Kunii and Levenspiel, 1991). Wall effects in the small-scale laboratory reactor could play a role as well.

It is important to note that the fitted average bubble diameter for the MAFBR increases only moderately with bed heights, which justifies to some extent the assumption of a constant bubble diameter in our model.

Finally, it is noted that the addition of gas via the membranes, even up to permeation fraction of 40%, hardly influenced the average bubble size, as expected, because of the relatively small effect of the fluidization velocity on the average bubble size.

4.3.1. Effect of bed height

In Figure 21 model predictions of methanol conversion and product selectivity at various bed height and various fractions of the total gas added via membranes, are compared with the experimental results. It is very clear from Figure 21 that selectivities to formaldehyde and carbon monoxide match quite nicely. The small deviations in the formaldehyde and carbon monoxide selectivity are mainly due to two reasons. Firstly, the DME is a bit over-predicted in our model due to unavoidable experimental errors in the DME kinetics originating from very small methanol conversion to DME (see Chapter 5). Secondly DME is directly converted to formaldehyde at the reactor operating temperatures, but at a very slow rate and it is not included in our reactor model. Hence it is expected that over-predicted DME should contribute to the formaldehyde and carbon monoxide selectivity correspondingly.

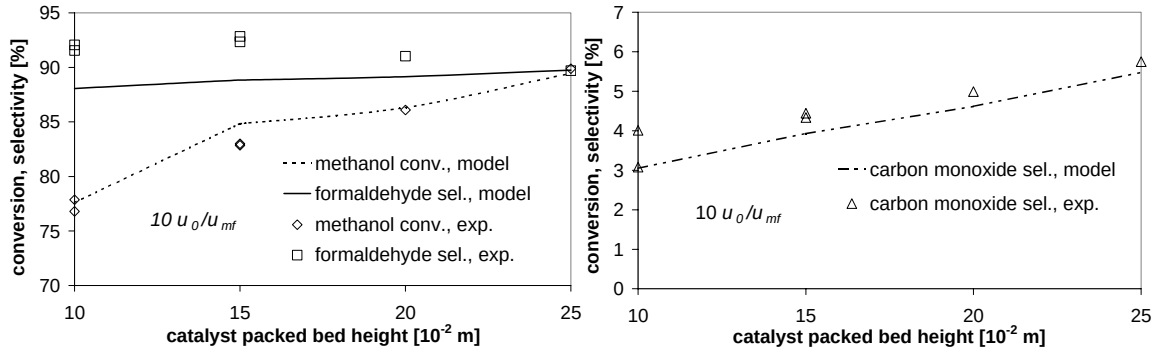

(a) 0 % permeation

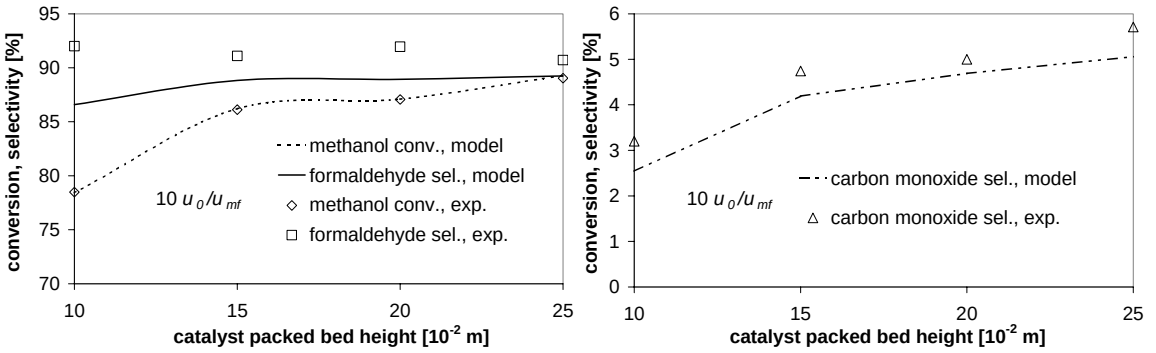

(b) 20% permeation

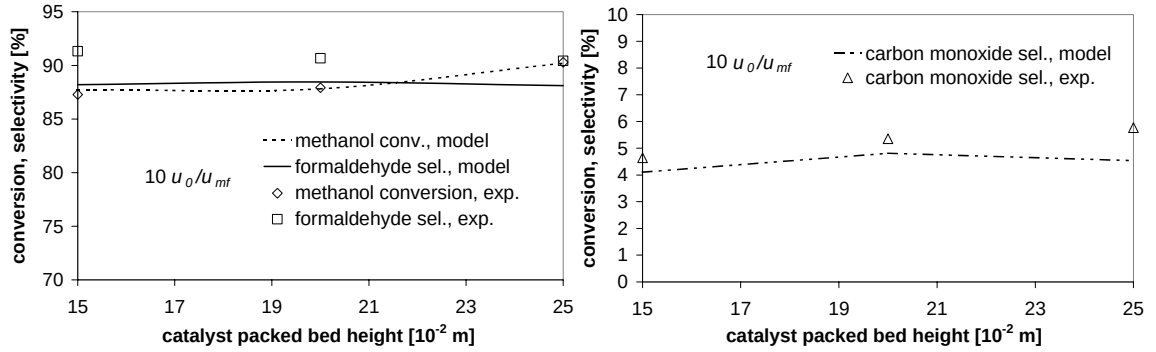

40% permeation

Figure 21. Comparison of the predicted methanol conversion and product selectivities by the two-phase model with the experimental results as function of the catalyst packed bed heights for 17% methanol and 9% oxygen overall feed composition at 275°C reactor temperature and three different permeation ratios.

4.3.2. Effect of permeation on reactants and products molar flow rate profiles

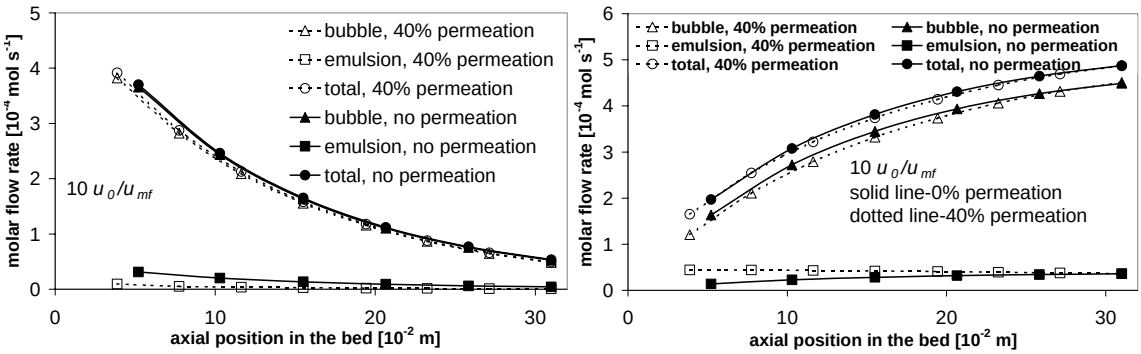

a) methanol b) formaldehyde

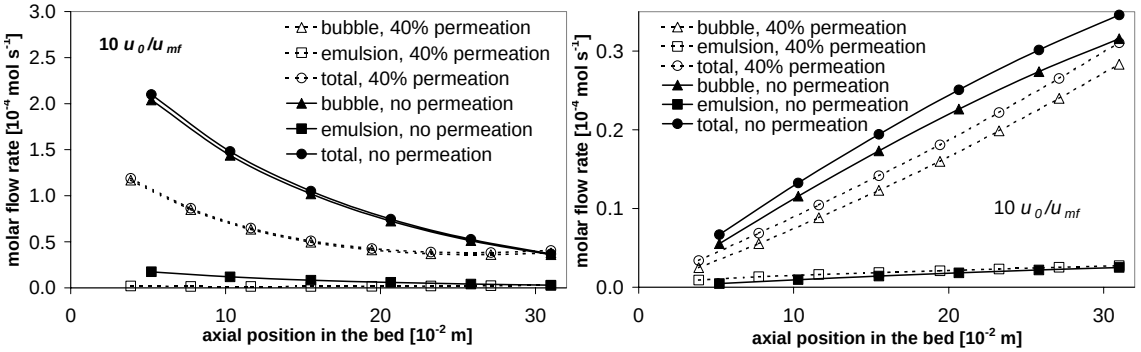

c) oxygen d) carbon monoxide

Figure 22. Comparison of the predicted bubble, emulsion phase and total molar flow rates for a) methanol, b) formaldehyde, c) oxygen and d) carbon monoxide as a function of the axial position in the bed, for inlet total molar flow rates for methanol and oxygen of $6.2 \cdot 10^{-4}$ and $3.2 \cdot 10^{-4}$ mol/s at a reactor temperature of 275°C and a catalyst packed bed height of 0.25 m for two different permeation ratios, where for the case without permeation 6 CISTRs and for the case with 40% permeation 8 CISTRs was taken respectively.

In Figure 22 the local bubble, emulsion phase and total molar flow rates for methanol, formaldehyde, oxygen and carbon monoxide as a function of the axial position in the bed, for overall inlet molar flow rates for methanol and oxygen of $6.2 \cdot 10^{-4}$ and $3.2 \cdot 10^{-4}$ mol/s at a reactor temperature of 275°C and a catalyst bed height of 0.25 m are compared for the case where no gas was added via the membranes with the case where 40% of the total flow was axially equally distributed via the membranes. The figure clearly shows that distributive feeding of oxygen (where all the methanol was fed via the bottom distributor for both cases) hardly influences the local total molar flow rates of methanol and formaldehyde, but strongly decreases the oxygen total molar flow rate causing also a significant reduction of the total CO molar flow rate. The little effect of the membrane permeation on the total and bubble phase methanol and formaldehyde molar flow rates can be explained by the dominant bubble-to-emulsion phase mass transfer limitations. Furthermore, the increased residence time for the methanol in the lower section of the reactor in case of gas addition via the membranes results in much lower methanol and oxygen concentrations (and corresponding molar flow rates) in the emulsion phase, where it is important to realize that the bubble phase molar flow rates are much larger than the emulsion phase molar flow rates due to the much higher superficial bubble phase velocity compared to the superficial emulsion phase velocity, as expected. Due to the low oxygen concentrations in the emulsion phase in case of gas addition via the membranes, the partial oxidation of formaldehyde is retarded thereby decreasing the CO formation rate. Thus, by feeding part of the oxygen distributively via the membranes the same formaldehyde throughput can be achieved at significantly reduced CO losses.

5. Summary and conclusions

The methanol partial oxidation to formaldehyde over an industrial Fe-Mo catalyst has been experimentally investigated in a membrane assisted fluidized bed reactor in order to demonstrate the reactor concept. A small laboratory scale membrane assisted fluidized bed reactor was constructed equipped with horizontal porous ceramic membranes and cooling tubes, in which the methanol conversion and the product selectivities towards formaldehyde, carbon monoxide, dimethyl ether and dimethoxy methane were measured at various overall fluidization velocities, reactor temperatures, methanol and oxygen overall feed concentrations, ratios of gas added via the membranes and the distributor and aspect ratios of the fluidized bed.

Firstly the extent of gas back-mixing in this MAFBR was quantified. Gas back-mixing studies employing steady state tracer injection experiments have demonstrated that for the experimental reactor effective compartmentalization of the fluidized bed is realized with the insertion of horizontal membranes and cooling tubes, especially in case of permeation flow through the membranes, so that the macro scale circulation patterns are effectively eliminated resulting in a close to plug flow behavior. The extent of the axial gas back-mixing in the membrane assisted fluidized bed reactor was quantified over a wide range of fluidization velocities by measuring the gas phase residence time distribution using an ultrasound technique, where the response of the reactor to step down concentration input was fitted by a model representing the reactor by number of CISTRs of equal volumes. The a number of CISTRs measured ranged from 6 to 10, depending on the superficial gas velocity and membrane permeation ratios, which indicates close to plug flow behavior of the MAFBR under all operating conditions employed for methanol partial oxidation to formaldehyde in this study.

Subsequently the MAFBR was demonstrated successfully for the partial oxidation of methanol to formaldehyde. High methanol conversions and high selectivities to formaldehyde were achieved with safe reactor operation at very high methanol concentrations, much higher than currently used in industrial processes. It was experimentally demonstrated that distributive feeding of oxygen in a MAFBR produces an increased overall formaldehyde yield and throughput without pronounced undesirable conversion of formaldehyde to carbon monoxide.

Finally, a reactor model has been developed considering the reactor as a series of ideally stirred tank reactors consisting of a bubble and emulsion phase. The addition of gas via the membranes and the gas production due to the reactions have been accounted for. For a MAFBR neither experimental data nor literature correlations are available for the prediction of the bubble size as a function of the axial position in the bed and superficial gas velocity. Therefore, the bubble size was assumed constant throughout the fluidized bed. The developed model is a two-parameter model, involving the number of CISTRs in series and average bubble size. The number of CISTRs was determined on the basis of independent RTD experiments and amounted 8 to 10.

The average bubble diameter was used as a fit parameter to match the methanol conversions in our experiments. The fitted bubble diameter as a function of the bed height and the superficial gas velocity was compared with well-known literature correlations obtained from cold-flow studies without chemical reaction in fluidized beds

without internals, and showed a quite nice correspondence. From the comparison it was concluded that the bubble size in the MAFBR is larger at low bed heights than predicted by the correlations, mainly due to the gas production by the reactions, but increases much slower with the bed height, mainly because of the enhanced break-up of the bubbles due to the presence of the membranes. Thus, the bubble size is much more constant in the MAFBR, supporting the assumption of a constant average bubble diameter to some extent. With the two-phase model all the experimentally observed influences of the operating conditions could be described well, and therefore our model can be used for further optimization of the MAFBR.

Acknowledgements

This research is part of the research program carried out within the Center for Separation Technology, as a cooperation between the University of Twente and TNO, the Netherlands Organization for Applied Scientific Research. The author wishes to thank Wim Leppink for construction and maintenance of the set-ups. Also contribution by Jan Albert Laverman in experimental as well as modeling work is greatly appreciated.

Notations

A_c	catchment area of the distributor, m^2
A_T	bed cross section, [m^2]
d_p	particle diameter, [micrometer]
D_g	gas diffusivity, [$m^2 \cdot s^{-1}$]
d_b	bubble diameter, [m]
$d_{b,0}$	initial bubble diameter, [m]
D_T	bed diameter, [m]
E	activation energy [$kJ \cdot mol^{-1}$]
F	permeation fraction [-]
g	gravitational acceleration, [$m \cdot s^{-2}$]
H_{mf}	minimum fluidization bed height, [m]
H_f	final fluidization bed height, [m]
k	reaction rate constant [s^{-1}]

K adsorption constant

K_{bc} volumetric interchange coefficient between bubble and cloud phase,[s^{-1}]

K_{ce} volumetric interchange coefficient between cloud and emulsion phase, [s^{-1}]

K^{eq} thermodynamic equilibrium constant [atm^{-1}]

m mass of catalyst [kg]

N number of CISTRs

P_i partial pressure of component i [atm]

R gas constant [= 8.314 J mol^{-1} K^{-1}]

R_i reaction rate of component i [$mol \cdot kg^{-1} \cdot s^{-1}$]

t time [s]

T temperature [K] or [°C]

u_0 superficial gas velocity to the reactor, [$m \cdot s^{-1}$]

u_b rise velocity of cloud of bubble in n^{th} compartment, [$m \cdot s^{-1}$]

u_{br} rise velocity of single bubble in n^{th} compartment, [$m \cdot s^{-1}$]

u_{bs} superficial bubble velocity, [$m \cdot s^{-1}$]

$u_{b,0,s}$ initial superficial bubble velocity, [$m \cdot s^{-1}$]

$u_{b,max,s}$ maximum superficial bubble gas velocity, [$m \cdot s^{-1}$]

u_{mf} minimum fluidization velocity, [$m \cdot s^{-1}$]

V_i volume of the i^{th} phase [m^3]

Greek letters

δ_{bo} initial bubble phase fraction [-]

δ_b bubble phase fraction in [-]

ε_{mf} bed voidage at minimum fluidization conditions, [-]

μ_g viscosity of gas, [Pa·s]

ρ_g density of gas, [$kg \cdot m^{-3}$]

ρ_p density of fluidizing particles, [$kg \cdot m^{-3}$]

θ_i surface fraction of component i [-]

Subscripts

0	initial
avg	average
b	bubble phase
be	bubble phase to emulsion phase
br	bubble rise
cat	catalyst
e	emulsion phase
eq	at thermodynamic equilibrium
exp	experimental
f	forward reaction, final height
g	gas phase
in	inlet
max	maximum
mf	minimum fluidization
n	nth
r	rise
s	superficial
tot	total

References

Abdalla, B.K. and Elnashaie, S.S.E.H. (1995), "Fluidized bed reactor without and with selective membranes for the catalytic dehydrogenation of ethylbenzene to styrene", Journal of Memb. Science, (101), 31.

Adris, A.M., Elnashaie, S.S.E.H. and Hughes, R. (1991),"A fluidized bed reactor for steam reforming of methane", The Canadian Journal of Chemical Engineering, (69), 1061.

Adris, A.M., Lim, C.J., and Grace J.R. (1994), " The fluid bed membrane reactor system: A pilot scale experimental study", Chem. Eng. Sci., (49), 5833.

Cents, A. H. G., Kersten, S. R. A. and Brilman, D. W. F. (2003), “Gas-phase RTD measurements in gas and gas-solid reactors using ultrasound”, Ind. Eng. Chem. Res., (42), 5506-5515.

Darton, R. C., La Nauze, R. D., Davidson, J. F and Harrison, D. (1977),“Bubble growth due to coalescence in fluidized beds”, Trans. Instn. Chem. Engrs, (55), 274.

Kato, K. and Wen, C. (1969), "Bubble assemblage model for fluidized bed catalytic reactors", Chem. Eng. Sci., (24), 1351.

Kunii, D. and Levenspiel, O. (1991), “Fluidization Engineering”, Wiley, New York.

Mori, S. and Wen, C. Y. (1975) “Estimation of bubble diameter in gaseous fluidized beds”, A.I.Ch.E.J., (21), 109.

Ostrowski, T., Giroir-Fendler, A., Mirodatos, C. and Mleczko, L. (1998), "Comparative study of the catalytic partial oxidation of Methane to synthesis gas in fixed bed and fluidized bed membrane reactors. Part II: Development of membranes and catalytic measurements", Cat. Today. , (40), 191.

Pyle, D. L., and Harrison, D. (1967), “An experimental investigation of the two-phase theory of fluidization”, Chem. Eng. Sci., (22), 1199.

Shiau, C. and Lin, C. (1991), “Equation for the superficial bubble-phase gas velocity in fluidized beds”, AICHE. J., (37),6, 953.

Shiau, C. and Lin, C. (1993), “An improved bubble assemblage model for fluidized bed catalytic reactors”, Chem. Eng. Sci., (48), 1299.

Toomey, R. D. and Johnstone, H. F. (1952), “Gaseous fluidization of solid particles”, Chem. Eng. Prog., (48), 220.

Werther, J. (1974), “Influence of the bed diameter on the hydrodynamics of gas fluidized beds”, AICHE Symp. Ser. No. 147, (70), 53.

Westerterp, K. R., van Swaaij, W. P. M. and Beenackers, A. A. C. M. (1993), “Chemical reactor design and operation”, John Wiley and Sons.

Yates, J. G., Ruiz-Martinez, R. S., Cheesman, D. J. (1990), “prediction of bubble size in a fluidized bed containing horizontal tubes”, Chem. Eng. Sci., 45 (4), 1105.

Publications

Deshmukh, S.A.R.K., van Sint Annaland, M. and Kuipers, J.A.M. (2003), “Effect of fluidization conditions on the membrane permeation rate in a membrane assisted fluidized bed”, Chem. Eng. J., 96, 125-131.

Deshmukh, S.A.R.K., Volkers, S., van Sint Annaland, M. and Kuipers, J.A.M. (2004), “Heat transfer in a membrane assisted fluidized bed with immersed horizontal tubes”, Fluidization XI Proceedings, 2004, Naples.

Deshmukh, S.A.R.K., Laverman, J.A., van Sint Annaland, M. and Kuipers, J.A.M. (2004) (2004), “Partial oxidation of methanol to formaldehyde in a membrane assisted fluidized bed reactor”, to be submitted to Industrial & Engineering Chemistry Research.

Deshmukh, S.A.R.K., van Sint Annaland, M. and Kuipers, J.A.M, “Reaction kinetics of the partial oxidation of methanol to formaldehyde reaction system over Fe-Mo catalyst”, to be submitted to Catalysis Today.

Deshmukh, S.A.R.K., van Sint Annaland, M. and Kuipers, J.A.M (2004), “Gas back-mixing in membrane assisted fluidized bed reactors”, to be submitted to Chem. Eng. Sci.

Acknowledgement

This is the last day before my thesis actually goes to printing press and I am still writing one of the most important parts of my thesis, the acknowledgement, trying my best not to discriminate any one. I would not have been here in the Netherlands without the absolute support of my parents and family; therefore I would like to thank them in the first place. I am highly indebted to my promoter, Hans Kuipers, who offered me a wonderful opportunity to pursue my research in a novel and industrially relevant field with a dynamic, multicultural and multinational group. His expertise in the field of fluidization has always helped me immensely during the entire period of the project. I sincerely appreciate his moral boosting and timely appreciation, which motivated me substantially during bad times of the research. I thank him from the bottom of my heart. It was a fantastic experience to have worked with Martin van Sint Annaland as my mentor. I admire his dedication, hard working ability and attitude to go to the bottom of any problem. His numerical and analytical skills are amazing. I am grateful to him for his easy access and persistent input during the entire project, which finally resulted in the form of my Ph.D. thesis. I want to thank Rob Klaassen for his coordination and continuous input during the project meetings. Special thanks to Dr. Paul Walter from Perstorp, Swidon for useful discussions and his generosity for giving the catalyst, without which demonstration of my reactor concept would have been difficult.

My research would have been incomplete without the contribution of excellent graduate students: Jan Stroomer, who performed experimental work to measure the axial gas back-mixing in fluidized bed with and without internals; Sander Volkers, who successfully measured the tube-to-bed heat transfer coefficient in the membrane assisted fluidized bed after overcoming initial hurdles and Jan Albert Laverman, who worked substantially for the experimental demonstration of membrane assisted fluidized bed reactor for partial oxidation of methane and its modeling. Furthermore, Mattijs van der Ham, who worked for three months, measured the effect of gas addition via the membranes on the axial back-mixing in the membrane assisted fluidized bed.

Since most of my project is based on experimental work, my research would not have been possible without expertise and easy availability of the technicians. First of all, I would like to thank Gerrit Schorfhaar for all the work he performed to construct the set-up to measure gas back-mixing in the fluidized bed. I also cherished the non-technical and humorous discussions with him apart from his contribution in improving my Dutch. I

am also thankful to Wim Leppink for construction of heat transfer set-up and also the lab scale demonstration unit of membrane assisted fluidized bed reactor, which was the heart of my thesis. I cannot forget the contribution of Benno Knaken for building the kinetics set-up and his innovative ideas to solve various technical problems during the experiments. Of course I would like to thank Robert Meijer for his assistance during the automation of the set-up and necessary safety measures. I appreciate the assistance of Toine Cents in measuring the gas phase RTD by ultrasound technique. Help by Mathijs Goldschmidt during my first year is greatly appreciated.

I would also like to thank Nicole Haitjema, Ria Steghuis-de Vegte, Brigitte Sanderink and Ria Hofs-Winkelman for their administrative support.

Furthermore, I had a wonderful time with all my colleagues and students of the FAP group. Sailing and Wadlopen experiences will always remain in my mind. My special thanks to Liesbeth Kuipers for organization of the FAP (Fun and Party) parties and winter sports and making my stay homely and lively. I also want to give special thanks to Dhaneshwar (Dani), Charu, Swapnil, Vinit, Girish, Ravi, Supriyo, Madhavi, Satyendra, Shashi, Kavitha-Kiran, Vijay, Kiran, Makarand, Valer, Mousa, Pramod, Shankar, Imran, Ubaid, Komal, Vasughi, Sheela and Arshad Bhai for their wonderful friendship and making my stay relatively peaceful. I sincerely thank them for their moral support during my bad times. I cannot forget the contribution of Seshan and Jayanti to keep the Indian community together by organizing various events and festivals. Moreover, I thank all the members of the Indian community for all the cooperation and enjoyment during my stay in the campus.

Finally I thank all of them who have contributed some way or other during my stay to reach this pinnacle of success. Thank you so much.

Salim Deshmukh

Résumé

Salim Abdul Rashid Khan Deshmukh was born on June 1st,1976 in Mahad, India. After having finished his higher secondary school education from Vahoor, he joined Dr. Babasaheb Ambedkar Technological University, Lonere, for his B. Tech. degree in Chemical Engineering. He successfully completed his Bachelor of Technology degree with first class distinction.

Subsequently, he was awarded the Junior Research Fellowship (JRF) from University Grants Commission (UGC) for excelling in All India level Graduate Aptitude Test in Engineering (GATE) exam and he joined University Department of Chemical Technology (UDCT) for his Master degree in chemical engineering. He worked on a dissertation titled “Novelties of multiphase reactions” under the able guidance of Prof. G. D. Yadav.

In November 1999, he got an opportunity to pursue his Ph. D. in the vibrant and dynamic group of Prof. J.A.M. Kuipers in the Department of Chemical Technology, University of Twente. He worked on the fundamental aspects of the novel Membrane Assisted Fluidized Bed Reactor (MAFBR) and successfully demonstrated the reactor concept for the industrially important partial oxidation reaction of methanol to formaldehyde. From November 2003, he has joined the Catalytic Processes and Materials group of Prof. L. Lefferts, University of Twente, as a Post Doctoral Researcher and working on Catalytic Flash Pyrolysis of Biomass.